Spectral and transport signatures of 1d topological superconductors of finite size in the sub- and supra-gap regime: An analytical study

Dissertation zur Erlangung des Doktorgrades der Naturwissenschaften (Dr. rer. nat.) der Fakultät für Physik

vorgelegt von

Nico Gerhard Leumer

aus Hamburg

im Jahre 2021

Promotionsgesuch eingereicht am: 11.06.2021
Die Arbeit wurde angeleitet von: Prof. Dr. Milena Grifoni

Prüfungsausschuss:
Prof. Dr. Christoph Strunk
Prof. Dr. Jaroslav Fabian
Prof. Dr. Tilo Wettig

Datum Promotionskolloquium: 28.7.2021

Let me complicate your life.

"You are clever man, friend John; you reason well, and your wit is bold; but you are too prejudiced. You do not let your eyes see nor your ears hear, and that which is outside your daily life is not of account to you. Do you not think that there are things which you cannot understand, and yet which are; that some people see things that others cannot? But there are things old and new which must not be contemplate by mens's eyes, because they know -or think they know- some things which other men have told them."

(Bram Stoker [1].)

Summary

We presented exact analytical results for the spectrum and the eigenstates of 1d models of finite size and considering open boundary conditions. This knowledge enables us to evaluate in exact close form the Green's function and transport characteristics of archetype models of 1d topological superconductors. Here I summarize major results.

Next nearest neighbour chain. The first technical non-trivial model we consider is a linear atomic chain with nearest neighbour hopping t and next nearest neighbour m, to which we refer as n.n.n. chain. We find a non equidistant quantization for the wavevectors, deviating from the standard particle in the box behaviour. We give an exact criterion for degenerate energy eigenvalues as a function of t/m. Furthermore, we find gap openings inside the spectrum for which we estimate the ratio t/m and the associated energy scale.

Kitaev chain. The methods used for the n.n.n. chain are the natural techniques to determine all eigenstates and the complete spectrum of the finite Kitaev chain with open boundary conditions. The Kitaev model is an archetype model for topological superconductivity and is has attracted much attention since it was proposed by Kitaev twenty years ago. Remarkably, exact analytical solutions for the spectrum and Green function of the finite chain were not known for generic parameter settings of the chain. We derive such exact expressions in the thesis for the generic parameter case. We summarize here major results and features of the chain.

The sub- and supra-gap spectrum of the finite sized Kitaev chain originates from a highly non-trivial wavevector quantization which depends on all the model parameters t, Δ and μ. Here, t denotes the nearest neighbor hopping amplitude and Δ is the p-wave superconducting mean-field pairing constant. Forced by the open boundary conditions and an interplay of the p-wave superconductivity with Pauli's exclusion principle, the chemical potential enters into the quantization constraint. Based on analytical facts, we show that this causes the energy eigenvalues below and above the superconducting gap to oscillate as a function of μ.

Closely related to this feature are two-fold degenerate energy eigenvalues (crossings) in the supra-gap regime. We give the exact criteria for their number and their position in the parameter space. Compared to the case of $\Delta = 0$, finite values of the pairing constant remove specific crossings from the spectrum transforming them into avoided crossings.

Concerning the sub-gap regime and thus Majorana fermions, the role of μ is crucial for the model and the prediction of edge states since otherwise the topologically trivial

and non-trivial phase are indistinguishable. We conclude that the setting of $\mu = 0$ represents a qualitative change and our results match perfectly with numerical treatments for generic parameter values.

Typically, one describes the spatial extension of Majorana fermions in terms of a decay length ξ which is extracted from the bulk dispersion relation [2, 3]. However, we show explicitly that in case of open boundary conditions and finite size of the model, the decay length adopts a quantization constraint itself. Pure bulk considerations for ξ have thus to be seen critically.

The transport signatures of the Kitaev chain are investigated in a normal-superconducting-normal (N-S-N) configuration and we consider both the sub- and supra-gap regime. We apply the non-equilibriums Green's function method and we find exact results for the necessary entries of the required Green's functions. Below the gap, we show exact results for the contribution of Andreev reflection, the crossed Andreev process and the ordinary charge transfer for generic parameters. We also discuss the effect of disorder. In order to conserve the current we adopt a symmetric bias configuration and find conductance values of e^2/h for near or exact zero energy modes due to the bias configuration between both leads in the charge conserving approach. We discuss how the ratio of Andreev reflection and direct charge transfer allows one to anticipate the spatial profile of the charge carrying state.

For generic energy eigenvalues and in particular for higher excitations, the physical quantity of our choice is the differential conductance. The mentioned crossings and avoided crossings in the Kitaev spectrum show unexpected transport behaviour. The contribution of the Andreev reflection to the differential conductance is unexpectedly large. At crossings it is a variable fraction of e^2/h, reaching e^2/h for $|t| = |\Delta|$ and decreasing for larger $|t/\Delta|$. At the avoided crossings it contributes exactly $e^2/(4h)$ to each of the split peaks. These findings arise from nearly perfect particle and hole mixing inside the eigenstates in the respective vicinity. In particular, the untypical high Andreev reflection is caused by the non-equidistant quantization rule of the Kitaev chain; here, the wavefunctions of ordinary extended states possess significant weight at the system's edges. Similar to situations of Majorana fermions inside the gap, we concluded that the Andreev process reflects the situation of the charge carrying state at the system's ends. These results have been partially published in [4, 5].

Minimal model. We made a minimalistic approach to the transport properties of generic 1d topological superconductors considering only the in-gap modes. We verified this method by reproducing correctly the exact conductance result from the Kitaev chain. The technical details of the model confirmed the connection of locality/ spatial extent of the charge carrying state and the ratio of Andreev and direct charge conductance. This approach is used in order to transfer the gained knowledge of the Kitaev chain to the more realistic physical devices, for instance the proximitized Rashba nanowires which are predicted to host Majorana fermions in the right circumstances [6].

Proximitized semiconducting Rashba nanowire. The low-energy physics of a semiconducting nanowire with Rashba spin-orbit coupling and in proximity to a s-wave superconductor mimics the sub-gap features of the Kitaev chain when exposed to an external magnetic field [6, 7]. Theoretically predicted, this model is able to host Majorana zero modes/ Majorana fermions and embodies a realization of the (sub-gap) Kitaev chain. In fact, the spectral and transport characteristics of the model have been object of intense investigation, see for instance Refs. [3, 8–11].

Since the complexity of the Rashba nanowire Hamiltonian exceed the one of the Kitaev chain, those studies were based mostly on numerical treatments, semi-infinite approaches or pure bulk considerations. In contrast, we consider here a finite length nanowire and we take explicitly the open boundary condition into account. The analogy to the Kitaev chain and the exact analytical results found by us, allows an analytical approach and understanding of spectral and transport signatures of the nanowire beyond earlier investigations. We shortly summarize our main results.

We derive an exact criterion for zero energy modes. Similar to the Kitaev chain, zero energy solutions are restricted to discrete lines in the μ-V_{Z} plane, where the parameter constraints on the chemical potential, the superconducting s-wave pairing constant and the Zeeman term associated to these lines are derived approximatively in the weak spin-orbit coupling limit. A numerical approach confirms our findings.

In the literature, energy oscillations as a function of chemical potential and/ or magnetic field in the sub- and supra gap regime have been found already [3, 9, 12–17]. A mapping of the low energy physics of the nanowire to the Kitaev chain around the Γ-point enabled us to investigate the underlying physical reasons qualitatively. The energy oscillations are caused by a non-trivial wavevector quantization imposed by the finite size and the open boundary conditions. This is also confirmed by the structure of the Bogoliubov -de Gennes Hamiltonian of the nanowire device.

Finally, we investigated the low-energy transport signatures and an exact analytical current formula was derived. We find that the conductance G reaches the conductance quantum along the discrete zero energy lines. As a consequence of the weak-spin orbit coupling limit, the Majorana fermions decay but may extend over long sections of the nanowire depending on the parameters. This behavior is reflected by the ratio of direct charge transfer G_{D} and Andreev reflection G_{A} in the conductance. In the vicinity of the phase boundary, the Majorana fermions are strongly localized at both edges of the system and thus the Andreev reflection is the dominant contribution to G. Still along the zero energy lines within the topologically non-trivial parameter section, but further away from the phase boundary, the Majorana fermions start to extend and thus G_{D} becomes more significant and finally dominant. Our findings are confirmed by numerical treatments and agree qualitatively with the expected behavior anticipated from the finite sized Kitaev chain with open boundary conditions. A publication is currently in preparation.

Contents

Symbols

Symbol	Meaning	Example
$:=$, $=:$	Definition	
$\equiv$	Identification	
Iff	If and only if	
$\approx$	Approximation	For $a = 1$, $b = 1.01$: $a \approx b$
$\lesssim$	Lesser & Approximation	For $a = 1$, $b = 1.001$: $a \lesssim b$
$\propto$	Proportionality	For $y = m \cdot x$: $y \propto x$
$\mathbb{1}_n$	Identity matrix of size n	$\mathbb{1}_2 = \begin{bmatrix} 1 & 0 \\ 0 & 1 \end{bmatrix}$
$0_{n,\,m}$	Zero matrix	$0_{2,\,3} = \begin{bmatrix} 0 & 0 & 0 \\ 0 & 0 & 0 \end{bmatrix}$
$[A,\, B]$	Commutator of A and B	
$\{A,\, B\}$	Anticommutator of A and B	
$\mathcal{K}$	Operator of complex conjugation	
$\mathcal{P}$	Particle-hole symmetry	
$\mathcal{C}$	Chiral symmetry	
$\mathcal{T}$	(Pseudo) time reversal symmetry	
$\mathcal{I}$	Inversion symmetry	

1. Motivation and introduction

Since the literature concerning the research field of Majorana physics is rapidly growing, we give a brief overview of the fundamental concepts. The idea of Majorana particles was born in particle physics and stretches into modern condensed matter theory, where one speaks about Majorana quasiparticles rather than particles. To emphasize the basic similarities and to provide the reader with the fundamental knowledge, we approach the topic via the Dirac equation.

The relativistic relation between energy E and momentum $p = \gamma m_0 v$ of a particle moving with speed v is

$$E^2 = c^2 p^2 + m_0^2 c^4, \tag{1.0.1}$$

where m_0 is the particles mass at rest and γ is the Lorentz factor. Imposing here directly the correspondence principle yields the Klein-Gordon equation

$$\left[\frac{1}{c^2}\partial_t^2 - \Delta + \frac{m_0^2 c^2}{\hbar^2}\right]\psi = 0 \tag{1.0.2}$$

in which both time and space derivatives enter quadratically. Notably, the corresponding time evolution does not capture the proper wave function dynamics [7, 18, 19]. Instead, a linear dependence on the time derivative is mandatory. The required Lorentz invariance of the relativistic quantum equation demands also linearity in $\hat{p}$ [18]. Finally, Paul Dirac found the solution. In terms of

$$\hat{H}_\mathrm{D} = c\,\boldsymbol{\alpha}\cdot\hat{\boldsymbol{p}} + \beta\, m_0 c^2 \tag{1.0.3}$$

the Dirac equation reads

$$\hat{H}_\mathrm{D}\,\psi = \mathrm{i}\hbar\,\partial_t\,\psi. \tag{1.0.4}$$

In Dirac representation the matrices $\boldsymbol{\alpha} = (\alpha_1, \alpha_2, \alpha_3)$ and β are given by

$$\alpha_i = \begin{pmatrix} & \sigma_i \\ \sigma_i & \end{pmatrix}, \quad \beta = \begin{pmatrix} \mathbb{1}_2 & \\ & -\mathbb{1}_2 \end{pmatrix}, \tag{1.0.5}$$

where σ_i denotes the Pauli matrices accounting for the particle spin. Here, $\boldsymbol{\alpha}$ and β possess the property that $\hat{H}_\mathrm{D}^2 = c^2\,\hat{\boldsymbol{p}}^2 + m_0^2 c^4$ holds, i.e. Eq. (1.0.1) can be recovered from Eq. (1.0.4).

Due to the square root, the stationary Dirac equation for free particles in Eq. (1.0.4) has positive and negative energy solutions. The latter were interpreted by Dirac as the antiparticle of the electron. Importantly, solutions for $E > 0$ and $E < 0$ are orthogonal and thus the wavefunction ψ describes either a particle or an antiparticle. However, there is a possible exception as noted by Ettore Majorana: a neutral particle with spin $1/2$ and zero energy has the opportunity to be its own antiparticle, referred to as Majorana particle [7, 19].

Regrettably, Majorana particles are so far not observed as fundamental building units of nature. In particle physics, the existence of Majorana particles is still an open issue. The neutrino is a natural candidate to be thought of as Majorana particle but, due to its only weak interactions, hard to detect and so its final fate to be a Dirac or Majorana particle remains experimentally undecided [7, 19–21].

The situation changes in condensed matter physics. Microscopically, ordinary s-wave superconductors can be described by [7, 19, 21, 22]

$$\hat{H} = \sum_{\sigma,\,\sigma'=\uparrow\downarrow} \int H_{\sigma\sigma'}(\boldsymbol{r})\, \hat{\psi}^\dagger_\sigma(\boldsymbol{r})\, \hat{\psi}_{\sigma'}(\boldsymbol{r})\, \mathrm{d}\boldsymbol{r} + \int \left(\Delta(\boldsymbol{r})\, \hat{\psi}^\dagger_\uparrow(\boldsymbol{r})\, \hat{\psi}^\dagger_\downarrow(\boldsymbol{r}) + \text{h.c.}\right) \mathrm{d}\boldsymbol{r}\,, \quad (1.0.6)$$

where $\hat{\psi}^\dagger_\sigma(\boldsymbol{r})$ creates an electron with spin σ at position $\boldsymbol{r}$. Here, $H_{\sigma\sigma'}$ is a single particle Hamiltonian and $\Delta(\boldsymbol{r})$ is the mean-field superconducting pairing potential. We consider $H_{\sigma\sigma'}$ initially as spin independent and diagonal in spin space for simplicity. Typically, the spectrum of a superconductor is gapped due to $\Delta(\boldsymbol{r}) \neq 0$, and Eq. (1.0.6) yields finite energy excitation above the gap. Those many body excitations are referred to as Bogoliubov quasiparticles being a combination of electrons and holes of opposite spin. For convenience, we introduce the Nambu spinor

$$\hat{\Psi}(\boldsymbol{r}) = \begin{pmatrix} \hat{\psi}_\uparrow(\boldsymbol{r}) \\ \hat{\psi}_\downarrow(\boldsymbol{r}) \\ \hat{\psi}^\dagger_\downarrow(\boldsymbol{r}) \\ -\hat{\psi}^\dagger_\uparrow(\boldsymbol{r}) \end{pmatrix} \quad (1.0.7)$$

and Eq. (1.0.6) adopts the Bogoliubov-de Gennes (BdG) form

$$\hat{H} = \frac{1}{2} \int \hat{\Psi}^\dagger(\boldsymbol{r})\, \mathcal{H}_{\text{BdG}}(\boldsymbol{r})\, \hat{\Psi}(\boldsymbol{r})\, \mathrm{d}\boldsymbol{r} \quad (1.0.8)$$

with

$$\mathcal{H}_{\text{BdG}}(\boldsymbol{r}) = \begin{pmatrix} H(\boldsymbol{r}) & \Delta(\boldsymbol{r}) \\ \Delta^*(\boldsymbol{r}) & -\sigma_y\, H^*(\boldsymbol{r})\, \sigma_y \end{pmatrix}. \quad (1.0.9)$$

The BdG construction doubles the degrees of freedom such that for each excitation associated to positive eigenvalues of $\mathcal{H}_{\text{BdG}}$, a negative one is introduced and they are

separated by the superconducting gap. The doubling introduces the so called (anti unitary) particle-hole symmetry operator $\mathcal{P}$, whose action is

$$\mathcal{P}\,\mathcal{H}_{\mathrm{BdG}}(\boldsymbol{r})\,\mathcal{P}^{\dagger} \;=\; -\mathcal{H}_{\mathrm{BdG}}(\boldsymbol{r}). \tag{1.0.10}$$

Thus $\mathcal{P}$ connects the eigenstates of $\mathcal{H}_{\mathrm{BdG}}$ with opposite energy. In matrix form we have $\mathcal{P} = \tau_y \otimes \sigma_y\,\mathcal{K}$, with τ_y (σ_y) as the Pauli matrix acting in particle-hole (spin) space and $\mathcal{K}$ the operator of complex conjugation [21].

Stationary solutions ϕ_E of the BdG equation $\mathcal{H}_{\mathrm{BdG}}\,\phi_E = E\,\phi_E$ are quite similar to the stationary ones of the Dirac equation [19, 23]. We notice that the Dirac equation in Eq. (1.0.4) possesses the charge conjugation symmetry, which connects solutions of opposite charge/ energy, i.e. particles and antiparticles [7]. Importantly, $\mathcal{P}$ adopts here a similar role in the BdG equation as the charge conjugation did for the Dirac equation. A particle-hole symmetric solution ϕ_E, i.e. whereby $\mathcal{P}\phi_E = \phi_E$, is called Majorana mode. Since $\mathcal{P}$ connects (orthogonal) states of opposite energy, only zero energy solutions are suitable candidates, referred to as Majorana zero (energy) modes.

An alternative and equivalent definition can be given in terms of field operators. An eigenstate of the BdG Hamiltonian $\phi_E = (u_{E,\uparrow},\, u_{E,\downarrow},\, v_{E,\downarrow},\, v_{E,\uparrow})^{\mathrm{T}}$ defines the operator

$$\hat{\psi}_E \;=\; \int \Big[u^{*}_{E,\uparrow}\,\hat{\psi}_{\uparrow}(\boldsymbol{r}) \;+\; u^{*}_{E,\downarrow}\,\hat{\psi}_{\downarrow}(\boldsymbol{r}) \;+\; v^{*}_{E,\downarrow}\,\hat{\psi}^{\dagger}_{\downarrow}(\boldsymbol{r}) \;-\; v^{*}_{E,\uparrow}\,\hat{\psi}^{\dagger}_{\uparrow}(\boldsymbol{r})\Big]\,\mathrm{d}\boldsymbol{r}, \tag{1.0.11}$$

using the Nambu spinor from Eq. (1.0.7). Supposing that ϕ_0 is a Majorana zero mode (MZM), i.e. $\mathcal{P}\phi_0 = \phi_0$ and $\mathcal{H}_{\mathrm{BdG}}\,\phi_0 = 0$ are true, the associated field

$$\hat{\psi}^{\dagger}_0 \;=\; \hat{\psi}_0 \tag{1.0.12}$$

is self-conjugate.

Next, we turn to Majorana fermions, which are closely related to Majorana zero modes. We define Majorana fermions $\hat{\psi}_{\mathrm{MF}}$ solely as self-conjugate

$$\hat{\psi}^{\dagger}_{\mathrm{MF}} = \hat{\psi}_{\mathrm{MF}}, \tag{1.0.13}$$

without the requirement to represent a (zero energy) eigenstate. Thus, a Majorana zero mode is also a Majorana fermion, but the reverse is not correct. For instance, imagine that the fermionic operator $\hat{\psi}_E$ corresponds to a non-zero energy eigenvalue of $\hat{H}$, i.e. the Hamiltonian contains the term $E\,\hat{\psi}^{\dagger}_E\,\hat{\psi}_E \neq 0$. We may define $\hat{\psi}_{\mathrm{A,\,B}}$ by

$$\begin{pmatrix}\hat{\psi}_{\mathrm{A}}\\ \hat{\psi}_{\mathrm{B}}\end{pmatrix} \;\coloneqq\; \frac{1}{\sqrt{2}}\begin{bmatrix}1 & 1\\ -\mathrm{i} & \mathrm{i}\end{bmatrix}\begin{pmatrix}\hat{\psi}_E\\ \hat{\psi}^{\dagger}_E\end{pmatrix}. \tag{1.0.14}$$

yielding $\hat{\psi}^{\dagger}_{\mathrm{A,\,B}} = \hat{\psi}_{\mathrm{A,\,B}}$ without restrictions [21]. Thus, $\hat{\psi}_{\mathrm{A,\,B}}$ are Majorana fermions and yet not Majorana zero modes.

Ordinary superconductors do not host MZM – their density of states is zero within the gap [22]. However, the so called topological superconductors are specific systems tailored from rather basic ingredients to host MZM. Also topological superconductors are gapped and thus the Majorana zero modes are energetically separated from the remaining excitations. For instance, semiconducting nanowires with intrinsic Rashba spin orbit coupling exposed to an external magnetic field when placed on a (s-wave) superconducting substrate is such a suitable platform [10, 24], see also [25–28]. As we are going to discuss in more detail, later in chapter 10, the physics is captured by the Hamiltonian in Eq. (1.0.6) for specific $H_{\sigma\sigma'}$. Proposals based on semiconducting nanowire structures in proximity to an s-wave superconductor beneath with Rashba spin orbit coupling and ferromagnetic insulator [29], or Rashba and Dresselhaus spin orbit coupling [6] give raise to similar scenarios. Remarkably, the basic mechanism in all scenarios is comparable; it relies on the Zeeman splitting, the superconducting proximity effect and Rashba spin orbit coupling to create effective p-wave superconductivity inside the device, which pairs electrons of the same spin. Alternatively, Majorana zero modes may exist also in semiconducting carbon nanotubes [30–33] or ferromagnetic chains in proximity to superconductors [34–38].

Topological superconductors can be identified in terms of topological invariants [39, 40]. The Hamiltonian is categorized following the Altand and Zirnbauer classification scheme [41], according to its present/ absent symmetries, which are related to topologically trivial or non-trivial invariants. In case of the latter, one finds a topological superconductor if the in-gap state is a MZM and otherwise a topological insulator.

The in-gap nature of MZMs has the important consequence that its wave vectors are complex [2, 3, 7, 19]. The associated imaginary part imposes a decay of the Majorana wave function in space, kept in form of a finite decay length. In turn, Majorana zero modes require defects or boundaries at which they are localised. Thus, MZM manifest themselves as boundary or edge modes at the surface of topological superconductor devices. In 1d or quasi 1d systems, they reside at both ends of the system.

In order to verify the existence of MZMs experimentally, several methods were proposed. For instance, the presence of MZMs should be reflected in transport measurements. In fact, Majorana zero modes change the periodicity of the Josephson effect from 2π to 4π [42–44]. Electrical transport phenomena are a further possibility and the presence of MZM in the in-gap regime is reflected by quantized zero bias peaks of the electrical conductance $G \coloneqq \lim_{V\to 0} \partial I/\partial V$ at zero temperature. Here, I is the observed current through the material hosting the MZM and V the applied bias. Theoretically predicted, Majorana zero modes cause quantized conductance peak values of e^2/h [45–47] or $2e^2/h$ [7, 27, 48, 49] or even $e^2/(2h)$ [50] depending on the considered setup. Alternatively, one can investigate the thermal transport properties [51].

However, small energy is unfortunately not uniquely limited to Majorans, and regrettably their transport signatures can be mimicked by topologically trivial Andreev bound states [27, 52–56] or level repulsion in multiband models [57, 58]. Further ideas, exploiting the non-locality of MZM, were thus proposed [59–61].

Up to modern days the clear and doubtless detection of Majoranas is debated and still an open issue, since also sources of disorder, interactions etc. in experimental devices may cause topological trivial features to mimic the fingerprints of their topological non-trivial counterparts [62]. Nonetheless the bar existence of Majorana quasiparticles is already widely accepted in the community and the experimental observations support this interpretation; only the final evidence seems to be missing. Although great effort has already been made, and more is undoubtedly required, the final promise in the quest for MZM may be worth the price: Majorana zero modes offer a solid platform for topological quantum computation [2, 63–65].

Most of the research in this area is necessarily based on numerical simulations. This embeds naturally a blind spot: the interpretation of the numerical data. The rare analytic results we know about Majorana zero modes and Majorana fermions are usually extracted from simple models which qualitatively reproduce the numerical findings. On the other side, the detection of Majorana quasiparticles is an experimental challenge and the devices possess a finite length. Typically, the analytical approaches do not cover all the implications due to technical difficulties. Nonetheless, exact solutions may be valuable for a deeper understanding and also for numerical aspects, or generally as inspiration. This is the main topic and contribution of this work.

Particularly, we will discuss in detail the Kitaev chain of *finite size* with open boundary conditions. As perspective, the Kitaev chain is a topological superconductor and its topological properties have been intensively studied [7, 19] since the model was published back in 2001 [2]. Kitaev's intention already went into the direction of quasi one dimensional quantum wires placed on a three-dimensional superconductor, but the concrete theoretical "realization" of his model came later [10, 30, 32, 66–68]. Importantly, the low energy degrees of freedom in the latter devices mimic the in gap situation in Kitaev's chain; thus, this model is the archetype of topological superconductors and some aspects are universal.

Contrary to this fact, only partial solutions of its finite size spectrum were known previously [69–72]. In the thesis, we derive exact results for the spectrum and all eigenvectors in case of generic parameter values. The findings agree and extend the known literature. For instance the Kitaev chain can be mapped onto an X-Y-model consisting of N spin $1/2$ particles for which diagonalization methods are known [73, 74]. Here too, our new approach extends the previous knowledge. As guidance for the reader, the open boundary condition and the finite length of the system imply an intricate wavevector quantization rule, as it has been shown more generally in Refs. [75–77]. This knowledge is then applied to investigate the transport properties of the Kitaev chain in a N-S-N symmetry.

The thesis is organized as follows. In part I, we focus on the spectra of simple 1d models in case of finite size and open boundary conditions. These chapters are considered as introduction and essentially the reader does not need extended pre-knowledge. Here, I introduce the non-standard technical methods used throughout the thesis based on given

examples in section 2 and 3. In section 4, we generalize the approach and consider a generic mathematical situation as preparation.

In the beginning of part II, the Kitaev chain as 1d topological superconductor is introduced and we discuss in chapter 5 some well known properties of the model. Then, we turn to the BdG spectrum and provide our results for the eigenvalues and the eigenvectors in case of a finite sized Kitaev chain with open boundary conditions. We give exact analytical results based on the methods from part I for all parameter scenarios. Once the results are known to the reader, we explain the physical implications.

Next, we investigate the transport signatures of the a finite sized Kitaev chain placed in between two normal conducting leads. In chapter 7, we apply the non-equilibrium Green's function method in order to derive an analytical expression for the (steady state) current through this N-S-N setup. We consider a generic bias $eV = \mu_L - \mu_R$ and arbitrary values of the chemical potentials $\mu_{L,R}$ of the respective lead. Partially based on our technical approach from section 4, we find exact expressions of the few entries of the retarded Green's function required for the current formula. In turn, we give exact expressions for the conductance formula G and its direct G_{D}, Andreev G_{A} and crossed Andreev G_{CA} contributions. We discuss the results in section 8.1 in and without the wide-band limit for varying values of $\mu_{L,R}$.

The supra-gap transport properties are discussed in section 8.2. The differential conductance $\partial I/\partial V$ and also the Andreev and direct charge transfer terms are investigated. Remarkably, the Andreev reflection is found to contribute significantly also at finite bias.

Finally, in part III, we use a minimal model to describe the linear transport of generic 1d topological superconductors. We demonstrate the validity of the model by reproducing the conductance of the Kitaev chain. In section 10, we introduce the proximitized semiconducting Rashba-nanowire. Based on the knowledge from the Kitaev chain and the minimal model, we discuss both the sub-gap spectrum and the associated transport properties of the finite sized nanowire.

Part I.

Simple finite size 1d models and their relation to Tetranacci polynomials

2. Linear chain

2.1. Model and spectrum using the k-space approach

As a first model, we consider spinless electrons in a chain of N atoms, each having one orbital degree of freedom, and which are coupled by a nearest neighbour hopping constant t. The Hamiltonian of this model reads

$$\hat{H}_{\mathrm{LC}} \;=\; -\mu \sum_{j=1}^{N} d_j^\dagger d_j \;- t \sum_{j=1}^{N-1} \left(d_{j+1}^\dagger d_j \;+\; d_j^\dagger d_{j+1} \right) \tag{2.1.1}$$

in terms of standard fermionic $d_j^\dagger$ (d_j) creation (annihilation) operators. The possible complex phase of the parameters can be gauged away inside the fermionic operators and thus we consider $t \in \mathbb{R}$ without restrictions. Readers familiar with the Kitaev chain [2, 7] will notice that Eq. (2.1.1) is recovered from the Kitaev chain in the absence of the superconducting pairing potential Δ.

The diagonalization of Eq. (2.1.1) is a truly textbook exercise, but we shortly refresh it. For periodic boundary conditions we use the Fourier approach: the transformation $d_j = \frac{1}{\sqrt{N}} \sum\limits_k e^{\mathrm{i}kdj}\, d_k$ diagonalizes the Hamiltonian from Eq. (2.1.1) in k-space

$$\hat{H}_{\mathrm{LC}} = \sum_k \epsilon(k)\, d_k^\dagger d_k, \tag{2.1.2}$$

with $\epsilon(k) = -\mu - 2t\, \cos(kd)$ yielding the dispersion relation, and d as the lattice constant. However, a chain of finite size with open boundary conditions demands that the wave function $\psi(j)$ vanishes at $j = 0$ and $j = N + 1$. Standing waves are readily constructed with the ansatz $\psi(j) = \sum\limits_{k \neq 0} \left(A\, e^{\mathrm{i}kdj} + B\, e^{-\mathrm{i}kdj} \right)$. Here, we used that the states with momentum $\pm k$ are degenerate, $\epsilon(k) = \epsilon(-k)$, and that we have only one atom per unit cell. The boundary condition implies $\psi(j) = 2\mathrm{i} \sum\limits_{k \neq 0} A \sin(kd)$ and yields the quantised values $k_n d = n\pi/(N+1)$ for $n = 1, \ldots, N$. Thus, the discrete energy levels of the linear chain are $\epsilon(k_n) = -\mu - 2t\, \cos\left(\frac{n\pi}{N+1}\right)$.

One could certainly question the necessity of repeating such a trivial and well-known result here. However, the results for the spectrum of the finite Kitaev chain discussed in Ch. 6 can be quite puzzling upon the first view, and we will see features of the linear chain spectrum reemerging. More importantly though, the spectrum of the finite Kitaev chain can be calculated in real space using similar techniques required to diagonalize the linear chain in the real space. Thus the diagonlization in k-space discussed above has to be seen as a benchmark for the real space approach presented below.

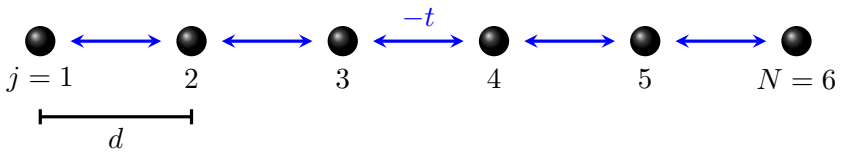

Figure 2.1.: Linear chain for N=6 atoms (black spheres), with lattice constant d and nearest neighbour hopping amplitude t.

2.2. Real space approach and generalisations

The so far unchallenging task to obtain the spectrum of the linear chain becomes seemingly more demanding if we rewrite Eq. (2.1.1) in matrix form and try to obtain its spectrum directly. Defining $\hat{\psi} \coloneqq (d_1, \ldots, d_N)^{\mathrm{T}}$ leads via $\hat{H}_{\mathrm{LC}} = \hat{\psi}^{\dagger}\, \mathcal{H}_{\mathrm{LC}}\, \hat{\psi}$ to

$$\mathcal{H}_{\mathrm{LC}} = \begin{bmatrix} -\mu & -t & & & & & & \\ -t & -\mu & -t & & & & & \\ & -t & -\mu & -t & & & & \\ & & \ddots & \ddots & \ddots & & & \\ & & & -t & -\mu & -t & & \\ & & & & -t & -\mu & -t & \\ & & & & & -t & -\mu & \end{bmatrix}_{N\times N} . \tag{2.2.1}$$

We calculate the spectrum of $\mathcal{H}_{\mathrm{LC}}$ from the characteristic polynomial $P_\lambda(\mathcal{H}_{\mathrm{LC}}) \coloneqq \det(\lambda \mathbb{1}_N - \mathcal{H}_{\mathrm{LC}})$ with $\mathbb{1}_N$ being the identity matrix of dimension N. For the diagonalization in k-space we have been exploiting the translational invariance of the infinite linear chain. Here, similarly, we look for peculiar structures of the matrix in Eq. (2.2.1). Indeed, the tridiagonal form in Eq. (2.2.1) allows a recursive solution of the characteristic polynomial, see Ref. [78], with $P_\lambda(\mathcal{H}_{\mathrm{LC}}) = f_N$ and $j \geq 1$:

$$f_j = (\lambda + \mu)\, f_{j-1} - t^2\, f_{j-2}, \qquad f_{-1} = 0,\ f_0 = 1. \tag{2.2.2}$$

The (banded) Toeplitz[1] character of $\mathcal{H}_{\mathrm{LC}}$ is manifested in the position independent coefficients $\lambda + \mu$ and $-t^2$. In order to obtain $P_\lambda(\mathcal{H}_{\mathrm{LC}})$, we have "simply" to solve the recursion relation for f_N. We calculate a few terms explicitly using Eq. (2.2.2). For example,

$$\begin{aligned} f_1 &= \lambda + \mu, \\ f_2 &= (\lambda + \mu)^2 - t^2, \\ f_3 &= (\lambda + \mu)^3 - 2t^2(\lambda + \mu), \\ f_4 &= (\lambda + \mu)^4 - 3t^2(\lambda + \mu)^2 + t^4, \end{aligned}$$

[1] A matrix is called Toeplitz, in case when each diagonal has only the same entry, for instance $T = \begin{bmatrix} a & b & c & d \\ e & a & b & c \\ f & e & a & b \end{bmatrix}$. The matrix is called further "banded", in case when only a finite number its elements are non zero [79, 80].

where the mixed terms in $\lambda + \mu$ and t^2 are problematic (independent of their precise values) and prevent the calculation of f_N for large values of N. We may get the idea not to solve Eq. (2.2.2) first, but rather ($j \geq 1$)

$$\tilde{f}_j = x\,\tilde{f}_{j-1} + y\,\tilde{f}_{j-2}, \qquad \tilde{f}_{-1} = 0,\ \tilde{f}_0 = 1 \tag{2.2.3}$$

for some $x,\ y \in \mathbb{R}$. Once the solution to the problem in Eq. (2.2.3) is known, we have automatically the one in Eq. (2.2.2) by replacing[2] $x,\ y$ by $\lambda + \mu,\ -t^2$ respectively. In fact, choosing specific values $x \neq 0,\ y \neq 0$, may point us towards the solution for arbitrary $x,\ y$. The most simple case $x = y = 1$, yields $(\tilde{f}_{-1},\ \tilde{f}_0,\ \tilde{f}_1,\ \tilde{f}_2,\ \tilde{f}_3,\ \tilde{f}_4,\ \tilde{f}_5,\ \ldots) = (0,\ 1,\ 1,\ 2,\ 3,\ 5,\ 8,\ \ldots)$ which is the famous Fibonacci sequence [81, 82].

Indeed, we deal here in general with "Fibonacci polynomials" [83, 84]. More precisely, Eq. (2.2.3) defines so called generalized Fibonacci polynomials [84] which reduce to Fibonacci polynomials [83] for $y = 1$. Both kinds are defined for arbitrary $x \in \mathbb{C}$ and initial values 0 and 1. These two types of polynomial sequences can be related by a transformation stated in Ref. [84]. Further generalizations to arbitrary initial values $\tilde{f}_{-1} \neq 0,\ \tilde{f}_0 \neq 1$ [85], granting so called generalized Fibonacci polynomials with generalized initial values, are possible. However, I will refer to all three kind of sequences simply as "Fibonacci polynomials" throughout[3] this work.

Returning to Eq. (2.2.3) with $\tilde{f}_{-1} = 0,\ \tilde{f}_0 = 1$, there exists a power law method to obtain $\tilde{f}_j$, namely $\tilde{f}_j \propto \tilde{R}^j$ ($\tilde{R} \in \mathbb{C} \setminus \{0\}$). From Eq. (2.2.3), we find that

$$\tilde{R}^2 \,-\, x\,\tilde{R} \,-\, y \,=\, 0 \tag{2.2.4}$$

after dividing by $\tilde{R}^{j-2}$ [85, 87]; the two solutions $\tilde{R}_{1,2}$ read

$$\tilde{R}_{1,2} = \frac{x \pm \sqrt{x^2 + 4y}}{2}. \tag{2.2.5}$$

The linearity of the recursion formula enables one to superpose the two solutions, thus $\tilde{f}_j = A\,\tilde{R}_1^j + B\tilde{R}_2^j$ holds, for $\tilde{R}_1 \neq \pm\tilde{R}_2$. The coefficients[4] $A,\ B$ are determined from $\tilde{f}_{-1} = 0,\ \tilde{f}_0 = 1$ and the solution of Eq. (2.2.3) is

$$\tilde{f}_j = \frac{\tilde{R}_1^{j+1} - \tilde{R}_2^{j+1}}{\tilde{R}_1 - \tilde{R}_2}, \tag{2.2.6}$$

which obviously satisfies the initial values. Inspecting the case $x = y = 1$ again gives $\tilde{R}_{1,2} = (1 \pm \sqrt{5})/2$, i.e $\tilde{R}_1$ turns into the golden ratio, and Eq. (2.2.6) becomes Binet's formula: the closed form for all Fibonacci numbers [81].

The replacement of $x,\ y$ by $\lambda + \mu,\ -t^2$ in Eq. (2.2.5) grants the solution for f_j. In terms of

$$R_{1,2} = \frac{\lambda + \mu \pm \sqrt{(\lambda + \mu)^2 \,-\, 4\,t^2}}{2} \tag{2.2.7}$$

[2] Simplification by complication.

[3] Indeed, there are also connections to Chebyshev polynomials of the second kind [86]. However, their application for generic situations is limited due to their mandatory initial values of 0 and 1.

[4] The condition $\tilde{f}_0 = 1$ entails $A = -B$. Does this sound familiar?

we find $f_j = (R_1^{j+1} - R_2^{j+1})/(R_1 - R_2)$. Finally, the characteristic polynomial we were looking for is

$$P_\lambda\left(\mathcal{H}_{\mathrm{LC}}\right) \,=\, f_N \,=\, \frac{R_1^{N+1} - R_2^{N+1}}{R_1 - R_2}, \tag{2.2.8}$$

for all $N \in \mathbb{N}$. Demanding $P_\lambda\left(\mathcal{H}_{\mathrm{LC}}\right) = 0$ using Eq. (2.2.8) in order to obtain the eigenvalues is seemingly complicated, since λ is hidden inside $R_{1,2}$. Nonetheless, we can define a useful variable[5] $\theta \in \mathbb{C}$ by

$$\lambda + \mu =: -2\,t\,\cos\theta \tag{2.2.9}$$

and we understand $\lambda = \lambda(\theta)$ from now on [83, 87]. Does Eq. (2.2.9) sound familiar? Indeed, by inspecting the dispersion relation of the linear chain which we first obtained in k-space, we see that the unknown θ is nothing else than the unquantized kd. We get $R_{1,2} = -t\exp(\mp\mathrm{i}\theta)$ and Eq. (2.2.8) becomes

$$P_\lambda\left(\mathcal{H}_{\mathrm{LC}}\right) = (-t)^N\,\frac{\sin\left[\theta\,(N+1)\right]}{\sin\theta}. \tag{2.2.10}$$

Hence, the eigenvalues of $\mathcal{H}_{\mathrm{LC}}$ follow for $\theta \equiv \theta_n = n\pi/(N+1)$ with $n = 1, \ldots, N$ and read $\lambda = -\mu - 2t\cos\left(\frac{n\pi}{N+1}\right)$ in agreement with the momentum space calculation.

Although more complicated, the real space approach we used here can be easily generalized, see [88–90]. Let us consider the, possibly non hermitian, matrix[6]

$$M \,=\, \begin{bmatrix} b & c_1 & & & & \\ a_1 & b & c_2 & & & \\ & a_2 & b & c_3 & & \\ & & \ddots & \ddots & \ddots & \\ & & & a_{N-2} & b & c_{N-1} \\ & & & & a_{N-1} & b \end{bmatrix}_{N\times N} \tag{2.2.11}$$

with b, a_j, $c_j \in \mathbb{C}$ for $j = 0, \ldots, N-1$ and the condition of $a_j\,c_j = -y$ for all j. Then, the corresponding characteristic polynomial $P_\lambda\left(M\right) = F_N$ can be calculated again by using the recursion technique [78] ($j \geq 1$)

$$F_j = (\lambda - b)\;F_{j-1} \,-\, a_{j-1}\,c_{j-1}\,F_{j-2}, \qquad F_{-1} = 0,\, F_0 = 1. \tag{2.2.12}$$

Calling $\lambda - b =: x \in \mathbb{C}$ and using $a_j\,c_j = -y$ yields

$$F_j = x\,F_{j-1} \,+\, y\,F_{j-2}, \quad j \geq 1, \tag{2.2.13}$$

[5] A complex θ satisfies the definition for all values of t, μ and λ.

[6] In [89] one finds an even further generalized case, where the first and the last diagonal element of M are shifted individually away from b. In terms of the Fibonacci polynomials, one can proof the result within a few lines.

a sequence of Fibonacci polynomials similar to $\tilde{f}_n$ in Eq. (2.2.3) discussed earlier. The Eqs. (2.2.5), (2.2.8) hold still, since we never made use of the *former realness* of x, y to derive them. Introducing $\theta \in \mathbb{C}$ again via[7] $x = 2\mathrm{i}\sqrt{y}\cos(\theta)$ yields now $\tilde{R}_{1,2} = \mathrm{i}\sqrt{y}\exp(\mp\mathrm{i}\theta)$ and we find $P_\lambda(M) = F_N$ to be

$$P_\lambda(M) = (\mathrm{i}\sqrt{y})^N \frac{\sin[\theta(N+1)]}{\sin\theta}. \tag{2.2.14}$$

The eigenvalues of M are given by $\theta_n = n\pi/(N+1)$ for $n = 1, \ldots, N$ and read

$$\lambda = b - 2\sqrt{a_1 c_1}\cos\left(\frac{n\pi}{N+1}\right) \tag{2.2.15}$$

following from the ansatz in θ and the use of $\sqrt{y} = i\sqrt{a_1 c_1}$.

Eq. (2.2.15) is valid for hermitian, skew-hermitian and general matrices of type M. Further, the condition $a_j\, c_j = -y \equiv$ const. allows for a large variety of changes in the matrix M, while keeping the same spectrum. For example, the replacement $c_j \to c_j/2$ and $a_j \to 2a_j$ for some (or all) $j = 1, \ldots, N$, changes M but not a single eigenvalue. One can also change c_j and a_j individually in a similar way (or even introduce entire new variables) without changing the eigenvalues.

The ideas and methods introduced in this chapter will be important to understand some of the steps needed to evaluate spectral properties of the finite Kitaev chain discussed in Ch. 6. Before attacking the Kitaev chain though, it is convenient to explore the properties of another, easier, 1D model, the linear chain with next nearest neighbor hoppings.

[7] These settings have always alternatives without changing the result. For example $x = -2\mathrm{i}\sqrt{y}\cos(\theta)$ can be rewritten as $\theta \to \theta + \pi$. Consequently, we would have $\tilde{R}_{1,2} \to -\tilde{R}_{1,2}$ and the negative sign can be absorbed into the superposition coefficients of $\tilde{R}_{1,2}$, i.e. it disappears. Further, I use always the positive square root of y, namely $\sqrt{y} = +i\sqrt{a_1\, c_1}$, since the possible negative sign is used to shift $\theta \to \theta + \pi$ again. Depending on how one reduces $\sqrt{x^2 + 4y}$ in Eq. (2.2.5) one might exchange $\tilde{R}_1 \to \tilde{R}_2$, but the description is invariant under this exchange, see for example Eq. (2.2.6). Last but not least, $a_j = c_j = -t$ (for $j = 0, \ldots, N$) yields $y = -t^2$ and the positive root is $\sqrt{y} = i|t|$. However, we can simply use $\sqrt{y} = it$ for $t \in \mathbb{R}$, since a sign change of t shifts θ by π again.

3. Atomic chain with next nearest neighbour hopping

3.1. The model and k-space approach to the spectrum

The model we consider bases on the linear chain from Eq. (2.1.1) where we now included next nearest neighbour (n.n.n.) hopping. The Hamiltonian in position space reads

$$\hat{H}_{\mathrm{EC}} = -\mu \sum_{j=1}^{N} d_j^\dagger d_j - t \sum_{j=1}^{N-1} \left(d_{j+1}^\dagger d_j + d_j^\dagger d_{j+1} \right) - m \sum_{j=1}^{N-2} \left(d_{j+2}^\dagger d_j + d_j^\dagger d_{j+2} \right), \tag{3.1.1}$$

with m as the n.n.n. hopping constant as illustrated in Fig. 3.1. Further, we use μ, t, $m \in \mathbb{R}$ without restrictions. Still, only one orbital degree of freedom per atom and spinless electrons are considered, as preparation for the Kitaev chain. Yet, a direct connection between both models is not visible on the level of their respective Hamiltonians.

Although it is intuitive to assume that the values of hopping amplitudes decrease for larger distances, i.e. $m < t$, we aim here to find the finite size spectrum of our new model for all parameter situations, even for $m > t$. We start our study by obtaining the bulk dispersion relation $\epsilon(k)$ belonging to Eq. (3.1.1) using the Fourier approach and periodic boundary conditions. We get

$$\hat{H}_{\mathrm{EC}} = \sum_k \epsilon(k)\, d_k^\dagger d_k, \tag{3.1.2}$$

with

$$\epsilon(k) = -\mu - 2t\cos(kd) - 2m\cos(2kd) \tag{3.1.3}$$

and d is the lattice constant. We find the dispersion relation to be symmetric in k, i.e. $\epsilon(k) = \epsilon(-k)$ due to the present time reversal symmetry. Further, we have the (spatial) inversion symmetry $\hat{I}$ since exchanging $d_j^{(\dagger)} \to d_{N+1-j}^{(\dagger)}$ $(j = 1, \ldots, N)$ maps the Hamiltonian in Eq. (3.1.1) onto itself. Finally, the two harmonics dispersion in Eq. (3.1.3) implies the presence of degenerate solutions, $\epsilon(k_1) = \epsilon(k_2)$, for momenta satisfying

$$\cos(k_1 d) + \cos(k_2 d) = -\frac{t}{2m}, \tag{3.1.4}$$

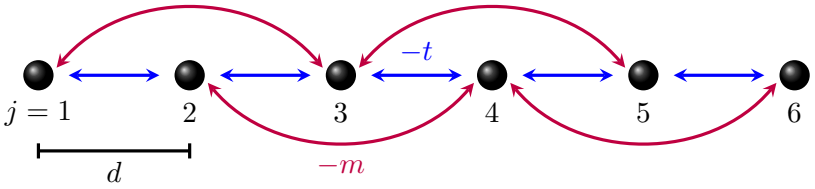

Figure 3.1.: Atomic chain with (next) nearest neighbour hopping amplitude (m) t for $N = 6$.

for $m \neq 0$. One can check easily that both momenta correspond to the same energy:

$$\begin{aligned}
\epsilon(k_1) + \mu &= -2t\,\cos(k_1 d) \;-\; 2m\cos(2k_1 d) \\
&= -2t\,\cos(k_1 d) \;-\; 2m\left[2\cos^2(k_1 d) \;-\; 1\right] \\
&\overset{(*)}{=} \frac{t^2}{m} \;+\; 2t\cos(k_2 d) \;-\; 2m\left[\frac{t^2}{2m^2} + 2\frac{t}{m}\cos(k_2 d) + 2\,\cos^2(k_2 d) - 1\right] \\
&= -2t\cos(k_2 d) - 2m\left[2\cos(k_2 d)^2 - 1\right] \\
&\equiv \epsilon(k_2) + \mu, \qquad (3.1.5)
\end{aligned}$$

using $\cos(2x) = 2\cos^2(x) - 1$ in the second/ second last step and Eq. (3.1.4) at $(*)$. Importantly, Eq. (3.1.4) does not quantise k_1 or k_2; it merely relates two points of equal energy in the Brillouin zone. The next step is to obtain the eigenvalues for finite length and open boundary conditions.

Similar to the simpler linear chain discussed in the former chapter, the spectrum of the finite model can be obtained with a genuine ansatz for a bulk wave function, containing left and right moving particles, which is able to satisfy the finite size constraints. The infinite long system with periodic boundary conditions is translation invariant and we first remind Bloch's theorem [91] which states that

$$\hat{T}_l\,\psi_k(j) \;=\; e^{\mathrm{i}kl}\psi_k(j), \qquad (3.1.6)$$

with $\hat{T}_l$ being the one dimensional translation operator shifting the state $\psi_k(j)$ of our single band by a distance $l = n\,d$, $n \in \mathbb{Z}$. Eq. (3.1.6) is a two point formula, giving the relation between an "initial" position j and a "final" position $j+n$ on the lattice without information about the underlying process. For example for $n = 2$ we can jump twice by one atom, i.e. using t, or once with m, see Fig. 3.1. Both processes are obviously independent, since if either $m = 0$ or $t = 0$, only one option remains, but Bloch's theorem must be satisfied. This leads to the two harmonics dispersion in Eq. (3.1.3). Thus, with $t \neq 0$ and $m \neq 0$, the ansatz for the wave function has to be

$$\psi(j) \;=\; A\,e^{\mathrm{i}k_1 dj} \;+\; B\,e^{-\mathrm{i}k_1 dj} \;+\; C\,e^{\mathrm{i}k_2 dj} \;+\; D\,e^{-\mathrm{i}k_2 dj}. \qquad (3.1.7)$$

Here, again, one exploits that $\epsilon(k_1) = \epsilon(k_2)$ and $\epsilon(k) = \epsilon(-k)$ is true. Further, compared to the former $m = 0$ case, the open boundary condition is now extended to

$$\psi(j) = 0, \quad \text{at } j = -1,\, 0,\, N+1,\, N+2, \qquad (3.1.8)$$

to properly account for the four constants A, B, C and D. The constraints at $j = -1$ and $j = N+2$ account for the next nearest neighbour hopping m. Alternatively, one can first derive the boundary condition and the ansatz in Eq. (3.1.7) follows then directly in order to avoid a trivial solution. The last implication from Eq. (3.1.7) is of course the linear independence in j of the plane waves, i.e. $k_{1,2} \neq 0$, $k_1 \neq \pm k_2$ and $k_1 d \neq (k_2 d + n\pi)$ for $n \in \mathbb{Z}$.

The parameter independent boundary conditions used together with Eq. (3.1.4) yield a quantization of $k_{1,2} = k_{1,2}(t, m)$ which depends on the values of m and t. In the following we arrive at the same dispersion relation and the associated quantization condition within the real space approach.

3.2. Position space calculation of the spectrum

The discreteness of the model in Eq. (3.1.1) allows a matrix representation, similar to the former $m = 0$ case, and we find

$$\mathcal{H}_{\mathrm{EC}} = \begin{bmatrix} -\mu & -t & -m & & & & \\ -t & -\mu & -t & -m & & & \\ -m & -t & -\mu & -t & -m & & \\ & \ddots & \ddots & \ddots & \ddots & \ddots & \\ & & -m & -t & -\mu & -t & -m \\ & & & -m & -t & -\mu & -t \\ & & & & -m & -t & -\mu \end{bmatrix}_{N\times N} \tag{3.2.1}$$

with $\hat{\psi} = (d_1, \ldots, d_N)^{\mathrm{T}}$ and $\hat{H}_{\mathrm{EC}} = \hat{\psi}^{\dagger}\, \mathcal{H}_{\mathrm{EC}}\, \hat{\psi}$. The matrix in Eq. (3.2.1) contains the onsite potential μ which shifts the eigenvalues λ only up or down and can thus be put to zero without restrictions.

The spectrum of the n.n.n chain is shown in Fig. 3.2. It is symmetric in $t \to -t$ and it displays a non-trivial behavior when $m \to -m$. The exact analytical solution is provided at the end of section 3.2.2, see Eq. (3.2.36). We find further degenerate energies, depicted in form of crossings, and avoided crossings in the spectrum with their numbers increasing with the system size as it is seen in panels a) and d) of Fig. 3.2. The precise positions and the corresponding mechanism of both features will be discussed below in chapter 3.3.

3.2.1. Recursion relation

Contrary to the linear chain with $m = 0$, we will not calculate the characteristic polynomial, rather aiming for the eigenvectors of $\mathcal{H}_{\mathrm{EC}}$ directly. The eigenvector problem $\mathcal{H}_{\mathrm{EC}}|\psi\rangle = \lambda|\psi\rangle$ for $N \geq 5$ with $|\psi\rangle = (\xi_1, \xi_2, \ldots, \xi_N)^{\mathrm{T}}$ yields

$$m\,\xi_{j+2} = -(\lambda + \mu)\,\xi_j - m\,\xi_{j-2} - t\,(\xi_{j-1} + \xi_{j+1}), \quad j = 3, \ldots, N-2, \tag{3.2.2}$$

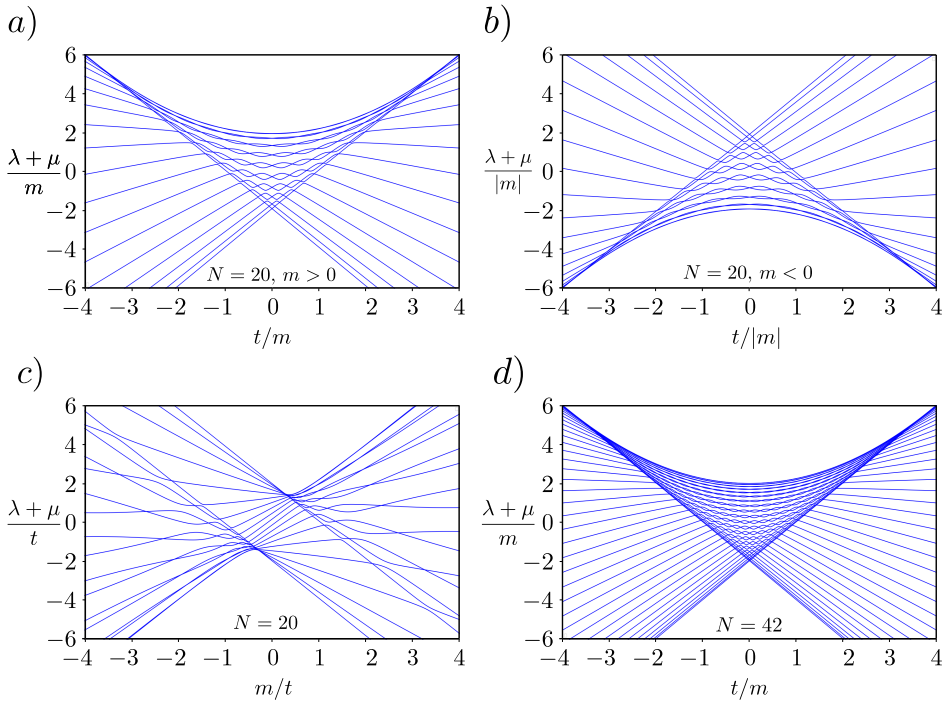

Figure 3.2.: Numerically calculated spectrum of a linear chain with next nearest neighbour hoppings. The parameter λ provides the eigenvalues, while t and m are the n.n and the n.n.n. hoppings, respectively. N is the number of lattice sites. a) $N = 20$ and $m > 0$. One observes a non trivial dependence of λ on t/m including several crossings, i.e. energy degeneracies. b) By changing the sign of m, the values of $\lambda + \mu$ invert their sign. The quantity $(\lambda + \mu)/m$ is thus invariant under the sign change of m. The spectrum is even in the hopping t. c) Spectrum as a function of m/t for $N = 20$ in units of t. d) Increasing the size to $N = 42$ does not change the overall shape of the spectrum, only the number of eigenvalues and crossings.

and four boundary conditions

$$m\,\xi_3 \;=\; -\,(\lambda+\mu)\;\xi_1 \;-\; t\,\xi_2, \tag{3.2.3}$$

$$m\,\xi_4 \;=\; -\,(\lambda+\mu)\;\xi_2 \;-\; t\,(\xi_1 \;+\; \xi_3)\,, \tag{3.2.4}$$

$$0 \;=\; -\,(\lambda+\mu)\;\xi_{N-1} \;-\; m\,\xi_{N-3} \;-\; t\,(\xi_N \;+\; \xi_{N-2})\,, \tag{3.2.5}$$

$$0 \;=\; -\,(\lambda+\mu)\;\xi_N \;-\; m\,\xi_{N-2} \;-\; t\,\xi_{N-1}, \tag{3.2.6}$$

with the terms being ordered according to Eq. (3.2.2). The cases for $N = 1, \ldots, 4$ can be included, as we show in the following.

Inspecting the Eqs. (3.2.3) - (3.2.6) closer, we realize that the boundary condition involves the interior of the system, not its exterior as usually used in k-space calculations. In the case of $m = 0$, we would expect the boundary condition to be $\xi_0 = \xi_{N+1} = 0$

as used in the calculation via the k-space in chapter 2. Imagine we solved our problem and know all entries of $|\psi\rangle$ for the known eigenvalues λ in the case of $N \geq 5$. We then might ask what is the value of ξ_{N+1}? Possibly a strange question since the largest index appearing in Eq. (3.2.2) is N, namely for $j = N-2$, due to the finite size, ξ_{N+1} is *not defined*. However, the recursion formula Eq. (3.2.2) requires only the knowledge about the last four terms to obtain the next one. Knowing $|\psi\rangle$ already, we might just continue to calculate further ξ_j. In other words, we do not ignore the upper limit of $j = N-2$ in Eq. (3.2.2), but rather we simply define ξ_{N+1}, ξ_{N+2}, ξ_{N+3}, ... as the continuation of $\xi_1, \ldots, \xi_N$ via Eq. (3.2.2), while keeping $|\psi\rangle = (\xi_1, \xi_2, \ldots, \xi_N)^{\mathrm{T}}$ fixed. We define ξ_0, ξ_{-1}, ... analogously, yielding

$$m\,\xi_{j+2} \;=\; -\,(\lambda+\mu)\;\xi_j \;-\,m\,\xi_{j-2} \;-\; t\,(\xi_{j-1} \;+\; \xi_{j+1})\,, \quad j \in \mathbb{Z}, \tag{3.2.7}$$

which defines so called Tetranacci polynomials. For more details, see Ch. 4.

Inspecting now the boundary conditions Eqs. (3.2.3) - (3.2.6) closer, we see "missing" terms compared to Eq. (3.2.7). The prior extension of the recursion formula allows to write them down. We find

$$\begin{aligned} 0 \;&=\; -m\,\xi_1 \;-\; t\,\xi_0, \\ 0 \;&=\; -m\,\xi_0, \\ 0 \;&=\; -m\,\xi_{N+1}, \\ 0 \;&=\; -m\,\xi_{N+2} - t\,\xi_{N+1}, \end{aligned}$$

and in the case of $t \neq 0$, $m = 0$ we get

$$\xi_0 = \xi_{N+1} = 0, \tag{3.2.8}$$

while

$$\xi_{-1} = \xi_0 = \xi_{N+1} = \xi_{N+2} = 0, \tag{3.2.9}$$

holds for $t \neq 0$, $m \neq 0$. We conclude that extending the recursion formula shifts the boundary condition from inside the Hamiltonian to its outside, onto *artificial* sites. This allows one to include the cases $N = 1, 2, 3, 4$ in the treatment.

For example, the $N = 1$ case follows directly from Eq. (3.2.7) with $j = 1$ and Eq. (3.2.9)

$$m\,\xi_3 \;=\; -\,(\lambda+\mu)\;\xi_1 \;-\,m\,\xi_{-1} \;-\; t\,(\xi_0 \;+\; \xi_2)\,. \tag{3.2.10}$$

Since $\xi_{N+1} \equiv \xi_2 = 0$, $\xi_{N+2} \equiv \xi_3 = 0$ holds, we find $0 = (\lambda+\mu)\,\xi_1$ which is $\mathcal{H}_{\mathrm{EC}}|\psi\rangle = \lambda|\psi\rangle$ for $N = 1$. Similarly, for $N = 2$ we find

$$m\,\xi_3 \;=\; -\,(\lambda+\mu)\;\xi_1 \;-\,m\,\xi_{-1} \;-\; t\,(\xi_0 \;+\; \xi_2)\,, \tag{3.2.11}$$

$$m\,\xi_4 \;=\; -\,(\lambda+\mu)\;\xi_2 \;-\,m\,\xi_0 \;-\; t\,(\xi_1 \;+\; \xi_3)\,, \tag{3.2.12}$$

and $\xi_{N+1} \equiv \xi_3 = 0$, $\xi_{N+2} \equiv \xi_4 = 0$ yields here

$$\left.\begin{aligned} 0 &= -(\lambda+\mu)\,\xi_1 - t\,\xi_2 \\ 0 &= -(\lambda+\mu)\,\xi_2 - t\,\xi_1 \end{aligned}\right\} \Rightarrow \begin{bmatrix} -\mu & -t \\ -t & -\mu \end{bmatrix} \begin{pmatrix} \xi_1 \\ \xi_2 \end{pmatrix} = \lambda \begin{pmatrix} \xi_1 \\ \xi_2 \end{pmatrix}, \tag{3.2.13}$$

or simply $\mathcal{H}_{\mathrm{EC}}|\psi\rangle = \lambda|\psi\rangle$ for $N = 2$. The cases $N = 3, 4$ are treated analogously. We thus conclude, that the Eqs. (3.2.7), (3.2.9) are valid for all N and solving the recursion problem will lead to the eigenvalues and eigenvectors of $\mathcal{H}_{\mathrm{EC}}$.

3.2.2. Spectral properties

In the case of $m \neq 0$ we may rewrite Eq. (3.2.7) as

$$\xi_{j+2} = -\frac{\lambda+\mu}{m}\,\xi_j - \xi_{j-2} - \frac{t}{m}\,(\xi_{j-1} + \xi_{j+1}), \qquad j \in \mathbb{Z}. \tag{3.2.14}$$

Let us recall that the Hamiltonian in Eq. (3.1.1) has inversion symmetry, i.e. it is invariant under the exchange $d_j^{(\dagger)} \to d_{N+1-j}^{(\dagger)}$. In the basis $\hat{\psi} = (d_1, \ldots, d_N)^{\mathrm{T}}$ for $\mathcal{H}_{\mathrm{EC}}$ in Eq. (3.2.1) we denote the inversion symmetry as I which has the representation

$$I = \begin{bmatrix} & & 1 \\ & \iddots & \\ 1 & & \end{bmatrix}_{N\times N}, \tag{3.2.15}$$

and $I\,\mathcal{H}_{\mathrm{EC}}\,I = \mathcal{H}_{\mathrm{EC}}$ holds indeed. The inversion symmetry, by definition, turns effectively the x axis and thus k into $-k$. In order to proceed, we repeat the same strategy as for Fibonacci polynomials. We define

$$\zeta := -\frac{\lambda+\mu}{m}, \tag{3.2.16}$$

$$\eta := -\frac{t}{m}, \tag{3.2.17}$$

for simplicity and the ansatz $\xi_j \propto r^j$ ($r \neq 0$) yields the characteristic equation

$$r^4 - \zeta\,r^2 + 1 - \eta\,(r + r^3) = 0 \tag{3.2.18}$$

after dividing by r^{j-2}. We can solve Eq. (3.2.18) easily, dividing by r^2. Solving first for $S := (r + r^{-1})$, i.e. $S^2 - 2 = r^2 + r^{-2}$, grants the condition

$$S^2 - \eta\,S - \zeta_{\mathrm{EC}} - 2 = 0 \tag{3.2.19}$$

and the two solutions $S_{1,2}$ read

$$S_{1,2} = \frac{\eta \pm \sqrt{\eta^2 + 4\,(\zeta+2)}}{2}. \tag{3.2.20}$$

Solving next for r, via $r^2 - S_{1,2}\, r + 1 = 0$, gives the four fundamental solutions r_{+1}, r_{-1}, r_{+2}, r_{-2}:

$$r_{\pm l} \;=\; \frac{S_l \,\pm\, \sqrt{S_l^2 - 4}}{2}, \quad l = 1, 2. \tag{3.2.21}$$

We can use the just derived Eqs. (3.2.20), (3.2.21) to discover some properties, namely

$$S_1 \,+\, S_2 \;=\; \eta \;=\; -\frac{t}{m}, \tag{3.2.22}$$

$$r_{+l}\, r_{-l} \;=\; 1, \quad l = 1, 2. \tag{3.2.23}$$

The apparent similarity between the solutions $r_{\pm l}$ and $\tilde{R}_{1,2}$ from Eq. (2.2.5) motivates the choice

$$S_l \;=:\; 2\cos(k_l d), \qquad l = 1, 2, \tag{3.2.24}$$

with[1] $k_l d \in \mathbb{C}$, yielding

$$r_{\pm l} = e^{\pm \mathrm{i} k_l d}. \tag{3.2.25}$$

For Fibonacci polynomials, the ansatz for θ (here k) was identified as the dispersion relation $\epsilon(k)$ and here it is correct for $k_{1,2}$ as well. Remembering that $S_{1,2}$ satisfy Eq. (3.2.19) and imposing Eq. (3.2.24) afterwards, yields

$$\zeta = S_{1,2}^2 - 2 - \eta\, S_{1,2} = \underbrace{4\cos^2(k_{1,2}d) - 2}_{=2\,\cos(2k_{1,2}d)} - \left(-\frac{t}{m}\right) \cos(k_{1,2}d)\,. \tag{3.2.26}$$

With $\zeta = -(\lambda + \mu)/m$ this reduces to the dispersion relation

$$\lambda \;=\; -\mu - 2t\, \cos(k_{1,2}d) - 2m\, \cos(2\, k_{1,2}d), \tag{3.2.27}$$

in agreement with the k-space treatment. Obviously, we have two descriptions for the same eigenvalue λ, one using $k_1 d$ and a second with $k_2 d$. Notice that $S_1 + S_2$ from Eq. (3.2.22) becomes

$$\cos(k_1 d) \,+\, \cos(k_2 d) \;=\; -\frac{t}{2m} \tag{3.2.28}$$

which is Eq. (3.1.4). This implies directly[2] $\lambda(k_1 d) = \lambda(k_2 d)$ as we have already demonstrated earlier in Eq. (3.1.5).

The connection between k_1 and k_2 drawn in the last expression demands $k_1 \neq \pm k_2$. Further, $k_l = 0$ is excluded since Eq. (3.2.21) demands $r_{+l} \neq r_{-l}$ for $l = 1, 2$. Inspecting the Eqs. (3.2.20), (3.2.21) closer, the four solutions $r_{\pm l}$ are distinct as long as $S_1 \pm S_2 \neq 0$,

[1] The realness of $k_{1,2}$ is a consequence of the quantization and the ansatz holds for complex values as well.

[2] We had only one "λ" from the very beginning.

i.e. $k_1 d \neq k_2 d \pm \pi$. In the case $t \neq 0$, ξ_j is a linear combination of the four fundamental solutions

$$\xi_j \;=\; A\, r_{+1}^{j} \;+\; B\, r_{-1}^{j} \;+\; C\, r_{+2}^{j} \;+\; D\, r_{-2}^{j}. \tag{3.2.29}$$

In terms of k_1 and k_2, Eq. (3.2.29) becomes

$$\xi_j \;=\; A\, e^{\mathrm{i}k_1 dj} \;+\; B\, e^{-\mathrm{i}k_1 dj} \;+\; C e^{\mathrm{i}k_2 dj} \;+\; D\, e^{-\mathrm{i}k_2 dj} \tag{3.2.30}$$

and one recovers Eq. (3.1.7) from the k-space approach. We conclude that all expressions in section 3.1 were correct, only limited to real values of $k_{1,2}$. The boundary conditions in Eq. (3.2.9) yield

$$\begin{bmatrix} e^{-\mathrm{i}k_1 d} & e^{\mathrm{i}k_1 d} & e^{-\mathrm{i}k_2 d} & e^{\mathrm{i}k_2 d} \\ 1 & 1 & 1 & 1 \\ e^{\mathrm{i}k_1 d(N+1)} & e^{-\mathrm{i}k_1 d(N+1)} & e^{\mathrm{i}k_2 d(N+1)} & e^{-\mathrm{i}k_2 d(N+1)} \\ e^{\mathrm{i}k_1 d(N+2)} & e^{-\mathrm{i}k_1 d(N+2)} & e^{\mathrm{i}k_2 d(N+2)} & e^{-\mathrm{i}k_2 d(N+2)} \end{bmatrix} \begin{pmatrix} A \\ B \\ C \\ D \end{pmatrix} = \begin{pmatrix} 0 \\ 0 \\ 0 \\ 0 \end{pmatrix}. \tag{3.2.31}$$

Demanding a singular matrix, to avoid a trivial solution, quantises $k_{1,2}d$. The result can be expressed in terms of $k_\Sigma \coloneqq (k_1 + k_2)/2$, $k_\Delta \coloneqq (k_1 - k_2)/2$ leading to the transcendental equation

$$\frac{\sin^2\left[k_\Sigma d\,(N+2)\right]}{\sin^2\left(k_\Sigma d\right)} \;=\; \frac{\sin^2\left[k_\Delta d\,(N+2)\right]}{\sin^2\left(k_\Delta d\right)}. \tag{3.2.32}$$

Iff Eq. (3.2.32) is satisfied the upper matrix is singular[3]. The dependence on $N+2$ originates from the N sites and the next nearest neighbour hopping $m \neq 0$. Importantly, Eq. (3.2.32) *selects* the allowed values of k_1 and k_2 for a finite model with N sites. The quantization rule is a single equation containing two unknowns $k_{\Sigma,\Delta}$. In order to solve for $k_{1,2}$, we have to respect also Eq. (3.2.28), which can be written as

$$\cos\left(k_\Sigma d\right)\,\cos\left(k_\Delta d\right) \;=\; -\frac{t}{4m}. \tag{3.2.33}$$

Let me clarify that Eq. (3.2.32) is the quantization rule, i.e. the finite size condition, while Eq. (3.2.33) is the equal energy constraint and in fact a bulk property, but both are required to obtain the finite size spectrum. The eigenvalues follow from inserting k_1 or k_2 into the dispersion relation in Eq. (3.2.27). The natural kind of representation of the momenta seems to be $k_{\Sigma,\Delta}$ and we thus rewrite the dispersion relation as follows. We know $\lambda(k_1 d) = \lambda(k_2 d)$, i.e. $2\lambda = \lambda(k_1 d) + \lambda(k_2 d)$ and hence

$$\begin{aligned} 2\,\lambda \;&=\; -2\mu \;-\; 2t\,\left[\cos\left(k_1 d\right) \;+\; \cos\left(k_2 d\right)\right] \;-\; 2m\,\left[\cos\left(2k_1 d\right) \;+\; \cos\left(2k_2 d\right)\right] \\ &=\; -2\mu \;+\; \frac{t^2}{m} \;-\; 4m\left[\cos\left(2k_\Sigma d\right)\,\cos\left(2k_\Delta d\right)\right], \end{aligned} \tag{3.2.34}$$

[3] If the determinant vanishes without constraint, the used ansatz is simply wrong.

holds after applying Eq. (3.2.28). In order to get a description in only k_Σ or k_Δ, we use further Eq. (3.2.33) stating that

$$\cos\left(2k_{\Delta,\Sigma}d\right) \;=\; 2\cos^2\left(k_{\Delta,\Sigma}d\right) - 1 = \frac{t^2}{8m^2}\,\frac{1}{\cos^2\left(k_{\Sigma,\Delta}d\right)} - 1 \tag{3.2.35}$$

is true. Combining the last two expressions give finally the form of $\lambda(k_{\Sigma,\Delta})$:

$$\lambda\left(k_{\Sigma,\Delta}\right) \;=\; -\mu \;+\; \frac{t^2}{4m} \;+\; 2m\,\cos\left(2k_{\Sigma,\Delta}d\right) \;+\; \frac{t^2}{4m}\,\tan^2\left(k_{\Sigma,\Delta}d\right), \qquad m \neq 0. \tag{3.2.36}$$

One can easily check that Eqs. (3.2.32), (3.2.33) and (3.2.36) are invariant under the exchanges $k_\Sigma \leftrightarrow k_\Delta$, $k_1 \leftrightarrow k_2$ and $k_{1,2} \leftrightarrow -k_{1,2}$. A second small check for the correctness of the results is the change of $t \to -t$ or similar $m \to -m$. Each sign change of these two parameters can be undone by shifting for example $k_\Delta \to k_\Delta + \pi/d$, see Eq. (3.2.33) and the quantization rule in (3.2.32) is invariant in $k_\Delta \to k_\Delta + \pi/d$. Thus, the values for k_Σ, k_Δ and k_Σ, $k_\Delta + \pi/d$ in both settings are the same. The dispersion relation in Eq. (3.2.36) is obviously π-periodic, i.e changing $t \to -t$ does not change the spectrum, but inverting the sign of m does. More precisely, $\lambda + \mu \to -(\lambda + \mu)$ for a sign change in m, which is exactly the numerical observed behaviour in Fig. 3.2. Apparently, we can demand $k_{\Sigma,\Delta} \in (0,\, \pi/d)$ without restrictions and similar for $k_{1,2}$. The correctness of the quantization rule in Eq. (3.2.32) can be confirmed analytically in the limit of $t = 0$. This case will turn out to be of importance also to understand some features of the Kitaev chain.

3.2.3. Special case of $t = 0$, $m \neq 0$

We calculate the eigenvalues of (3.2.1) starting from the original definition of the model in Eq. (3.1.1) at $t = 0$

$$\hat{H}_{\mathrm{EC}}\Big|_{t=0} \;=\; -\mu \sum_{j=1}^{N} d_j^\dagger d_j \;- m \sum_{j=1}^{N-2} \left(d_{j+2}^\dagger d_j \;+\; d_j^\dagger d_{j+2}\right), \tag{3.2.37}$$

in order to formulate an expectation for the derivation starting from the quantization rule in Eq. (3.2.32). Once the spectrum for this case is known, we re-engineer the values for $k_{\Sigma,\Delta}$ from our findings and inspect whether Eq. (3.2.32) is satisfied or not.

Before we diagonalise Eq. (3.2.37) in position space, we draw the model once more. Inspecting Fig. 3.3 a), we recognize only connections between every second atom. Thus, the odd and even values for the position index j belong to distinct sublattices as visualised in Fig. 3.3 b). The independent parts of our system mimic each a linear chain with nearest neighbour hopping amplitude m, lattice constant $2d$ and N_1 (N_2) sites for

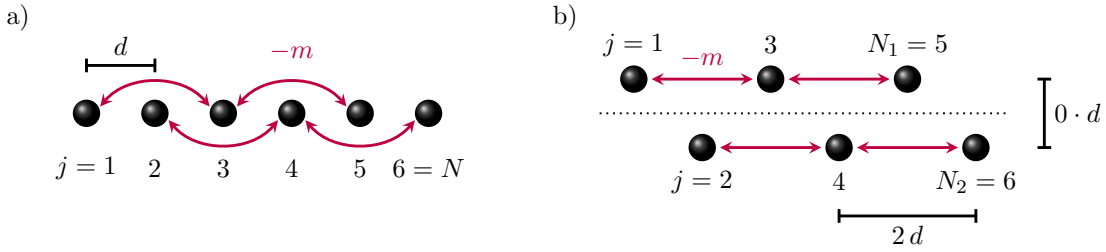

Figure 3.3.: In the case $t = 0$ the chain with n.n.n hopping amplitude m and N sites in a) decouples into two distinct sublattices with $N_{1,2}$ atoms as shown in b). Each imitates a nearest neighbour chain with hopping constant m and lattice constant $2d$. The two chains are both lying on the x-axis.

the slice formed by the odd (even) values of j. The number of atoms in each piece is

$$N_1 = \begin{cases} \frac{N}{2}, & N \text{ even} \\ \frac{N+1}{2}, & N \text{ odd} \end{cases}, \tag{3.2.38}$$

$$N_2 = \begin{cases} \frac{N}{2}, & N \text{ even} \\ \frac{N-1}{2}, & N \text{ odd} \end{cases}, \tag{3.2.39}$$

following from the constraint $N_1 + N_2 = N$ and $N_1 = N_2$ ($N_1 = N_2 + 1$) for even (odd) N[4]. We will verify our insight from the Fig. 3.3 and call

$$\begin{aligned} a_j &= d_{2j-1}, \quad j = 1, \ldots, N_1, \\ b_j &= d_{2j}, \qquad j = 1, \ldots, N_2 \end{aligned}$$

temporarily. The Hamiltonian in Eq. (3.2.37) indeed certifies the pictorial finding and transforms into

$$\hat{H}_{\mathrm{EC}}\Big|_{t=0} = -\mu \sum_{j=1}^{N_1} a_j^\dagger a_j - m \sum_{j=1}^{N_1-1} \left(a_{j+1}^\dagger a_j + a_j^\dagger a_{j+1} \right) \tag{3.2.40}$$

$$- \mu \sum_{j=1}^{N_2} b_j^\dagger b_j - m \sum_{j=1}^{N_2-1} \left(b_{j+1}^\dagger b_j + b_j^\dagger b_{j+1} \right). \tag{3.2.41}$$

We obtain two distinct but structurally identical, copies of Eq. (2.1.1) for $N_{1,2}$ sites. We may define $\hat{\psi} \coloneqq (a_1, \ldots, a_{N_1}, b_1, \ldots, b_{N_2})^{\mathrm{T}}$ and we find via $\hat{H}_{\mathrm{EC}} = \hat{\psi}^\dagger \mathcal{H}_{\mathrm{EC}} \hat{\psi}$ a block

[4]The values for $N_{1,2}$ immediately tell us the form of the spectrum just by looking at Fig. 3.3 b), as demonstrated next.

diagonal matrix

$$\mathcal{H}_{\mathrm{EC}} = \left[\begin{array}{cccccc|cccccc} -\mu & -m & & & & & & & & & & \\ -m & -\mu & -m & & & & & & & & & \\ & -m & -\mu & -m & & & & & & & & \\ & & \ddots & \ddots & \ddots & & & & 0_{N_1,\,N_2} & & & \\ & & & -m & -\mu & -m & & & & & & \\ & & & & -m & -\mu & & & & & & \\ \hline & & & & & & -\mu & -m & & & & \\ & & & & & & -m & -\mu & -m & & & \\ & & & & & & & -m & -\mu & -m & & \\ & & & 0_{N_2,\,N_1} & & & & & \ddots & \ddots & \ddots & \\ & & & & & & & & & -m & -\mu & -m \\ & & & & & & & & & & -m & -\mu \end{array}\right] \tag{3.2.42}$$

$$\equiv \begin{bmatrix} \mathcal{H}_{\mathrm{a}} & \\ & \mathcal{H}_{\mathrm{b}} \end{bmatrix},$$

where $\mathcal{H}_{\mathrm{a}} \in \mathbb{R}^{N_1 \times N_1}$, $\mathcal{H}_{\mathrm{b}} \in \mathbb{R}^{N_2 \times N_2}$ describe the sublattices. Obviously, the characteristic polynomial corresponding to $\mathcal{H}_{\mathrm{EC}}$ is given by the product of the ones associated with $\mathcal{H}_{\mathrm{a,b}}$, exploiting the block diagonal structure. The eigenvalues $\lambda_{\mathrm{a,b}}$ of $\mathcal{H}_{\mathrm{a,b}}$,

$$\lambda_{\mathrm{a}} = -\mu - 2m\cos(k_{a,n}d), \qquad k_{a,n}d = \frac{n\pi}{N_1+1},\ n = 1, \ldots,\ N_1, \tag{3.2.43}$$

$$\lambda_{\mathrm{b}} = -\mu - 2m\cos(k_{b,n}d), \qquad k_{b,n}d = \frac{n\pi}{N_2+1},\ n = 1, \ldots,\ N_2, \tag{3.2.44}$$

follow directly from the discussion in section 2.2, more specifically from Eqs. (2.2.11), (2.2.15). The spectrum of $\mathcal{H}_{\mathrm{EC}}$ is the set containing all values $\lambda_{\mathrm{a,b}}$. However, by virtue of Eq. (3.2.27) one would expect the eigenvalues to depend on twice $k_{a,n}$ ($k_{b,n}$) rather than once, since m is the n.n.n. hopping constant. Reminding Eq. (3.2.38) we may understand $k_{a,n}$ as ($n = 1, \ldots,\ N_1$)

$$k_{a,n}d = \frac{2\,n\pi}{2N_1+2} = 2\,n\pi \cdot \begin{cases} \frac{1}{N+2} & N \text{ even} \\ \frac{1}{N+3} & N \text{ odd} \end{cases}. \tag{3.2.45}$$

Analogously, we have ($n = 1, \ldots,\ N_2$)

$$k_{b,n}d = \frac{2\,n\pi}{2N_2+2} = 2\,n\pi \cdot \begin{cases} \frac{1}{N+2} & N \text{ even} \\ \frac{1}{N+1} & N \text{ odd} \end{cases}. \tag{3.2.46}$$

Hence, we find the "missing" factor two and the spacing $1/(N+2)$ between the closest values of $k_{a,n}d$ ($k_{b,n}d$) for at least even N as one probably anticipated from Eq. (3.2.32). In the case of N even the eigenvalues of $\mathcal{H}_{\mathrm{EC}}$ read

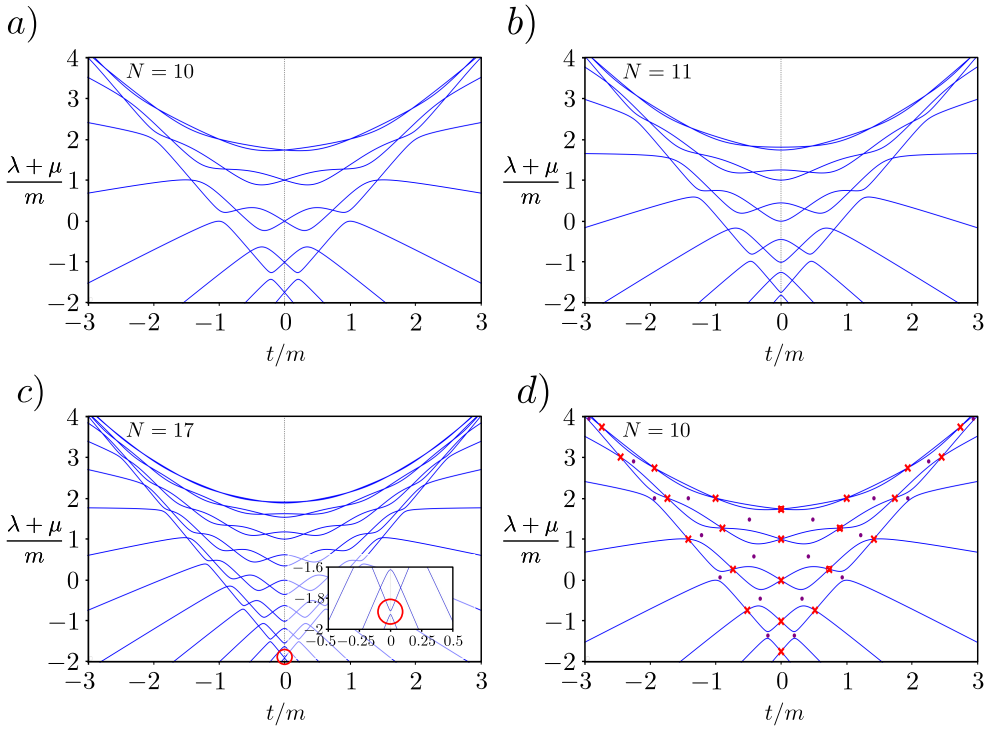

Figure 3.4.: Spectrum of the atomic chain with n.n.n. hopping for even and odd number of atoms. a) The spectrum is degenerate for $N = 10$ along the $t/m = 0$ line. In contrast, for odd number of atoms, $N = 11$ in b), no energy degeneracy occurs at $t/m = 0$. c) For larger odd N some energies become close (○) and may appear as degenerate depending on the resolution, see in panel zoom. d) Pictorial definition of "crossings" (C), marked as "×", and "avoided crossings" (AC) visualized by "•" for $N = 10$. Note that the precise positions of the avoided crossings are debatable.

$$\lambda = -\mu - 2m\cos\left(2\frac{n\pi}{N+2}\right), \quad n = 1, \ldots, N/2 \quad (N \text{ even, each twofold degenerate}), \tag{3.2.47}$$

and each value is twice degenerate since $N_1 = N_2$ for even N, i.e. both sublattices are physically indistinguishable see Fig. 3.3. In the case of N odd, we find

$$\lambda = -\mu - 2m\cos\left(2\frac{n\pi}{N+3}\right), \quad n = 1, \ldots, (N+1)/2 \quad (N \text{ odd, part 1}), \tag{3.2.48}$$

$$\lambda = -\mu - 2m\cos\left(2\frac{n\pi}{N+1}\right), \quad n = 1, \ldots, (N-1)/2 \quad (N \text{ odd, part 2}), \tag{3.2.49}$$

and we have no degeneracy.

The spectrum for $t = 0$, $m \neq 0$ is now known. The values of $k_{a,n}/2$ ($k_{b,n}/2$) can be understood as those for k_1; k_2 follows then from Eq. (3.1.4) at $t = 0$, thus $k_2 = k_1 + \pi/d$.

Alternatively, one can exchange the roles of k_1, k_2 and independently $\pi \to -\pi$ without loss of generality. Still, the quantization rule in Eq. (3.2.32) is written in terms of $k_{\Sigma,\,\Delta}$, but we can simply construct them from $k_{1,2}$. Reminding $k_2 = k_1 + \pi/d$ for $t = 0$ and $k_{\Sigma,\Delta} = (k_1 \pm k_2)/2$ grants

$$k_\Sigma \;=\; k_1 + \frac{\pi}{2d}, \tag{3.2.50}$$

$$k_\Delta \;=\; \frac{\pi}{2d}. \tag{3.2.51}$$

As shown in appendix A, those values of $k_{\Sigma,\,\Delta}$ indeed satisfy the quantization rule from Eq. (3.2.32) at $t = 0$ for odd and even N respectively.

3.3. Crossings and avoided crossings in the spectrum

In general the quantization rule shapes the entire finite size spectrum of the n.n.n. chain including in particular the crossings and the avoided crossings. Nonetheless, they exist only for specific values of t/m, hinting that an extra criterion for their appearance is required. In the current status of the introduction however, we cannot show the details of the derivation since more advanced knowledge of the recursion formula stated back in Eq. (3.2.14) is mandatory. The approach is exposed in appendix B for completeness, but only recommended for readers already familiar with the results for the Kitaev chain given in section 6 or at least with chapter 4. Here we summarize the results and we turn first to the spectral crossings. The given results should be taken as motivation for later further studies of the recursion formula from Eq. (3.2.14).

3.3.1. The criterion for spectral crossings

For the purpose of demonstration, we have chosen in Fig. 3.5 the small, gentle $N = 4$ case. Most importantly, the entire criterion bases only on integers i, j associated to $k_{\Sigma,\,\Delta}d$ which one can further convert into values for t/m and $(\lambda + \mu)/m$ as we explain in the following. In Fig. 3.6, we have shown the scenario for $N = 5$.

Before we give the result, two short remarks: First, the model is invariant under exchange of $k_{1,2}$ and thus allows the choice $k_1 > k_2 > 0$, i.e. $k_\Sigma > k_\Delta > 0$, without restrictions. Second, the symmetry of the spectrum in $t/m \to -t/m$ is respected by two separated selection rules.

The values for $k_{\Sigma,\Delta}d$ at energetic crossings are

$$\textbf{(C)} \quad (k_\Sigma d,\, k_\Delta d) = \left(\frac{i\,\pi}{N+2},\, \frac{j\,\pi}{N+2}\right), \quad i = 2, \ldots, i^{\mathrm{C}}_{\mathrm{max}},\, j = 1, \ldots,\, i-1, \tag{3.3.1}$$

with $\pi/2 \geq k_\Sigma d > k_\Delta d > 0$ and

$$\textbf{(C)} \quad (k_\Sigma d,\, k_\Delta d) = \left(\pi\frac{N+2-i}{N+2},\, \frac{j\,\pi}{N+2}\right), \quad i = 2, \ldots, i^{\mathrm{C}}_{\mathrm{max}},\, j = 1, \ldots,\, i-1 \tag{3.3.2}$$

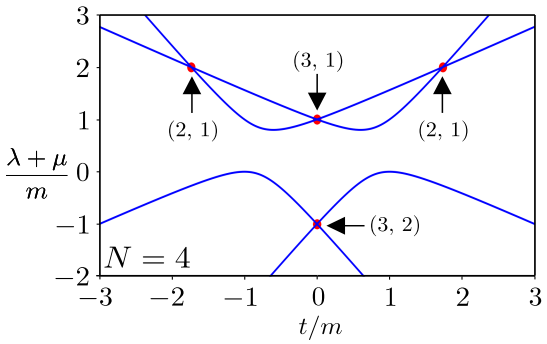

(i,j)	$k_\Sigma d$	$k_\Delta d$	$\frac{t}{m}$	$\frac{\lambda+\mu}{m}$
$(2,1)$	$\frac{2\pi}{6}$	$\frac{\pi}{6}$	-1.73	2.00
$(3,1)$	$\frac{3\pi}{6}$	$\frac{\pi}{6}$	0.00	1.00
$(3,2)$	$\frac{3\pi}{6}$	$\frac{2\pi}{6}$	0.00	-1.00
$(2,1)$	$\frac{4\pi}{6}$	$\frac{\pi}{6}$	1.73	2.00

Figure 3.5.: Numerically calculated eigenvalues as a function of t/m, and predicted crossings, marked as "•" for $N = 4$ (left panel). The analytical values for the $k_\Sigma d$, $k_\Delta d$ pairs and the corresponding values for t/m, $(\lambda+\mu)/m$ (rounded) are given in the right panel. The numbers in the brackets, for example $(2,1)$, correspond to (i,j) in the notation of Eqs. (3.3.1), (3.3.2) determining $k_{\Sigma,\Delta}d$ and in turn t/m, $(\lambda+\mu)/m$. Values in the last line of the right panel belong to $k_\Sigma d > \pi/2$, i.e. to (i,j) from Eq. (3.3.2).

satisfying $\pi > k_\Sigma d \geq \pi/2 > k_\Delta d > 0$. The largest integer $i^{\mathrm{C}}_{\max} \geq 2$ is

$$i^{\mathrm{C}}_{\max} = \begin{cases} \frac{N+2}{2}, & N \text{ even} \\ \frac{N+1}{2}, & N \text{ odd} \end{cases} \tag{3.3.3}$$

and formally allows a unification of the crossing criteria for even and odd N. Note the value $i^{\mathrm{C}}_{\max} = (N+2)/2$ for even N yields $k_\Sigma d = \pi/2$ in both Eqs. (3.3.1), (3.3.2) and is twice represented, but exists in fact only once.

The smallest number of atoms allowing the formation of crossings is $N = 2$ following from the condition $i_{\max} \geq 2$. Let us turn back to the separation of $k_\Sigma d \leq \pi/2$ and $k_\Sigma d \geq \pi/2$ in Eqs. (3.3.1), (3.3.2). This specific choice embodies the symmetry of the spectrum in $t/m \to -t/m$ as we show next. The equal energy constraint on $k_{\Sigma,\Delta}$ was not used so far, but has to be satisfied per se in order to obey the open boundary condition. Here, the situation changed slightly as we know already the values for $k_{\Sigma,\Delta}$; thus,

$$\frac{t}{m} = -4\cos(k_\Sigma d)\cos(k_\Delta d) \tag{3.3.4}$$

predicts the exact ratios t/m, i.e. the horizontal positions in Figs. 3.5, 3.6, at which the crossings occur. One can easily verify that the values for $k_{\Sigma,\Delta}d$ in Eqs. (3.3.1), (3.3.2) satisfy the quantization rule and thus $k_{\Sigma,\Delta}d$ are associated to energy eigenvalues. The value for λ, or better $(\lambda+\mu)/m$, follows by inserting the selected $k_{\Sigma,\Delta}d$ and the associated t/m into the dispersion relation. Please notice, the given criterion is exact and moreover, only crossings correspond to the equidistantly quantized values of $k_{\Sigma,\Delta}d$.

The values for $k_\Sigma d$ in Eq. (3.3.2) are received by subtracting the ones from Eq. (3.3.1) from π and thus causing a sign change of $t/m \to -t/m$ in Eq. (3.3.4). This sign can be absorbed into t, which does not affect the spectrum. Thus, the two sets $k_{\Sigma,\Delta}d$ inherit

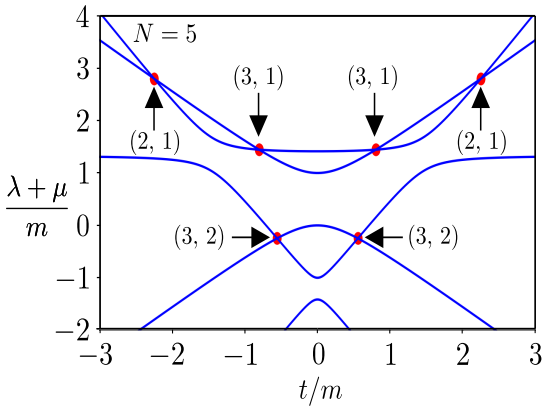

(i,j)	$k_\Sigma d$	$k_\Delta d$	$\frac{t}{m}$	$\frac{\lambda+\mu}{m}$
$(2,1)$	$\frac{2\pi}{7}$	$\frac{\pi}{7}$	-2.25	2.80
$(3,1)$	$\frac{3\pi}{7}$	$\frac{\pi}{7}$	-0.80	1.45
$(3,2)$	$\frac{3\pi}{7}$	$\frac{2\pi}{7}$	-0.55	-0.25
$(2,1)$	$\frac{5\pi}{7}$	$\frac{\pi}{7}$	2.25	2.80
$(3,1)$	$\frac{4\pi}{7}$	$\frac{\pi}{7}$	0.80	1.45
$(3,2)$	$\frac{4\pi}{7}$	$\frac{2\pi}{7}$	0.55	-0.25

Figure 3.6.: Numerically calculated eigenvalues and predicted crossings (•) as function of t/m for $N = 5$. The last three lines in the right panel originate from Eq. (3.3.2) and the first three from Eq. (3.3.1).

the symmetry of the spectrum.

Note, the previous special case for $t = 0$ and N even can be recovered from Eq. (3.3.1). We have to use $i = i_{\max}$ here, i.e. $k_\Sigma d = \pi/2$, setting $t = 0$, but mind the roles of k_Σ and k_Δ w.r.t to Eqs. (A.1.1), (A.1.2) are exchanged. Exploiting the π periodicity of the quantization rule and the spectrum, we have to regard $k_\Sigma d - \pi$ in Eq. (A.1.2) instead yielding the values of $k_\Delta d$ from Eq. (3.3.1) for $j = 1, \ldots, N/2$.

The left hand side in Eq. (3.3.4) is limited by ± 4 and thus the crossings occur exclusively for $-4 < t/m < 4$, see Figs. 3.5, 3.6 for comparison. Similarly, we have limitations on $(\lambda + \mu)/m$. Returning to Eq. (3.2.36), we find $(m \neq 0)$

$$\begin{aligned} \frac{\lambda(k_\Sigma) + \mu}{m} &= 2\cos(2k_\Sigma d) + \frac{t^2}{4m^2}\left[1 + \tan^2(k_\Sigma d)\right] \\ &= 2\cos(2k_\Sigma d) + \frac{t^2}{4m^2}\frac{1}{\cos^2(k_\Sigma d)} \\ &= 2\cos(2k_\Sigma d) + 4\cos^2(k_\Delta d), \end{aligned} \tag{3.3.5}$$

where we used Eq. (3.3.4) in the last step[5]. The last expression holds also for exchanged roles of k_Σ, k_Δ. We do know already the values of k_Σ, k_Δ for the crossings and thus they occur exclusively in the region

$$-2 \leq \frac{\lambda + \mu}{m} \leq 6, \qquad \text{and} \qquad -4 \leq \frac{t}{m} \leq 4, \tag{3.3.6}$$

where the equalities hold only in the limit $N \to \infty$. In general, the values for i, j from Eq. (3.3.1) (Eq. (3.3.2)) belong to the negative (positive) ratios of t/m. The larger

[5]We know that $i_{\max}$ yields $k_\Sigma d = \pi/2$ for even N. Nonetheless, the corresponding prefactor and Eq. (3.3.4) avoids the divergence. For comparison, see the crossings in Fig. 3.5 at $t/m = 0$.

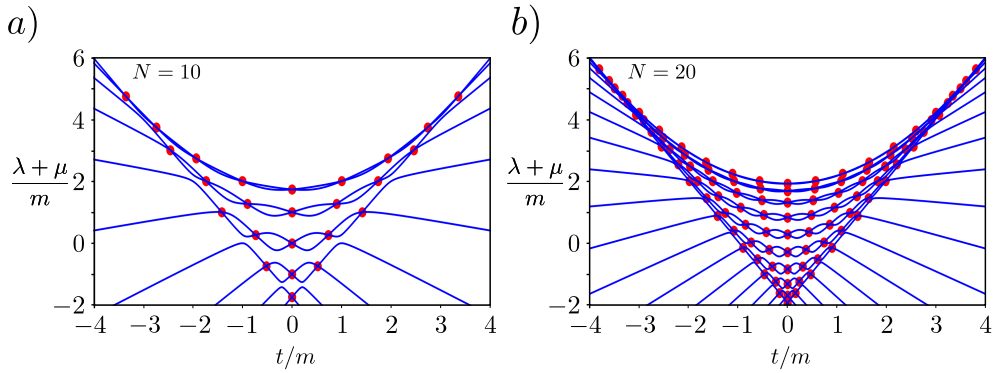

Figure 3.7.: Crossings for $N = 10$ in a) and $N = 20$ in b) and numerical eigenvalues. Increasing the system size floods the area between $-2 \leq (\lambda+\mu)/m \leq 6$ and $|t/m| \leq 4$ with crossings, since N_{C} scales with the square of N. In case of $N = 10$ ($N = 20$), we have $N_{\mathrm{C}} = 25$ ($N_{\mathrm{C}} = 100$).

i, j become, the closer $k_{\Sigma,\Delta}d$ get to $\pi/2$, i.e. t/m approaches zero due to Eq. (3.3.4) visible especially for $(i, j) = (3, 1)$ and $(i, j) = (3, 2)$ in Fig. 3.6. Moreover, the number of crossings N_{C} follows by counting the allowed combinations of k_Σ and k_Δ in the Eqs. (3.3.1), (3.3.2). We find

$$N_{\mathrm{C}} = \begin{cases} \frac{N^2}{4}, & N \text{ even}, \\ \frac{N^2-1}{4}, & N \text{ odd} \end{cases}, \tag{3.3.7}$$

in agreement with the numerics. As the number of crossings increased with N and since the limits in Eq. (3.3.6) do not, the region in which the crossings are found becomes more and more crowded for increasing N, as shown in Fig. 3.7. A similar discussion will help us to track the avoided crossings (AC).

3.3.2. The criterion for avoided crossings

Avoided crossings do not correspond to eigenvalues and reside instead between them, see e.g. Fig. 3.4 d). In turn, they are associated to values of $k_{1,2}$ which do not satisfy the quantization rule. In this matter of failing, the avoided crossings are not unique per se, as many $k_{1,2}$ do not obey Eq. (3.2.32). The only reliable information is about their number N_{AC}. Nonetheless, for our current purpose the precise value of N_{AC} is not important, but rather that $N_{\mathrm{AC}} \lesssim N_{\mathrm{C}} \propto N^2$ (at least for sufficient large N) holds, as two crossings often sandwich an avoided one.

Deriving the criterion for the crossings in appendix B, yields initially more values of $k_{\Sigma,\,\Delta}$ than those actually corresponding to degenerate energy eigenvalues. Among them are half-integer multiples of $\pi/(N+1)$, which do not satisfy the quantization rule in Eq.

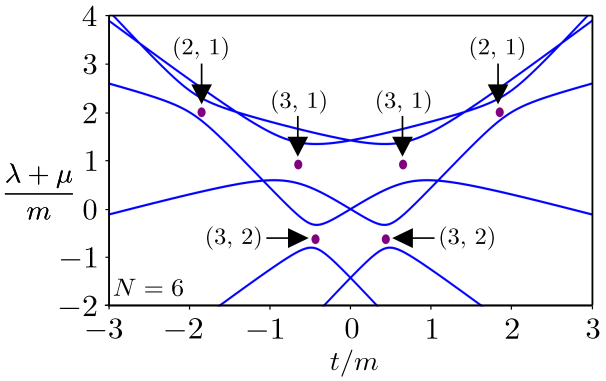

(i,j)	$k_\Sigma d$	$k_\Delta d$	$\frac{t}{m}$	$\frac{\lambda+\mu}{m}$
$(2,1)$	$\frac{5\pi}{16}$	$\frac{3\pi}{16}$	-1.85	2.00
$(3,1)$	$\frac{7\pi}{16}$	$\frac{3\pi}{16}$	-0.65	0.92
$(3,2)$	$\frac{7\pi}{16}$	$\frac{5\pi}{16}$	-0.43	-0.61
$(2,1)$	$\frac{11\pi}{16}$	$\frac{3\pi}{16}$	1.85	2.00
$(3,1)$	$\frac{9\pi}{16}$	$\frac{3\pi}{16}$	0.65	0.92
$(3,2)$	$\frac{9\pi}{16}$	$\frac{5\pi}{16}$	0.43	-0.61

Figure 3.8.: Numerically calculated eigenvalues as function of t/m and the avoided crossings (•) for $N = 6$ in the left panel. Right panel: analytical values for the k_Σ, k_Δ pairs and the corresponding values for t/m, $(\lambda+\mu)/m$ (rounded). Note that the values for λ in the table do not correspond to eigenvalues.

(3.2.32), as one can verify easily[6]. After some simplifications, we found

$$\textbf{(AC)} \quad (k_\Sigma d,\, k_\Delta d) = \left(\pi\frac{i+\frac{1}{2}}{N+2}, \pi\frac{j+\frac{1}{2}}{N+2}\right), \quad i = 2,\ldots,i^{\mathrm{AC}}_{\max},\, j = 1,\ldots,i-1, \tag{3.3.8}$$

with $\pi/2 \geq k_\Sigma d > k_\Delta d > 0$, and

$$\textbf{(AC)} \quad (k_\Sigma d,\, k_\Delta d) = \left(\pi\frac{N-i+\frac{3}{2}}{N+2}, \pi\frac{j+\frac{1}{2}}{N+2}\right), \quad i = 2,\ldots,i^{\mathrm{AC}}_{\max},\, j = 1,\ldots,i-1 \tag{3.3.9}$$

with $\pi > k_\Sigma d > \pi/2 > k_\Delta d > 0$ only for avoided crossings. The upper limit $i^{\mathrm{AC}}_{\max}$ is

$$i^{\mathrm{AC}}_{\max} = \begin{cases} \frac{N}{2}, & N \text{ even} \\ \frac{N+1}{2}, & N \text{ odd} \end{cases}. \tag{3.3.10}$$

The value of $i = i_{\max} = (N+1)/2$ for odd N, leading to $k_\Sigma d = \pi/2$ and formally represented in both sets, occurs in fact only once. This prevents a general distinction of the criterion between even and odd N outside of the definition for $i^{\mathrm{AC}}_{\max}$. Before we continue, notice the apparent similarity of the Eqs. (3.3.8), (3.3.9) with Eqs. (3.3.1), (3.3.2).

[6]Similar half-integer values correspond to avoided crossings for the Kitaev chain as well. However, there one can prove actually that the avoided crossings are former crossings. In this respect, this ansatz is an analogy we have to adapt from the Kitaev chain back to the n.n.n. chain.

The equal energy constraint from Eq. (3.3.4) has to be obeyed and defines, as for the crossings, the ratio for t/m, where we have to expect the avoided crossings. Although not defining eigenvalues, inserting a pair k_Σ, k_Δ with the corresponding value of t/m into the dispersion relation estimates finally the position of an avoided crossing. Moreover, this implies directly that crossings and avoided crossing share the same region in Eq. (3.3.6). As we see in Fig. 3.8, our findings indeed agree with the numerics.

The number of avoided crossings N_{AC} can be determined from the upper criterion and we find

$$N_{\mathrm{AC}} = \begin{cases} \frac{N\,(N-2)}{4}, & N \text{ even}, \\ \frac{(N-1)^2}{4}, & N \text{ odd} \end{cases} . \tag{3.3.11}$$

Thus, N_{AC} scales as N^2, is always smaller than N_{C} and yet comparable to N_{C} for sufficient large N. Further, Eq. (3.3.11) implies that avoided crossings exists for only $N \geq 3$. The precise value of N_{AC} and the lower limit on N are both in exact agreement with the numerics.

3.3.3. Inversion symmetry

The implications of the inversion symmetry I as regards the spectrum of the n.n.n. chain may help in developing a more intuitive understanding of crossing and avoided ones. A representation for I can be found in Eq. (3.2.15), written in the same basis as $\mathcal{H}_{\mathrm{EC}}$ in Eq. (3.2.1). Since $I^2 = \mathbb{1}_N$ holds, the spectrum of I is solely composed of ± 1. The atomic chain studied here is inversion symmetric, i.e. $I\,\mathcal{H}_{\mathrm{EC}}\,I = \mathcal{H}_{\mathrm{EC}}$ is true, and thus the commutator $[I,\, \mathcal{H}_{\mathrm{EC}}] = 0$ vanishes. Therefore, we can diagonalize both I and $\mathcal{H}_{\mathrm{EC}}$ simultaneously and the eigenstates of our system are either even (eigenvalue $+1$) or odd (eigenvalue -1) w.r.t I. In Fig. 3.9 the even (odd) eigenstates of $\mathcal{H}_{\mathrm{EC}}$ are visualized by a red (blue) line colour.

As discussed previously, the spectrum of $\mathcal{H}_{\mathrm{EC}}$ is mostly non-degenerate and there we can have exclusively even or odd eigenstates. The nature of these states is determined by k_1, k_2 (or equivalently k_Σ, k_Δ) as follows from Eq. (3.2.30). There, the coefficients A, B, C and D must be chosen appropriately, following from the boundary condition, and thus depend on k_1, k_2. In turn the values for k_1, k_2 follow from the quantization rule in Eq. (3.2.32), which is the reason to avoid a deeper analytic treatment and to rather focus on a numerical approach. At crossings, the eigenvalue of $\mathcal{H}_{\mathrm{EC}}$ is twice degenerate, i.e we have to find both inversion characters there in agreement with Fig. 3.9. We discover further that the avoided crossings are positioned between eigenstates of the same inversion character. We conclude that inversion symmetry protects the crossings for $t \neq 0$, $m \neq 0$.

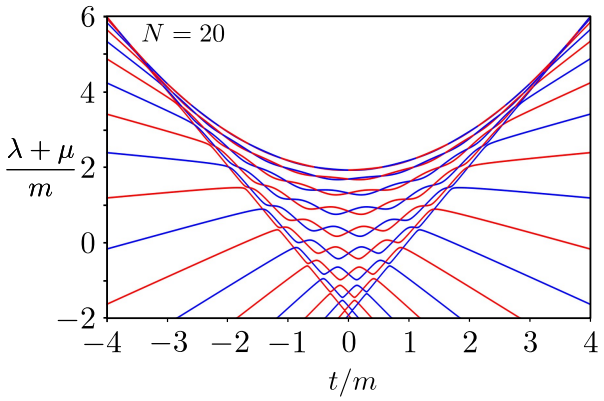

Figure 3.9.: Behavior of the numerically calculated eigenstates under inversion symmetry I for $N = 20$. The eigenstates are either even (red) or odd (blue) w.r.t. I. The crossings arise from states with different inversion character and the avoided crossings from states with the same behaviour.

3.4. Complex momenta

Although the n.n.n. chain is topologically trivial, one can indeed find complex solutions $k_{\Sigma,\Delta}$ of Eq. (3.2.32). This can best be seen from Eq. (3.3.5), which imposes $-2 \leq (\lambda + \mu)/m \leq 4$ for $k_{\Sigma,\Delta} \in \mathbb{R}$ and Fig. 3.2 in comparison. We observe $(\lambda + \mu)/m < -2$ being possible only for $k_{\Sigma,\Delta} \in \mathbb{C}$. Similar, we find $(\lambda + \mu)/m \geq 4$ as depicted in Fig. 3.9. These values indeed satisfy Eq. (3.2.32) and the equal energy constraint from Eq. (3.2.33).

We investigated spectrum numerically. In case of either $(\lambda+\mu)/m < -2$ or $(\lambda+\mu)/m \geq 4$, we found that exclusively k_1 or k_2 is purely imaginary for $(\lambda + \mu)/m \leq -4$, i.e. $k_{\Sigma,\Delta} \in \mathbb{C}$ is confirmed. We found further no decaying states, and instead the respective eigenstates were close to the ones of the linear chain from chapter 2. We can explain this result by returning to the open boundary conditions for $m = 0$ Eq. (3.2.8) and for $m \neq$ in Eq. (3.2.9). In case of $m \neq 0$, one has to obey four boundary conditions and the ansatz from Eq. (3.2.30) is mandatory, independent of the precise value of m. However, for $t/m \gg 1$, we expect that the n.n.n. chain recovers the situation of the linear chain from chapter 2 since the energy scale given by m becomes unimportant. Indeed, we found that the coefficients in Eq. (3.2.30) belonging to the pure imaginary value k_1 or k_2 get seemingly suppressed. Thus, effectively only one momentum in Eq. (3.2.30) contributes and the ansatz for the linear chain is recovered.

3.5. Final remarks

The announced "pure mathematical" study brought us to a deeper yet exact and analytic insight into the spectrum of an atomic chain with nearest and next nearest neighbour hopping defined in Eq. (3.1.1). The rather unorthodox treatment via real space coincides

with the momentum space discussion and we had a perfect agreement of analytical and numerical findings. In other words, we achieved full control over the spectrum of $\mathcal{H}_{\mathrm{EC}}$. However, realistic models obey usually the constraint $|t| > |m|$, which makes the crossings and avoided crossings experimentally at least hard if not impossible to observe.

One could ask why did we study a toy model with probably not measurable features, such as crossings/ avoided crossings, with potentially absent easy special cases, and why did we go through this technical approach? Not to mention the so far- missing link to the Kitaev chain, if there is even one? Indeed everything we did so far was done for one strategic reason; understanding the implication of the recursion formula

$$\xi_{j+2} = \zeta\,\xi_j - \xi_{j-2} + \eta\,(\xi_{j-1} + \xi_{j+1})\,. \tag{3.5.1}$$

In fact, all properties of the Kitaev chain, its spectrum, its eigenstates and even the transport properties, rely on precisely this formula, for the appropriate ζ, η and a specific boundary condition in real space. The atomic chain with n.n.n. hopping was engineered exclusively for the purpose of Eq. (3.5.1); no more no less. From the perspective of the recursion formula, both models are so similar, that without telling the context nor the constants ζ, η, no distinction can be made.

Nonetheless, we need a more general and even deeper mathematical treatment outside of a model's context in order to gain a better understanding, which is the topic of the next section. Surely, the objects defined by Eq. (3.5.1) deserve a special name of their own. They are called Tetranacci polynomials; we explain the reason for the naming later: The readers who are more interested in the physical applications of these polynomials can directly jump to the end of chapter 4 where a summary is provided.

4. The very basics of Fibonacci & Tetranacci polynomials

The results concerning the Tetranacci polynomials inside this chapter have been published only partially and for special cases in [4, 5].

4.1. On Fibonacci polynomials

The previous chapters were inspired to give an introduction into specific polynomial sequences and to show their usefulness in condensed matter physics. Correctly handled, they enable us to find eigenvalues and eigenvectors, yet the treatment sometimes prevents an intuitive physical understanding. Here, we summarize the important technical steps done so far and generalize them. Further, we unite all Fibonacci sequences we had earlier into one object with a single notation.

Definition 4.1.1 (Fibonacci sequence/ polynomial)
The Fibonacci sequence $\{f_j \,|\, j \in \mathbb{Z}\}$ *is the set of all Fibonacci polynomials* f_j *[83, 84] defined by the initial values*[1] f_{-1}, $f_0 \in \mathbb{C}$ *and the recursion formula*

$$f_{j+1} = x\, f_j + y\, f_{j-1}, \tag{4.1.1}$$

with x, $y \in \mathbb{C}$.

Earlier in chapter 2, we discussed the linear chain and its connection to Fibonacci polynomials [78, 83, 84] in Eq. (2.2.2), generated by the recursion formula in Eq. (4.1.1) for $x = \lambda + \mu$, $y = -t^2$ and $f_{-1} = 0$, $f_0 = 1$. We will now determine the closed formula for f_j for the general case in def. 4.1.1. For clarity, we do not consider any concrete or physical situation temporarily and thus x, y are general. The closed form of f_j is already known and given in [85]. Nonetheless, we re-derive the solution using the power law ansatz and the superposition of the solutions, due to the linearity of the recursion formula. The ansatz $f_j \propto R^j \neq 0$ yields

$$R_\pm = \frac{x \pm \sqrt{x^2 + 4y}}{2}. \tag{4.1.2}$$

The cases relevant for us are $x^2 + 4\,y \neq 0$ or $x \neq 0$, i.e. $R_+ \neq \pm R_-$; the coefficients A, B in the ansatz for $f_j = A\, R_+^j + B\, R_-^j$ are determined by f_{-1}, f_0. We find

$$A = R_+ \frac{f_0 - f_{-1}\, R_-}{R_+ - R_-}, \quad B = -R_- \frac{f_0 - f_{-1}\, R_+}{R_+ - R_-}. \tag{4.1.3}$$

[1] I avoided here to introduce new variables as initial values for simplicity.

Since both constants depend on the initial values, we may re-arrange the terms and get

$$f_j \;=\; f_0\,\frac{R_+^{j+1}-R_-^{j+1}}{R_+-R_-} \;-\; f_{-1}\,R_+R_-\frac{R_+^{j}-R_-^{j}}{R_+-R_-}. \tag{4.1.4}$$

Obviously, we generalized the earlier result in Eq. (2.2.6) to which Eq. (4.1.4) reduces back for $f_0 = 1$, $f_{-1} = 0$. We can make the result in Eq. (4.1.4) even more compact, defining

$$\mathcal{F}(j) \coloneqq \frac{R_+^{j}-R_-^{j}}{R_+-R_-}. \tag{4.1.5}$$

Using $R_+\,R_- = -y$ yields

$$f_j \;=\; f_0\,\mathcal{F}(j+1) \;+\; f_{-1}\,y\,\mathcal{F}(j), \qquad j\in\mathbb{Z}. \tag{4.1.6}$$

Of course the prefactor y in the second term is disturbing, but absorbing it into another function is more distracting. Let us focus on $\mathcal{F}(j)$ next. A superposition of $R_\pm$, i.e. $\mathcal{F}(j)$ must be itself a specific solution of Eq. (4.1.1) with the initial values

$$\mathcal{F}(0) \;=\; 0, \tag{4.1.7}$$
$$\mathcal{F}(1) \;=\; 1. \tag{4.1.8}$$

One can verify easily that $\mathcal{F}(j)$ indeed satisfies Eq. (4.1.1), exploiting $R_\pm$ from Eq. (4.1.2) in the form $x = R_+ + R_-$, $y = -R_+R_-$ which yields for all $j\in\mathbb{Z}$

$$\begin{aligned} x\,\mathcal{F}(j) \;+\; y\,\mathcal{F}(j-1) \;&=\; (R_+ + R_-)\,\frac{R_+^{j}-R_-^{j}}{R_+-R_-} \;-\; R_+\,R_-\frac{R_+^{j-1}-R_-^{j-1}}{R_+-R_-} \\ &=\; \frac{R_+^{j+1}-R_-^{j+1}}{R_+-R_-} + \frac{R_-\,R_+^{j}-R_-\,R_+^{j}}{R_+-R_-} \;-\; \frac{R_-\,R_+^{j}-R_-\,R_+^{j}}{R_+-R_-} \\ &\equiv \mathcal{F}(j+1). \end{aligned} \tag{4.1.9}$$

We can understand f_j in Eq. (4.1.6) now as composition of the special solutions $\mathcal{F}(j+1)$, $y\mathcal{F}(j)$; we see next that both of them become 0, 1 on the level of the initial values f_0, f_{-1}, i.e. for $j = -1,\,0$. We observe $y\,\mathcal{F}(-1) = 1$, for example following from Eq. (4.1.5):

$$y\,\mathcal{F}(-1) \;=\; -R_+\,R_-\frac{R_+^{-1}-R_-^{-1}}{R_+-R_-} \;=\; -\frac{R_- - R_+}{R_+-R_-} \;=\; 1. \tag{4.1.10}$$

This ensures f_j to meet its initial values at $j = -1,\,0$:

$$f_j|_{j=-1} \;=\; f_0\,\mathcal{F}(0) \;+\; f_{-1}\,y\,\mathcal{F}(-1) \;\equiv\; f_{-1}, \tag{4.1.11}$$
$$f_j|_{j=0} \;=\; f_0\,\mathcal{F}(1) \;+\; f_{-1}\,y\,\mathcal{F}(0) \;\equiv\; f_0. \tag{4.1.12}$$

We conclude that the prior cases for $f_0 = 1$ and $f_{-1} = 0$ discussed in chapter 2.2, and embodied now by $\mathcal{F}(j)$, were sufficient for the general case. Next, we define[2] $kd \in \mathbb{C}$ via

$$x =: 2\mathrm{i}\sqrt{y}\,\cos(kd) \tag{4.1.13}$$

granting

$$R_\pm = i\sqrt{y}\,e^{\mp \mathrm{i}kd}, \tag{4.1.14}$$

a more suitable form for $R_\pm$. This new form is fully equivalent to the prior one in Eq. (4.1.2) and still obeys $R_+ R_- = -y$ and $R_+ + R_- = 2i\sqrt{y}\cos(kd) \equiv x$. We find now the familiar expression

$$\mathcal{F}(j) \;=\; (\mathrm{i}\sqrt{y})^{j-1}\;\frac{\sin\left(kd\,j\right)}{\sin(kd)} \tag{4.1.15}$$

for $\mathcal{F}(j)$ from Eq. (4.1.5). Finally, f_j in Eq. (4.1.6) becomes

$$f_j = (\mathrm{i}\sqrt{y})^j \left(f_0\,\frac{\sin\left[kd\;(j+1)\right]}{\sin(kd)} \;- \mathrm{i}\sqrt{y}\,f_{-1}\frac{\sin\left(kd\,j\right)}{\sin(kd)}\right), \qquad j \in \mathbb{Z}. \tag{4.1.16}$$

Importantly, Eq. (4.1.16) unites the former distinct cases to obtain the spectrum of the tridiagonal matrices of size N using either the characteristic polynomial $f_{-1} = f_N = 0$, see for example Eqs. (2.2.2), (2.2.8), or the eigenstates $f_0 = f_{N+1} = 0$ in Eq. (3.2.8). Further, the results presented in this chapter do not require a concrete context, i.e. are usable always if Eq. (4.1.1) is given, and various examples were discussed in the sections 2, 3.

A change of the initial values from f_{-1}, f_0 to exemplarily f_0, f_1 does not require another calculation and can be anticipated directly from Eq. (4.1.6). One can define $\bar{f}_j \coloneqq f_{j+1}$ which obeys the recursion relation in Eq. (4.1.1). Thus Eq. (4.1.6) applies for $\bar{f}_j$ instead of f_j, and converting back to f_j grants

$$f_j \;=\; f_1\,\mathcal{F}(j) \;+\; f_0\,y\,\mathcal{F}(j-1). \tag{4.1.17}$$

All manipulations on $\mathcal{F}$, as for example Eq. (4.1.15), are still true and the use of Eq. (4.1.6) or Eq. (4.1.17) is merely a question of convenience.

4.2. An introduction to Tetranacci polynomials

Definition 4.2.1 (Tetranacci polynomial/sequence)
The sequence of the Tetranacci polynomials $\{\xi_j \,|\, j \in \mathbb{Z}\}$ *considered throughout this work is the set of all Tetranacci polynomials* ξ_j *defined by the arbitrary initial values* ξ_{-2}, ξ_{-1}, ξ_0, $\xi_1 \in \mathbb{C}$ *and the recursion formula*

$$\xi_{j+2} \;=\; \zeta\,\xi_j \;-\; \xi_{j-2} \;+\; \eta\,\left(\xi_{j+1} + \xi_{j-1}\right), \tag{4.2.1}$$

with ζ, $\eta \in \mathbb{C}$.

[2]Strictly speaking we have no lattice constant d here, since we operate currently outside of any physical context. Yet, we will use it on the Kitaev chain afterwards and I want to avoid later confusion by calling this object now θ, but later kd. Any change of the lattice as $d \to 2d$ can be absorbed into k and kd is not quantised so far.

An example for a Tetranacci sequence was treated in chapter 3, where the boundary condition demanded $\xi_{-1} = \xi_0 = 0$. The reason for the naming becomes probably clearer if we consider Tribonacci numbers [92, 93] or Tribonacci polynomials [94]; here the next element of the sequence is determined by the last three elements. The difference between the number and the polynomial sequence arises as in the Fibonacci case in the used coefficients and the initial values, without touching further details. Inspecting now Eq. (4.2.1), we see the last four terms define the next one and we thus call ξ_j a *Tetra*nacci polynomial. In the literature one can find publications regarding Tetranacci numbers, for example [92, 95, 96] (to give only a few), but the author of this manuscript is still unaware of probably existent previous works on Tetranacci polynomials, despite multiple attempts to find them. Therefore, we call this sequence simply "Tetranacci polynomials", although this is only a special case with the coefficient in front of ξ_{j-2} being -1 rather than an arbitrary, complex coefficient.

The general closed form for ξ_j can be lengthy (depending on the representation) and is maybe counterintuitive. As a warm up, we consider first the special case of $\eta = 0$.

4.2.1. The special case of $\eta = 0$

The recursion formula in Eq. (4.2.1) for $\eta = 0$ reads

$$\xi_{j+2} = \zeta\,\xi_j - \xi_{j-2}, \qquad j \in \mathbb{Z} \tag{4.2.2}$$

and we still have the initial values[3] ξ_{-2}, ξ_{-1}, ξ_0, ξ_1. As we directly observe from Eq. (4.2.2), the even and odd indices decay into two distinct subsequences. Further, Eq. (4.2.2) looks somehow very familiar; the *last two* even (odd) indexed members of the sequence give the next one. Indeed we face here two Fibonacci sequences, becoming apparent by defining $u_n \coloneqq \xi_{2n+1}$ ($v_n \coloneqq \xi_{2n}$) for all $n \in \mathbb{Z}$,

$$u_{n+1} = \zeta\,u_n - u_{n-1}, \qquad u_{-1} = \xi_{-1},\, u_0 = \xi_1, \tag{4.2.3}$$

$$v_{n+1} = \zeta\,v_n - v_{n-1}, \qquad v_{-1} = \xi_{-2},\, v_0 = \xi_0. \tag{4.2.4}$$

Importantly, the recursion formula for u_n and v_n is the same and differences arise only from the in general distinct initial values. We now can simply use the knowledge gained through the previous chapter and write down the closed form for u_n, v_n for $x \to \zeta$ and $y = -1$. Thus, we find from Eq. (4.1.6)

$$\xi_{2n+1} = u_n = \xi_1\,\mathcal{F}(n+1) - \xi_{-1}\,\mathcal{F}(n), \tag{4.2.5}$$

$$\xi_{2n} = v_n = \xi_0\,\mathcal{F}(n+1) - \xi_{-2}\,\mathcal{F}(n), \tag{4.2.6}$$

for $\zeta \neq -2$ ($x^2 + 4y \neq 0$), $\zeta \neq 0$ ($x \neq 0$). The expression $\mathcal{F}(n) = \sin(kd\,n)/\sin(kd)$ follows again with $x = 2\mathrm{i}\sqrt{y}\cos(kd)$, i.e. $\zeta = -2\cos(kd)$. Here, we used[4] $\mathrm{i} = \sqrt{-1}$ without restrictions; the function $R_\pm$ from Eq. (4.1.2) are

$$R_\pm = \frac{\zeta \pm \sqrt{\zeta^2 - 4}}{2} = -e^{\mp ikd}. \tag{4.2.7}$$

[3] In case of η dependent ξ_{-2}, ξ_{-1}, ξ_0, ξ_1, one has to apply this limit on them as well.

[4] The case of $\sqrt{-1} = -\mathrm{i}$ is equivalent, since we can shift $kd \to kd + \pi$ without any constraint.

We would like to stress that the reader was already confronted with this separation into even/ odd index Fibonacci sequences earlier in chapter 3.2.3. There, we used a basis transformation and avoided this discussion. We had $\eta = -t/m = 0$ ($t = 0$) and $\zeta = -(\lambda + \mu)/m$; the dispersion relation $\lambda = -\mu - 2m\cos(kd)$ follows from $\zeta = -2\cos(kd)$. The boundary condition on the eigenstate $|\psi\rangle$, whose entries were $\xi_1, \ldots, \xi_N$, was $\xi_{-1} = \xi_0 = \xi_{N+1} = \xi_{N+2} = 0$ and the system separated into the parts $\mathcal{H}_{\mathrm{a,\,b}}$ see Eq. (3.2.42). This boundary condition on Eqs. (4.2.5), (4.2.6) yields

$$u_n \;=\; \xi_1\, \mathcal{F}(n+1), \tag{4.2.8}$$

$$v_n \;=\; -\,\xi_{-2}\, \mathcal{F}(n). \tag{4.2.9}$$

Recall that the index j of ξ_j referred to the atomic positions, and the odd (even) sites were placed in $\mathcal{H}_\mathrm{a}$ ($\mathcal{H}_\mathrm{b}$) due to the basis transformation, i.e. the u_n (v_n) form the eigenstates[5] of $\mathcal{H}_\mathrm{a}$ ($\mathcal{H}_\mathrm{b}$). The values of ξ_1, ξ_{-2} for the eigenvector problem can be understood as the normalisation factors. Further, the realisation of the boundary condition on u_n, v_n depends on whether N is even or odd

$$v_{\frac{N+2}{2}} \;=\; \xi_{N+2}, \quad u_{\frac{N}{2}} \;=\; \xi_{N+1} \qquad (N \text{ even}), \tag{4.2.10}$$

$$v_{\frac{N+1}{2}} \;=\; \xi_{N+1}, \quad u_{\frac{N+1}{2}} \;=\; \xi_{N+2} \quad (N \text{ odd}). \tag{4.2.11}$$

In order to obtain the quantization rules for kd, one has to use Eqs. (4.2.8), (4.2.9) together with $\mathcal{F}(n) = \sin(kd\,n)/\sin(kd)$ leading back to the Eqs. (3.2.47)-(3.2.49). We just saw that boundary conditions can be transformed into initial values and that a specific case defines the proper coefficients of the recursion formula(s). We discuss these aspects later in section 4.3.

4.2.2. The closed Form of ξ_j and the Fibonacci decomposition for $\eta \neq 0$

In the later discussion of the finite sized Kitaev chain, we will be confronted with Tetranacci polynomials on several occasions. For instance, we meet them in the characteristic polynomial, the eigenvector entries, or inside the retarded Green's function for the transport properties. In this respect, the main goal here is to derive the closed formula for ξ_j from Eq. (4.2.1) while $\eta \neq 0$. Meanwhile, we guide the reader through some possibly surprising observations. Initially, we give the first few terms for ξ_j to demonstrate the issue of finite η. We find

$$\xi_2 \;=\; -\xi_{-2} \,+\, \eta\,\xi_{-1} \,+\, \zeta\,\xi_0 \,+\, \eta\,\xi_1, \tag{4.2.12}$$

$$\xi_3 \;=\; -\eta\,\xi_{-2} \,+\, \left(\eta^2 - 1\right)\,\xi_{-1} \,+\, \eta\,(\zeta+1)\,\xi_0 \,+\, \left(\eta^2 + \zeta\right)\xi_1, \tag{4.2.13}$$

$$\begin{aligned}\xi_4 \;=\; &-\left(\eta^2 + \zeta\right)\,\xi_{-2} \,+\, \eta\left(\eta^2 + \zeta - 1\right)\xi_{-1} \\ &+\, \left(\zeta^2 + \eta^2\,\zeta + \eta^2 - 1\right)\,\xi_0 \,+\, \eta\,(\eta + 2\zeta + 1)\,\xi_1,\end{aligned} \tag{4.2.14}$$

and the former separated Fibonacci sequences are coupled. Apparently, $\eta \neq 0$ is a qualitative change and we have seemingly no "Fibonacci feature" here anymore. Surprisingly,

[5] Alternatively, one can see this relation in Eqs. (4.2.10), (4.2.11) below from the index of ξ, since $\mathcal{H}_\mathrm{a}$ has one atom more than $\mathcal{H}_\mathrm{b}$ for odd N.

this is wrong; there are specific Fibonacci polynomials which are Tetranacci polynomials simultaneously and do satisfy Eq. (4.2.1), as we show next.

Theorem 4.2.1 (The hidden Fibonacci solutions)

There exists up to two Fibonacci polynomials φ_l $(l = 1, 2)$ *defined by*

$$\varphi_l(j+1) \;=\; S_l\,\varphi_l(j) - \varphi_l(j-1), \quad j \in \mathbb{Z}, \tag{4.2.15}$$

with $2\,S_{1,2} \;=\; \eta \pm \sqrt{\eta^2 + 4\,(\zeta+2)}$ *and arbitrary initial values* $\varphi_{1,2}(0)$, $\varphi_{1,2}(1) \in \mathbb{C}$ *which satisfy the Tetranacci recursion formula in Eq.* (4.2.1). *Later, we choose* $\varphi_{1,2}(0) = 0$, $\varphi_{1,2}(1) = 1$ *for simplicity.*

Proof 4.2.1

First, let me comment on why we find "up to two" solutions; it is a matter of counting. In the case $\eta^2 + 4\,(\zeta+2) = 0$, we will have $S_1 = S_2$ and the recursion formulas for $\varphi_{1,2}$ are the same. Nonetheless, their initial values may differ yielding obviously $\varphi_1(j) \neq \varphi_2(j)$ and otherwise $\varphi_1(j) = \varphi_2(j)$. We may then say that different initial values create still distinct sequences, but Eq. (4.1.6) reduces every Fibonacci polynomial back to two which use the initial values $0, 1$. Hence, "up to two". Second, the "proof" is essentially only a straightforward construction, equivalent for both φ_1, φ_2, and we thus drop the index $l = 1, 2$ without loss of generality. Let us assume that we have an object φ obeying

$$\varphi(j+1) \;=\; x\,\varphi(j) \;+\; y\,\varphi(j-1) \tag{4.2.16}$$

with arbitrary values $\varphi(0)$, $\varphi(1) \in \mathbb{C}$ and some x, $y \in \mathbb{C}$. The idea is to use the ansatz in Eq. (4.2.16) multiple times on Eq. (4.2.1), such that the latter gets reshaped into the structure of the former. This procedure then leads directly to a read out of x and y. Please notice that the structure $j+1$, j, $j-1$ is fundamental for a successful approach.

The first step is to use (4.2.16) to eliminate the $j+2$ and the $j+1$ term in (4.2.1). We find

$$x\,\varphi(j+1) \;+\; y\varphi(j) \;=\; \zeta\,\varphi(j) \;-\; \varphi(j-2) \;+\; \eta\,[x\,\varphi(j) \;+\; y\,\varphi(j-1)] \;+\; \eta\,\varphi(j-1),$$

where the r.h.s depends only on the indices j, $j-1$, $j-2$. The use of Eq. (4.2.16) on $\varphi(j+1)$ another time grants upon reordering

$$\left(x^2 + y - \eta x - \zeta\right)\,\varphi(j) \;=\; (\eta y + \eta - xy)\,\varphi(j-1) \;-\; \varphi(j-2), \tag{4.2.17}$$

the same structure as in our ansatz Eq. (4.2.16). Comparing the coefficients in both expressions yields first $y = -1$. Second, we have to demand that $\eta y + \eta - xy \stackrel{!}{=} x$, but $y = -1$ implies automatically $\eta y + \eta - xy = -\eta + \eta + x = x$ without any constraint on x. The value(s) of x is (are) determined by demanding $x^2 + y - \eta x - \zeta \stackrel{!}{=} 1$, which is equivalent to finding the zero(s) of $x^2 - \eta x - \zeta - 2 \;=\; 0$ due to $y = -1$. Hence we

find $2\,x \;=\; \eta \pm \sqrt{\eta^2 + 4\,(\zeta + 2)} \equiv 2\,S_{1,2} \neq 0$ $(\eta \neq 0)$ and the functions $\varphi(j)$ generated by (4.2.16) satisfy Eq. (4.2.1) as well. Since we have not used any specific initial values $\varphi(0)$, $\varphi(1)$ this technique holds for all of them. Importantly, Eq. (4.2.1) requires four "initial" values for $\varphi(j)$ in order to use this formula. This is not a problem, because the "missing" values for $\varphi(j)$ at $j = -2$ and $j = -1$ can be obtained from our ansatz in Eq. (4.2.16) and $\varphi(0)$, $\varphi(1)$, since x, y are already known. In other words: $\varphi(j)$ is now (uniquely) fixed by $\varphi(0)$, $\varphi(1)$, as it is true for all Fibonacci polynomials, and the definition 4.1.1 demands only to have four initial values. Thus, $\varphi(j)$ is simultaneously a Fibonacci and a Tetranacci polynomial.

Please notice, this implication: These Fibonacci also satisfy the Tetranacci definition but the reverse is not true for a general Tetranacci polynomial, simply due to the arbitrariness of $\xi_{-2}, \ldots, \xi_1$. □

This rather surprising feature in theorem 4.2.1 allows one to describe a general Tetranacci ξ_j from definition 4.2.1 in terms of $\varphi_{1,2}$ later, where the combinations of $\varphi_{1,2}(j)$ with specific, but distinct, initial values $\varphi_{1,2}(0)$, $\varphi_{1,2}(1)$ account for the four[6] initial values for ξ_j. We call this the Fibonacci decomposition of ξ_j. Importantly, if we use Fibonacci sequences of distinct recursion formulas $(S_1 \neq S_2)$ ξ_j is not a Fibonacci, only a Tetranacci polynomial. We return now back to Eqs. (4.2.12)-(4.2.14) to derive the closed form.

Clearly, we see that ξ_2, ξ_3 and ξ_4 are composed of the generic initial values $\xi_{-2}, \ldots, \xi_1$ and ζ, η. The idea to use specific initial values in order to reduce the number of terms in Eqs. (4.2.12)-(4.2.14) might seem tempting, as we never excluded the scenario in which $\xi_{-2}, \ldots, \xi_1$ depend on η and/ or ζ. Then, in a second step one could try to generalize the findings. This is indeed a legitimate strategy, but complicates the matter more than necessary. In fact, ξ_2, ξ_3, ξ_4 in their current status contain the most important information: the separation into initial values each being multiplied by an object arising solely from the recursion formula. We treat the initial values as their own entities, as done similarly for Fibonacci polynomials in Eq. (4.1.6) before. By triviality, this separation of ξ_2, ξ_3, ξ_4 holds particularly for the initial values themselves, since

$$\xi_1 \;=\; 0 \cdot \xi_{-2} \,+\, 0 \cdot \xi_{-1} \,+\, 0 \cdot \xi_0 \,+\, 1 \cdot \xi_1, \tag{4.2.18}$$

is true and analogously for ξ_{-2}, ξ_{-1}, ξ_0. This motivates the ansatz

$$\xi_j \;=\; \mathcal{T}_{-2}(j)\,\xi_{-2} \,+\, \mathcal{T}_{-1}(j)\,\xi_{-1} \,+\, \mathcal{T}_0(j)\,\xi_0 \,+\, \mathcal{T}_1(j)\,\xi_1, \qquad j \in \mathbb{Z} \tag{4.2.19}$$

where $\mathcal{T}_{-2}(j), \ldots, \mathcal{T}_1(j)$ account for the recursion formula and are meant to be independent of $\xi_{-2}, \ldots, \xi_1$. For instance, we have $\mathcal{T}_{-2}(2) \equiv -1$, $\mathcal{T}_{-2}(3) \equiv -\eta$ from Eqs. (4.2.12), (4.2.13) etc.. Importantly, a set of implications are imposed by Eq. (4.2.19) in order to be correct. First of all, we have to ensure that ξ_j adopts its initial values. Therefore, we demand

$$\mathcal{T}_1(j) \;=\; 0, \qquad j = -2, -1, 0, \tag{4.2.20}$$

$$\mathcal{T}_1(1) \;=\; 1, \tag{4.2.21}$$

[6] In a sloppy way: $2 \cdot 2 = 4$.

and similar for $\mathcal{T}_{-2}(j)$, $\mathcal{T}_{-1}(j)$, $\mathcal{T}_0(j)$; thus, we want

$$\mathcal{T}_i(j) \,=\, \delta_{ij}, \qquad \text{for } \underline{\textbf{only}}\ i,j \in \{-2,\,-1,\,0,\,1\}\,, \tag{4.2.22}$$

where δ_{ij} denotes the Kronecker-delta. We call Eq. (4.2.22) the selective property of $\mathcal{T}_i(j)$ (on the level of the initial values) which ensures that ξ_j indeed meets its initial values. Second, since ξ_j has to obey the Tetranacci recursion formula by definition, thus $\mathcal{T}_{-2}(j)$, $\mathcal{T}_{-1}(j)$, $\mathcal{T}_0(j)$ and $\mathcal{T}_1(j)$ do so too. An alternative way to understand this property exploits the initial values; setting temporarily three values for ξ_{-2}, ξ_{-1}, ξ_0, ξ_1 to zero and the remaining value to one, grants $\xi_j \,=\, \mathcal{T}_i(j)$ for $i \,=\, -2,\,1,\,0,\,1$. By definition, Tetranacci polynomials require initial values and the ones for $\mathcal{T}_i(j)$ are given in Eq. (4.2.22). We summarize the findings in the following theorem and prove its validity.

Theorem 4.2.2 (Linear combinations of basic Tetranacci polynomials)
Any Tetranacci polynomial ξ_j from definition 4.2.1 can be expressed as[7]

$$\xi_j \,=\, \sum_{i=-2}^{1} \xi_i\, \mathcal{T}_i(j), \qquad j \in \mathbb{Z}, \tag{4.2.23}$$

in terms of the Tetranacci polynomials $\mathcal{T}_{-2}(j)$, $\mathcal{T}_{-1}(j)$, $\mathcal{T}_0(j)$, $\mathcal{T}_1(j)$ for all $\eta,\,\zeta \in \mathbb{C}$. The latter posses the selective property $\mathcal{T}_i(j) \,=\, \delta_{ij}$ for $i,j \,=\, -2,\,\ldots,\,1$ on the level of the initial values of ξ_j. We call further $\mathcal{T}_{-2}(j)$, $\mathcal{T}_{-1}(j)$, $\mathcal{T}_0(j)$, $\mathcal{T}_1(j)$ the basic Tetranacci polynomials.

Proof 4.2.2

The proof is straightforward by induction over j. Since $j \in \mathbb{Z}$ we have a forward, for positive j, and a backward direction for negative j. The selective property of $\mathcal{T}_i(j)$ shows the correctness of Eq. (4.2.23) for $j \,=\, -2,\,-1,\,0,\,1$ and is the starting point of the proof.

We treat the "forward" case first. Let us assume that Eq. (4.2.23) holds already for fixed integers $j+1$, j, $j-1$, $j-2$ and that the $\mathcal{T}_i(j)$ are Tetranacci polynomials. Then we have to show its correctness for $j+2$. Since ξ_j is stated to be a Tetranacci, from definition 4.2.1 it has four initial values and obeys the Tetranacci recursion formula. The assumptions grant immediately after reordering that

$$\begin{aligned}
\xi_{j+2} \,&=\, \zeta\,\xi_j - \xi_{j-2} \,+\, \eta\,(\xi_{j+1} + \xi_{j-1}) \\
&=\, \sum_{i=-2}^{1} \xi_i\, \{\zeta\,\mathcal{T}_i(j) \,-\, \mathcal{T}_i(j-2) \,+\, \eta\,[\mathcal{T}_i(j+1) \,+\, \mathcal{T}_i(j-1)]\} \\
&\equiv\, \sum_{i=-2}^{1} \xi_i\, \mathcal{T}_i(j+2),
\end{aligned} \tag{4.2.24}$$

[7] A similar approach for 3, 5, 6, ..., n term recursion formulae is possible by adapting the range of i.

where the identification holds due to the Tetranacci character of $\mathcal{T}_i(j)$. This concludes the proof for the forward direction. The backward case can be proven similarly: Exchange the terms ξ_{j+2}, ξ_{j-2} in Eq. (4.2.1), assume Eq. (4.2.23) to hold at the fixed integers $j+2$, $j+1$, j, $j-1$ and look at ξ_{j-2}. The starting point of the induction cycle at $j = -2, -1, 0, 1$ is still correct. Thus, Eq. (4.2.23) is true. □.

In order to find now the closed form for ξ_j with arbitrary ξ_{-2}, ξ_{-1}, ξ_0, ξ_1, we only need to find the closed form for the basic Tetranacci polynomials. We next use the ansatz $\xi_j \propto r^j$ ($r \neq 0$) from chapter 3.2.2 to do so. For shortness, we write ξ_j rather than $\mathcal{T}_i(j)$ since the expressions for the latter follow by imposing the associated initial values. From Eq. (4.2.1) it follows directly

$$r^4 - \zeta r^2 + 1 - \eta (r + r^3) = 0 \tag{4.2.25}$$

with division by r^{j-2}. We define $S \coloneqq (r + r^{-1})$, i.e. $S^2 - 2 = r^2 + r^{-2}$, and a further division by r^2 in Eq. (4.2.25) yields

$$S^2 - \eta S - \zeta - 2 = 0. \tag{4.2.26}$$

Solving the upper equation grants precisely $S_{1,2}$,

$$S_{1,2} = \frac{\eta \pm \sqrt{\eta^2 + 4(\zeta + 2)}}{2}, \tag{4.2.27}$$

found earlier in theorem 4.2.1. The two solutions obey always

$$S_1 + S_2 = \eta, \qquad S_1 S_2 = -\zeta - 2. \tag{4.2.28}$$

The fundamental solutions $r_{\pm 1,2}$ to Eq. (4.2.1) follow then from $r^2 - S_{1,2} r + 1 = 0$ as

$$r_{\pm l} = \frac{S_l \pm \sqrt{S_l^2 - 4}}{2}, \quad l = 1, 2, \tag{4.2.29}$$

with the properties

$$r_{+l} r_{-l} = 1, \qquad r_{+l} + r_{-l} = S_l, \quad l = 1, 2. \tag{4.2.30}$$

The linearity of (4.2.1) allows the construction of any Tetranacci by a proper (linear independent) combination of the fundamental solutions $r_{\pm 1}$, $r_{\pm 2}$, but the used combination depends critically on the relation between η and ζ. We focus here on the most important case of $\eta^2 + 4(\zeta + 2) \neq 0$, $\eta \neq 0$, while the situation for degenerate roots, i.e. $\eta^2 + 4(\zeta + 2) = 0$, is given in appendix D. The former case allows a decomposition of Tetranacci polynomials into the Fibonacci polynomials $\varphi_{1,2}$.

4.2.2.1. The Fibonacci decomposition ($\eta^2 + 4\,(\zeta + 2) \neq 0$, $\eta \neq 0$)

The relation between ζ, η implies $S_1 \neq \pm S_2$ and thus $r_{\pm 1}$ is not related to $r_{\pm 2}$. Hence, the ansatz for ξ_j is simply

$$\xi_j \;=\; A\, r_{+1}^j \;+\; B\, r_{-1}^j \;+\; C\, r_{+2}^j \;+\; D\, r_{-2}^j \tag{4.2.31}$$

and the coefficients A, B, C, $D \in \mathbb{C}$ are fixed by the initial values ξ_{-2}, ξ_{-1}, ξ_0 and ξ_1. We find the unique solution from

$$\begin{pmatrix} A \\ B \\ C \\ D \end{pmatrix} \;=\; \begin{bmatrix} \frac{1}{r_{+1}^2} & r_{+1}^2 & \frac{1}{r_{+2}^2} & r_{+2}^2 \\ \frac{1}{r_{+1}} & r_{+1} & \frac{1}{r_{+2}} & r_{+2} \\ 1 & 1 & 1 & 1 \\ r_{+1} & \frac{1}{r_{+1}} & r_{+2} & \frac{1}{r_{+2}} \end{bmatrix}^{-1} \begin{pmatrix} \xi_{-2} \\ \xi_{-1} \\ \xi_0 \\ \xi_1 \end{pmatrix}, \tag{4.2.32}$$

and a replacement of $\xi_{-2}, \ldots, \xi_1$ by the initial values of $\mathcal{T}_i(j)$ yields the coefficients for $\mathcal{T}_i(j)$ respectively. Our strategy "banishes the entire evilness" of Tetranacci polynomials into the $\mathcal{T}_i(j)$'s. Their expression is initially unhandy. The formulas however can be rapidly shortened with the help of two distinct and specific Fibonacci/ Tetranacci polynomials $\varphi_{1,2}$ from theorem 4.2.1 with $\varphi_l(0) = 0$, $\varphi_l(1) = 1$, since $\eta^2 + 4\,(\zeta + 2) \neq 0$ is true. We define $\varphi_{1,2}$ explicitly as

$$\varphi_l(j) \;\coloneqq\; \frac{r_{+l}^j - r_{-l}^j}{r_{+l} - r_{-l}}, \qquad l = 1, 2, \tag{4.2.33}$$

being obviously a Tetranacci polynomial as linear combination of r_{+l}, r_{-l} w.r.t Eq. (4.2.1) and still imitating the closed form of a Fibonacci polynomial, see Eq. (4.1.5) for example. Note that $\varphi_{1,2}(j)$ adopt similar roles as $\mathcal{F}(j)$ did in chapter 4.1. Now we have to check whether $\varphi_l(j)$ from Eq. (4.2.33) indeed satisfies Eq. (4.2.15), i.e. if

$$\varphi_l(j+1) \;=\; S_l\, \varphi_l(j) \;-\; \varphi_l(j-1), \tag{4.2.34}$$

holds true. Recall the properties of $r_{\pm l}$ in Eq. (4.2.30), namely $r_{+l}\, r_{-l} \;=\; 1$, $r_{+l} + r_{-l} \;=\; S_l$ for $l = 1$, 2 and we find

$$\begin{aligned} S_l\, \varphi_l(j) \;-\; \varphi_l(j-1) \;&=\; (r_{+l} \;+\; r_{-l})\, \frac{r_{+l}^j - r_{-l}^j}{r_{+l} - r_{-l}} \;-\; \frac{r_{+l}^{j-1} - r_{-l}^{j-1}}{r_{+l} - r_{-l}} \\ &=\; \frac{r_{+l}^{j+1} - r_{-l}^{j+1}}{r_{+l} - r_{-l}} + \frac{r_{+l}^{j-1} - r_{-l}^{j-1}}{r_{+l} - r_{-l}} - \frac{r_{+l}^{j-1} - r_{-l}^{j-1}}{r_{+l} - r_{-l}} \\ &\equiv \varphi_l(j+1) \end{aligned} \tag{4.2.35}$$

for all $j \in \mathbb{Z}$. Thus, $\varphi_{1,2}$ are indeed simultaneously Fibonacci and Tetranacci polynomials. We soon need the explicit values of $\varphi_l(j)$ for some j, and $l = 1$, 2 in order to verify

the closed formula for $\mathcal{T}_i(j)$. The use of Eq. (4.2.34) and $\varphi_l(0) = 0$, $\varphi_1(1) = 1$ yields quickly ($l = 1, 2$)

$$\varphi_l(2) \;=\; S_l\,\varphi_l(1) - \varphi_l(0) \;=\; S_l, \tag{4.2.36}$$

$$\varphi_l(3) \;=\; S_l\,\varphi_l(2) - \varphi_l(1) \;=\; S_l^2 - 1, \tag{4.2.37}$$

and solving Eq. (4.2.34) backwards for $\varphi_l(j-1)$ yields

$$\varphi_l(-1) \;=\; S_l\,\varphi_l(0) - \varphi_l(1) \;=\; -1, \tag{4.2.38}$$

$$\varphi_l(-2) \;=\; S_l\,\varphi_l(-1) - \varphi_l(0) \;=\; -S_l, \tag{4.2.39}$$

$$\varphi_l(-3) \;=\; S_l\,\varphi_l(-2) - \varphi_l(-1) \;=\; -\left(S_l^2 - 1\right). \tag{4.2.40}$$

Apparently, we have $\varphi_l(j) = -\varphi_l(-j)$ for $j = 2, 3$. This is also true for all $j \in \mathbb{Z}$, as we observe from Eq. (4.2.33) by exploiting the properties of $r_{\pm l}$

$$\varphi_l(-j) \;=\; \frac{r_{+l}^{-j} - r_{-l}^{-j}}{r_{+l} - r_{-l}} \;=\; \frac{r_{+l}^{-j} - r_{-l}^{-j}}{r_{+l} - r_{-l}}\,(\underbrace{r_{+l}\,r_{-l}}_{=1})^j \;=\; \frac{r_{-l}^{j} - r_{+l}^{j}}{r_{+l} - r_{-l}} \equiv -\varphi_l(j). \tag{4.2.41}$$

The closed form expressions for $\mathcal{T}_{-2}(j), \ldots, \mathcal{T}_1(j)$ can be written in combinations of $\varphi_{1,2}(j)$ and we use a specific notation where $\bar{l}$ denotes "not l": For $l = 1$ ($l = 2$) we have $\bar{l} = 2$ ($\bar{l} = 1$). One finds

$$\mathcal{T}_{-2}(j) \;=\; \frac{\varphi_2(j) - \varphi_1(j)}{S_1 - S_2}, \tag{4.2.42}$$

$$\mathcal{T}_{-1}(j) \;=\; \sum_{l=1,2} \frac{\varphi_l(j+2) \;+\; \varphi_l(j)\,\varphi_{\bar{l}}(-3) \;+\; \varphi_l(j-1)\,\varphi_{\bar{l}}(2)}{(S_1 - S_2)^2}, \tag{4.2.43}$$

$$\mathcal{T}_{0}(j) \;=\; \sum_{l=1,2} \frac{\varphi_l(j+2)\,\varphi_{\bar{l}}(-2) \;+\; \varphi_l(j+1)\,\varphi_{\bar{l}}(3) \;-\; \varphi_l(j-1)}{(S_1 - S_2)^2}, \tag{4.2.44}$$

and finally

$$\mathcal{T}_{1}(j) \;=\; \sum_{l=1,2} \frac{\varphi_l(j+2) \;+\; \varphi_l(j+1)\,\varphi_{\bar{l}}(-2) \;+\; \varphi_l(j)}{(S_1 - S_2)^2}. \tag{4.2.45}$$

First of all, let us discuss the r.h. sides in Eqs. (4.2.42) - (4.2.45). We have to question whether they are or are not Tetranacci polynomials. On the first view, we see products like $\varphi_l(j+1)\,\varphi_{\bar{l}}(-2)$ in $\mathcal{T}_1(j)$ being non-linear. Inspecting their nature closer, we find always just a single j dependent term and terms like $\varphi_{\bar{l}}(-2)$ are in fact a constant prefactor. Hence, we have linear combinations of $\varphi_l(j+2)$, $\varphi_l(j+1)$, $\varphi_l(j)$, $\varphi_l(j-1)$ and the r.h.s in Eqs. (4.2.42) - (4.2.45) are thus Tetranacci polynomials. Further, the use of φ_1 and φ_2 prohibits $\mathcal{T}_{-2}(j), \ldots, \mathcal{T}_1(j)$ to be Fibonacci polynomials as in Eq. (4.2.34), since $\eta^2 + 4\,(\zeta + 2) \neq 0$ excludes $S_1 = S_2$.

Second, the selective property in Eq. (4.2.22) is easily verified, done exemplarily for $\mathcal{T}_{-2}(j)$ and $\mathcal{T}_{-1}(j)$ next. The upper Eqs. (4.2.36)-(4.2.40) together with the initial values $\varphi_l(0) = 0$, $\varphi_l(1) = 1$ for $l = 1, 2$ yield

$$\mathcal{T}_{-2}(-2) = \frac{\varphi_2(-2) - \varphi_1(-2)}{S_1 - S_2} = \frac{-S_2 + S_1}{S_1 - S_2} = 1, \tag{4.2.46}$$

$$\mathcal{T}_{-2}(-1) = \frac{\varphi_2(-1) - \varphi_1(-1)}{S_1 - S_2} = \frac{-1 + 1}{S_1 - S_2} = 0, \tag{4.2.47}$$

$$\mathcal{T}_{-2}(0) = \frac{\varphi_2(0) - \varphi_1(0)}{S_1 - S_2} = \frac{0 - 0}{S_1 - S_2} = 0, \tag{4.2.48}$$

$$\mathcal{T}_{-2}(1) = \frac{\varphi_2(1) - \varphi_1(1)}{S_1 - S_2} = \frac{1 - 1}{S_1 - S_2} = 0, \tag{4.2.49}$$

as expected. Similarly, we have

$$\mathcal{T}_{-1}(-2) = \sum_{l=1,2} \frac{\varphi_l(0) + \varphi_l(-2)\,\varphi_{\bar{l}}(-3) + \varphi_l(-3)\,\varphi_{\bar{l}}(2)}{(S_1 - S_2)^2} \overset{\text{Eq. (4.2.41)}}{=} 0, \tag{4.2.50}$$

$$\begin{aligned} \mathcal{T}_{-1}(-1) &= \sum_{l=1,2} \frac{\varphi_l(1) + \varphi_l(-1)\,\varphi_{\bar{l}}(-3) + \varphi_l(-2)\,\varphi_{\bar{l}}(2)}{(S_1 - S_2)^2} \\ &= \sum_{l=1,2} \frac{1 + S_{\bar{l}}^2 - 1 - S_l\,S_{\bar{l}}}{(S_1 - S_2)^2} \\ &= \frac{S_1^2 - 2\,S_1\,S_2 + S_2^2}{(S_1 - S_2)^2} = 1, \end{aligned} \tag{4.2.51}$$

$$\begin{aligned} \mathcal{T}_{-1}(0) &= \sum_{l=1,2} \frac{\varphi_l(2) + \varphi_l(0)\,\varphi_{\bar{l}}(-3) + \varphi_l(-1)\,\varphi_{\bar{l}}(2)}{(S_1 - S_2)^2} \\ &= \sum_{l=1,2} \frac{\varphi_l(2) - \varphi_{\bar{l}}(2)}{(S_1 - S_2)^2} = 0, \end{aligned} \tag{4.2.52}$$

and last but not least

$$\begin{aligned} \mathcal{T}_{-1}(1) &= \sum_{l=1,2} \frac{\varphi_l(3) + \varphi_l(1)\,\varphi_{\bar{l}}(-3) + \varphi_l(0)\,\varphi_{\bar{l}}(2)}{(S_1 - S_2)^2} \\ &= \sum_{l=1,2} \frac{\varphi_l(3) - \varphi_{\bar{l}}(3)}{(S_1 - S_2)^2} = 0, \end{aligned} \tag{4.2.53}$$

as demanded from Eq. (4.2.22). Analogously, one can verify the selective property for $\mathcal{T}_0(j)$, $\mathcal{T}_1(j)$ and $j = -2, \ldots, 1$. Obviously, Tetranacci polynomials are uniquely identified by their initial values, if η, ζ are kept fixed, as we see from Eq. (4.2.1) or Eq. (4.2.32). Thus, we found in Eqs. (4.2.42)-(4.2.45) the closed form expressions for $\mathcal{T}_{-2}(j)$,

$\mathcal{T}_{-1}(j)$, $\mathcal{T}_0(j)$ and $\mathcal{T}_1(j)$. Together with the explicit from of ξ_j, given by Eq. (4.2.23) in theorem 4.2.2 this is a major result of this work. An even more compact and symmetric form of the Tetranacci polynomials found at the end of writing this thesis, can be found in appendix C.

The last paragraph of this chapter addresses the limiting case $\eta \to 0$ as last verification.

4.2.2.2. The limit $\eta = 0$ ($\eta^2 + 4\,(\zeta + 2) \neq 0$)

The basic Tetranacci polynomials are well behaving functions in ζ, η; for real ζ, η even smooth in $\mathbb{R}$,[8] as one can prove directly from Eq. (4.2.1) via induction over j. We demonstrate this behaviour by considering the case of $\eta = 0$ on $\mathcal{T}_{-2}(j)$, $\mathcal{T}_{-1}(j)$, $\mathcal{T}_0(j)$, $\mathcal{T}_1(j)$ which grants in turn $\xi_j|_{\eta=0}$ and we compare it to our prior solutions in Eqs. (4.2.5), (4.2.6). First, we find $S_1|_{\eta=0} = -S_2|_{\eta=0}$ from Eq. (4.2.27) implying $r_{\pm1}|_{\eta=0} = -r_{\mp2}|_{\eta=0}$ in Eq. (4.2.29). The former clear distinction between the solutions $\varphi_{1,2}$ nearly vanishes

$$\varphi_1|_{\eta=0}\,(j) \;=\; (-1)^{j-1}\;\varphi_2|_{\eta=0}\,(j), \tag{4.2.54}$$

for all $j \in \mathbb{Z}$. The last equation is invariant under exchanging $\varphi_{1,2}$ and we can write in general

$$\varphi_l|_{\eta=0}\,(j) \;=\; (-1)^{j-1}\;\varphi_{\bar{l}}|_{\eta=0}\,(j), \tag{4.2.55}$$

for l, $\bar{l} = 1, 2$. We apply now Eq. (4.2.55) first on $\mathcal{T}_{-2}(j)$ in Eq. (4.2.42) and observe that

$$\mathcal{T}_{-2}(j)|_{\eta=0} \;=\; \left[\frac{\varphi_2(j) - \varphi_1(j)}{S_1 - S_2}\right]_{\eta=0} \;=\; -\left[1 + (-1)^j\right]\;\left.\frac{\varphi_1(j)}{2\,S_1}\right|_{\eta=0}, \tag{4.2.56}$$

where $r_{\pm1}$ inside $\varphi_1(j)$ has still to be evaluated at $\eta = 0$. Apparently, we have a separation into even and odd j

$$\mathcal{T}_{-2}(j)|_{\eta=0} \;=\; \begin{cases} -\left.\frac{\varphi_1(j)}{S_1}\right|_{\eta=0}, & j \text{ even} \\ 0, & j \text{ odd} \end{cases} \tag{4.2.57}$$

[8] This is not true for an arbitrary Tetranacci ξ_j, due to possible initial values like $\xi_{-2} = 1/(\zeta\eta)$. Further, the statement in the text is independent of the relation between η and ζ.

reproducing our earlier finding in the $\eta = 0$ case. Similarly, we obtain for $\mathcal{T}_{-1}(j)$ from Eq. (4.2.43)

$$\begin{aligned}
\mathcal{T}_{-1}(j)|_{\eta=0} &= \left[\sum_{l=1,2} \frac{\varphi_l(j+2) \,+\, \varphi_l(j)\,\varphi_{\bar{l}}(-3) \,+\, \varphi_l(j-1)\,\varphi_{\bar{l}}(2)}{(S_1 - S_2)^2}\right]_{\eta=0} \\
&= \left.\frac{\varphi_1(j+2)\,\left[1+(-1)^{j+1}\right] \,+\, \varphi_1(j)\varphi_2(-3)\,\left[1+(-1)^{j-1-3-1}\right]}{4\,S_1^2}\right|_{\eta=0} \\
&\quad + \left.\frac{\varphi_1(j-1)\varphi_2(2)\,\left[1+(-1)^{j-2+2-1}\right]}{4\,S_1^2}\right|_{\eta=0} \\
&= \left[1+(-1)^{j-1}\right]\,\left.\frac{\varphi_1(j+2) \,-\, \varphi_1(j)\,\varphi_1(3) \,-\, \varphi_1(j-1)\,\varphi_1(2)}{4\,S_1^2}\right|_{\eta=0}, \quad (4.2.58)
\end{aligned}$$

where we used Eq. (4.2.55) multiple times and twice Eq. (4.2.41) in the last step. The last equation is a typical example for expressions we obtain for $\mathcal{T}_i(j)$ ($i = -1,\, 0,\, 1$) at $\eta = 0$, and there are several options to simplify it. We use Eq. (4.2.34) to replace $\varphi_1(j+2)$, $\varphi_1(j+1)$ and the values of $\varphi_1(2)$ and $\varphi_1(3)$ from Eqs. (4.2.36), (4.2.37) to continue. We find

$$\mathcal{T}_{-1}(j)|_{\eta=0} \,=\, -\left[1+(-1)^{j-1}\right]\,\frac{\varphi_1(j-1)}{2\,S_1} \,=\, \begin{cases} 0, & j \text{ even} \\ -\left.\frac{\varphi_1(j-1)}{S_1}\right|_{\eta=0}, & j \text{ odd} \end{cases}. \quad (4.2.59)$$

Analogously, one obtains

$$\mathcal{T}_0(j)|_{\eta=0} \,=\, \left[1+(-1)^{j}\right]\,\frac{\varphi_1(j+2)}{2\,S_1} \,=\, \begin{cases} \left.\frac{\varphi_1(j+2)}{S_1}\right|_{\eta=0}, & j \text{ even} \\ 0, & j \text{ odd} \end{cases} \quad (4.2.60)$$

and

$$\mathcal{T}_1(j)|_{\eta=0} \,=\, \left[1+(-1)^{j-1}\right]\,\frac{\varphi_1(j+1)}{2\,S_1} \,=\, \begin{cases} 0, & j \text{ even} \\ \left.\frac{\varphi_1(j+1)}{S_1}\right|_{\eta=0}, & j \text{ odd} \end{cases}. \quad (4.2.61)$$

As an intermediate result, now Eq. (4.2.23) reduces to

$$\xi_j|_{\eta=0} \,=\, \begin{cases} [\xi_{-1}\,\mathcal{T}_{-1}(j) \,+\, \xi_1\,\mathcal{T}_1(j)]_{\eta=0} & j \text{ odd} \\ [\xi_{-2}\,\mathcal{T}_{-2}(j) \,+\, \xi_0\,\mathcal{T}_0(j)]_{\eta=0} & j \text{ even} \end{cases} \quad (4.2.62)$$

adopting already the proper structure of Eqs. (4.2.5), (4.2.6). In order to do the final step, we have to return to Eqs. (4.2.27), (4.2.29) at $\eta = 0$. The former reveals $S_1|_{\eta=0} = \sqrt{\zeta+2}$ and the latter offers

$$r_{\pm 1}^2\big|_{\eta=0} \,=\, \frac{\zeta \pm \sqrt{\zeta^2-4}}{2} \,\equiv\, R_\pm \quad (4.2.63)$$

according to Eq. (4.2.7). We can relate now $\varphi_1(j)$ ($\varphi_2(j)$) to $\mathcal{F}(j)$. For even j we simply set $j = 2n$ ($n \in \mathbb{Z}$) and inspecting the expressions like $\varphi_1(j)/S_1$ in $T_{-2}(j)$ at both $\eta = 0$ closer, reveals

$$\begin{aligned}\left.\frac{\varphi_1(j)}{S_1}\right|_{\eta=0} &= \left\{\frac{r_{+1}^j - r_{-1}^j}{r_+ - r_-}\,\frac{1}{r_+ + r_-}\right\}_{\eta=0} \\ &= \left\{\frac{r_{+1}^{2n} - r_{-1}^{2n}}{r_+^2 - r_-^2}\right\}_{\eta=0} \\ &= \frac{R_+^n - R_-^n}{R_+ - R_-} \equiv \mathcal{F}(n), \end{aligned} \tag{4.2.64}$$

where we used $S_1 = r_{+1} + r_{-1}$ in the first and Eq. (4.1.5) in the last step. Importantly, for odd j, where we can set $j = 2n + 1$ ($n \in \mathbb{Z}$), the expressions for $\mathcal{T}_{\pm 1}(j)|_{\eta=0}$ depend on $\varphi_1(j \pm 1)|_{\eta=0}$; thus we can use Eq. (4.2.64) for them as well. The proper application of Eq. (4.2.64) in Eq. (4.2.62) gives ($n \in \mathbb{Z}$)

$$\xi_j|_{\eta=0}^{j=2n+1} = \xi_1\,\mathcal{F}(n+1) - \xi_{-1}\,\mathcal{F}(n), \tag{4.2.65}$$

$$\xi_j|_{\eta=0}^{j=2n} = \xi_0\,\mathcal{F}(n+1) - \xi_{-2}\,\mathcal{F}(n). \tag{4.2.66}$$

for η independent initial values and agrees indeed with our prior findings in Eqs. (4.2.5), (4.2.6).

4.3. General remarks and the application to physical systems

The purpose of this section is to relate our mathematical object, the Tetranacci sequence, back to physics. We will see its appearance in the Kitaev chain later. Further, even within the same model, Tetranacci polynomials can emerge multiple times for different tasks. For example the characteristic polynomial, the eigenstates and the Green's function (all in real space) of the Kitaev chain can be written naturally in terms of Tetranacci polynmials In the following, we work out the details for the eigenstate problem. The equations themselves are universal and apply always.

In the beginning we have a given Hamiltonian $\hat{H}$ describing a certain discrete and/or finite sized model containing the necessary parameters, interactions etc. The class of systems we consider here is given in terms of field operators. Independent of whether the latter are bosonic, fermionic or Majorana like fields, we can construct a Hamiltonian density which adopts a matrix form. We want to solve the corresponding eigenvalue/eigenvector problem. Some entries of our model obey the Tetranacci recursion formula Eq. (4.2.1) in position space. Thus, the quantities ζ and η contain the parameters of our system; its symmetries may -or may not- be directly visible in ζ, η. That said, all the quantities $r_{\pm l}$, S_l for $l = 1, 2$ are defined for our model and have a certain value. As done already in chapter 3, we can always define the quantities $k_{1,2}d \in \mathbb{C}$ by

$$S_l =: 2\cos(k_l d), \quad l = 1, 2, \tag{4.3.1}$$

and, since $S_1 + S_2 = \eta$ holds, we have the relation

$$\cos(k_1 d) + \cos(k_2 d) = \frac{\eta}{2} \tag{4.3.2}$$

between $k_1 d$ and $k_2 d$. So far, we should understand $k_l d$ as a complex object which depends on ζ, $\eta \in \mathbb{C}$, since $S_{1,2}$ as solutions of Eq. (4.2.26) grants

$$\zeta = S_{1,2}^2 - \eta\, S_{1,2} - 2 = 4\cos^2(k_{1,2} d) - 2\eta\cos(k_{1,2} d) - 2. \tag{4.3.3}$$

Generally, only a complex $k_{1,2} d$ can satisfy the last expression seen at best in case of $\zeta \gg \eta$. Further, $k_{1,2} d$ does not adopt discrete values for now, since $S_{1,2}$, ζ and/ or η do not. The fundamental solutions $r_{\pm l}$ from Eq. (4.2.29) become simply

$$r_{\pm l} = e^{\pm \mathrm{i}\, k_l d}, \quad l = 1,\, 2. \tag{4.3.4}$$

Apart from being convenient to have a description of $r_{\pm l}$ as in Eq. (4.3.4), we notice that the situation of the physical problem in the Eqs. (4.3.1)-(4.3.3) is turned upside down: If we knew $k_{1,2} d$ we could obtain the quantities ζ, η, $S_{1,2}$ and $r_{\pm 1,2}$. So far, all the manipulations above are universal and not specific for eigenvalue/ eigenvector problems. Nonetheless, the latter have the unique feature that in the models we consider here, the probably unknown eigenvalue λ will enter exclusively into $\zeta \equiv \zeta(\lambda)$.

This may not sound impressive, but it is. We translate the unknown eigenvalue via Eq. (4.3.3) into $k_{1,2} d$, and since η is fixed by the model, Eq. (4.3.2) relates k_1 and k_2. Thus, we trade one unknown, namely λ, for another say $k_1 d$. This seemingly unremarkable deal bypasses effectively the recursion cycle in Eq. (4.2.1) as we explain next.

Suppose we expressed our model Hamiltonian already in terms of a matrix. The spectrum can be determined then either by calculating the associated characteristic polynomial P_λ or directly from the eigenvector problem as we did in section 3. Either way, the generic system size enters in the latter via the open boundary conditions. Imagine that P_λ or the eigenvector entries are related to Tetranacci polynomials; then, we need ultimately Tetranacci polynomials whose index correlates with the system's size. Clearly, the recursive approach Eq. (4.2.1) is for analytical treatments not a suitable method. Instead, we use for instance Eq. (4.2.31) together with Eq. (4.3.4) granting

$$\xi_j = A\, e^{\mathrm{i} k_1 d\, j} + B\, e^{-\mathrm{i} k_1 d\, j} + C\, e^{\mathrm{i} k_2 d\, j} + D\, e^{-\mathrm{i} k_2 d\, j}, \tag{4.3.5}$$

where the recursion is satisfied by construction of $r_{\pm l}$. Here, we can directly insert the boundary condition or required index and one is left to find the constants A, B, C and D. Specifically for the eigenvector equation and the open boundary condition, the knowledge of the four coefficients is only necessary in case one is interested in the eigenvector: The eigenvalues can be obtained via a quantization rule imposed by the open boundary condition which do not demand to know the coefficients. In this scope, we avoid the explicit recursion cycle and we find the values for $k_{1,2}$. In turn, the explicit values for $r_{\pm l}$ and S_l are known and one is left to read out the eigenvalues. Indeed, Eq. (4.3.3) is the dispersion relation for the models considered in this work (in a very unfamiliar form), as the eigenvalues enter only in $\zeta \equiv \zeta(\lambda)$. The extreme is Eq. (4.3.1),

which is actually the shortest form of the bulk dispersion relation. Moreover, Eq. (4.3.2) is the equal energy constraint on $k_{1,2}$ such that $\lambda(k_1) = \lambda(k_2)$.

Depending on the character of the problem, Eq. (4.3.5) may not be the best choice to determine ξ_j. As we have shown, the use of the basic Tetranacci polynomials representation, that is

$$\xi_j \;=\; \sum_{i=-2}^{1} \xi_i \, \mathcal{T}_i(j), \qquad j \in \mathbb{Z}, \tag{4.3.6}$$

and Eq. (4.3.6) is absolutely equivalent to Eq. (4.3.5) supposed that the coefficients A, B, C, D are converted properly. Further, Eq. (4.3.6) is universal for Tetranacci polynomials and applies always, though it may not be advantageous in specific situations.

The basic Tetranacci polynomials are written in terms of $\varphi_{1,2}(j)$ defined in Eq. (4.2.33). Importantly for the physical intuition, $\varphi_{1,2}(j)$ are reshaped into the form of standing waves

$$\varphi_l(j) \;=\; \frac{\sin\left(k_l d\, j\right)}{\sin\left(k_l d\right)}, \quad l = 1,\, 2 \tag{4.3.7}$$

by applying Eq. (4.3.4). In turn, we can understand $T_i(j)$ $(i = -2, -1, 0, 1)$ following Eqs. (4.2.42)-(4.2.45) as specific superposition. This is independent of whether $k_{1,2}$ are quantized and again a universal feature. The next time we are confronted with the recursion formula from Eq. (4.2.1), we have already the solution independent of the context. Finally, the basic Tetranacci polynomials $\mathcal{T}_i(j)$ $(\varphi_{1,2}(j))$ are real in case ζ, η $(S_{1,2})$ are also real.

Part II.

Spectral and transport properties of the finite Kitaev chain

5. The Kitaev chain

5.1. Topological phase diagram and k-space representation

In his original work [2] in 2001, Alexei Kitaev investigated the possibility for fault tolerant quantum computation based on isolated Majorana fermions. He concluded that these Majorana fermions are "immune to any kind of error" and thus predestined as qubits for quantum computers. But Majorana fermions are quasiparticle states, and thus not a fundamental element in solid state physics. Majorana bound states exist in so called topological superconductors as Bogoliubov quasiparticles [7, 19, 20, 23]. Specific devices with the ability to host Majorana fermions have thus to be engineered [66], for example based on nanowires [10, 67] or carbon nanotubes [30, 32, 68]. In these setups, intrinsic spin-orbit coupling and an external magnetic field create effective p-wave superconductivity based on ordinary s-wave pairing. The effort realizes the archetypal model of 1d topological superconductors: the Kitaev chain.

The Kitaev chain is a toy model based on a chain of N atoms, each with only one orbital degree of freedom; in principle up to two electrons can occupy a single orbital, but nonetheless *spinless* fermions are considered [2, 7, 19, 21, 66]. Alternatively, one can think of a spin polarized system, say only spin up, where the electron's spin is "frozen out" by a magnetic field. The Kitaev mean field Hamiltonian reads

$$\hat{H}_{\mathrm{KC}} \,=\, -\mu \sum_{j=1}^{N} \left(d_j^\dagger d_j \,-\, \frac{1}{2} \right) \,+\, \sum_{j=1}^{N-1} \left(\Delta\, d_{j+1}^\dagger d_j^\dagger \,-\, t\, d_{j+1}^\dagger d_j \,+\, \mathrm{h.c.} \right), \tag{5.1.1}$$

in terms of standard fermionic operators d_j, $d_j^\dagger$, where t is the nearest neighbor hopping constant, Δ the short range p-wave superconducting pairing constant, and μ accounts for the chemical potential. The unusual p-wave superconductivity, contrary to the common s-wave type, pairs electrons of the same spin, where the dominant contribution appears only between nearest neighbors. As we shall see, the Hamiltonian in Eq. (5.1.1) is the archetype of a one-dimensional topological superconductor. We consider t, $\Delta \in \mathbb{R}$ without restrictions.

In section 5.2, we analyze the symmetries of the Kitaev chain in k-space in more detail. We find the particle-hole symmetry $\mathcal{P}$, the chiral symmetry $\mathcal{C}$, the (pseudo) time reversal symmetry $\mathcal{T}$ and the inversion symmetry $\hat{I}$. Here, in real space the action of $\hat{I}$ is seen at best. The mapping $d_j^{(\dagger)} \to d_{N+1-j}^{(\dagger)}$ for $j = 1, \ldots, N$ on Eq. (5.1.1) yields

$$\hat{I}\, \hat{H}_{\mathrm{KC}} \hat{I}^{-1} \,=\, \hat{H}_{\mathrm{KC}}\Big|_{-\Delta}, \tag{5.1.2}$$

where the sign change of Δ arises from the now opposite binding direction reflecting the p-wave superconductivity.

Considering now periodic boundary conditions on the Hamiltonian in Eq. (5.1.1), which grants also discrete translational invariance, allows a Fourier analysis with $d_j = \frac{1}{\sqrt{N}} \sum_k d_k \, e^{\mathrm{i}kj\,d}$ and lattice constant d. We find [7]

$$\hat{H}_{\mathrm{KC}} = \sum_k \left[-\mu - 2t\cos(kd)\right] d_k^\dagger d_k + \Delta \sum_k \left(d_k^\dagger \, d_{-k}^\dagger \, e^{-\mathrm{i}\,kd} + d_{-k} \, d_k \, e^{\mathrm{i}\,kd} \right) + \frac{\mu\, N}{2}. \tag{5.1.3}$$

Expressing the Kitaev Hamiltonian in momentum space via

$$\hat{H}_{\mathrm{KC}} = \frac{1}{2} \sum_k \hat{\Psi}_k^\dagger \, \mathcal{H}(k) \, \hat{\Psi}_k, \quad \hat{\Psi}_k := \begin{pmatrix} d_k \\ d_{-k}^\dagger \end{pmatrix}, \tag{5.1.4}$$

yields the BdG matrix

$$\mathcal{H}(k) = \begin{pmatrix} -\mu - 2t\,\cos(kd) & -2\mathrm{i}\Delta \sin(kd) \\ 2\mathrm{i}\Delta \sin(kd) & \mu + 2t\,\cos(kd) \end{pmatrix} \tag{5.1.5}$$

up to an overall constant. The dispersion relation for the excitation spectrum

$$E_\pm(k) = \pm \sqrt{\left[\mu + 2t\,\cos(kd)\right]^2 + 4\Delta^2 \sin^2(kd)} \tag{5.1.6}$$

follows from diagonalising $\mathcal{H}(k)$ [2, 7, 19, 66]. A finite superconducting pairing constant Δ causes a gapped spectrum; the gap width for $\mu = 0$ is $4\min\{t, \Delta\}$, supposing that non of them is zero. Please notice that the periodicity of the dispersion relation in kd changes for finite chemical potential.

The gap closing condition for finite $\Delta \neq 0$ at $kd = 0, \pi$ is $\mu = \mp 2t$ and marks the phase boundary between distinct topological phases depicted in Fig. 5.1. Still, the identification of the topological trival and non-trivial phases cannot be achieved from the gap closing and relies on topological invariants, which are determined by the dimensionality of the system and the involved symmetries.

5.2. Symmetries and topological invariant

Naturally, the dispersion relation Eq. (5.1.6) reflects the symmetries present in the system's BdG Hamiltonian in Eq. (5.1.5). The Kitaev chain has three important ones: The particle-hole $\mathcal{P}$, the chiral $\mathcal{C}$ and the (pseudo) time reversal symmetry $\mathcal{T}$. Thus, the Kitaev chain is placed in the BDI class [41, 97] related to a $\mathbb{Z}$ topological invariant in one dimension.

The antiunitary particle-hole symmetry arises directly from the BdG construction. Explicitly, we have $\mathcal{P} = \mathcal{K}\,\sigma_{\mathrm{x}}$ w.r.t $\mathcal{H}(k)$ in Eq. (5.1.5), where σ_{x} is the Pauli matrix and

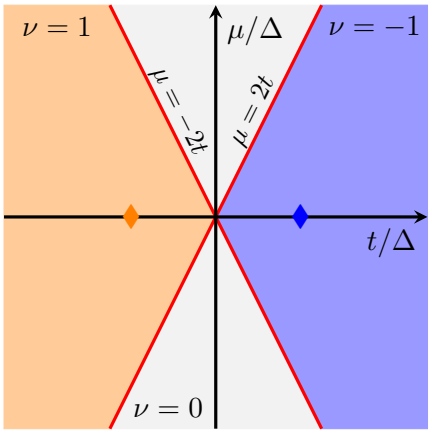

Figure 5.1.: Topological phase diagram of the Kitaev chain. The phase boundary (red line) separates the topological non trivial phases ($\nu = \pm 1$) from the trivial one ($\nu = 0$ in gray). The Kitaev points at $(t/\Delta, \mu/\Delta) = (\pm 1, 0)$ are highlighted.

$\mathcal{K}$ denotes the operator of complex conjugation. One can easily verify that $\mathcal{P}\,\mathcal{H}(k)\,\mathcal{P}^{-1} = -\mathcal{H}(-k)$ and $\mathcal{P}^2 = \mathbb{1}_2$ holds [39]. Thus, acting with $\mathcal{P}$ on an eigenstate $\vec{v}(k)$ of $\mathcal{H}(k)$ with energy E and wavevector k gives

$$\mathcal{H}(k)\;\mathcal{P}\,\vec{v}(-k) \;=\; -E\;\mathcal{P}\,\vec{v}(-k), \tag{5.2.1}$$

the eigenvector $\mathcal{P}\,\vec{v}(-k)$ belonging to $-E$ and $-k$. Most notably, the particle-hole symmetry $\mathcal{P}$ implies a doubly degenerated zero energy level (if present) and thus Majorana zero energy modes (MZM) can only emerge in pairs.

The (pseudo) time reversal symmetry $\mathcal{T} = \mathcal{K}\,\mathbb{1}_2$ ($\mathcal{T}^2 = \mathbb{1}_2$) changes $k \to -k$ and $\mathcal{T}\,\mathcal{H}(k)\,\mathcal{T}^{-1} = \mathcal{H}(-k)$ is true [40]. The presence of $\mathcal{T}$ originates from the fermion's spinless nature in Eq. (5.1.1). The chiral symmetry $\mathcal{C} = \sigma_\mathrm{x}$ ($\mathcal{C}^2 = \mathbb{1}_2$) acts as $\mathcal{C}\,\mathcal{H}(k)\,\mathcal{C}^{-1} = -\mathcal{H}(k)$, thereby changing the eigenstate $\vec{v}(k)$ with energy E

$$\mathcal{H}(k)\;\mathcal{C}\,\vec{v}(k) \;=\; -E\;\mathcal{C}\,\vec{v}(k) \tag{5.2.2}$$

into $\mathcal{C}\,\vec{v}(k)$ corresponding to $-E$. Thus, $\mathcal{C}$ indicates the presence of the pseudo time reversal symmetry by $\mathcal{T} = \mathcal{P}\,\mathcal{C}$.

Finally acting similar to the (pseudo) time reversal symmetry by inverting the momentum's sign, the inversion symmetry $\mathcal{I}$ is also relevant for the Kitaev chain. One can distinguish it from $\mathcal{T}$ noting that the former is unitary, while the latter antiunitary. Explicitly, we have

$$\mathcal{I} \;=\; \begin{pmatrix} 1 & \\ & -1 \end{pmatrix} \;=\; \sigma_\mathrm{z}, \tag{5.2.3}$$

replacing indeed $k \to -k$ in Eq. (5.1.5); thus, effectively only the sign of the superconducting pairing constant is reverted, in agreement with Eq. (5.1.2) in real space.

Nonetheless, the inversion symmetry as global symmetry does not enter into the topological classification by Altland and Zirnbauer contrary to the local acting ones: $\mathcal{P}$, $\mathcal{C}$ and $\mathcal{T}$ [41].

The chiral symmetry allows one to introduce the winding number ν as the topological invariant [39, 98]

$$\nu = \frac{1}{2\pi} \int_{-\pi/d}^{\pi/d} \mathrm{d}k \, \partial_k w(k), \tag{5.2.4}$$

with $w(k) = \arg\left[2\Delta \sin(kd) + \mathrm{i}\left(\mu + 2t\cos(kd)\right)\right]$ for $N \to \infty$ [4]. The entire topological phase diagram is determined by the values of ν with $\nu = \pm 1$ ($\nu = 0$) corresponding to the topological non trivial (trivial) phase. The evaluation of Eq. (5.2.4) yields $\nu = \pm 1$ ($\nu = 0$) for $|\mu| < 2\,|t|$ (otherwise) and thus to the topological phase diagram in Fig. 5.1.

Significantly, in the thermodynamic limit of $N \to \infty$ Majorana zero modes are present for all parameters assigned to the topological non trivial phases. In the case of a finite system size (with open boundary condition) we have to correct this point of view slightly; the non trivial phase is merely the parameter frame where we expect Majorana fermions, since finite size effects may prohibit their presence for certain values of μ/Δ, t/Δ within the topological non trivial region.

5.3. Kitaev's approach

The remarkable feature of Kitaev's model is the simplicity in proving the existence of Majorana fermions as emergent boundary states [2, 7, 19, 21]. This can be demonstrated for example by using (local) Majorana operators γ_j^A, γ_j^B defined via the unitary transformation

$$\begin{pmatrix} \gamma_j^A \\ \gamma_j^B \end{pmatrix} \coloneqq \frac{1}{\sqrt{2}} \begin{bmatrix} 1 & 1 \\ -\mathrm{i} & \mathrm{i} \end{bmatrix} \begin{pmatrix} d_j \\ d_j^\dagger \end{pmatrix}. \tag{5.3.1}$$

Apart from the anticommutation relation ($\alpha, \beta = A, B$; $l, j = 1, \ldots, N$)

$$\left\{\gamma_j^\alpha, \gamma_l^\beta\right\} = \delta_{\alpha\beta}\,\delta_{jl}, \tag{5.3.2}$$

the Majorana operators are hermitian and square to $1/2$

$$\left(\gamma_j^\alpha\right)^\dagger = \gamma_j^\alpha, \tag{5.3.3}$$

$$\left(\gamma_j^\alpha\right)^2 = \frac{1}{2}. \tag{5.3.4}$$

As Eq. (5.3.1) suggests, the Majorana operators are in perfect balance between particle creation and annihilation, thus they treat superconducting pairing and hopping processes similarly. Since a unitary (or any invertible) basis transformation cannot cause a loss

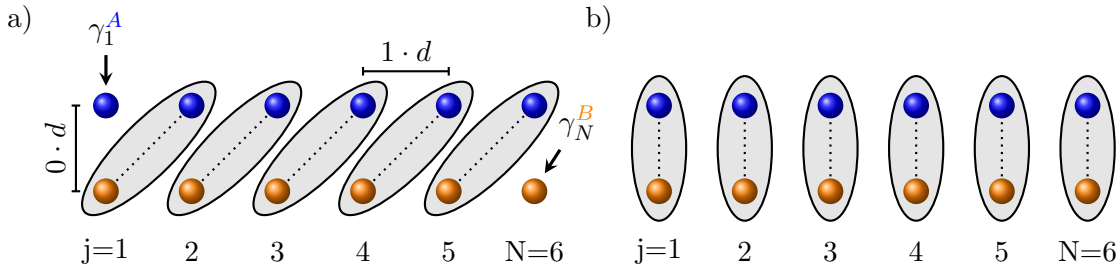

Figure 5.2.: The Kitaev chain with $N = 6$ sites, lattice constant d and open boundary, visualized for $\mu = 0$, $\Delta = t \neq 0$ in a) and $\mu \neq 0$, $t = \Delta = 0$ in b). The Majorana orbitals (•, •) associated to γ_j^A, γ_j^B at site j are sketched along the vertical axis. The enclosed pairs are bound together along the displayed dotted lines and form fermions.

of information, Δ, t get reshaped into the linear combinations $\Delta \pm t$ and the Kitaev Hamiltonian from Eq. (5.1.1) becomes

$$\hat{H}_{\mathrm{KC}} = -\mathrm{i}\mu \sum_{j=1}^{N} \gamma_j^A \gamma_j^B + \mathrm{i}(\Delta - t) \sum_{j=1}^{N-1} \gamma_j^A \gamma_{j+1}^B + \mathrm{i}(\Delta + t) \sum_{j=1}^{N-1} \gamma_j^B \gamma_{j+1}^A. \tag{5.3.5}$$

The actual decomposition of a particle into the two Majorana operators gives rise to two degrees of freedom per atom, namely A and B. These two "orbitals" are bound together by the chemical potential μ and we may think of $-\mathrm{i}\mu$ as a kind of hopping parameter between both. Importantly, avoid over-interpreting Eq. (5.3.1): it does not require superconductivity at all, nor does it give rise to the presence of Majorana fermions; it is merely a basis transformation applicable to many systems. Nonetheless, the new shape of the Hamiltonian suggests to investigate the cases $\Delta = t$ and $\Delta = -t$. The situation for zero chemical potential and $\Delta = t \neq 0$, belonging to the topological non-trivial phase, is depicted in Fig. 5.2 a). The Hamiltonian becomes peculiar

$$\hat{H}_{\mathrm{KC}} = 2\mathrm{i}\, t \sum_{j=1}^{N-1} \gamma_j^B \gamma_{j+1}^A, \tag{5.3.6}$$

since γ_1^A and γ_N^B do not appear. In doubt, we can calculate the commutators $\left[\hat{H}_{\mathrm{KC}}, \gamma_1^A\right] = \left[\hat{H}_{\mathrm{KC}}, \gamma_N^B\right] = 0$. The result shows the absence of γ_1^A, γ_N^B in $\hat{H}_{\mathrm{KC}}$. Indeed, the absence of γ_1^A, γ_N^B indicates the presence of zero energy end modes in a finite chain (with open boundary conditions). A similar situation occurs for $\Delta = -t$ and $\mu = 0$. We call the points $(t/\Delta, \mu/\Delta) = (\pm 1, 0)$ in the parameter space the Kitaev points. Since two Majorana operators of type A, B form a fermion (created by $q_\pm^\dagger$ defined in Eqs. (5.3.7), (5.3.8)), one can show that such a single fermion is localized at both ends of the chain

simultaneously

$$q_+^\dagger = \frac{1}{\sqrt{2}}\left(\gamma_1^A - \mathrm{i}\,\gamma_N^B\right), \quad [\Delta = t], \tag{5.3.7}$$

$$q_-^\dagger = \frac{1}{\sqrt{2}}\left(\gamma_1^B - \mathrm{i}\,\gamma_N^A\right), \quad [\Delta = -t]. \tag{5.3.8}$$

Single Majorana operators γ_j^A, γ_j^B cannot enter into the Hamiltonian as they do not preserve the fermionic parity. Thus, isolated Majorana fermions associated for instance with γ_1^A, γ_N^B are stable against errors, i.e. predestined for fault tolerant quantum computations. Furthermore, zero energy states cause fermionic parity switches, since it costs no energy to change the occupation. For more details see [7] and in particular [2].

Zero energy edge modes are not always present in the Kitaev chain as we can see clearly from Eq. (5.3.5) at $t = \Delta = 0$, $\mu \neq 0$

$$\hat{H}_{\mathrm{KC}} = -\mathrm{i}\mu \sum_{j=1}^{N} \gamma_j^A \gamma_j^B, \tag{5.3.9}$$

which belongs to the topological trivial phase. The Majorana operators on each site get bound into fermions with finite energy as visualized in Fig. 5.2 b). The scenarios drawn in Eqs. (5.3.7) - (5.3.9) allow a more practical understanding of the topological phase diagram as we discuss in the following.

5.4. Finite size effects and spatial overlap

A finite system length with boundaries is mandatory to observe Majorana fermions since they possess as in-gap excitation a complex wavevector κ. The associated imaginary part causes a decay in the spatial profile of the wavefunction. Typically, one defines a decay length $\xi = d/\mathrm{Im}(\kappa)$ in order to quantify the spatial behavior of the Majarana wavefunctions in comparison to the system size L. In case of $\xi/L \ll 1$ ($\xi/L \gg 1$), the wave function is localized closely to the systems ends (extended over the entire system).

The extreme case is shown in Eqs. (5.3.7), (5.3.8), where the fermion is composed by two Majorana fermions residing on the first and last sites. Here, the decay length is zero as the wave functions drops immediately to zero on the nearest neighboring site.

For the Kitaev chain at zero chemical potential, one finds [2]

$$\xi|_{\mu=0} = \frac{2d}{\left|\ln\left|\frac{t-\Delta}{t+\Delta}\right|\right|}, \tag{5.4.1}$$

for arbitrary values of t, Δ.

In the community it is widely believed that the spatial profile of Majorana fermions at finite system length L causes the energy to shift from zero to finite values, as stated in Refs. [3, 7, 8, 19, 66] to give only a few. Explicitly, in the situation where the two

Majorana fermions are not remotely far away, their wavefunctions may possess a spatial overlap. Numerical investigations, and some analytic treatments [2, 3, 72], conclude that this overlap causes an energy shift from zero, whose upper value is proportional to $\exp(-L/\xi)$.

6. Spectral analysis of the finite Kitaev chain

The main aspects of the chapter have been published in [4, 5].

We start the discussion of the spectrum and the eigenstates of the finite Kitaev chain in real space by defining our default BdG basis $\hat{\psi}_{\mathrm{BdG}} = \left(d_1, \ldots, d_N, d_1^\dagger, \ldots, d_N^\dagger\right)$. The Kitaev Hamiltonian in Eq. (5.1.1) becomes

$$\hat{H}_{\mathrm{KC}} = \frac{1}{2}\, \hat{\psi}_{\mathrm{BdG}}^\dagger\, \mathcal{H}_{\mathrm{BdG}}\, \hat{\psi}_{\mathrm{BdG}}. \tag{6.0.1}$$

As a first impression, the matrix $\mathcal{H}_{\mathrm{BdG}}$ contains a particle C and a hole block $-C$

$$\mathcal{H}_{\mathrm{BdG}} = \begin{bmatrix} C & S \\ S^\dagger & -C \end{bmatrix}, \tag{6.0.2}$$

both coupled by the superconducting pairing matrices S, $S^\dagger$. All matrices inside $\mathcal{H}_{\mathrm{BdG}}$ are *tridiagonal* and the matrix C is hermitian,

$$C = \begin{bmatrix} -\mu & -t & & & & & & \\ -t & -\mu & -t & & & & & \\ & -t & -\mu & -t & & & & \\ & & \ddots & \ddots & \ddots & & & \\ & & & -t & -\mu & -t & & \\ & & & & -t & -\mu & -t & \\ & & & & & -t & -\mu & \end{bmatrix}_{N\times N}. \tag{6.0.3}$$

It displays essentially the same structure as the linear chain from section 2, see in particular Eq. (2.2.1). The matrix

$$S = \begin{bmatrix} 0 & \Delta & & & & & & \\ -\Delta & 0 & \Delta & & & & & \\ & -\Delta & 0 & \Delta & & & & \\ & & \ddots & \ddots & \ddots & & & \\ & & & -\Delta & 0 & \Delta & & \\ & & & & -\Delta & 0 & \Delta & \\ & & & & & -\Delta & 0 & \end{bmatrix}_{N\times N}. \tag{6.0.4}$$

is skew hermitian, i.e. $S^\dagger = -S$, since Δ is considered real.The default basis introduced here will not be the best basis choice for the latest stages of our approach, but in the beginning it will serve us well. Later during the discussions of the transport properties, we will express the retarded Green's function w.r.t to this default basis $\hat{\psi}_{\mathrm{BdG}}$ enabling hopefully an intuitive understanding.

The tridiagonal structure of C, S originates from the Kitaev Hamiltonian owing exclusively nearest neighbour processes, either the hopping t or the p-wave pairing constant Δ. Notice that in section 2.2, we dealt with exactly this type of matrices. Before using the formalism of section 2.2, we obtain the eigenvalues together with the quantization of the wavevector k for special parameter settings with very small effort.

6.1. The humble beginnings in real space: $\Delta = 0$ vs. $t = 0$

In this short section, we calculate the spectrum of the Kitaev chain for the rather trivial cases $\Delta = 0$ and $t = 0$, the former only for completeness. We use the most elementary and error resistant method: the characteristic polynomial. In case of $\Delta = 0$ only C and $-C$ in $\mathcal{H}_{\mathrm{BdG}}$ remain, since $S = S^\dagger = 0_{N,\,N}$ drops out. Obviously, we have that

$$\begin{aligned} P_\lambda\left(\mathcal{H}_{\mathrm{BdG}}|_{\Delta=0}\right) \;=\; \det\left(\lambda\mathbb{1}_{2N} - \mathcal{H}_{\mathrm{BdG}}|_{\Delta=0}\right) \;=\; \det\begin{bmatrix} \lambda\mathbb{1}_{\mathbb{N}} - C & \\ & \lambda\mathbb{1}_{\mathbb{N}} + C \end{bmatrix} \\ = \det\left(\lambda\mathbb{1}_N - C\right)\det\left(\lambda\mathbb{1}_N + C\right), \quad (6.1.1) \end{aligned}$$

and the last step follows from the block diagonal structure of $\mathcal{H}_{\mathrm{BdG}}|_{\Delta=0}$. The spectrum of C is the one of the linear chain. Observing that $\lambda = E_\pm^{\Delta=0}$ with $E_\pm$ from Eq. (5.1.6) holds, the eigenvalues of the Kitaev chain are

$$E_\pm^{\Delta=0}(k_j d) \;=\; \pm\left[\mu \;+\; 2\,t\cos\left(k_j d\right)\right] \tag{6.1.2}$$

with $k_j d \;=\; j\pi/(N+1)$, $j = 1, \ldots, N$. We continue with the situation of $t = 0$, $\Delta \neq 0$, where we find a naively unexpected result for the eigenvalues and quantized wavevectors. This advantageous strategy provides us with the possibility to check the more advanced results to be presented later.

6.1.1. Spectrum for $\mu = t = 0$, $\Delta \neq 0$.

We simplify our life further by first considering $\mu = t = 0$; we include $\mu \neq 0$ in a second step. The parameter setting sets now $C = 0_{N,\,N}$ following Eq. (6.0.3), and only S, $S^\dagger$ remain in $\mathcal{H}_{\mathrm{BdG}}$

$$\mathcal{H}_{\mathrm{BdG}}|_{t=\mu=0} \;=\; \begin{bmatrix} & S \\ S^\dagger & \end{bmatrix}. \tag{6.1.3}$$

Obtaining eigenvalues can involve the calculation of determinants and the latter are not only determined by the value of the individual entries for the corresponding matrix, but

their arrangement as well; the geometry of the elements so to speak, as follows from Laplace's expansion. Nevertheless, here we wish to point out the specific arrangement of physical quantities inside Eq. (6.1.3), since S, $S^\dagger$ are tridiagonal. Clearly, only Δ remains; but the way how Δ enters into S, and S, $S^\dagger$ into $\mathcal{H}_{\mathrm{BdG}}$ is delicate. The tempting structure provided by $\mathcal{H}_{\mathrm{BdG}}$ grants the characteristic polynomial

$$P_\lambda(\mathcal{H}_{\mathrm{BdG}}|_{t=\mu=0}) = \det\left(\lambda \mathbb{1}_{2N} - \mathcal{H}_{\mathrm{BdG}}|_{t=\mu=0}\right) = \det\begin{bmatrix} \lambda\,\mathbb{1}_N & -S \\ S & \lambda\,\mathbb{1}_N \end{bmatrix}, \tag{6.1.4}$$

where we used $S^\dagger = -S$. We thus work in the frame of partitioned matrices. In particular, the commutator $[\lambda\,\mathbb{1}_N, S] = 0$ vanishes[1] and one obtains[99]

$$P_\lambda(\mathcal{H}_{\mathrm{BdG}}|_{t=\mu=0}) = \det\left[\lambda^2\,\mathbb{1}_N + S^2\right]. \tag{6.1.5}$$

Exploiting that S and $\mathbb{1}_N$ commute, we can simplify P_λ again

$$P_\lambda(\mathcal{H}_{\mathrm{BdG}}|_{t=\mu=0}) = \det\left[\lambda\,\mathbb{1}_N + \mathrm{i}S\right]\det\left[\lambda\,\mathbb{1}_N - \mathrm{i}S\right] = P_\lambda(\mathrm{i}S)\,P_\lambda(-\mathrm{i}S). \tag{6.1.6}$$

The eigenvalues of $\mathcal{H}_{\mathrm{BdG}}$ follow now from the ones of the hermitian matrices $\pm\mathrm{i}S$. The matrix $\mathrm{i}S$ is tridiagonal

$$\mathrm{i}S = \begin{bmatrix} 0 & \mathrm{i}\Delta & & & & & \\ -\mathrm{i}\Delta & 0 & \mathrm{i}\Delta & & & & \\ & -\mathrm{i}\Delta & 0 & \mathrm{i}\Delta & & & \\ & & \ddots & \ddots & \ddots & & \\ & & & -\mathrm{i}\Delta & 0 & \mathrm{i}\Delta & \\ & & & & -\mathrm{i}\Delta & 0 & \mathrm{i}\Delta \\ & & & & & -\mathrm{i}\Delta & 0 \end{bmatrix}_{N\times N} \tag{6.1.7}$$

and imitates a linear chain with imaginary "hopping" $\mathrm{i}\Delta$. We can directly read out the eigenvalues of $\pm\mathrm{i}S$ using Eqs. (2.2.11), (2.2.15). The spectrum of $\mathcal{H}_{\mathrm{BdG}}$ is simply

$$\lambda = \pm 2\Delta\cos\left(\frac{n\pi}{N+1}\right), \quad n = 1, \ldots, N. \tag{6.1.8}$$

Surprisingly, we find a cosine dependence, while the dispersion relation from Eq. (5.1.6) gives $E_\pm(k) = \pm 2\Delta\sin(kd)$ at $t = \mu = 0$. Thus, the quantised values of kd w.r.t to $E_\pm(k)$ are

$$kd = k_n d + \frac{\pi}{2} = \frac{n\pi}{N+1} + \frac{\pi}{2}, \quad n = 1, \ldots, N. \tag{6.1.9}$$

Next, we consider finite values of the chemical potential.

[1] The technique provided by Ref. [99] applies even for non invertible diagonal blocks, in contrary to the standard determinant formula for partitioned 2×2 matrices. We will find $\lambda = 0$ as eigenvalue for odd N, since the reality of Δ implies $S^\dagger = S^{\mathrm{T}} = -S$ and in turn $\det(S) = \det(S^{\mathrm{T}}) = (-1)^N\det(S)$ yielding $\det(S) = 0$ for odd N. Silvester's formula states $\det\begin{bmatrix} A & B \\ C & D \end{bmatrix} = \det[AD - CB]$, iff $[C, D] = 0$, for equal sized, square matrices A, B, C, D.

6.1.2. Eigenvalues for $t = 0$, $\mu \neq 0$ $\Delta \neq 0$.

We can include $\mu \neq 0$ using the same techniques as before. Revisiting Eq. (6.0.3) displays $C = -\mu \mathbb{1}_N$ at $t = 0$ and thus the characteristic polynomial belonging to $\mathcal{H}_{\mathrm{BdG}}$ is now

$$P_\lambda(\mathcal{H}_{\mathrm{BdG}}|_{t=0}) = \det\left(\lambda \mathbb{1}_{2N} - \mathcal{H}_{\mathrm{BdG}}|_{t=0}\right) = \det\begin{bmatrix}(\lambda+\mu)\,\mathbb{1}_N & -S \\ S & (\lambda-\mu)\,\mathbb{1}_N\end{bmatrix}. \quad (6.1.10)$$

Still, $\mathbb{1}_N$ and S commute granting again [99]

$$P_\lambda(\mathcal{H}_{\mathrm{BdG}}|_{t=0}) = \det\left[\left(\lambda^2 - \mu^2\right)\mathbb{1}_N + S^2\right] = \det\left[\Lambda^2\,\mathbb{1}_N + S^2\right] \quad (6.1.11)$$

where we set $\Lambda^2 \coloneqq \lambda^2 - \mu^2$ in order to imitate the structure from the former $\mu = 0$ zero case. Similarly as before, we get $P_\lambda(\mathcal{H}_{\mathrm{BdG}}|_{t=0}) = P_\Lambda(\mathrm{i}S)\,P_\Lambda(-\mathrm{i}S)$. The hermiticity of $\pm\mathrm{i}S$ ensures $\Lambda \in \mathbb{R}$, i.e. $\lambda^2 \geq \mu^2$, and we get $\Lambda = \pm 2\Delta\cos[n\pi/(N+1)]$ with $n = 1, \ldots, N$. The spectrum of the Kitaev chain follows by solving for λ. In terms of the dispersion relation from Eq. (5.1.6) the eigenvalues are

$$E_\pm^{t=0}(k) = \pm\sqrt{\mu^2 + 4\Delta^2\sin^2\left(\frac{n\pi}{N+1} + \frac{\pi}{2}\right)}, \quad n = 1, \ldots, N, \quad (6.1.12)$$

with the displayed quantized wavevectors.

Including the chemical potential μ into the eigenvalues was not a challenge and only $t \neq 0$ remains. However, we have a competition between t and Δ, as it becomes completely apparent by comparing the situation $t = \mu = 0$, $\Delta \neq 0$ with $\Delta = \mu = 0$, $t \neq 0$. This conflict prevents us from including $t \neq 0$ into the eigenvalues via the scheme discussed above as shown in appendix E and is in fact essential for the Kitaev chain.

6.2. The SSH-like chain limit: $\mu = 0$

The prior section used the default BdG Basis $\hat{\psi}_{\mathrm{BdG}} = \left(d_1, \ldots, d_N, d_1^\dagger, \ldots, d_N^\dagger\right)$ and we showed its inappropriate character to deal with t and Δ simultaneously in appendix E. Further progress in real space is possible by choosing a suitable basis. In particular, the Hamiltonian in terms of Majorana operators γ_j^A, γ_j^B $(j = 1, \ldots, N)$ from Eq. (5.3.5) is the most adequate, since t, Δ are reshaped into $a \coloneqq \mathrm{i}(\Delta - t)$ and $b \coloneqq \mathrm{i}(\Delta + t)$. For $\mu = 0$ we have that

$$\hat{H}_{\mathrm{KC}}\Big|_{\mu=0} = a\sum_{j=1}^{N-1}\gamma_j^A\gamma_{j+1}^B + b\sum_{j=1}^{N-1}\gamma_j^B\gamma_{j+1}^A. \quad (6.2.1)$$

Notice that without chemical potential the onsite bonding $-\mathrm{i}\mu$ between $\gamma_j^A\,\gamma_j^B$ dropped. As depicted in Fig. 6.1, we find two independent Su–Schrieffer–Heeger-like (SSH-like) chains α, β with lattice constant $2d$, respectively [97, 100]. The α (β) chain starts always

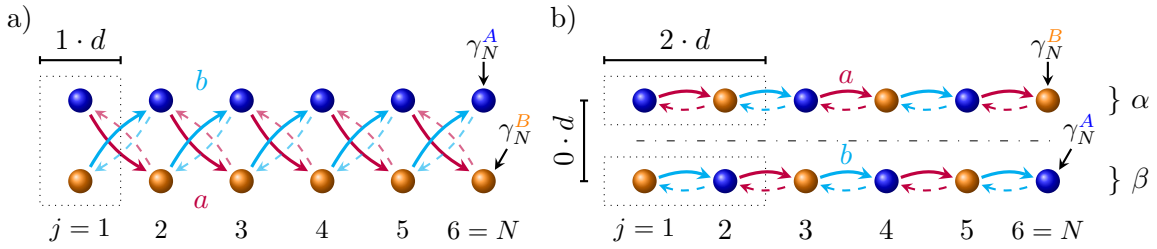

Figure 6.1.: The Kitaev BdG Hamiltonian for $\mu = 0$ and $N = 6$ depicted in terms of the Majorana operators γ_j^A, γ_j^B (●, ●) and with n.n.n. hoppings $a = \mathrm{i}\,(\Delta - t)$ (purple), $b = \mathrm{i}\,(\Delta + t)$ (cyan) as solid arrows; the dashed ones are associated with $-a$, $-b$. a) The Majorana operators form connected sublattices and the dotted rectangle indicates the unit cell. b) No length scale is assigned to the vertical axis and exchanging every second pair γ^A, γ^B reduces the former intertwined structure into two independent subsystems α, β. Each of them is a Su–Schrieffer–Heeger-like (SSH)-like chain with the given unit cell and lattice constant $2d$ [97, 100].

with γ_1^A (γ_1^B) and contains only γ_j^A with even (odd) and only γ_j^B with odd (even) position j. In fact, a reordering of the terms in Eq. (6.2.1) yields

$$\begin{aligned}\hat{H}_{\mathrm{KC}}\Big|_{\mu=0} = \frac{1}{2}\left(a\sum_{l=1}^{N_1}\gamma_{2l-1}^A\gamma_{2l}^B + b\sum_{l=1}^{N_2}\gamma_{2l}^B\gamma_{2l+1}^A\right) + \text{h.c.} \\ + \frac{1}{2}\left(b\sum_{l=1}^{N_1}\gamma_{2l-1}^B\gamma_{2l}^A + a\sum_{l=1}^{N_2}\gamma_{2l}^A\gamma_{2l+1}^B\right) + \text{h.c.},\end{aligned} \tag{6.2.2}$$

with $N_1 = N/2$, $N_2 = N_1 - 1$ for even N and $N_1 = N_2 = (N-1)/2$ for odd N. Here, the first (second) line is the Hamiltonian for the α (β) chain.

Next, we calculate the BdG matrix from Eq. (6.2.2) defining

$$\hat{\psi}_{\mathrm{SSH}}^{\mathrm{even}} \coloneqq \left(\gamma_1^A, \gamma_2^B, \ldots, \gamma_{N-1}^A, \gamma_N^B \middle| \gamma_1^B, \gamma_2^A, \ldots, \gamma_{N-1}^B, \gamma_N^A\right)^{\mathrm{T}}, \tag{6.2.3}$$

$$\hat{\psi}_{\mathrm{SSH}}^{\mathrm{odd}} \coloneqq \left(\gamma_1^A, \gamma_2^B, \ldots, \gamma_{N-1}^B, \gamma_N^A \middle| \gamma_1^B, \gamma_2^A, \ldots, \gamma_{N-1}^A, \gamma_N^B\right)^{\mathrm{T}}, \tag{6.2.4}$$

where "$|$" indicates the end of the α chain and we understand $\hat{\psi}_{\mathrm{SSH}}^{\mathrm{even,\ odd}} = \left(\hat{\psi}_\alpha \,\middle|\, \hat{\psi}_\beta\right)^{\mathrm{T}}$. Please notice that $\hat{\psi}_\alpha$ ($\hat{\psi}_\beta$) is precisely depicted by the spheres of chain α (β) in Fig. 6.1 b). In terms of $\hat{\psi}_{\mathrm{SSH}}$, Eq. (6.2.2) becomes

$$\hat{H}_{\mathrm{KC}}\Big|_{\mu=0} = \frac{1}{2}\,\hat{\psi}_{\mathrm{SSH}}^\dagger\,\mathcal{H}_{\mathrm{KC}}^{\mathrm{SSH}}\,\hat{\psi}_{\mathrm{SSH}} = \frac{1}{2}\,\hat{\psi}_{\mathrm{SSH}}^\dagger\begin{bmatrix}\mathcal{H}_\alpha & 0_{N,N}\\ 0_{N,N} & \mathcal{H}_\beta\end{bmatrix}\hat{\psi}_{\mathrm{SSH}}, \tag{6.2.5}$$

for even and odd N, respectively. $\mathcal{H}_{\alpha,\beta}$ are tridiagonal as indicated by Fig. 6.1 b), and

we find for even N

$$\mathcal{H}_\alpha = \begin{bmatrix} 0 & a & & & & & \\ -a & 0 & b & & & & \\ & -b & 0 & a & & & \\ & & \ddots & \ddots & \ddots & & \\ & & & -a & 0 & b & \\ & & & & -b & 0 & a \\ & & & & & -a & 0 \end{bmatrix}_{N\times N}, \tag{6.2.6}$$

and similarly

$$\mathcal{H}_\beta = \begin{bmatrix} 0 & b & & & & & \\ -b & 0 & a & & & & \\ & -a & 0 & b & & & \\ & & \ddots & \ddots & \ddots & & \\ & & & -b & 0 & a & \\ & & & & -a & 0 & b \\ & & & & & -b & 0 \end{bmatrix}_{N\times N}. \tag{6.2.7}$$

The odd N expressions follow from removing both the last line and last column in Eqs. (6.2.6), (6.2.7). We observe that the SSH-like chain matrices convert into each other by exchanging the hopping a with b: $\mathcal{H}_\alpha = \mathcal{H}_\beta|_{a\leftrightarrow b}$. Still, $\mathcal{H}_{\alpha,\,\beta}$ are written in a distinct basis, i.e. w.r.t different operators. Nonetheless, the relation between both chains can be seen directly in Fig. 6.1 b) as well, where we pictorially replace the color of the arrows, i.e. purple with cyan and vice versa, but we do not change the blue/ orange spheres. This property is very useful and will simplify the calculation of the eigenvalues, as we see next.

6.2.1. Derivation of the characteristic polynomial

The spectrum can be obtained with the characteristic polynomial. In order to avoid the longer and more technical discussion from appendix F, we exploit some properties of the SSH-like representation granting a faster, intuitive yet exact calculation. The characteristic polynomial of $\mathcal{H}_{\mathrm{KC}}^{\mathrm{SSH}}$ in Eq. (6.2.5)

$$\begin{aligned} P_\lambda(\mathcal{H}_{\mathrm{KC}}^{\mathrm{SSH}}) = \det\left(\lambda\mathbb{1}_{2N} - \mathcal{H}_{\mathrm{KC}}^{\mathrm{SSH}}\right) &= \det\begin{bmatrix} \lambda\,\mathbb{1}_N - \mathcal{H}_\alpha & \\ & \lambda\,\mathbb{1}_N - \mathcal{H}_\beta \end{bmatrix} \\ &= P_\lambda(\mathcal{H}_\alpha)\,P_\lambda(\mathcal{H}_\beta), \end{aligned} \tag{6.2.8}$$

is a product of the characteristic polynomials of the individual SSH-like chains. The relations between $\mathcal{H}_{\alpha,\beta}$ are the key to solve for the spectrum of the Kitaev chain and allow a rather simple treatment, as we show.

The tridiagonal structure of $\mathcal{H}_\alpha$ from Eq. (6.2.6) allows the use of the recursion method provided by Ref. [78]. We have $P_\lambda(\mathcal{H}_\alpha) = \epsilon_N$ ($P_\lambda(\mathcal{H}_\beta) = \zeta_N$) and ϵ_N (ζ_N) is

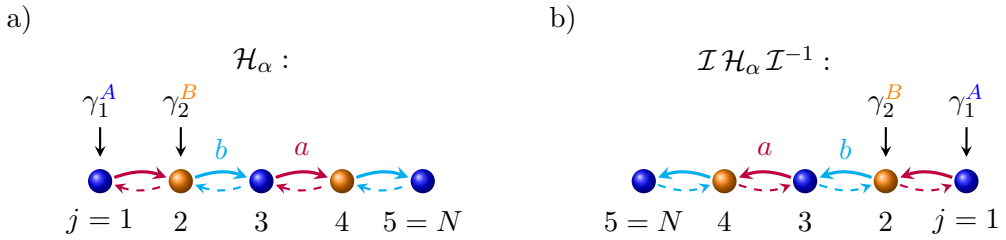

Figure 6.2.: The α-chain for odd $N = 5$ in a) and after spatial inversion in b). By comparison, the structure of $\mathcal{I}\,\mathcal{H}_\alpha\,\mathcal{I}^{-1}$ is essentially the one of $\mathcal{H}_\alpha$ after changing $a \to b$. Both differ only by an overall sign, since the solid arrows point now in the opposite direction.

obtained from

$$\epsilon_l \;=\; \lambda\,\epsilon_{l-1} \;+\; \left(a^2\,\delta_{l,\mathrm{even}} \;+\; b^2\,\delta_{l,\mathrm{odd}}\right)\epsilon_{l-2}, \tag{6.2.9}$$

$$\zeta_l \;=\; \lambda\,\zeta_{l-1} \;+\; \left(b^2\,\delta_{l,\mathrm{even}} \;+\; a^2\,\delta_{l,\mathrm{odd}}\right)\zeta_{l-2}, \tag{6.2.10}$$

for $l = 1, \ldots, N$. The initial values are $\epsilon_0 = 1$, $\epsilon_{-1} = 0$ and $\zeta_0 = 1$, $\zeta_{-1} = 0$. The second term of the r.h.s in Eqs. (6.2.9), (6.2.10) differs between even and odd index, which makes it problematic to directly access the final result. However, one can circumvent this term by exploiting the properties of $\mathcal{H}_{\alpha,\beta}$ in several simple steps. Apparently, Eqs. (6.2.6), (6.2.7) imply

$$\zeta_l|_{a\to b} = \epsilon_l\,, \quad l \geq -1 \tag{6.2.11}$$

and vice versa. This property alone will not simplify the calculation, but there is in fact a second relation between ζ_l, ϵ_l.

As shown in Fig. 6.1 a spatial inversion of $\mathcal{H}_\alpha$ ($\mathcal{H}_\beta$ analogously) acts similar as exchanging a and b. The spatial inversion $\mathcal{I}$ reads

$$\mathcal{I} = \begin{bmatrix} & & 1 \\ & \iddots & \\ 1 & & \end{bmatrix}_{N\times N} \tag{6.2.12}$$

w.r.t. $\mathcal{H}_{\alpha,\beta}$. Indeed, the application of $\mathcal{I}$ on $\mathcal{H}_\alpha$ yields

$$\mathcal{I}\,\mathcal{H}_\alpha\,\mathcal{I}^{-1} \;=\; -\,\mathcal{H}_\alpha|_{a\to b} \;=\; -\mathcal{H}_\beta, \quad \text{(odd } N \text{ only)} \tag{6.2.13}$$

only if N is odd and analogously for $\mathcal{H}_\beta$. For even N, this connection breaks down as one can see from Fig. 6.1 by removing one site. The first hopping process and the last one would be the same; thus the inversion exchanges only $a \to -a$, $b \to -b$ and no mapping between $\mathcal{H}_{\alpha,\beta}$ is achievable with $\mathcal{I}$.

Importantly, Eq. (6.2.13), the hermiticity of $\mathcal{H}_\beta$ and the properties of the determinant yield

$$\begin{aligned}\epsilon_N \;=\; P_\lambda(\mathcal{H}_\alpha) \;=\; \det(\mathcal{I})\,\det(\lambda\mathbb{1}_N - \mathcal{H}_\alpha)\det\left(\mathcal{I}^{-1}\right) \;&=\; \det\left(\lambda\mathbb{1}_N - \mathcal{I}\,\mathcal{H}_\alpha\,\mathcal{I}^{-1}\right)\\ &=\; \det\left(\lambda\,\mathbb{1}_N \,+\, \mathcal{H}_\beta^\dagger\right)\\ &=\; \det\left(\lambda\,\mathbb{1}_N \,+\, \mathcal{H}_\beta^*\right)\\ &=\; \det\left(\lambda\mathbb{1}_N - \mathcal{H}_\beta\right)\\ &=\; P_\lambda(\mathcal{H}_\beta) \equiv \zeta_N \qquad (6.2.14)\end{aligned}$$

for odd N. Thus, $\mathcal{H}_{\alpha,\,\beta}$ share the same spectrum for odd N. Notice that Eq. (6.2.14) may actually imply that

$$\epsilon_l \;=\; \zeta_l, \quad (l \text{ odd}) \qquad (6.2.15)$$

is true for all odd l due to the recursive approach. Next, recall that λ is meant as parameter so far and not as eigenvalue. Since Eq. (6.2.11) is also correct, we find that ϵ_l, ζ_l are invariant under the exchange of a's and b's from Eq. (6.2.15).

The crucial step to solve the recursion in Eqs. (6.2.9), (6.2.10) is to consider even and odd l independently. Due to the property shown in Eq. (6.2.15), one finds in both cases the common and simplified expressions ($l = 1, \ldots, N$)

$$\epsilon_l \;=\; \lambda\,\zeta_{l-1} \,+\, a^2\,\epsilon_{l-2}, \qquad (6.2.16)$$

$$\zeta_l \;=\; \lambda\,\epsilon_{l-1} \,+\, b^2\,\zeta_{l-2}. \qquad (6.2.17)$$

We can disentangle the last two expressions and we find

$$\epsilon_{l+2} \;=\; \left(\lambda^2 + a^2 + b^2\right)\,\epsilon_l \;-\; a^2b^2\,\epsilon_{l-2}, \qquad (6.2.18)$$

$$\zeta_{l+2} \;=\; \left(\lambda^2 + a^2 + b^2\right)\,\zeta_l \;-\; a^2b^2\,\zeta_{l-2}. \qquad (6.2.19)$$

Here, we extended the sequences to all integers l for simplicity. The appearance of $\boldsymbol{\lambda^2}$ in the last expressions reflects the chiral and the particle-hole symmetry of the Kitaev chain, rather than λ in the Eqs. (6.2.10), (6.2.9). Further, the Eqs. (6.2.18), (6.2.19) show a distinction for even and odd number of sites, which is a known feature of SSH chains [101].

We have already shown in Ch. 4.2.1 that the Eqs. (6.2.18), (6.2.19) define Fibonacci polynomials $u_n \coloneqq \epsilon_{2n+1}$, $v_n \coloneqq \epsilon_{2n}$. We find the initial values $u_0 = \epsilon_1 \;=\; \lambda$, $u_{-1} = \epsilon_{-1} = 0$, $v_0 = \epsilon_0 = 1$, $v_{-1} = \epsilon_{-2} = 1/a^2$, see Eq. (6.2.9). The value for ϵ_{-2} is extracted from Eq. (6.2.9) by inserting $l = 0$. The closed form expressions for u_n, v_n are given in Eq. (4.1.6). Here, we have $x = \lambda^2 + a^2 + b^2$ and $y = -a^2b^2$. The solutions for ϵ_{2n+1} and ϵ_{2n} read

$$\epsilon_{2n+1} \;=\; \lambda\,\mathcal{F}(n+1), \qquad (6.2.20)$$

$$\epsilon_{2n} \;=\; \mathcal{F}(n+1) \;-\; b^2\,\mathcal{F}(n), \qquad (6.2.21)$$

in terms of the notation implemented in Ch. 4.1. Since both x and y are invariant under the exchange of a's and $b's$, the Fibonacci $\mathcal{F}(n)$ is, see Eq. (4.1.2), (4.1.5). Thus, ζ_{2n+1}, ζ_{2n} follow from Eqs. (6.2.20), (6.2.21) as

$$\zeta_{2n+1} \;=\; \lambda\,\mathcal{F}(n+1), \tag{6.2.22}$$

$$\zeta_{2n} \;=\; \mathcal{F}(n+1) \;-\; a^2\,\mathcal{F}(n), \tag{6.2.23}$$

using Eq. (6.2.11). The characteristic polynomial is $P_\lambda(\mathcal{H}_{\mathrm{KC}}^{\mathrm{SSH}}) = \epsilon_N\,\zeta_N$ and fully determined, see Eq. (6.2.8). From our results in Eqs. (6.2.20) - (6.2.23), we can see that the spectra for the SSH-like chains α and β are non-degenerate (doubly degenerate) for even (odd) N.

A final remark before we turn directly to the eigenvalues. The results for $P_\lambda(\mathcal{H}_{\mathrm{KC}}^{\mathrm{SSH}})$ do not require the hermiticity of $\mathcal{H}_{\alpha,\,\beta}$ as can be extracted from Ref. [78]; hermiticity was only a special case. The results for ϵ_N and ζ_N hold for all a, b independently of whether they are real, pure imaginary or complex. An alternative approach to the spectrum at $\mu = 0$ can be found in Ref. [70].

6.2.2. Spectrum for $\mu = 0$ and N odd

The zeros of ϵ_N and $\zeta_N = 0$ yield the eigenvalues. Since the lattice constant for the α and the β chain is $2d$ as shown in Fig. 6.1, we thus set $\lambda^2 + a^2 + b^2 \;=\; 2ab\,\cos(2\,kd)$ following Eq. (4.1.13). Indeed, we find the dispersion relation $\lambda = E_\pm|_{\mu=0}$

$$E_\pm^{\mu=0} \;=\; \pm\sqrt{4t^2\,\cos^2(kd) \;+\; 4\Delta^2\sin^2(kd)} \tag{6.2.24}$$

in agreement with Eq. (5.1.6), after converting $a = \mathrm{i}(\Delta - t)$, $b = \mathrm{i}(\Delta + t)$ back into t, Δ. From Eq. (4.1.15), we have $\mathcal{F}(n) \propto \sin(2kd\,n)\,/\,\sin(2kd)$ and demanding $\epsilon_N = \zeta_N = 0$ gives the quantization constraints.

In case of N odd, we evaluate Eqs. (6.2.20), (6.2.22) at $n = (N-1)/2$ and the spectrum reads[2]

$$E_\pm^{\mu=0} \;=\; 0, \quad \text{(twofold degenerate)} \tag{6.2.25}$$

$$E_\pm^{\mu=0}(k_j d) \;=\; \pm\sqrt{4t^2\,\cos^2(k_j d) \;+\; 4\Delta^2\sin^2(k_j d)} \tag{6.2.26}$$

with $k_j d = j\pi/(N+1)$, $j = 1, \ldots, N$, $j \neq (N+1)/2$. Since each value of kd corresponds to two energy eigenvalues, we have in total $2N$, as expected. The excluded value $j = (N+1)/2$ corresponds to $2kd = \pi$, originating from the denominator $\sin(2kd)$ in both ϵ_N, ζ_N. For $N = 1$ we have only zero energy modes.

The limiting cases of either $t = 0$ and $\Delta = 0$ on the Eqs. (6.2.25), (6.2.26) reproduce our earlier findings in Eq. (6.1.2), (6.1.12) at $\mu = 0$ and odd N. Note, the zero energy mode from Eq. (6.2.25) enforces the $\pi/2$ shift of kd for $\Delta = 0$ in order to be incorporated into the equidistant quantization.

[2]The $\mu = 0$ case is intricate since the periodicity of the bulk dispersion relation is different from that of finite μ. One can restrict $kd \in (0,\,\pi/2)$ ($kd \in (\pi/2,\,\pi)$) for the α (β) chain and both together yield Eq. (6.2.26).

In the general case of both finite t and Δ, the Eqs. (6.2.25), (6.2.26) do not differentiate between $t/\Delta > 1$, $t/\Delta < 1$ and especially, we find one zero energy mode on each SSH-like chain. This originates from the peculiar bonding situation of the α, β chains in case of odd N as can be seen from Fig. 6.2 a). Since $|a| \neq |b|$, one end is always more weakly connected to the rest of the SSH-like chain. In Ch. 6.2.5, we demonstrate that the zero energy mode is an edge state residing at this end.

6.2.3. Spectrum for $\mu = 0$ and N even

In case of even N the bonding scenario changes as depicted in Fig. 5.2. Both ends of a given SSH-like chain are connected equally strong to the interior. This causes the presence of two decaying states on the SSH-like chain with the smaller hoppings value of a or b at its end and simultaneously none on the other. Still, the spatial distance between both chains is zero and experimentally one would observe two edge states at opposite ends of the Kitaev chain; this discrepancy is expressed in distinct quantization rules for both SSH-like chains.

6.2.3.1. Quantization rule for extended states

The quantization is generally not equidistant, but kept in terms of a transcendental equation as we discover soon. Here, the ratios $t/\Delta > 1$ and $t/\Delta < 1$ correspond to distinct situations. The ansatz $\lambda^2 + a^2 + b^2 = 2ab\,\cos(2kd)$ uses the convention $\mathrm{i}\sqrt{y} = ab$ in $x = 2\,\mathrm{i}\sqrt{y}\cos(2kd)$ from Eq. (4.1.13) with $x = \lambda^2 + a^2 + b^2$ and $y = -a^2b^2$.

Since $\zeta_N \neq \epsilon_N$ for even N, we get two quantization rules, one for each SSH-like chain. Eq. (4.1.15) states $\mathcal{F}(n) = (\mathrm{i}\sqrt{y})^{n-1}\sin(2kd\,n)/\sin(2kd)$ and from $\epsilon_N = 0$, we find

$$a\,\frac{\sin\left[kd\,(N+2)\right]}{\sin\left(2kd\right)} \;-\; b\,\frac{\sin\left(kd\,N\right)}{\sin\left(2kd\right)} \;=\; 0, \tag{6.2.27}$$

which can be simplified to

$$\Delta\,\frac{\cos\left[kd\,(N+1)\right]}{\cos(kd)} \;-\; t\,\frac{\sin\left[kd\,(N+1)\right]}{\sin(kd)} \;=\; 0. \tag{6.2.28}$$

The expression for $\zeta_N = 0$ follows from $\epsilon_N = 0$ by exchanging $a = \mathrm{i}(\Delta - t))$ with $b = \mathrm{i}(\Delta + t)$, i.e. $t \to -t$. Thus, the quantization rules for the Kitaev chain for even N and at $\mu = 0$ is

$$\tan\left[kd\,(N+1)\right] \;=\; \pm\frac{\Delta}{t}\,\tan\left(kd\right), \quad kd \neq 0 \tag{6.2.29}$$

where the positive (negative) sign is associated to the α (β) SSH-like chain. The solutions of Eq. (6.2.29) inserted into the dispersion relation from Eq. (5.1.6) at $\mu = 0$ give the eigenvalues, see Fig. 6.3. Notice that one can restrict the solutions of kd to be positive. We continue with discussing the properties of Eq. (6.2.29).

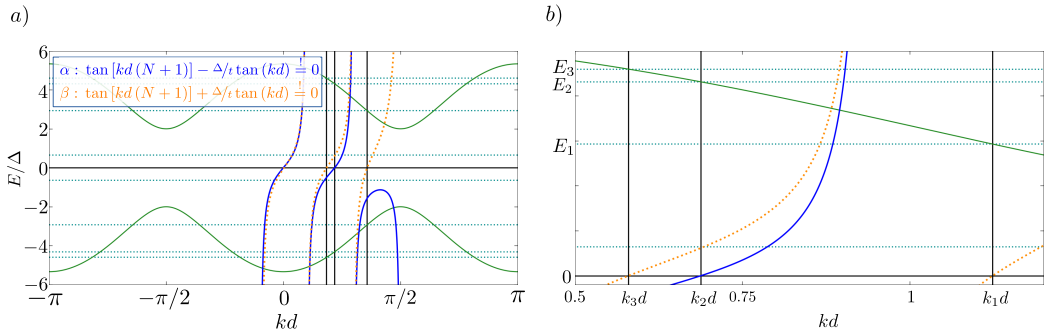

Figure 6.3.: Numerically calculated eigenvalues $\pm E_j (j = 0, 1, 2, 3)$ of the Kitaev chain with $N = 4$ sites, $t/\Delta = 4/1.5 \approx 2.66$, $\mu = 0$ depicted as horizontal dotted lines. The bulk dispersion relation $E_\pm(k)$ (green) in units of Δ is shown as a function of $kd \in [-\pi, \pi]$. a) The zeros of $\tan[kd(N+1) - \Delta/t \tan(kd)]$ (blue) and $\tan[kd(N+1) + (\Delta/t)\tan(kd)]$ (orange, dotted) quantize the real momenta $kd = k_j d$ as $k_{3,2,1} d \in \{0.58012, 0.68813, 1.12386\}$. The eigenvalues $\pm E_j \in \{\pm 4.59, \pm 4.31, \pm 2.93\}$ are correctly reproduced. b) Zoom of a) for $kd \in [0.5, 1.2]$. The in-gap energies $\pm E_0$ require a complex wavevector shown in Fig. 6.4.

First, the case of $\Delta = 0$ implies $\tan[kd(N+1)] = \sin[kd(N+1)] = 0$ and we receive our prior result from Eq. (6.1.2) at $\mu = 0$ back. Second, the effect of $t = 0$ is better visible from Eq. (6.2.28). Since $\cos[kd(N+1)] = 0$ is imposed, the wavevectors are shifted by $\pi/2$ compared to the prior $\Delta = 0$ case.

Alternatively, we can set $kd \to \tilde{k}d + \pi/2$ in Eq. (6.2.29) and one finds

$$\tan\left[\tilde{k}d(N+1)\right] = \pm\frac{t}{\Delta}\tan\left(\tilde{k}d\right), \quad \tilde{k}d \neq 0, \tag{6.2.30}$$

Eq. (6.2.29) with inverted ratio Δ/t. Here, the positive (negative) sign is still associated to the α (β) chain. The applied $\pi/2$ shift affects also the dispersion relation in Eq. (5.1.6) changing $\cos^2(kd) \to \sin^2\left(\tilde{k}d\right)$ etc. Thus, we recover the results from Eq. (6.1.12) at $\mu = 0$.

6.2.3.2. Quantization rule for edge states and criterion for their existence

Strictly speaking, we have not specified kd as real quantity and indeed Eq. (6.2.29) accounts also for the in-gap states. However, we can derive a more suitable quantization rule for them. We revisit our ansatz $\lambda^2 + a^2 + b^2 = 2ab\cos(2kd)$, which imposes only $\cos(2kd)$ to be real in general. Leaving the $\pi/2$ shift aside, we can simply replace $kd \to \mathrm{i}qd$ in order to receive a condition for edge states. We find

$$\tanh[qd(N+1)] = \pm\frac{\Delta}{t}\tanh(qd), \quad qd \neq 0 \tag{6.2.31}$$

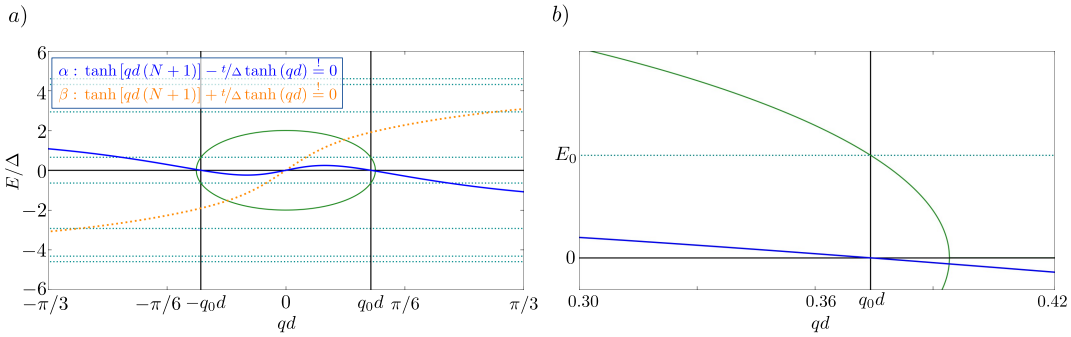

Figure 6.4.: Spectrum and the quantized wavevector $k_0 d = \mathrm{i}q_0 d + \pi/2$ for the Kitaev molecule with four sites and $t/\Delta = 4/1.5 \approx 2.66$ at $\mu = 0$. a) The ellipse in green shows the dispersion relation in units of Δ as a function of $kd = \mathrm{i}qd + \pi/2$, i.e. Eq. (6.2.32) with exchanged roles of t, Δ. The blue curve depicts $\tanh[qd(N+1)] - (t/\Delta)\tanh(qd)$, while $\tanh[qd(N+1)] + (t/\Delta)\tanh(qd)$ is shown dotted and in orange. The zero of the former quantizes the imaginary part of $k_0 d$ as $q_0 d = 0.37416$ and this yields the correct in gap energy $\pm E_0 = \pm 0.97$. b) Zoom of a) for better visibility of the intersection points.

and in case of $\tilde{k}d = kd + \pi/2 \to \mathrm{i}qd$ only the ratio Δ/t is inverted. For generic parameters, one is not able to extract the solution from Eq. (6.2.31) analytically. However, for specific values of t, Δ we can obtain qd and we discuss the implications in the next paragraph. As preparation, we give the restrictions on t, Δ such that provides Eq. (6.2.31) a solution.

We can understand the value of qd as the criterion for an intersection point of both sides in Eq. (6.2.31). Due to the symmetry of the quantization rule, we can restrict ourselves to positive qd. Solutions to Eq. (6.2.31) exist in case of $1 \leq |\Delta/t| \leq N+1$ ($kd \to \mathrm{i}qd$) or $1 \leq |t/\Delta| \leq N+1$ ($\tilde{k}d = kd + \pi/2 \to \mathrm{i}qd$). Only in the special case that $|t/\Delta| = N+1$ ($|\Delta/t| = N+1$) is true, we have the solution $qd = 0$ as can be seen better from Eq. (6.2.28). Our finding agrees with known results for ordinary SSH chains [101, 102].

Please note that the solution qd of Eq. (6.2.31) is always associated to the positive value $\pm\Delta/t$ ($\pm t/\Delta$). Thus, for $\Delta/t > 0$ ($\Delta/t < 0$) both decaying states are associated to the α (β) chain. This finding is intuitively clear from Fig. 6.1 b) as the ends of the α (β) chain are bound more weakly to the next Majorana sites in case of $\Delta/t > 0$ ($\Delta/t < 0$).

Before we turn to the physical implications imposed by the quantization rule in Eq. (6.2.31), we discuss the energy associated to qd. The replacement $kd \to \mathrm{i}qd$ on the

dispersion relation from Eq. (6.2.24) yields

$$E_{\pm}^{\mu=0}(qd) \;=\; \pm\sqrt{4t^2\cosh^2(qd) \;-\; 4\Delta^2\sinh^2(qd)}, \quad (|\Delta| \geq |t|) \tag{6.2.32}$$

and with exchanged roles of t and Δ for $|t| > |\Delta|$. More suitable is

$$E_{\pm}^{\mu=0}(qd) \;=\; \pm 2\min\left(\{|t|,\, |\Delta|\right\} \;\frac{\cosh(qd)}{\cosh\left[qd\,(N+1)\right]} \tag{6.2.33}$$

received via Eq. (6.2.31). The energy is usually finite and lies always inside the gap at $\mu = 0$.

6.2.3.3. Physical implication of the quantization rule

Since qd is the imaginary part of kd, we can define a decay length ξ_q by $1/\xi_q \coloneqq |q|/d = |\mathrm{Im}(k)|/d$. Then, Eq. (6.2.33) yields the exponential behavior $E_{\pm}^{\mu=0}(qd) \propto \exp(-L/\xi_q)$ setting[3] $L = Nd$. This behavior is typical for the energy of Majorana fermions and not restricted to the Kitaev chain [3, 7, 8, 19, 66].

Notice an important difference to the statement in section 5.4. We use here the decay length ξ_q extracted from the solution of the quantization rule and not ξ from Eq. (5.4.1) as one may expect. Although ξ_q is a continuous function in t, Δ, its value is quantized and we have in fact $\xi_q \equiv \xi_q(N)$.

The effect of different number of atoms N on ξ_q depends highly on the parameters t/Δ as we discuss next. In case of $|\Delta/t| \to 1$, i.e. around the Kitaev points, qd approaches infinity independent of N. Thus, $\xi_q \to 0$ in agreement with the Eq. (5.4.1). Remember, that ξ from Eq. (5.4.1) does not know about the system size. Since ξ and ξ_q differ not much close to the Kitaev point, a numerical investigation of the energy $E_{\pm}^{\mu=0}(qd)$ with ξ rather than ξ_q will show a good agreement.

In the limit $N \to \infty$ and $|\Delta/t| > 1$, the solution of Eq. (6.2.31) is $qd = \mathrm{arctanh}(|t/\Delta|)$. For $|t/\Delta| > 1$, the roles of t and Δ have to be exchanged. Since the argument inside the arctanh function is smaller than one, we can rewrite our findings. After some manipulations, we find the remarkable result

$$\lim_{N\to\infty} \xi_q \;=\; \frac{2d}{\left|\ln\left|\frac{\Delta-t}{\Delta+t}\right|\right|} \equiv \xi. \tag{6.2.34}$$

These two limiting cases wrongly suggest, that the quantization of qd provided by Eq. (6.2.31) has no implication. Next, we consider the rather non trivial case of finite N and $|\Delta/t| \to N+1$ ($|t/\Delta| \to N+1$), which is more interesting. Here, we have $qd \to 0$ as discussed above. In turn, we find $\xi_q(N) \to \infty$ and the associated eigenvalues $\pm 2\min\left(\{|t|,\, |\Delta|\right\}$ settle exactly on the upper/lower value of the bulk gap at $\mu = 0$. We demonstrate in the next section 6.2.4 that the associated eigenstates still decay, contrary to the intuitive interpretation of $\xi_q(N) \to \infty$.

[3] In order to be precise, the length of the Kitaev chain is actually $(N-1)d$.

Importantly though, Eq. (5.4.1) still claims a finite value for ξ, since this quantity does not depend on N. In perspective, ξ misses entirely the open boundary condition and the systems finite length. We return to this issue in more detail in section 6.7 after we discussed the quantization rule for generic parameters. As conclusion, the argumentation that the Kitaev chain hosts MZM in the limit of $\xi \ll N$ using the decay length from Eq. (5.4.1), is not justified for finite N without taking into account the systems parameters.

A final remark. The number of eigenvalues is always constant $2N$. The situation in which $|\Delta/t| \to N+1$ or $|t/\Delta| \to N+1$ holds marks a transition of a former in-gap to an extended out of gap state.

6.2.4. Eigenstates for even N

The technique to obtain the eigenvectors for the Kitaev chain is similar for both odd and even N, but appears to be more natural for the latter case. We denote the eigenvector to the Kitaev Hamiltonian in Eq. (6.2.5) as $\vec{\psi} = (\vec{v}_\alpha,\, \vec{v}_\beta)^{\mathrm{T}}$ in terms of the sublattice vectors $\vec{v}_{\alpha,\beta}$ associated to the SSH-like chains α and β. The spectrum of both subchains is non-degenerate. As such, we can treat both α and β independently and solve for

$$\vec{\psi}^{\alpha} = \begin{pmatrix} \vec{v}_\alpha \\ 0 \end{pmatrix}, \quad \vec{\psi}^{\beta} = \begin{pmatrix} 0 \\ \vec{v}_\beta \end{pmatrix} \tag{6.2.35}$$

as the eigenvectors of the entire system. Thus, the eigenvector problem $\mathcal{H}_{\mathrm{KC}}^{\mathrm{SSH}} \vec{\psi}^{\alpha,\,\beta} = \lambda\, \vec{\psi}^{\alpha,\,\beta}$ reduces to the one of the separated SSH-like states: $\mathcal{H}_\alpha\, \vec{v}_\alpha = \lambda\, \vec{v}_\alpha$, $\mathcal{H}_\beta\, \vec{v}_\beta = \lambda\, \vec{v}_\beta$. Mathematically, we obtain the eigenvectors of tridiagonal matrices based on and extending the results of [102]. Motivated by the unit cell associated to both SSH-like chains, we define $\vec{v}_{\alpha,\,\beta}$ as

$$\vec{v}_\alpha = \big(x_1,\, y_1,\, x_2,\, y_2,\, \ldots,\, x_{N/2},\, y_{N/2}\big)^{\mathrm{T}}, \tag{6.2.36}$$

$$\vec{v}_\beta = \big(\mathcal{X}_1,\, \mathcal{Y}_1,\, \mathcal{X}_2,\, \mathcal{Y}_2,\, \ldots,\, \mathcal{X}_{N/2},\, \mathcal{Y}_{N/2}\big)^{\mathrm{T}}, \tag{6.2.37}$$

where $l = 1, \ldots, N/2$ accounts for one cell and x_l, $\mathcal{X}_l$ (y_l, $\mathcal{Y}_l$) belong to the real space positions $j = 2l-1$ ($j = 2l$). As the notation suggests, x_1 (y_l) and $\mathcal{X}_1$ ($\mathcal{Y}_1$) are related and convert into each other by replacing $t \to -t$. This originates in the relation of $\mathcal{H}_{\alpha,\,\beta}$ which map into each other by replacing all $a = \mathrm{i}(\Delta - t)$ with $b = \mathrm{i}(\Delta + t)$ and vice versa, see Eqs. (6.2.6), (6.2.7). Thus, it is sufficient to solve only $\mathcal{H}_\alpha\, \vec{v}_\alpha = \lambda\, \vec{v}_\alpha$; we find two boundary equations

$$a\, y_1 = \lambda\, x_1, \tag{6.2.38}$$

$$-a\, x_{N/2} = \lambda\, y_{N/2} \tag{6.2.39}$$

and

$$a\, y_{l+1} - b\, y_l = \lambda\, x_{l+1}, \tag{6.2.40}$$

$$b\, x_{l+1} - a\, x_l = \lambda\, y_l \tag{6.2.41}$$

for $l = 1, \ldots N/2 - 1$ from the interior of the matrix in case of $N \geq 2$. Before we solve for x_l, y_l in case of arbitrary $a \neq 0$ and $b \neq 0$, we first turn to the special cases at the Kitaev points $t = \pm\Delta$, i.e. $a = 0$ or $b = 0$.

The eigenvector equations can be used to determine whether zero energy is possible or not. Demanding $\lambda = 0$ and $a \neq 0$ (b arbitrary) yields $x_1 = \ldots, = x_{N/2} = y_1 = \ldots = y_{N/2} = 0$, i.e. $\vec{v}_\alpha = \vec{0}$, and we thus do not find an eigenvector. Instead only for $a = 0$, zero energy is allowed and corresponds to an eigenstate localized at both ends of the Kitaev chain on subchain α with $x_1 \neq 0$, $y_{N/2} \neq 0$ as the only non zero entries.

A second rather simple case is $a = 0$, but λ finite. This implies $b = 2\mathrm{i}t \neq 0$ (otherwise the Kitaev Hamiltonian is zero). The Eqs. (6.2.40), (6.2.41) yield the energies $\lambda = \pm 2t$, each being $(N-2)/2$ times degenerate, which belong to dimerized pairs $(y_l,\, x_{l+1}) = \frac{1}{\sqrt{2}}(1,\, \pm\mathrm{i})$ with $l = 1, \ldots,\, N/2 - 1$.

The last remaining case is $b = 0$ and thus $a = -2\mathrm{i}t \neq 0$. The Eqs. (6.2.40), (6.2.41) imply now $\lambda = \pm 2t$ and we find $(x_l,\, y_l) = \frac{1}{\sqrt{2}}(1,\, \pm\mathrm{i})$ with $l = 1, \ldots,\, N/2$.

All special cases were analyzed and we turn next to $a \neq 0$, $b \neq 0$, where the constraint on a excludes directly $\lambda = 0$. Next, we use the Eqs. (6.2.40), (6.2.41) to extend $x_1, \ldots,\, x_{N/2},\, y_1, \ldots,\, y_{N/2}$ to the sequences x_l, y_l with $l \in \mathbb{Z}$; the implicit dependence on N of the recursion relations drops and yet $\vec{v}_\alpha$ in Eq. (6.2.36) remains unchanged. Further, the boundary conditions from Eqs. (6.2.38), (6.2.39) simplifies to

$$y_0 \;=\; x_{\frac{N}{2}+1} \;=\; 0 \tag{6.2.42}$$

using Eqs. (6.2.40) (6.2.41). Hence, the wave function $\vec{\psi}^\alpha$ vanishes on the "sites" $j = 0$ and $j = N + 1$. Since $\lambda \neq 0$, we can disentangle x_l and y_l by multiplication with λ on the recursion relations Eqs. (6.2.40), (6.2.41) yielding

$$x_{l+1} \;=\; \frac{\lambda^2 \,+\, a^2 \,+\, b^2}{ab}\, x_l \;-\; x_{l-1}, \tag{6.2.43}$$

$$y_{l+1} \;=\; \frac{\lambda^2 \,+\, a^2 \,+\, b^2}{ab}\, y_l \;-\; y_{l-1} \tag{6.2.44}$$

and $l \in \mathbb{Z}$. The solution to x_l, y_l can be adopted from Eqs. (4.1.1) - (4.1.17) with $x = (\lambda^2 + a^2 + b^2)/(ab)$, $y = -1$ and $2d$ as lattice constant, i.e. $d \to 2d$. We choose further $\sqrt{y} = -i$ without restrictions. The bulk dispersion relation of the Kitaev chain at $\mu = 0$ in Eq. (5.1.6) is reproduced from the standard ansatz $x = 2\mathrm{i}\sqrt{y}\cos(2kd)$, where $\lambda^2 + a^2 + b^2 = 2ab\cos(2kd)$ and $E_\pm^{\mu=0}(k) = \lambda$ holds. Thus, Eq. (4.1.17) gives the solutions for x_l, y_l as

$$x_l \;=\; x_1\, \mathcal{F}(l) \;-\; x_0\, \mathcal{F}(l-1), \tag{6.2.45}$$

$$y_l \;=\; y_1\, \mathcal{F}(l), \tag{6.2.46}$$

$$\mathcal{F}(l) \;=\; \frac{\sin(2kd\, l)}{\sin(2kd)} \tag{6.2.47}$$

where we directly used the boundary condition $y_0 = 0$ from Eq. (6.2.42). Leaving the required quantization for kd aside for a moment, we need the initial values x_1, x_0 and

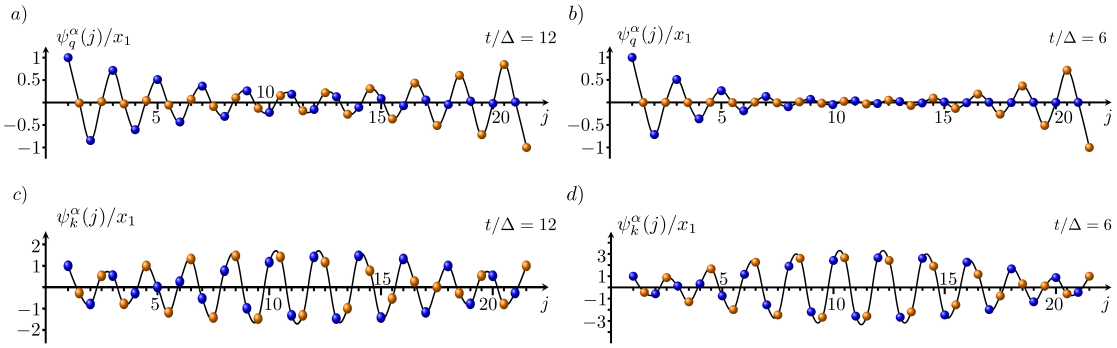

Figure 6.5.: The in-gap ψ_q^α and lowest energy bulk state ψ_k^α of the Kitaev chain with $N = 42$ sites for $t/\Delta = 12$ (left column) and $t/\Delta = 6$ (right column) at $\mu = 0$ are illustrated. All states are associated with the α chain. The blue (orange) spheres display x_l/x_1, $(\mathrm{i}y_l/x_1)$ at site $j = 2l-1$ ($j = 2l$) for $l = 1, l \ldots, N/2$ and the black line is given as guide to the eye. a) The decaying state associated with $qd = 0.0833983$, $E/\Delta = 0.1111$ is mostly localised around both ends of the system, yet reaches into the interior. b) For smaller t/Δ, the decaying state belongs now to $qd = 0.168236$, $E/\Delta = 2.923 \times 10^{-3}$ and gets more localized. c) The extended states for $t/\Delta = 12$ is associated with $kd = 1.47822$, $E/\Delta = 2.98132$ and largest around the chain's center. d) The weight of the extended state ($kd = 1.48686$, $E/\Delta = 2.14094$) diminishes around the ends for decreasing t/Δ.

y_1 in order to determine the eigenvectors. Since an eigenvector is only defined up to multiples, we can choose at least one entry freely. From Eq. (6.2.40) at $l = -1, 0$ we find $y_1 = E_\pm^{\mu=0}(k)\, x_1/a$, $y_1 = E_\pm^{\mu=0}(k) x_0/b$; thus, if we choose a value for x_1, y_1 and x_0 are fixed due to $E_\pm^{\mu=0}(k) \neq 0$, $a \neq 0$, $b \neq 0$. We find

$$\frac{x_l}{x_1} = \frac{\sin(2kd\,l)}{\sin(2kd)} - \frac{b}{a}\frac{\sin\left[2kd\;(l-1)\right]}{\sin(2kd)}, \tag{6.2.48}$$

$$\frac{y_l}{x_1} = \frac{E_\pm^{\mu=0}(k)}{a}\frac{\sin(2kd\,l)}{\sin(2kd)}, \tag{6.2.49}$$

where x_1 as the only one degree of freedom excludes any energy degeneracy. Note x_1 can be set as the normalization constant once kd is known. As we see, the values of x_l can be chosen as real and then y_l becomes imaginary.

Despite having a form for x_l, y_l we do not have their values, since the boundary condition from Eq. (6.2.42) is not yet satisfied. Demanding $x_{\frac{N}{2}+1} = 0$ grants directly Eq. (6.2.27) and the wave vectors k get quantized according to Eq. (6.2.29) (with the positive sign). For real kd, the values for x_l, y_l in Eqs. (6.2.48), (6.2.49) correspond to the extended states; by replacing $kd \to \mathrm{i}qd$ ($kd \to \mathrm{i}qd + \pi/2$) for $|\Delta| > |t|$ ($|t| > |\Delta|$), x_l, y_l belong to decaying states.

Although we have solved the problem, one can find a simplified expression for x_l, y_l

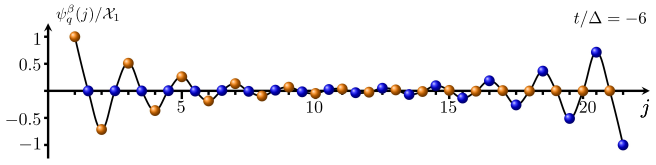

Figure 6.6.: In-gap state ψ_q^β for $N = 42$ and $t/\Delta = -6$ at $\mu = 0$. The blue (orange) spheres belong to $\mathcal{X}_l/\mathcal{X}_1$ ($\mathrm{i}\mathcal{Y}_l/\mathcal{X}_1$) at the positions $j = 2l - 1$ ($j = 2l$) and the black line is a guide to the eye. The Majorana operators γ_j^A, γ_j^B are exchanged w.r.t to the α chain, reflected by the sphere's colour change. The decaying state is associated with $qd = 0.168236$ and $E/\Delta = 2.923 \times 10^{-3}$.

namely

$$x_l = \mathcal{F}(N/2 + 1 - l), \tag{6.2.50}$$

$$y_l = \mp \mathrm{i}\,\mathcal{F}(l) \tag{6.2.51}$$

as we showed in appendix G. The value of x_1 was set such that $x_{N/2} = 1$; thus all x_l (y_l) are real (pure imaginary). The signs in Eq. (6.2.51) account for the negative/positive energy at a given kd and have to be chosen in accordance to Eqs. (6.2.38), (6.2.39). The particle-hole symmetry $\mathcal{P} = \mathbb{1}_{2N}\mathcal{K}$ converts the positive and negative energy solutions at given wavevector into each other, since $\mathcal{F}(l)$ is always real[4]. Please notice, the boundary condition from Eq. (6.2.42) is satisfied automatically in this representation, but still kd follows from the quantization rule in Eq. (6.2.27) with the positive sign for the α chain. Further, the expressions for x_l, y_l hold also for the decaying states and are again obtained by the replacement $kd \to \mathrm{i}qd$ ($kd \to \mathrm{i}qd + \pi/2$) for $|\Delta| > |t|$ ($|t| > |\Delta|$).

In Fig. 6.5, we visualized the entries x_l, $\mathrm{i}y_l$ for decaying states and the bulk states with smallest positive energy belonging to the SSH-like chain α for the parameters $t/\Delta = 12$ and $t/\Delta = 6$, respectively. As expected for ratios of $|t/\Delta|$ (analogously $|\Delta/t|$) close to one, the decaying states localize mostly around the edges but extend further into the system for larger ratios. Surprisingly, the extended states are enhanced around both ends. This is not due to a complex wavevector but rather a consequence of the non-equidistant quantization of kd and the Majorana sublattices. The entries x_l, y_l behave as separate standing waves, see Eqs. (6.2.50), (6.2.51) and the quantized real kd moves their respective nodes away from the system's ends. Therefore, the increase of x_l (y_l) towards the first (last) site reflects the beginning of the next oscillation and the finite size prevents simply a new full period, i.e. x_l (y_l) are *locally* larger around the ends. A complex wavevector, on the contrary, puts the global maximum of the wavefunction at the ends. We will see later that the enhanced weight of the bulk wave functions causes a revival of the Andreev reflection process in the non-linear transport regime later.

In section 6.2.2, we discussed the implications of $|t/\Delta| \to N + 1$ or $|\Delta/t| \to N + 1$ associated to $qd \to 0$. Here, we can finally discuss the corresponding eigenstates and

[4] $\mathcal{F}(l)$ obeys the Eqs. (6.2.43), (6.2.44) as well, and the statement follows immediately since the coefficients there and the initial values 0, 1 of $\mathcal{F}(l)$ are all real.

their energy is $\pm 2\min\{t, \Delta\}$. Since $\sinh(2qd\,j)/\sinh(2qd) \to j$ for $qd \to 0$ holds with some number j, we find from Eqs. (6.2.50), (6.2.51) that

$$\lim_{qd\to 0} x_l = \frac{N}{2} + 1 - l, \tag{6.2.52}$$

$$\lim_{qd\to 0} y_l = \mp \mathrm{i}\, l. \tag{6.2.53}$$

Thus, the eigenstate decays (grows) linearly on the Majorana sites A (B) associated to the SSH-like chain α. Since $qd = 0$ implies $\xi_q = \infty$ as discussed earlier, the fact that this state still decays is remarkable.

Last but not least, the eigenstates formed by x_l, y_l are fermionic as one can see at best from Eqs. (6.2.50), (6.2.51). The operator $\hat{\psi}_\alpha^\dagger$ creating the eigenstate $\vec{\psi}^\alpha$ from Eq. (6.2.35) is

$$\hat{\psi}_\alpha^\dagger = \frac{1}{v_\alpha} \sum_{l=1}^{N/2} \left[x_l \left(\gamma_{2l-1}^A\right)^\dagger + y_l \left(\gamma_{2l}^B\right)^\dagger \right] \tag{6.2.54}$$

since x_l (y_l) is associated to γ_j^A (γ_j^B) at the real space position $j = 2l - 1$ ($j = 2l$) and v_α is the norm of $\vec{v}_\alpha$. The anticommutation relation of the Majorana operators γ^A, γ^B given in Eq. (5.3.2) shows that

$$\left(\hat{\psi}_\alpha^\dagger\right)^2 = \frac{1}{2v_\alpha^2} \sum_{l=1}^{N/2} \left(x_l^2 + y_l^2\right), \tag{6.2.55}$$

where we used $\left(\gamma_l^A\right)^2 = \left(\gamma_l^B\right)^2 = 1/2$. Reordering the sum in Eq. (6.2.55) and using the relations of y_l and x_l given in Eqs. (6.2.50), (6.2.51), i.e. $E_\pm(k) \neq 0$, impose $\left(\hat{\psi}_\alpha^\dagger\right)^2 = 0$ and we have a fermionic state. This holds analogously for the eigenstates assigned to the β chain, since one has only to exchange a's and b's, i.e. $t \to -t$, inside the expressions of chain α. We are left to deal with odd N at $\mu = 0$.

6.2.5. Eigenstates for odd N

We follow here the same strategy as for the N even case. Although for odd N both SSH-like chains share the same spectrum, one can still decompose the eigenstates as

$$\vec{\psi}^\alpha = \begin{pmatrix} \vec{v}_\alpha \\ 0 \end{pmatrix}, \quad \vec{\psi}^\beta = \begin{pmatrix} 0 \\ \vec{v}_\beta \end{pmatrix}. \tag{6.2.56}$$

Only the structure of $\vec{v}_\alpha$ ($\vec{v}_\beta$)

$$\vec{v}_\alpha = \left(x_1, y_1, x_2, y_2, \ldots, x_{\frac{N-1}{2}}, y_{\frac{N-1}{2}}, x_{\frac{N+1}{2}}\right)^{\mathrm{T}}, \tag{6.2.57}$$

$$\vec{v}_\beta = \left(\mathcal{X}_1, \mathcal{Y}_1, \mathcal{X}_2, \mathcal{Y}_2, \ldots, \mathcal{X}_{\frac{N-1}{2}}, \mathcal{Y}_{\frac{N-1}{2}}, \mathcal{X}_{\frac{N+1}{2}}\right)^{\mathrm{T}}, \tag{6.2.58}$$

has to be adapted. We still need only to solve the eigenvector problem for one chain, since both problems convert into each other and solving $\mathcal{H}_{\mathrm{KC}}^{\mathrm{SSH}}\vec{\psi}^{\alpha} = \lambda\,\vec{\psi}^{\alpha}$ reduces to $\mathcal{H}_{\alpha}\,\vec{v}_{\alpha} = \lambda\,\vec{v}_{\alpha}$ again. The entries of $\vec{v}_{\alpha}$ obey

$$b\,x_{i+1} - a\,x_i = \lambda\,y_i, \tag{6.2.59}$$

$$a\,y_{l+1} - b\,y_l = \lambda\,x_{l+1}, \tag{6.2.60}$$

with $l = 1, \ldots \frac{N-3}{2}$, $i = 1, \ldots, \frac{N-1}{2}$ accounting for the different numbers of x's and y's. We use the abbreviations $a = \mathrm{i}(\Delta - t)$, $b = \mathrm{i}(\Delta + t)$ as usual. The realisation of the open boundary condition changes

$$a\,y_1 = \lambda\,x_1, \tag{6.2.61}$$

$$-b\,y_{\frac{N-1}{2}} = \lambda\,x_{\frac{N+1}{2}} \tag{6.2.62}$$

only at the r.h.s of the Kitaev chain, since we added (removed) there a single site compared to N even. Let us shortly discuss the Kitaev points $a = 0$ or $b = 0$ for completeness and we give only results for non zero entries of $\vec{v}_{\alpha}$. At $a = 0$, $b \neq 0$, we can find the energy $\lambda = \pm 2t \neq 0$ corresponding to the dimerized pairs $(y_i,\, x_{i+1}) = \frac{1}{\sqrt{2}}(1,\, \mp\mathrm{i})$, $i = 1, \ldots (N-1)/2$ between neighbouring sites. In contrast, $b = 0$, $a \neq 0$ amounts to the on-site pairing $(x_i,\, y_i) = \frac{1}{\sqrt{2}}(1,\, \pm i)$ with energy $\lambda = \pm 2t \neq 0$ and $i = 1, \ldots (N-1)/2$. Next, we consider zero energy. The eigenvector system yields only a single one zero mode[5], which is fully localized at the left (right) end $x_1 = 1$ ($x_{\frac{N+1}{2}} = 0$) for $a = 0$, $b \neq 0$ ($a \neq 0$, $b = 0$).

Generally, even for both $a \neq 0$, $b \neq 0$ a zero energy mode exists in agreement with our prior findings in Ch. 6.2.2. One can use Eq. (6.2.59) at $\lambda = 0$ repeatedly and after converting a, b back into t, Δ respectively, one finds

$$x_l = \left(\frac{\Delta - t}{\Delta + t}\right)^{l-1} x_1 \tag{6.2.63}$$

for $l = 1, \ldots, (N+1)/2$. Notice that Eq. (6.2.60) and the boundary condition always impose $y_1 = y_2 = \ldots = y_{\frac{N-1}{2}} = 0$ and the value for x_1 is chosen as the normalization constant. As we see, the relative sign between t, Δ determines which end this zero energy mode is localized; for $t/\Delta > 0$ ($t/\Delta < 0$) it decays away from the left (right) end, starting from the first (last) site. This behaviour becomes clear by inspecting Fig. 6.2 a), where we see that the zero energy mode is always localized at the end connected by the weaker binding a or b to next site. Further, the decay length extracted from Eq. (6.2.63) agrees with the one given in Eq. (5.4.1) prior.

Next, we turn to the extended states with real wave vector kd for $a \neq 0$, $b \neq 0$ and as a first step we extend x_l, y_l to $l \in \mathbb{Z}$. Thus, the index limitations in Eqs. (6.2.59),

[5]The second zero energy mode of the Kitaev chain belongs to the SSH-like chain β, not to α. This state is localized always at the opposite end compared to the one of the α chain, due to the exchange of a and b.

(6.2.60) drop, i.e. they imitate Eqs. (6.2.40), (6.2.41) from the former even N case. The solutions of x_l, y_l follow from the same steps as for even N and using Eq. (4.1.17) grants

$$x_l = x_1\,\mathcal{F}(l) - x_0\,\mathcal{F}(l-1), \tag{6.2.64}$$

$$y_l = y_1\,\mathcal{F}(l) - y_0\,\mathcal{F}(l-1), \tag{6.2.65}$$

$$\mathcal{F}(l) = \frac{\sin(2kd\,l)}{\sin(2kd)} \tag{6.2.66}$$

and $\lambda = E_{\pm}^{\mu=0}(k)$ is the dispersion relation of the Kitaev chain from Eq. (5.1.6) at $\mu = 0$. Further, the open boundary conditions from Eqs. (6.2.61), (6.2.62) transform into

$$y_0 = y_{\frac{N+1}{2}} = 0, \tag{6.2.67}$$

i.e. we have that $\vec{\psi}^{\alpha}$ vanishes on the sites $j = 0$ and $j = N+1$. However, the realization of the boundary condition changed solely to y and from Eq. (6.2.65) we get immediately that $0 = y_{\frac{N+1}{2}} \propto \mathcal{F}(N+1/2)$. Hence, the quantization of kd follows from

$$\frac{\sin\left[2kd\left(\frac{N+1}{2}\right)\right]}{\sin(2kd)} = 0. \tag{6.2.68}$$

and we find $kd = n\pi/(N+1)$ for $n = 1, \ldots, (N-1)/2$. The spectrum and the quantization for the β chain follows by exchanging a's and b's, i.e. $t \to -t$; thus, both SSH-like chains share the same spectrum. The momenta assigned to the β chain can be shifted by $\pi/2$ without changing the spectrum and one receives Eq. (6.2.26) back, for α, β together. However, this imposes a phase shift for the eigenvectors and so we use still $kd = n\pi/(N+1)$, $n = 1, \ldots, (N-1)/2$ for them. At last, Eq. (6.2.59) and Eq. (6.2.61) at $i = 0$, yield $y_1 = E_{\pm}^{\mu=0}(k)\,x_1/a$, $x_0 = b\,x_1/a$ and our solutions for x_l, y_l become

$$\frac{x_l}{x_1} = \mathcal{F}(l) - \frac{b}{a}\,\mathcal{F}(l-1), \tag{6.2.69}$$

$$\frac{y_l}{x_1} = \frac{E_{\pm}^{\mu=0}(k)}{a}\,\mathcal{F}(l) \tag{6.2.70}$$

and x_1 can be chosen freely, for example as the normalization constant. The results are in agreement with Ref. [101, 102]. The last two expressions for x_l, y_l determine the vector $\vec{v}_{\alpha}$ and in turn the eigenstate $\vec{\psi}^{\alpha}$ is found.

Similar to the N even case, the operator $\hat{\psi}_{\alpha}^{\dagger}$

$$\hat{\psi}_{\alpha}^{\dagger} = \frac{1}{v_{\alpha}}\left[\sum_{l=1}^{\frac{N+1}{2}} x_l\,\left(\gamma_{2l-1}^{A}\right)^{\dagger} + \sum_{l=1}^{\frac{N-1}{2}} y_l\,\left(\gamma_{2l}^{B}\right)^{\dagger}\right] \tag{6.2.71}$$

creates the eigenstate $\vec{\psi}^{\alpha}$ from Eq. (6.2.56), since x_l y_l is associated to γ_j^A (γ_j^B) at position $j = 2l-1$ ($j = 2l$) and v_{α} is the norm of $\vec{v}_{\alpha}$. In case of $E_{\pm}^{\mu=0}(k) \neq 0$, i.e. for x_l, y_l from Eqs. (6.2.69), (6.2.70) we find that $\left(\hat{\psi}_{\alpha}^{\dagger}\right)^2 = 0$, since x_l/x_1 (y_l/x_1) is real (pure

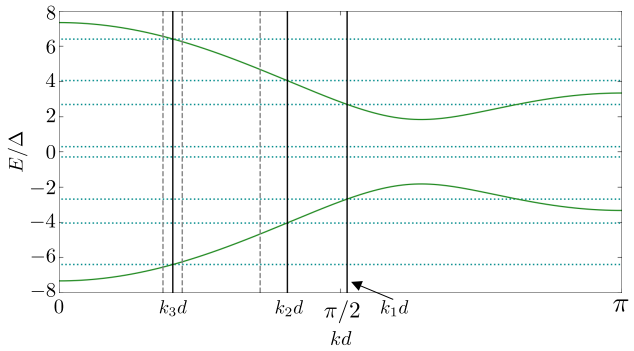

Figure 6.7.: Spectrum and quantized wavevectors of the Kitaev chain with four sites and non zero chemical potential. The dispersion relation is shown in units of Δ (green) and its former π periodicity at $\mu = 0$ switches to 2π, see Eq. (5.1.6). The momenta $k_{3,2,1}d \in \{0.6360, 1.2753, 1.6086\}$ obeying the general quantization rule from Eq. (6.3.28), reproduce the numerically calculated eigenvalues. The gray dashed lines display the former wavevectors at $\mu = 0$. Significantly, the quantization is influenced by the chemical potential. As parameters were chosen $t/\Delta = 4/1.5 \approx 2.66$ and $\mu/\Delta = 2$ corresponding to the energies $\{\pm 0.29, \pm 2.69, \pm 4.05, \pm 6.402\}$ (in units of Δ).

imaginary) and x_l, y_l exactly cancel each other. In contrast the zero energy mode given in Eq. (6.2.63) corresponds to $\left(\hat{\psi}_\alpha^\dagger\right)^2 = 1/2$, since the value of all y_l for this particular state are zero; thus, a cancellation of the x_l terms is prevented.

We have now investigated all special parameter settings and we have merely to generalize the results at $\mu = 0$ for finite chemical potential.

6.3. The chiral basis

A first impression the influence of a finite μ on the eigenvalues can be extracted from Fig. 6.7. We discover not only that the eigenvalues changed compared to the prior $\mu = 0$ case as indicated by the bulk dispersion relation in Eq. (5.1.6), but the quantized wavevectors as well. We have thus to understand $k = k(\mu, t, \Delta)$ for a finite system, which is possibly surprising, but we do not discuss the reasons immediately and rather prepare for the discussion.

From the analytical point of view, we have to adjust to the new situation. As we see from Fig. 6.8, the former separated SSH-like chains couple due to a finite chemical potential; thus the representation in terms of these chains lost its advantage. Since we aim particularly for the parameter setting $t \neq \pm\Delta$, the problem of solving for the eigenvalues of the Kitaev chain cannot be reduced to independent subparts of the system anymore. For further calculation, we chose the so called chiral basis $\hat{\psi}_\mathrm{c} \coloneqq \left(\gamma_1^A, \gamma_2^A, \ldots, \gamma_N^A, \gamma_1^B, \gamma_2^B, \ldots, \gamma_N^B\right)^\mathrm{T}$ as a new representation, because the Kitaev Hamiltonian does not include $\gamma_j^A\,\gamma_{j'}^A$ nor $\gamma_j^B\,\gamma_{j'}^B$ $(j, j' = 1, \ldots, N)$ contributions. In terms

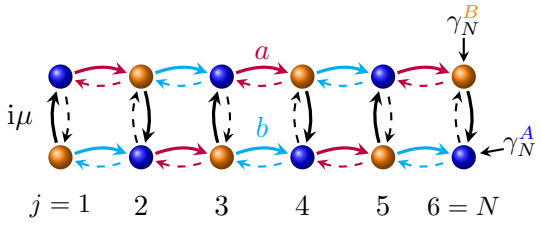

Figure 6.8.: For finite μ, both SSH-like chains are coupled by $\mathrm{i}\mu$ ($-\mathrm{i}\mu$) depicted as solid (dashed) arrows. At finite chemical potential, the SSH-like chains are not separated and no qualitative distinction between even and odd N can be found.

of $\hat{\psi}_\mathrm{c}$ we find that the Kitaev BdG Hamiltonian

$$\hat{H}_\mathrm{KC} = \frac{1}{2}\hat{\psi}_\mathrm{c}^\dagger \mathcal{H}_\mathrm{c}\, \hat{\psi}_\mathrm{c} \tag{6.3.1}$$

is expressed by a block off-diagonal matrix $\mathcal{H}_\mathrm{c}$

$$\mathcal{H}_\mathrm{c} = \begin{bmatrix} 0_{N,N} & h \\ h^\dagger & 0_{N,N} \end{bmatrix}. \tag{6.3.2}$$

The matrix h accounts for terms of the form $\gamma_j^A \gamma_{j'}^B$ and is thus not hermitian, but tridiagonal

$$h = \begin{bmatrix} -\mathrm{i}\,\mu & a & & & & & \\ -b & -\mathrm{i}\,\mu & a & & & & \\ & -b & -\mathrm{i}\,\mu & a & & & \\ & & \ddots & \ddots & \ddots & & \\ & & & -b & -\mathrm{i}\,\mu & a & \\ & & & & -b & -\mathrm{i}\,\mu & a \\ & & & & & -b & -\mathrm{i}\,\mu \end{bmatrix}_{N\times N}, \tag{6.3.3}$$

since Eq. (5.3.5) contains only nearest neighbor and onsite terms. In this basis all A-type and B-type Majorana form sublattices and the chiral symmetry $\mathcal{C}$ becomes diagonal

$$\mathcal{C} = \begin{bmatrix} \mathbb{1}_N & \\ & -\mathbb{1}_N \end{bmatrix}, \tag{6.3.4}$$

hence the name: chiral basis. For an arbitrary parameter setting, $\hat{\psi}_\mathrm{c}$ is possibly the best way to express the Kitaev Hamiltonian and as first verification we turn directly to the zero energy criterion.

6.3.1. Zero energy lines and the determinant formula

Contrary to generic eigenvalues, zero energy can be found from a vanishing determinant. This treatment avoids the usage of the otherwise required quantization rule. Although

the determinant is basis invariant, the chiral basis especially allows an immediate access due to the block off diagonal character of $\mathcal{H}_{\mathrm{c}}$. We exploit Eq. (6.3.2) and apply exemplarily the theorem provided in Ref. [99]. This yields

$$\det\left[\mathcal{H}_{\mathrm{c}}\right] \,=\, \det\left[-hh^{\dagger}\right] \,=\, (-1)^{N}|\det\left[h\right]|^{2}, \tag{6.3.5}$$

where we used standard properties of determinants in the second step. The prefactor $(-1)^{N}$ reflects the particle-hole symmetry of the Kitaev chain. Besides the fact that we need only to estimate $\det\left[h\right]$ to get $\det\left[\mathcal{H}_{\mathrm{c}}\right]$, the striking advantage of Eq. (6.3.5) resides in the fact that the zeros of the former are the zeros of the latter. Even better: there is no necessity to calculate $\det\left[h\right]$, as we know the eigenvalues η_{n} of h. They are complex (h is not hermitian) and read [88–90]

$$\eta_{n} \,=\, -\mathrm{i}\mu \,+\, 2\sqrt{\Delta^{2}-t^{2}}\,\cos\left(\frac{n\pi}{N+1}\right), \quad n=1\,\ldots,\,N \tag{6.3.6}$$

for all values of t, $\Delta \in \mathbb{R}$, as instantly follows from Eq. (2.2.15), since the matrix M given in (2.2.11) matches h. In fact, the Kitaev chain hosts zero energy modes if a single η_{n} vanishes. The condition $\eta_{n}=0$ imposed on Eq. (6.3.6) grants

$$\mu_{n} \,=\, 2\sqrt{t^{2}-\Delta^{2}}\,\cos\left(\frac{n\pi}{N+1}\right), \quad n=1\,\ldots,\,N, \tag{6.3.7}$$

where we replaced $\mu \to \mu_{n}$ in order to separate it from generic values of the chemical potential and to reflect its discreteness. Naively, one might expect that Eq. (6.3.7) holds for all values of t, Δ, since the parental expression in Eq. (6.3.6) does. Nonetheless, the chemical potential is restricted to real values[6] and thus Eq. (6.3.7) generally indicates zero energy only for $t^{2} \geq \Delta^{2}$, with exactly one exception: For odd N, n can assume the value $1 \leq (N+1)/2 \leq N$ causing the cosine in Eq. (6.3.7) to vanish, such that $\mu_{N+1/2}=0$ holds for arbitrary t, Δ. This specific situation refers back to our prior findings of the spectrum in Eq. (6.2.25) and to the related zero energy mode from Eq. (6.2.63). Our zero energy criterion in Eq. (6.3.7) agrees with the findings in [69–72, 75]. Notice that the zero energy criterion are associated to fermionic parity switches [3, 71, 103, 104]

For illustration, the zero energy lines, which we henceforth call "Majorana lines", following from Eq. (6.3.7) are depicted in Fig. 6.9 for both even and odd N and a numerical result for the smallest positive eigenvalue of $\mathcal{H}_{\mathrm{c}}$ is given in 6.10 for comparison. Although we cannot discuss now the physical reasons behind Eq. (6.3.7) without analysing the quantization rule, we are certainly on the correct track in our attempt to include a finite chemical potential.

We return now to Eq. (6.3.5) and determine $\det\left[h\right]$ next as an intermediate step for $\det\left[\mathcal{H}_{\mathrm{c}}\right]$. The tridiagonal structure of h allows us to use the recursion formula given in Ref. [78] and straightforwardly one finds

$$\det\left[h\right] \,=\, i^{N}\,\frac{r_{+}^{N+1}-r_{-}^{N+1}}{r_{+}-r_{-}} \tag{6.3.8}$$

[6] In a mathemtical context, where μ does not denote the chemical potential and is allowed to be complex, Eq. (6.3.7) holds without any restriction as Eq. (6.3.6) does.

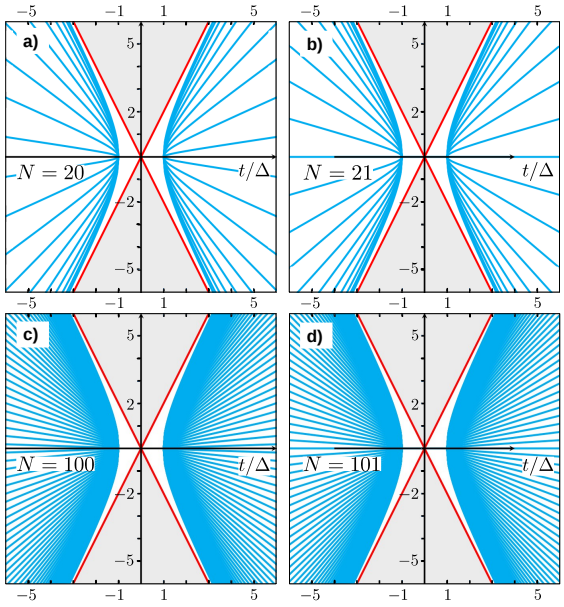

Figure 6.9.: Zero energy lines of the finite size Kitaev chain with open boundary conditions. Zero energy is restricted to parameters given in Eq. (6.3.7) associated to the blue curves. The phase boundary in the topological phase diagram is visualized by the red lines. a) For small even N and $\mu = 0$, zero energy is reached only at the Kitaev points $|t| = |\Delta|$, from which generally all Majorana lines depart. b) For (small) odd N, the entire horizontal axis corresponds now to $E = 0$. c) Increasing the number of sites causes a larger density of lines. d) Apart from the horizontal axis, large odd N behave similar as large even N. (Figure is taken from [4])

with $2\,r_\pm = -\mu \pm \sqrt{\mu^2 + 4\,(\Delta^2 - t^2)}$ for all μ, t and Δ. Thus, we find

$$\det\left[\mathcal{H}_\mathrm{c}\right] = (-1)^N \left| \frac{r_+^{N+1} - r_-^{N+1}}{r_+ - r_-} \right|^2 . \tag{6.3.9}$$

and a deeper analytic investigation of Eq. (6.3.9) confirms our earlier findings that zero energy is exclusively reached for the parameter settings given by Eq. (6.3.7).

Further, Eq. (6.3.9) contains the main information about the in-gap energies, although they may be finite as we explain now. As we see from Fig. 6.10 and as is stated in the literature [3, 13, 72] the energy of the topological edge states can abruptly increase for small parameter changes. Though all energies depend on the parameters in a complicated manner, the in-gap energy is more sensitive in this respect. Thus, the product of all eigenvalues, i.e. Eq. (6.3.9), contains a slow varying piece, namely the product of all out-of gap excitations, and the possibly rabidly changing in-gap energies. Although we cannot separate both contributions in Eq. (6.3.9), we can nonetheless hope for a qualitative agreement between the parameter regions in which the in-gap energy is

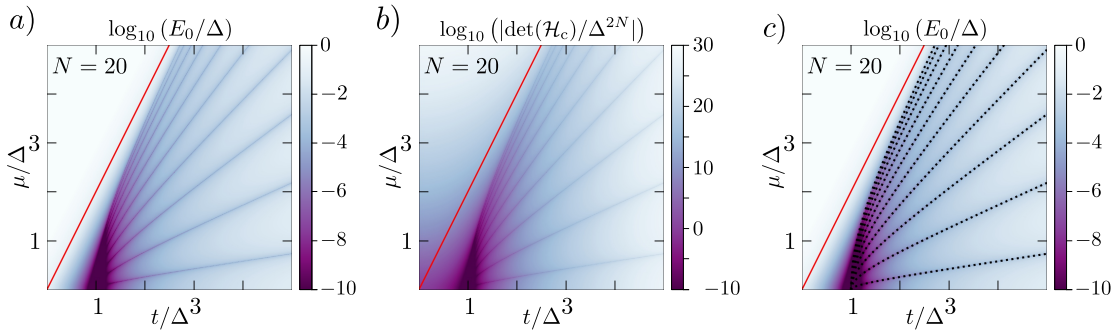

Figure 6.10.: Numerical investigation of the in-gap energies for $N = 20$ as function of μ/Δ, t/Δ. The topological phase boundary $\mu = 2t$ is depicted in red. a) The smallest positive energy E_0 of $\mathcal{H}_c$ diminishes within the triangular-like region around the Kitaev point $|t/\Delta| = 1$, $\mu = 0$ and branches into separated Majorana lines for larger t/Δ. b) As explained in the text, the determinant of the Kitaev chain Hamiltonian mimics qualitatively the in-gap energies. Note that the smearing of the purple colour in the bottom left corner is solely caused by the scaling. c) Same as a) only with added zero energy lines (dotted, black) following Eq. (6.3.7) as their numerical investigation is difficult with a chosen grid.

exponentially suppressed and those where $\det[\mathcal{H}_c]$ is sufficiently small, since the effect of the out-of gap energies is limited by the bulk dispserion relation in Eq. (5.1.6). This approach is justified as we see from Fig. 6.10. We finally aim now for the general quantization rule.

6.3.2. Derivation of the quantization rule for arbitrary t, Δ and μ

Initially, we observe that the characteristic polynomial associated to $\mathcal{H}_c$ from Eq. (6.3.2) reads [99]

$$P_\lambda(\mathcal{H}_c) = \det(\lambda \mathbb{1}_{2N} - \mathcal{H}_c) = \det\left(\lambda^2 \mathbb{1}_N - hh^\dagger\right). \tag{6.3.10}$$

Although we have the eigenvalues η_n of h, see Eq. (6.3.6), and thus those of $h^\dagger$ are known to us, the spectrum for the Kitaev chain follows not simply as $\lambda^2 = |\eta_n|^2$, since h, $h^\dagger$ cannot be diagonalised simultaneously; their commutator does not vanish. Explicitly, $\left[h, h^\dagger\right]$ has only two non-zero entries

$$\left[h, h^\dagger\right]_{n,m} = \begin{cases} -4\,\Delta\,t & n = m = 1, \\ 4\,\Delta\,t & n = m = N, \\ 0 & \text{otherwise}, \end{cases} \tag{6.3.11}$$

supposed $N \geq 2$, and for one site we have $\left[h, h^\dagger\right] = 0$, because hopping and pairing do not enter into the Hamiltonian. Essentially all possible surprising features of the Kitaev chain's spectrum originate from Eq. (6.3.11). In appendix E we discuss the competition

between t and Δ arising from the electronic creation (annihilation) operator's d_j, $d_j^\dagger$ fermionic nature, used to set up the BdG Kitaev Hamiltonian, which reappears here.

For either $t = 0$ or $\Delta = 0$, h, $h^\dagger$ commute and from Eq. (6.3.6) follows indeed the correct spectrum of the Kitaev chain as $\lambda = |\eta_n|$. Considering $4\,|\Delta\, t| \ll 1$, i.e. small but finite, we can approximate $\lambda \approx |\eta_n|$; though it is sufficient for some eigenvalues λ, at least the in-gap energies cannot be reproduced accurately since (6.3.6) relies on real wave vectors.

Notably, $\left[h,\, h^\dagger\right]$ is independent of μ and from Eq. (6.3.11) we may naively expect that the chemical potential adopts only a minor role, though Fig. 6.7 tells us differently. As we will soon experience, it is the superconducting pairing constant which forces the chemical potential into a possible unexpected role, given that both t and Δ are finite. Temporarily, one can extract this information by revisiting the Hamiltonian in the default BdG basis in Eq. (6.0.1), where electron and hole parts are formed. Importantly, the chemical potential enters with *opposite* signs into the Hamiltonian, such that a basis transformation may has severe consequences. In the cases of either $t = 0$ or $\Delta = 0$, we found that the chemical potential enters into the Hamiltonian via the identity, thus shifting merely the energy eigenvalues. However, this is not completely true anymore.

Since determining the characteristic polynomial of the Kitaev chain for a general parameter setting turns out to be lengthy and complicated (the result is given in appendix N), we do not evaluate the l.h.s of Eq. (6.3.10). Nonetheless, Eq. (6.3.10) is indeed powerful: the matrix size of $hh^\dagger$ is N, half the Hamiltonian's original dimension. The experience gained during the investigations in Ch. 6.2.4, implies that one can find the spectrum of well-conditioned matrices, such as Toeplitz matrices, by focusing simply on their eigenvectors instead, rather then at the eigenvalues directly [79, 102]. The characteristic polynomial $P_\lambda\left(\mathcal{H}_\mathrm{c}\right)$ from Eq. (6.3.10) originates as well from the eigenvector equation

$$hh^\dagger\,|\text{🕭}\rangle \;=\; \lambda^2\,|\text{🕭}\rangle, \tag{6.3.12}$$

so that this λ is indeed an eigenvalue of the Kitaev chain. Though we have no interest in $|\text{🕭}\rangle$ per se, we can possibly hope to solve Eq. (6.3.12) for $|\text{🕭}\rangle$; thus, granting us in turn the eigenvalues $\Lambda = \lambda^2$. In this scope we bypass the difficult calculation of $P_\lambda\left(\mathcal{H}_\mathrm{c}\right)$, yet we find its zeros. Notice that $|\text{🕭}\rangle$ is of course not an eigenvector of the Kitaev chain.

By virtue of Eq. (6.3.12), we have to first verify that $hh^\dagger$ is a matrix of suitable character. Indeed, from Eq. (6.3.3) we find that $(n,\, m = 1, \ldots,\, N)$

$$\begin{aligned}\left(hh^\dagger\right)_{nm} \;=\; &\left[\mu^2 - a^2\,\left(1 - \delta_{n,N}\right) - b^2\,\left(1 - \delta_{n,1}\right)\right]\,\delta_{nm} \\ &+ \mathrm{i}\mu\,(a-b)\,\left(\delta_{n\,m+1} \,+\, \delta_{m\,n+1}\right) \,+\, ab\,\left(\delta_{n\,m+2} \,+\, \delta_{m\,n+2}\right)\end{aligned} \tag{6.3.13}$$

holds for all N. In terms of the temporary abbreviations $\bar{t} = \mathrm{i}\mu\,(a-b)$, $\bar{m} = ab$ and

$\bar{\mu} = \mu^2 - a^2 - b^2$, the matrix form of $hh^\dagger$ can be more appreciated[7]

$$hh^\dagger = \begin{bmatrix} \bar{\mu}+b^2 & \bar{t} & \bar{m} & & & & \\ \bar{t} & \bar{\mu} & \bar{t} & \bar{m} & & & \\ \bar{m} & \bar{t} & \bar{\mu} & \bar{t} & \bar{m} & & \\ & \ddots & \ddots & \ddots & \ddots & \ddots & \\ & & \bar{m} & \bar{t} & \bar{\mu} & \bar{t} & \bar{m} \\ & & & \bar{m} & \bar{t} & \bar{\mu} & \bar{t} \\ & & & & \bar{m} & \bar{t} & \bar{\mu}+a^2 \end{bmatrix}. \tag{6.3.14}$$

In particular, $hh^\dagger$ falls mathematically in the same category as the Hamiltonian of the chain with n.n.n. hopping[8], see Eq. (3.2.1). A single discrepancy comprises in the first and last diagonal elements, which can be absorbed into the boundary conditions as we show now.

We express Eq. (6.3.12) by the elements of $|\text{𝕊}\rangle = (\xi_1, \xi_2, \ldots, \xi_N)^{\mathrm{T}}$ and granting first

$$\xi_{j+2} = \frac{\lambda^2 + a^2 + b^2 - \mu^2}{ab}\,\xi_j - \xi_{j-2} - \mathrm{i}\mu\frac{a-b}{ab}\,(\xi_{j+1} + \xi_{j-1}), \tag{6.3.15}$$

for $j = 3, \ldots, N-2$, supposed $ab \neq 0$ ($\Delta \neq \pm t$) and $N \geq 5$. Secondly, the boundary conditions imposed by Eq. (6.3.12) are

$$\xi_3 = \frac{\lambda^2 + a^2 - \mu^2}{ab}\,\xi_1 - \mathrm{i}\mu\frac{a-b}{ab}\,\xi_2, \tag{6.3.16}$$

$$\xi_4 = \frac{\lambda^2 + a^2 + b^2 - \mu^2}{ab}\,\xi_2 - \mathrm{i}\mu\frac{a-b}{ab}\,(\xi_3 + \xi_1), \tag{6.3.17}$$

$$0 = \frac{\lambda^2 + a^2 + b^2 - \mu^2}{ab}\,\xi_{N-1} - \xi_{N-3} - \mathrm{i}\mu\frac{a-b}{ab}\,(\xi_N + \xi_{N-2}), \tag{6.3.18}$$

$$0 = \frac{\lambda^2 + a^2 + b^2 - \mu^2}{ab}\,\xi_N - \xi_{N-2} - \mathrm{i}\mu\frac{a-b}{ab}\,\xi_{N-1}. \tag{6.3.19}$$

We follow now the same strategy as explained in depth in Ch. 3.2.2 and we extend directly the entries ξ_j beyond the lattice sites via Eq. (6.3.15) for all $j \in \mathbb{Z}$. In this scope the boundary condition can be simplified as

$$\xi_0 = \xi_{N+1} = b\,\xi_{N+2} - a\,\xi_N = b\,\xi_1 - a\,\xi_{-1} = 0. \tag{6.3.20}$$

Next, we define the abbreviations

$$\zeta := \frac{\lambda^2 + a^2 + b^2 - \mu^2}{ab}, \tag{6.3.21}$$

$$\eta := -\mathrm{i}\,\mu\frac{a-b}{ab}, \tag{6.3.22}$$

[7]The commutator $\left[h, h^\dagger\right]$ from Eq. (6.3.11) can directly be obtained from Eq. (6.3.14), because h and $h^\dagger$ convert into each other for $a \leftrightarrow b$ and $\mu \to -\mu$.

[8]Thus, we find crossings and avoided crossings for the same mathematical, but distinct physical reasons, as we discuss later.

such that the recursion formula adopts the Tetranacci form

$$\xi_{j+2} = \zeta\, \xi_j - \xi_{j-2} + \eta\, (\xi_{j+1} + \xi_{j-1}), \quad j \in \mathbb{Z}, \tag{6.3.23}$$

of Eq. (4.2.1). By means of the extension performed above, the condition $N \geq 5$ dropped. Without specifying ζ and η, no distinction between the Kitaev chain and the atomic chain with n.n.n. hopping can be made by inspecting Eq. (6.3.23) alone, as promised earlier. Please let me remind you that our investigations for $\eta = 0$ back in Ch. 4.2.1, where we found that ξ_j separates into two Fibonacci sequences corresponding to even and odd indices, respectively. In the case of $\mu = 0$, we called those two sequences x_j and y_j, see especially Eqs. (6.2.36), (6.2.43), (6.2.44). Already for the n.n.n. hopping chain in section 3.2.3, we noticed that the absence of nearest neighbor hopping, in the present scope $\eta = 0$, signaled the presence of two independent sublattice structures; for $\mu = 0$, the Kitaev chain segmented into the two SSH-like chains α and β. Importantly, Eq. (6.3.23) generalizes our prior findings for the Kitaev chain and we can apply our knowledge about Tetranacci polynomials from Ch. 4.2.

Unfortunately, our current situation offers several ways to proceed and many questions may rise simultaneously, such as the physical reasons behind Eq. (6.3.23) or its implications etc. We will discuss all of this in detail soon including also a intuitive and nearly complete pictorial derivation of Eq. (6.3.13) in section 6.6, but we finish first the calculation.

The duty of $|\text{🔔}\rangle$ was to bring us into the proper position, i.e. granting us the Tetranacci recursion formula in Eq. (6.3.23) for the Kitaev chain and the boundary condition in Eq. (6.3.20); thus, $|\text{🔔}\rangle$ served its purpose and is left aside. As we have shown in Ch. 4, consult Eqs. (4.2.25) - (4.2.30) and especially Eqs. (4.3.4) -(4.3.1), Tetranacci polynomials can be written as

$$\xi_j = A\, e^{\mathrm{i}k_1 d\, j} + B\, e^{-\mathrm{i}k_1 d\, j} + C\, e^{\mathrm{i}k_2 d\, j} + D\, e^{-\mathrm{i}k_2 d\, j}, \tag{6.3.24}$$

with suitable complex constants A, B, C, D. Since we consider the most general case, the boundary condition from Eq. (6.3.23) always involves all four coefficients in Eq. (6.3.24) implying $k_{1,2} \neq 0$ and $k_{1,2} \neq \pi$. Consequently, the open boundary condition prevents the gap closing to occur for $\mu = \pm 2t$.

The definition of $k_{1,2}d \in \mathbb{C}$ via the quantity $S_{1,2}$ from Eq. (4.2.27), is

$$S_{1,2} = \frac{\eta \pm \sqrt{\eta^2 + 4\,(\zeta + 2)}}{2} =: 2\, \cos\left(k_{1,2} d\right) \tag{6.3.25}$$

using now the present expressions of ζ, η from Eqs. (6.3.21), (6.3.22). The last expression relates the eigenvalues λ, hidden in ζ, with $k_{1,2}$ and Eq. (6.3.25) is the bulk dispersion relation from Eq. (5.1.6). The last statement can be straightforwardly shown, at best with Eq. (4.2.26) which both $S_{1,2}$ satisfy. So we may exchange $\lambda \to E_{\pm}(k_{1,2}d)$. Further, the bulk equal energy constraint for $E_{\pm}(k_1) = E_{\pm}(k_2)$ embedded in Eq. (6.3.25) reads

$$\cos\left(k_1 d\right) + \cos\left(k_2 d\right) = -\frac{\mu t}{t^2 - \Delta^2} \tag{6.3.26}$$

where we expressed η in terms of t, Δ rather then $a = \mathrm{i}(\Delta - t)$ or $b = \mathrm{i}(\Delta + t)$. However, a more useful expression for Eq. (6.3.26) is received in terms of $k_\Sigma \coloneqq (k_1 + k_2)/2$, $k_\Delta \coloneqq (k_1 - k_2)/2$, namely

$$\cos(k_\Sigma d)\cos(k_\Delta d) = -\frac{1}{2}\frac{\mu t}{t^2 - \Delta^2}. \tag{6.3.27}$$

Since the relation between $k_{\Sigma,\Delta}$ ($k_{1,2}$) is known, we are left to demand that ξ_j from Eq. (6.3.24) satisfies the boundary condition from Eq. (6.3.20). This grants a set of homogeneous equations and the constraint that the determinant of the coefficient matrix vanishes yields the quantization rule. After several simplifications, the quantization rule becomes

$$\frac{\sin^2[k_\Sigma d(N+1)]}{\sin^2[k_\Delta d(N+1)]} = \frac{1 + \left(\frac{\Delta}{t}\right)^2 \cot^2(k_\Delta d)}{1 + \left(\frac{\Delta}{t}\right)^2 \cot^2(k_\Sigma d)}, \tag{6.3.28}$$

where we used the representation in terms of fractions only for shortness, rather than the proper product form. Notice that this quantization rule applies also for X-Y model consisting of N spin 1/2 particles in transverse magnetic field [73, 74].

Similar, to the n.n.n. chain in Ch. 3, both the equal energy constraint in Eq. (6.3.27), which is in fact a bulk property, and the finite size quantization in Eq. (6.3.28) have to be used in order to determine the values of $k_{\Sigma,\Delta}$ or alternatively $k_{1,2}$. Both equations reproduce the numerically calculated eigenvalues accurately and complex solutions can be found.

A fast verification of the quantization rule is the limit of $\mu = 0$. As we see, Eq. (6.3.27) imposes either $k_\Sigma d = \pi/2$ or (exclusively) $k_\Delta = \pi/2$. We freely choose the latter since the entire description is invariant under the exchange of $k_{\Sigma,\Delta}$. Rearranging the terms in Eq. (6.3.28) before we demand $\mu = 0$ and then exploiting that $\cot^2(k_\Delta d) = \cot^2(\pi/2) = 0$ holds, yields

$$\sin^2[k_\Sigma d(N+1)] = \frac{\sin^2[k_\Delta d(N+1)]}{1 + \left(\frac{\Delta}{t}\right)^2 \cot^2(k_\Sigma d)}. \tag{6.3.29}$$

Next, note that

$$\sin^2[k_\Delta d(N+1)] = \begin{cases} 1, & N \text{ even} \\ 0, & N \text{ odd} \end{cases} \tag{6.3.30}$$

since $k_\Delta d = \pi/2$. For odd N, we receive directly $\sin^2[k_\Sigma d(N+1)] = 0$; however for the proper expression, we exploit that $k_\Delta d = \pi/2$ implies $k_\Sigma d = k_1 d - \pi/2$. Thus, we have $\sin^2[k_1 d(N+1)] = 0$ and we recover our prior results $k_1 = n\pi/(N+1)$, $n = 1, \ldots, N$, $n \neq (N+1)/2$ from Eq. (6.2.26). The excluded value for n would imply $k_\Sigma d = \pi/2$, which is forbidden due to $k_\Sigma \neq k_\Delta$.

In case of N even, we find first

$$\cot^2[k_\Sigma d(N+1)] = \left(\frac{\Delta}{t}\right)^2 \cot^2(k_\Sigma d) \tag{6.3.31}$$

and using $k_\Sigma d = k_1 d + \pi/2$ yields

$$\tan\left[k_1 d\,(N+1)\right] \;=\; \pm\frac{\Delta}{t}\,\tan\left(k_1 d\right) \tag{6.3.32}$$

which is Eq. (6.2.29). For $\mu = 0$, as we experienced earlier, the Kitaev chain separates into the two SSH-like chains, and the four boundary conditions separate as well. Because of this, we do not need both momenta $k_{1,2}$ in this limit, rather one of them, either k_1 or k_2. In general this is not true, as we discuss in more detail in Ch. 6.5.

In preparation for the discussion in the next section, we convert the bulk dispersion relation for $k_{1,2}$ in Eq. (5.1.6) into a more adequate form, where $k_{\Sigma,\Delta}$ can directly be inserted. Straightforwardly one finds that

$$\begin{aligned} E_\pm^2 \;&=\; \mu^2 \,+\, 4\Delta^2 \,+\, 4(t^2-\Delta^2)\,\cos(k_1 d)\,\left[\frac{\mu t}{t^2-\Delta^2} \,+\, \cos(k_1 d)\right] \\ &=\; \mu^2 \,+\, 4\Delta^2 \,-\, 4(t^2-\Delta^2)\,\cos(k_1 d)\,\cos(k_2 d) \end{aligned} \tag{6.3.33}$$

where we used Eq. (6.3.26) in the last step. This procedure holds similar for exchanged roles of $k_{1,2}$. Further, we use that $2\cos(k_1 d)\,\cos(k_2 d) = 2\cos^2(k_\Delta d) + 2\cos^2(k_\Sigma d) - 2$ granting

$$E_\pm^2(k_{\Sigma,\Delta}) \;=\; \frac{1}{\cos^2(k_{\Sigma,\Delta} d)}\,\left[4(t^2-\Delta^2)\,\cos^2(k_{\Sigma,\Delta} d) - \mu^2\right]\,\left[\frac{t^2}{t^2-\Delta^2} - \cos^2(k_{\Sigma,\Delta} d)\right] \tag{6.3.34}$$

after a few steps and Eq. (6.3.27) ensures $E_\pm(k_\Sigma) = E_\pm(k_\Delta)$. We can finally discuss the physics behind the excitation spectrum of the Kitaev chain with open boundary conditions for generic parameters, but nonetheless the recent results demand first some general remarks.

6.4. The Kitaev chain's BdG spectrum

6.4.1. General remarks about the quantization rule and the impact of the chemical potential

We begin our analysis by inspecting Eqs. (6.3.27), (6.3.28) and their behaviour under $t \to -t$, $\Delta \to -\Delta$ and/ or $\mu \to -\mu$. As we clearly observe the quantization rule depends only implicitly on the chemical potential and t, Δ enter as squares. The bulk equal energy constraint in Eq. (6.3.27) behaves differently. Inverting the sign of either μ or t can be counteracted by shifting one wavevector, say k_Σ, by π/d. Since the quantization rule in Eq. (6.3.28) is invariant under $k_\Sigma d \to k_\Sigma d \pm \pi$, the quantized wavevectors are as well. Further, the dispersion relation given in Eq. (6.3.34) above remains unchanged as well; thus, the excitation spectrum is symmetric in t, Δ and μ, in agreement with Fig. 6.11.

As we clearly see from Fig. 6.11 a) and c), inverting the ratio t/Δ into its opposite changes the spectrum drastically. Unlike in the prior $\mu = 0$ case, the situations for $t > \Delta$

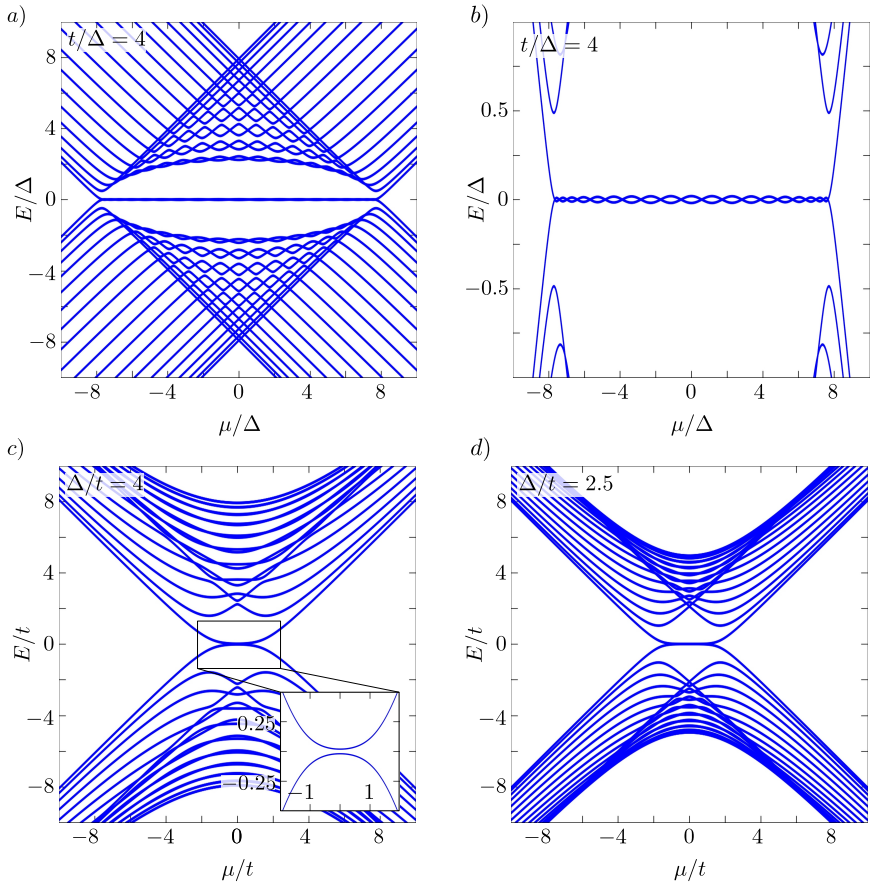

Figure 6.11.: Numerically calculated (BdG) spectrum of the Kitaev chain for $N = 20$ as function of μ for different ratios of t/Δ. a) The excitation spectrum is symmetric in μ and the Kitaev chains hosts in-gap states for $|\mu| \leq 2|t|$. The excitations show crossings and avoided crossings. b) Zoom of a). The in-gap energies are finite and oscillate with varying μ. Zero energy is only met at the discrete values μ_n from Eq. (6.3.7). c) Inverting the ratio of t/Δ into its opposite changes drastically the shape of the excitation spectrum, yet we observe again crossings and avoided crossings. Zero energy is not present, see the inset. d) For $t \lesssim \Delta$, the region around $\mu \approx 0$ and $2 \leq E/\Delta \leq 4$ appears similar to the triangular shaped region in a) but inverted.

and $t < \Delta$ cannot be mapped into each other by shifting the momenta, as we see from the quantization rule in Eq. (6.3.28). We discuss this issue in more detail in Ch. 6.4.3, where we also analyse the crossings and avoided crossings in depth.

More urgent is to clarify the implicit appearance of the chemical potential in the quantization, contrary to the usual way we think of it, as a mere constant shift of the energy levels up or down. However, the quantization rule shows that this is not true –as

it has to be, since topologically trivial and non-trivial features of the Kitaev chain is a question about the ratio $\mu/2t$, not t/Δ per se. The ordinary understanding of topological superconductors is that the topological non-trivial predictions for $N \to \infty$ impose constraints on finite size systems. Here, we expect localized in-gap states with exponentially small energy to be present for $|\mu| \leq 2|t|$ and suitable ratios t/Δ. Suppose that the chemical potential does not influence the quantization; consequently the scenarios of $|\mu| \geq 2|t|$ (trivial) and $|\mu| \leq 2|t|$ (non trivial) are indistinguishable. Thus, one would either find decaying in both regimes states or none at all. However, we do find them not only numerically, but we gave already analytical results at $\mu = 0$, i.e. there is no point in denying that μ influences the quantization[9]. Further, the topological phase diagram from Fig. 5.1 can be re-obtained from the quantization rule in the limit of $N \to \infty$. This approach is very technical and for more details consult appendix H.

One might ask what is so special about the chemical potential of the Kitaev chain. The answer is simple, yet possibly confusing: Absolutely nothing. Its important role is entirely due to the fact that the system is superconducting. We can understand this by simply revisiting the Eqs. (6.0.1), (6.0.2) where we wrote the Kitaev Hamiltonian in the form of a BdG matrix with separated particle and hole subspaces. Most importantly though, we deal with fermions, not bosons; this causes a sign inversion of all elements in the hole compared to the particle block. In particular, the chemical potential as diagonal entry switches sign, such that μ does not solely enter as $\mu\mathbb{1}_{2N}$ into this matrix. Without special parameter choices and $\Delta \neq 0$, the system cannot be reduced to independent subparts where only $\mu\mathbb{1}_N$ may enter; consequently, the chemical potential cannot only shift the energies and will influence the entire spectrum in a non trivial way. In summary, the superconductivity and the fermionic nature of the electrons force the chemical potential into this role[10].

The method to engineer non-trivial topological phases relies on a specific coupling of degrees of freedom. Done appropriately, the actual quantization rule depends on the Hamilonian's parameters and has the property that solutions corresponding to real kd, i.e. extended states with energies from the bulk regime, get missing for certain parameters. These "missing" solutions are then replaced by in-gap or generally decaying state solution with non-real kd and the associated parameters may belong to the topological non trivial phase.

The influence of the chemical potential is not limited to the wavevectors for in-gap states of a finite system with open boundary conditions, but it in fact stretches to all modes. Remember that the Kitaev chain has only a single (independent) band, either the one associated to the positive, namely $E_+(k)$, or the negative energy $E_-(k)$, due

[9] In turn $\mu = 0$ is a qualitative change for a finite system.

[10] Note, only for the Kitaev chain this behaviour is restricted to μ, simply because of limited number of parameters here. Similar energy oscillations as function of the Zeeman term V_Z (or in the chemical potential) are observed for semiconducting nanowires with Rashba spin orbit coupling in proximity to a superconducting substrate [3, 9, 12–17]; V_Z enters into the Hamiltonian similar as μ does for the Kitaev chain: switching signs. For more details consult Ch. 10.

to the particle-hole symmetry. In this scope, the quantization rule from Eq. (6.3.28) was obtained for a certain band with unspecified energy $E_{\pm}(k)$, not necessarily zero nor inside the bulk gap. Thus, whenever μ influences the in-gap regime, the higher, out-of gap excitations are automatically affected as well. This can be seen in Fig. 6.11 a) as the same oscillatory pattern, originating from μ, affects both in-gap and out of gap energies.

6.4.2. Discussion of the BdG spectrum for the finite length Kitaev chain

The quantization rule in Eq. (6.3.28) and Eq. (6.3.27) are seriously responseable for the appearance and the features of the Kitaev chain's BdG spectrum. In general, one has to read out numerically the solutions for $k_{\Sigma,\,\Delta}d$ which in turn contain all the required information. However, this is a rather unsatisfying answer if our aim is to understand the excitation spectrum; therefore, we first re-investigate analytically the zero energy condition. Practically, the most important issue is how the constraint of $E_{\pm} = 0$ enters into Eq. (6.3.28). This can be achieved in two steps from the dispersion relation using $k_{\Sigma,\,\Delta}$ given in Eq. (6.3.34). As we see directly, Eq. (6.3.34) is predestined for a zero energy discussion, since we can demand that one of the two brackets for either k_{Σ} or k_{Δ} has to vanish. We set

$$\mu^2 \;=\; 4(t^2 - \Delta^2)\,\cos^2(k_{\Sigma}d) \tag{6.4.1}$$

since Eq. (6.3.27) translates the last expression into

$$\frac{t^2}{t^2 - \Delta^2} \;-\; \cos^2(k_{\Delta}d) \;=\; 0 \tag{6.4.2}$$

which implies $E_{\pm}(k_{\Delta}) = 0$ in Eq. (6.3.34). Notice that Eq. (6.4.1) is almost Eq. (6.3.7), only $k_{\Sigma}d$ is not quantized so far. As one can show, Eq. (6.4.2) is equivalent to

$$1 \;+\; \left(\frac{\Delta}{t}\right)^2 \cot^2(k_{\Delta}d) \;=\; 0. \tag{6.4.3}$$

Notice, that the last expression also enters in the quantization rule. Thus, Eq. (6.3.28) reduces to

$$\sin^2\left[k_{\Sigma}d\,(N+1)\right] \;=\; 0. \tag{6.4.4}$$

Inserting the solutions $k_{\Sigma}d = n\pi/(N+1)$, $n = 1, \ldots, N$ in Eq. (6.4.1) grants the zero energy condition from Eq. (6.3.7) after the replacement $\mu \to \mu_n$. We discuss these zero energy lines and the associated in-gap eigenstates in more detail in Ch. 6.5.3.

In their occurrence, the bulk energy constraint Eq. (6.3.27) and the quantization rule Eq. (6.3.28) generally manifest a non trivial, i.e. a non equidistant quantization, of the wave vectors $k_{1,2}$. For example, the standard particle in the box behavior is associated to $\sin^2\left[k_{\Sigma,\Delta}d\,(N+1)\right] = 0$ (simultaneously). Clearly this satisfies Eq. (6.3.28), since both of its sides vanish independently. However, this quantization upon further selection criteria is reserved for the crossings, i.e. out-of-gap degenerate energies only, as we show

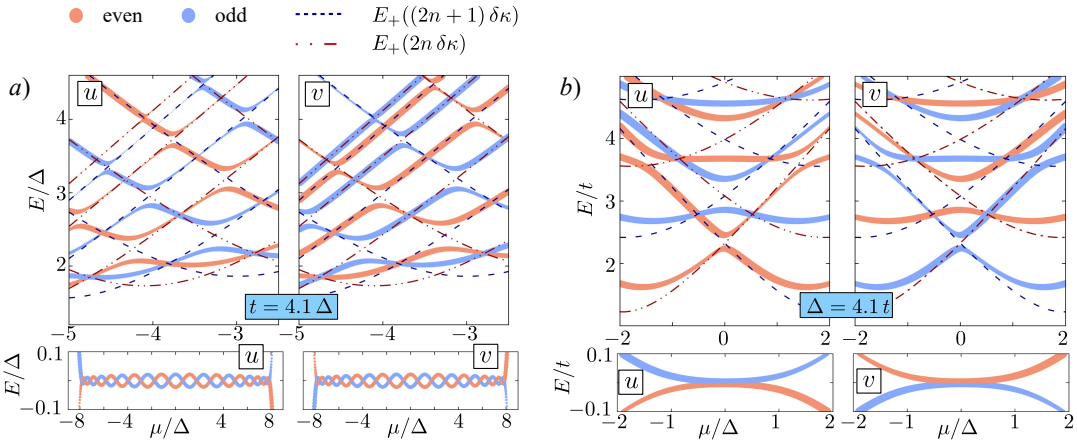

Figure 6.12.: Spatial parity $I_{u,v}$ for the particle u and hole v sectors of the eigenstates for $t/\Delta = 4.1$ in a) and $\Delta/t = 4.1$ in b). The quantities $I_u = \langle u|\mathcal{I}_s|u\rangle/\langle u|u\rangle$, $I_v = \langle v|\mathcal{I}_s|v\rangle/\langle v|v\rangle$, with $\mathcal{I}_s$ from Eq. (6.5.21), are either $+1$ (even, red) or -1 (odd, blue) and the line thickness illustrates $|u|$, $|v|$. The dark dashed (dot-dot-dashed) lines display the energy $E_+((2n+1)\delta k)$ ($E_+((2n)\delta k)$ in terms of odd (even) multiples of $\delta k = \pi/(N+1)$ and E_+ is taken from Eq. (5.1.6). Clearly, crossings form at intersection points where even/ odd multiples of δk meet, while the avoided crossings occur at intersections of even and an odd multiples of δk. More details are given in Ch. 6.4.3 below. (This Figure is published in Ref. [5])

in section 6.4.3. The derivation is given in Ch. 6.5.2. In this respect, the bulk energy constraint Eq. (6.3.27) determines the parameter, for instance the values of μ, at which these degeneracies occur for given t, Δ since k_Σ, k_Δ are fixed.

The similarity between finite energy crossings and zero energy resides in the fact that both demand $\sin^2[k_\Sigma d\,(N+1)] = 0$ (without restriction). The difference originates solely in the way how the quantization rule is satisfied: The former rely on $\sin^2[k_\Delta d\,(N+1)] = 0$ and the latter on Eq. (6.4.2). These are the possibilities for equidistant quantized wavevectors, see Eq. (6.3.28), but their number is limited. Thus, non-degenerate energies and especially the oscillatory behavior of the energy on the chemical potential, in and outside of the gap, arises from the non-equidistant quantization.

This clarified, we can discuss the physics in more detail. The BdG spectrum for $|t| > |\Delta|$ ($|t| < |\Delta|$) can be roughly understood as the one for $\Delta = 0$ ($t = 0$) with the important difference that the quantization rule from Eq. (6.3.28) introduces extra features, for instance the gap openings in the higher excitation spectrum which we call avoided crossings. These avoided crossings are caused by a finite superconducting pairing constant Δ and the associated gaps vanish for $\Delta = 0$, as we proof in section 6.4.3 analytically. The avoided crossings have to be understood as former crossings at $\Delta = 0$

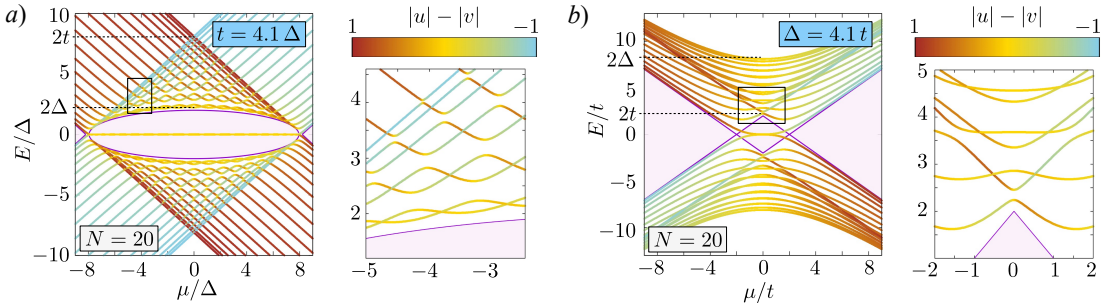

Figure 6.13.: The complete excitation spectrum of the Kitaev chain for $N = 20$ and $t/\Delta = 4.1$ in a), Δ/t in b). The quasi-particle character $|u| - |v|$ of the associated eigenstates at a given energy ranges from pure particles (red) via perfectly balanced quasiparticles (yellow) to completely hole-like (blue). The bulk gap is shown in violet. (This Figure is published in Ref. [5])

between states with same inversion character of the electron (u)/ hole (v) components which hybridize under the action of Δ and thereby open these gaps. This behavior is illustrated in Fig. 6.12. More technically phrased, avoided crossings originate from two $\Delta = 0$ BdG eigenstates, where one corresponds to an even and the other one to an odd multiple of $\pi/(N+1)$ for $k_{1,2}$. Contrary to the avoided crossings, the electron and hole components of degenerate energy eigenstates are protected by inversion symmetry and correspond to even (odd) multiple of $\pi/(N+1)$ for $k_{1,2}$.

Let us turn to the particle and hole character of the eigenstates. For $|t| > |\Delta|$, we find unsurprisingly perfectly balanced quasiparticle states within the gap as shown in Fig. 6.13. Possibly unexpected though, the same holds for all avoided crossings independently of the precise energy value. Only as the absolute value of the energy grows, this feature is restricted closer to the avoided crossings and this mixing becomes thus less dominant. On the contrary, *around* finite degenerate energies we find the extreme cases of nearly perfect electron and hole states. Numerically, we find that the crossings and avoided crossings are restricted to $|E/\Delta| < 2|t/\Delta|$ and $|\mu/\Delta| < 2|t/\Delta|$ which we confirm analytically in Ch. 6.4.3 soon. Thus, crossings and avoided crossings occur for parameters associated to the topological non trivial phase for $|t| > |\Delta|$. We find similar results for $|t| < |\Delta|$, but the mixing of particle and holes occurs now even outside of the topological non trivial phase for $|\mu/\Delta| > 2|t/\Delta|$.

6.4.3. Degenerate energies and gap openings inside the excitation regime

We start the discussion of the non zero degeneracies and avoided crossings with an inspection of Fig. 6.14. Clearly, the action of a finite superconducting pairing is to open gaps inside the higher excitations, i.e. former crossings turn into avoided ones. Further, several energy degeneracies still exist, though their position in the E/t, μ/t plane may have changed. We derive the criterion for crossings and avoided crossings later in Ch. 6.5.2 and they allow a better understanding of the excitation spectrum.

As we will show, the general parameter setting of $\mu \neq 0$, $t \neq \pm\Delta$, $t \neq 0$, $\Delta \neq 0$ allows

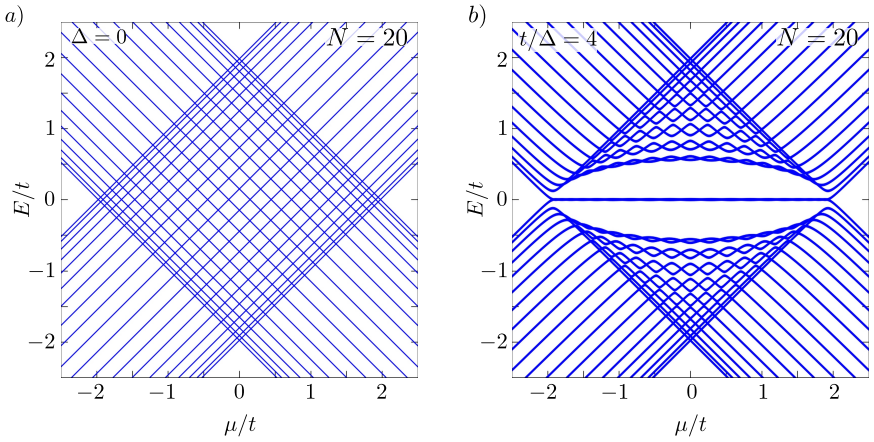

Figure 6.14.: BdG Spectrum of the Kitaev chain with $N = 20$ for $\Delta = 0$ in a) and $t/\Delta = 4$ in b). a) No superconducting gap exists and the eigenvalues are $E_{\pm}(k_n d) = \pm[\mu + 2t\cos(k_n d)]$ with $k_n d = n\pi/(N+1)$ and $n = 1, \ldots, N$. We find N^2 crossings and no avoided ones. b) For finite superconducting pairing Δ, degenerate energies are still found outside the gap, while simultaneously avoided crossings are formed.

only up to twofold degeneracies. Considering Fig. 6.14 panel a) or Fig. 6.12, it is not surprising that the first quantitative criterion for degeneracies which we obtain is

$$k_{1,2}d = \frac{n\pi}{N+1}, \quad n = 1 \ldots, N \tag{6.4.5}$$

even for $\Delta \neq 0$. Here, the values for $k_{1,2}$ can for the moment be chosen completely independently. However, only specific combinations of $k_{1,2}d$ from Eq. (6.4.5) satisfy the quantization rule and are thus associated to crossings. We discuss the results in the next section.

6.4.3.1. Finite energy crossings

The model is invariant under exchange of $k_{1,2}$ and one can set $k_1 > k_2 > 0$, i.e. $k_\Sigma > k_\Delta > 0$, without restrictions. The values for $k_{\Sigma,\Delta}d$ associated to finite energy crossings are

$$(k_\Sigma d,\, k_\Delta d) = \left(\frac{i\pi}{N+1}, \frac{j\pi}{N+1}\right), \quad i = 2, \ldots, i^{\mathrm{c}}_{\max},\, j = 1, \ldots, i^{\mathrm{c}}_{\max} - 1, \tag{6.4.6}$$

with $\pi/2 \geq k_\Sigma d > k_\Delta d > 0$ and

$$(k_\Sigma d,\, k_\Delta d) = \left(\pi\frac{N+1-i}{N+1}, \frac{j\pi}{N+1}\right), \quad i = 2, \ldots, i^{\mathrm{c}}_{\max},\, j = 1, \ldots, i^{\mathrm{c}}_{\max} - 1, \tag{6.4.7}$$

with $\pi \geq k_\Sigma d \geq \pi/2 > k_\Delta d > 0$. Here, $i^{\mathrm{c}}_{\mathrm{max}}$ is

$$i^{\mathrm{c}}_{\mathrm{max}} = \begin{cases} \frac{N+1}{2}, & N \text{ odd} \\ \frac{N}{2}, & N \text{ even} \end{cases}. \tag{6.4.8}$$

Note the value $i = i^{\mathrm{c}}_{\mathrm{max}}$ in case of N is odd yields $k_\Sigma d = \pi/2$ in both Eqs. (6.4.6), (6.4.7) and is twice represented, but occurs only once.

The position of the crossings as a function of t, Δ or μ follows from the equal energy constraint. For convenience we use Eq. (6.3.27)

$$\mu = 2\frac{\Delta^2 - t^2}{t} \cos(k_\Sigma d) \cos(k_\Delta d) \tag{6.4.9}$$

solved for μ. The value of $k_\Sigma d$ of both sets is connected by π, such that the symmetry of the spectrum in μ is automatically respected. The energy eigenvalue is found by inserting the parameters t, Δ and μ with $k_{\Sigma,\Delta}$ into the dispersion relation, for instance Eq. (6.3.34). Our results are illustrated by Fig. 6.15.

The number of the finite energy crossings $N_{\mathrm{C,E}\neq 0}$ is

$$N_{\mathrm{C,E}\neq 0} = \begin{cases} \frac{(N-1)^2}{2}, & N \text{ odd} \\ \frac{N^2}{2} - N, & N \text{ even} \end{cases}. \tag{6.4.10}$$

Please notice $N_{\mathrm{C,E}\neq 0}$ is independent of t, Δ and μ, contrary to the N zero energy crossings which exist only for $t^2 \geq \Delta^2$. Including them, gives N_{C} as

$$N_{\mathrm{C}} = \begin{cases} \frac{N^2+1}{2}, & N \text{ odd} \\ \frac{N^2}{2} & N \text{ even} \end{cases} \quad (t^2 \geq \Delta^2). \tag{6.4.11}$$

At last, let us discuss the parameter regions where crossings occur. We see directly from Eq. (6.4.9) that

$$0 \leq |\mu| < 2\left|\frac{\Delta^2 - t^2}{t}\right| = 2\left|\frac{1 - t^2/\Delta^2}{t/\Delta^2}\right| \tag{6.4.12}$$

holds and especially for $|t/\Delta| > 1$ we find $|\mu/\Delta| < 2|t/\Delta|$.

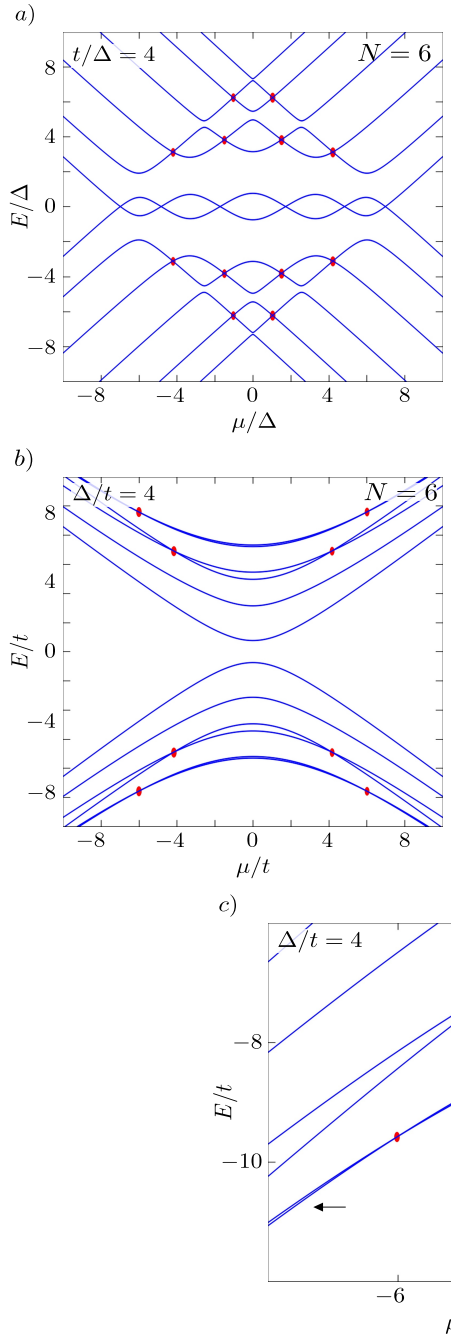

(i,j)	$k_\Sigma d$	$k_\Delta d$	$\frac{\mu}{\Delta}$	$\lvert\frac{E}{\Delta}\rvert$
$(2,1)$	$\frac{2\pi}{7}$	$\frac{\pi}{7}$	-4.21	3.12
$(3,1)$	$\frac{3\pi}{7}$	$\frac{\pi}{7}$	-1.50	3.82
$(3,2)$	$\frac{3\pi}{7}$	$\frac{2\pi}{7}$	-1.04	6.23
$(2,1)$	$\frac{5\pi}{7}$	$\frac{\pi}{7}$	4.21	3.12
$(3,1)$	$\frac{4\pi}{7}$	$\frac{\pi}{7}$	1.50	3.82
$(3,2)$	$\frac{4\pi}{7}$	$\frac{2\pi}{7}$	1.04	6.23

(i,j)	$k_\Sigma d$	$k_\Delta d$	$\frac{\mu}{t}$	$\lvert\frac{E}{t}\rvert$
$(2,1)$	$\frac{2\pi}{7}$	$\frac{\pi}{7}$	-16.85	19.00
$(3,1)$	$\frac{3\pi}{7}$	$\frac{\pi}{7}$	-6.01	9.58
$(3,2)$	$\frac{3\pi}{7}$	$\frac{2\pi}{7}$	-4.16	6.90
$(2,1)$	$\frac{5\pi}{7}$	$\frac{\pi}{7}$	16.85	19.00
$(3,1)$	$\frac{4\pi}{7}$	$\frac{\pi}{7}$	6.01	9.58
$(3,2)$	$\frac{4\pi}{7}$	$\frac{2\pi}{7}$	4.16	6.90

Figure 6.15.: Finite energy crossings (●) in the Kitaev BdG spectrum for $N = 6$. The analytical predictions for the finite energy crossings are stated in the table to the right of the respective panel. a) The predicted $N_{\mathrm{C,\,E\neq 0}} = 12$ finite energy crossings for $t/\Delta = 4$ are reproduced numerically. b) Same as a) only for inverted ratio $\Delta/t = 4$. Contrary to the first impression the number of crossings remains $N_{\mathrm{C,\,E\neq 0}} = 12$, since four crossings are outside of the plot range. c) Zoom of b) in order to demonstrate the degeneracy. The arrows point to line openings.

To find the energy range where the crossings occur, we use (6.3.34) and replace the chemical potential with Eq. (6.4.9) such that

$$E_{\pm}^2 = \frac{4}{t^2}\left[(t^2-\Delta^2)\cos^2(k_\Sigma) - t^2\right]\left[(t^2-\Delta^2)\cos^2(k_\Delta) - t^2\right] \tag{6.4.13}$$

we find a mixed description in k_Σ and k_Δ. The last expression for the energy implies

$$\frac{\Delta^4}{t^2} < \frac{E_{\pm}^2}{4} < t^2, \quad t^2 > \Delta^2 \tag{6.4.14}$$

$$t^2 < \frac{E_{\pm}^2}{4} < \frac{\Delta^4}{t^2}, \quad \Delta^2 > t^2. \tag{6.4.15}$$

where changing the ratio of t, Δ exchanges the limits. This "inversion" reflects the counter movement of the crossings from Eq. (6.4.6) and Eq. (6.4.7) upon exchanging t/Δ. We now turn to the avoided crossings.

6.4.3.2. The avoided crossings

The avoided crossings are associated to specific half integer multiples of $\pi/(N+1)$ for which the quantization rule from Eq. (6.3.28) reduces to

$$\left(\frac{\Delta}{t}\right)^2 \cot^2(k_\Sigma d) = \left(\frac{\Delta}{t}\right)^2 \cot^2(k_\Delta d)\,. \tag{6.4.16}$$

Since $k_\Sigma d$ and $k_\Delta d$ do not differ by π, the quantization rule is only satisfied at $\Delta = 0$. In turn, the half integer multiples do not correspond to eigenvalues unless $\Delta = 0$. Thus, the superconducting pairing is responsible for the gap openings in the supra gap excitation regime. Similarly as done before, we can reduce the combinations of k_Σ, k_Δ to $k_\Sigma > k_\Delta$ and divide them into two sets. We find,

$$(k_\Sigma d,\, k_\Delta d) = \left(\pi\frac{i+1/2}{N+1}, \pi\frac{j+1/2}{N+1}\right), \quad i = 1,\ldots,i_{\max}^{\mathrm{AC}},\, j = 0,\ldots i-1 \tag{6.4.17}$$

with $\pi/2 \geq k_\Sigma d > k_\Delta d > 0$ and

$$(k_\Sigma d,\, k_\Delta d) = \left(\pi\frac{N-i+1/2}{N+1}, \pi\frac{j+1/2}{N+1}\right), \quad i = 1,\ldots,i_{\max}^{\mathrm{AC}},\, j = 0,\ldots i-1 \tag{6.4.18}$$

with $\pi \geq k_\Sigma d \geq \pi/2 > k_\Delta d > 0$ to respect the symmetry of the spectrum. Here, we set

$$i_{\max}^{\mathrm{AC}} := \begin{cases} \frac{N-1}{2} & N \text{ odd} \\ \frac{N}{2} & N \text{ even} \end{cases}. \tag{6.4.19}$$

Note, that $k_\Sigma d = \pi/2$ for $i_{\max}^{\mathrm{AC}}$ in case of even N is twice represented in Eqs. (6.4.17) (6.4.18) but exists only once.

Analogously to the crossings, the values for μ where the avoided crossings occur are given by the equal energy constraint in Eq. (6.4.9). The "energy" around the center of

the anticrossing follows simply by inserting the half integer pairs into the bulk dispersion relation with the corresponding value of μ. Note, to speak about avoided crossings for $\Delta^2 > t^2$ is not fully proper as the BdG spectrum follows then more the one for $t = 0$, i.e. the spectrum is gaped everywhere. Furthermore, the avoided crossings turn into finite size crossings at $|t| = |\Delta|$.

Finally the number of avoided crossings N_{AC} is

$$N_{\mathrm{AC}} = \begin{cases} \frac{N^2-1}{2} & N \text{ odd} \\ \frac{N^2}{2} & N \text{ even} \end{cases} . \tag{6.4.20}$$

The total number of crossings and avoided crossings from Eqs. (6.4.11), (6.4.20) sums of to N^2, which is indeed the number of crossings at $\Delta = 0$, see Fig. 6.14.

The criterion for crossings and the avoided ones can be extracted from the eigenvector equation, which we discuss next.

6.5. Eigenvectors for generic parameter values

The calculation of eigenvectors is generally straightforward using the chiral basis, i.e. the Kitaev Hamiltonian in the form of Eq. (6.3.2). We start with general remarks, before we discuss the different cases. Further, we intend for the parameter settings $a \neq 0$, $b \neq 0$, i.e. $\Delta^2 \neq t^2$, and $\mu \neq 0$ as these special cases were already handled earlier. Our ansatz for the eigenvectors $\vec{v}_{\mathrm{c}} = (\vec{v}_{\mathrm{A}}, \vec{v}_{\mathrm{B}})^{\mathrm{T}}$ respects both Majorana sublattices A and B; thus, the eigenvector equation reads

$$\begin{bmatrix} & h \\ h^\dagger & \end{bmatrix} \begin{pmatrix} \vec{v}_{\mathrm{A}} \\ \vec{v}_{\mathrm{B}} \end{pmatrix} = \lambda \begin{pmatrix} \vec{v}_{\mathrm{A}} \\ \vec{v}_{\mathrm{B}} \end{pmatrix} \tag{6.5.1}$$

where h is taken from Eq. (6.3.3). We find the coupled equations

$$h\,\vec{v}_{\mathrm{B}} = \lambda\,\vec{v}_{\mathrm{A}}, \tag{6.5.2}$$

$$h^\dagger\,\vec{v}_{\mathrm{A}} = \lambda\,\vec{v}_{\mathrm{B}}, \tag{6.5.3}$$

for finite λ. Not only in case of zero energy, even generally we can demand $|\vec{v}_{\mathrm{A}}| = |\vec{v}_{\mathrm{B}}|$ since

$$\vec{v}_{\mathrm{A}}^\dagger\,h\,\vec{v}_{\mathrm{B}} = \lambda\,|\vec{v}_{\mathrm{A}}|^2, \tag{6.5.4}$$

$$\vec{v}_{\mathrm{B}}^\dagger\,h^\dagger\,\vec{v}_{\mathrm{A}} = \lambda\,|\vec{v}_{\mathrm{B}}|^2, \tag{6.5.5}$$

implies $|\vec{v}_{\mathrm{A}}|^2 = |\vec{v}_{\mathrm{B}}|^2$. For λ finite, we are left to find only $\vec{v}_{\mathrm{A}}$ or $\vec{v}_{\mathrm{B}}$, since the other follows directly from Eqs. (6.5.2), (6.5.3) above. We will solve always for $\vec{v}_{\mathrm{A}}$.

A disentanglement of $\vec{v}_{\mathrm{A,B}}$ or squaring the eigenvector equation, yields the familiar expressions

$$hh^\dagger\,\vec{v}_{\mathrm{A}} = \lambda^2\vec{v}_{\mathrm{A}}, \tag{6.5.6}$$

$$h^\dagger h\,\vec{v}_{\mathrm{B}} = \lambda^2\vec{v}_{\mathrm{B}}. \tag{6.5.7}$$

For comparison let us revisit Eq. (6.3.12) and identify $\vec{v}_{\mathrm{A}} \equiv |\text{🕸}\rangle$. Since the matrices h, $h^\dagger$ convert into each other by exchanging a's and b's while turning $\mu \to -\mu$, the entries of both sublattice vectors

$$\vec{v}_{\mathrm{A}} = (\xi_1, \ldots, \xi_N)^{\mathrm{T}}\,, \tag{6.5.8}$$

$$\vec{v}_{\mathrm{B}} = (\sigma_1, \ldots, \sigma_N)^{\mathrm{T}} \tag{6.5.9}$$

obey the same Tetranacci recursion relation, namely

$$\xi_{j+2} \;=\; \frac{\lambda^2 + a^2 + b^2 - \mu^2}{ab}\,\xi_j \;- \xi_{j-2} \;- \mathrm{i}\mu\frac{a-b}{ab}\,(\xi_{j+1} \,+\, \xi_{j-1})\,, \tag{6.5.10}$$

$$\sigma_{j+2} \;=\; \frac{\lambda^2 + a^2 + b^2 - \mu^2}{ab}\,\sigma_j \;- \sigma_{j-2} \;- \mathrm{i}\mu\frac{a-b}{ab}\,(\sigma_{j+1} \,+\, \sigma_{j-1})\,. \tag{6.5.11}$$

Here, we extended ξ_j, σ_j to the full sequence and set $j \in \mathbb{Z}$. The open boundary condition of the entire eigenstate $\vec{v}_{\mathrm{c}} = (\vec{v}_{\mathrm{A}}, \vec{v}_{\mathrm{B}})^{\mathrm{T}}$, i.e. $\xi_0 = \xi_{N+1} = \sigma_0 = \sigma_{N+1} = 0$ imposed by Eq. (6.5.1), becomes after the decoupling process

$$\xi_0 \;=\; \xi_{N+1} \;=\; b\,\xi_{N+2} \;-\; a\,\xi_N \;=\; b\,\xi_1 \;-\; a\,\xi_{-1} \;=\; 0. \tag{6.5.12}$$

These conditions act on $\vec{v}_{\mathrm{A}}$ alone, see Eq. (6.3.20). A similar condition holds for $\vec{v}_{\mathrm{B}}$ as well. Nonetheless, we need only to find $\vec{v}_{\mathrm{A}}$, as $\vec{v}_{\mathrm{B}}$ follows from Eq. (6.5.3). In section 4, we discussed the necessity of two left and two right moving quasi-particles to construct a Tetranacci polynomial, see for instance Eq. (4.3.5). As we have shown in Ch. 6.3.2 this ansatz and the boundary condition yield the quantization rule in Eq. (6.3.28). Still, the equal energy constraint given in Eq. (6.3.27) must be obeyed. Thus, we know implicitly all eigenvalues and the associated wavevectors $k_{1,2}$, or alternatively $k_{\Sigma,\,\Delta} = (k_1 \pm k_2)/2$. In turn, the value for the coefficients in Eq. (6.5.10) are now completely known to us. Please notice, that the Eqs. (6.5.10), (6.5.11) are universal for all eigenstates, but the value of $(\lambda^2 + a^2 + b^2 - \mu^2)/(ab)$ differs for each eigenstate. Further, we consider λ to be from now on an arbitrary but fixed eigenvalue of the Kitaev Hamiltonian.

Although our eigenvector problem involves boundary conditions, we can translate them into constraints on the initial values, as we show explicitly in the next sections 6.5.1, 6.5.2 for the individual cases. Consequently, we need only to determine ξ_{-2}, ξ_{-1}, ξ_0 and ξ_1 since Eq. (4.2.23) yields

$$\xi_j \;=\; \sum_{i=-2}^{1} \xi_i\,\mathcal{T}_i(j) \tag{6.5.13}$$

which determines in turn all entries of $\vec{v}_{\mathrm{A}}$. Notice, the values of $\mathcal{T}_i(j)$ are in fact known to us as we explain next. Further, we have chosen Eq. (6.5.13), which is fully equivalent to the superposition of left and right moving quasiparticles, due to its practicality. The initial values of $\mathcal{T}_i(j)$ are defined by their selective property

$$\mathcal{T}_i(j) \;=\; \delta_{i,j}, \quad \text{for only } i,\, j \;=\; -2,\, -1,\, 0,\, 1. \tag{6.5.14}$$

For $j > 1$, $\mathcal{T}_i(j)$ can be obtained in principle from the recursion formula Eq. (6.5.10). Be aware of the fact that the values for $\mathcal{T}_i(j)$ change with the eigenvalue since they depend on $(\lambda^2 + a^2 + b^2 - \mu^2)/(ab)$ or alternatively on the wavevectors associated to λ. The only exceptions are the particle-hole partners as λ enters squared into Eq. (6.5.10).

More advantageous though, is the use of the closed form for $\mathcal{T}_i(j)$ taken from the Eqs. (4.2.42)-(4.2.45) in terms of $\varphi_{1,2}(j)$ or their simplified version in appendix C. As we discussed in Ch. 4.2, the usage of these formulae demands $\eta^2 + 4(\zeta + 2) \neq 0$, i.e. two independent left (right) moving quasiparticles, which is always valid here. The involved Fibonacci decomposition of $\mathcal{T}_i(j)$ into $\varphi_{1,2}$ allows a direct use of the quantized wavevectors. We have

$$\varphi_l(j) \,=\, \frac{\sin\left(k_l d\, j\right)}{\sin\left(k_l d\right)}, \quad l \,=\, 1\,, 2, \tag{6.5.15}$$

according to Eq. (4.3.7), rather than the fully equivalent energy description following Eq. (4.2.33). Please notice, Eq. (6.5.15) holds in general for complex wavevectors and is not restricted to real ones.

Depending on the precise nature of the energy, i.e. finite but non degenerate, finite and degenerate or even zero, the relation between ξ_j and σ_j changes such that we focus temporarily only on $\vec{v}_{\mathrm{A}}$. In all of these cases, we are left to find ξ_{-2}, ξ_{-1}, ξ_0 and ξ_1. Actually, the boundary condition from Eq. (6.5.12) reduces the task further, since $\xi_0 = 0$ and $\xi_{-1} = b\,\xi_1/a$ holds. Thus, only ξ_1 and ξ_{-2} have to be found[11]. In this respect, the cases of non-degenerate and finite degenerate energies, i.e. crossings, differ as we discuss in the sections 6.5.1, 6.5.2. We consider first non-degenerate, finite eigenstates associated to the sub- and supra-gap regime.

6.5.1. Non-degenerate finite energy eigenstates

We derive here the eigenvector formula for nearly all eigenstates, since degenerate energies appear extremely rare for the Kitaev chain compared to the non-degenerate ones.

Initially, we translate the boundary conditions into constraints on the initial values of ξ_j. Please recall that eigenvectors are only defined up to their non zero multiples. This and exploiting the absence of degeneracy[12], means that we can choose exactly one entry freely (without loss of generality); we use $\xi_1 \in \mathbb{R} \setminus \{0\}$. Consequently, the value of ξ_{-1} is set by the boundary condition as $\xi_{-1} = b\xi_1/a$ and we are left to find ξ_{-2}.

Notice that all four boundary equations are linearly dependent for the proper quantized wavevectors $k_{1,2}$. Since already two boundary conditions, namely $\xi_0 = 0$ and $\xi_{-1} = b\xi_1/a$, are satisfied, only one of the remaining two contains further information in order to (uniquely) determine ξ_{-2}. For instance from $\xi_{N+1} = 0$ follows

$$\xi_{-2} \,=\, -\xi_1\, \frac{a\,\mathcal{T}_1(N+1) \,+\, b\,\mathcal{T}_{-1}(N+1)}{a\,\mathcal{T}_{-2}(N+1)}, \tag{6.5.16}$$

[11] This is the most ungrateful part of the work, as simple expressions are only available in the degenerate energy cases.

[12] The eigenspace has thus dimension one.

supposing $\mathcal{T}_{-2}(N+1) \neq 0$. Otherwise $b\,\xi_{N+2} - a\,\xi_N = 0$ grants

$$\xi_{-2} = \frac{\xi_1\,[a\,\mathcal{T}_1(N) - b\,\mathcal{T}_1(N+2)] + \xi_{-1}\,[a\,\mathcal{T}_{-1}(N) - b\,\mathcal{T}_{-1}(N+2)]}{b\,\mathcal{T}_{-2}(N+2) - a\,\mathcal{T}_{-2}(N)} \tag{6.5.17}$$

for $b\,\mathcal{T}_{-2}(N+2) - a\,\mathcal{T}_{-2}(N) \neq 0$. Note, the case when the denominators in both Eq. (6.5.16) and Eq. (6.5.17) are simultaneously zero belongs to degenerate energy states as we show in Ch. 6.5.2 in more detail. In the case that neither $\mathcal{T}_{-2}(N+1)$ nor $b\,\mathcal{T}_{-2}(N+2) - a\,\mathcal{T}_{-2}(N)$ is zero, both expressions give the same value of ξ_{-2}, due to the linear dependency of the boundary condition imposed by the quantization rule. However, an approximated, numerical or an inaccurate value for the wavevectors may result in small difference between the Eqs. (6.5.16), (6.5.17). Since ξ_{-2} is fixed, we found all initial values and thus $\vec{v}_\mathrm{A}$ is fully determined.

Before we continue though, notice that the recursion coefficients in Eq. (6.5.10) are in fact real numbers. Thus, the basic Tetranacci polynomials $\mathcal{T}_i(j)$ are real[13] valued due to their initial values from Eq. (6.5.14). In turn, all ξ_j are real, since ξ_1 was chosen so.

We are left to give the formula for $\vec{v}_\mathrm{B} = (\sigma_1, \ldots, \sigma_N)^\mathrm{T}$. In principle we can repeat the procedure of finding $\vec{v}_\mathrm{A}$, since

$$\sigma_j = \sum_{i=-2}^{1} \sigma_i\,\mathcal{T}_i(j) \tag{6.5.18}$$

holds. Notice, that these values for $\mathcal{T}_i(j)$ are exactly the same as for ξ_j. The initial values σ_{-2}, σ_{-1}, σ_0 and σ_1 can be read out from $\vec{v}_\mathrm{A}$ using Eqs. (6.5.2), (6.5.3). We find $\sigma_0 = 0$, $\sigma_{-1} = a\sigma_1/b$ and

$$\sigma_{-2} = \frac{-\mathrm{i}\mu\,\sigma_1 - \lambda\,\xi_1}{a}. \tag{6.5.19}$$

The value of σ_1 is

$$\sigma_1 = \frac{\mathrm{i}\mu\,\xi_1 + b\,\xi_2}{\lambda}. \tag{6.5.20}$$

Consequently, σ_1 is purely imaginary and so are in turn all σ_j. This is in agreement with the eigenvector equation and $\vec{v}_\mathrm{B}$ is now fully determined. However, there is a much simpler, alternative approach using the (sublattice) inversion symmetry $\mathcal{I}_\mathrm{s}$

$$\mathcal{I}_\mathrm{s} = \begin{bmatrix} & & 1 \\ & \iddots & \\ 1 & & \end{bmatrix}_{N\times N}, \tag{6.5.21}$$

as we discuss now. For shortness, we define

$$\mathcal{I} \coloneqq \begin{pmatrix} \mathcal{I}_\mathrm{s} & \\ & \mathcal{I}_\mathrm{s} \end{pmatrix}. \tag{6.5.22}$$

[13] In particular, this is true for decaying states associated to finite energy.

The action of $\mathcal{I}$ on the full Hamiltonian $\mathcal{H}_\mathrm{c}$ from Eq. (6.3.2) is

$$\mathcal{I} \begin{pmatrix} & h \\ h^\dagger & \end{pmatrix} \mathcal{I} = \begin{pmatrix} & h \\ h^\dagger & \end{pmatrix}_{\Delta \to -\Delta} \tag{6.5.23}$$

in agreement with Eq. (5.1.2). Since h, $h^\dagger$ contain $a = \mathrm{i}(\Delta - t)$, $b = \mathrm{i}(\Delta + t)$ and $a|_{-\Delta} = -b$, $b|_{-\Delta} = -a$ holds, we find $h^\dagger|_{-\Delta} = -h$ ($h|_{-\Delta} = -h^\dagger$) according to Eq. (6.3.3). Thus, we have

$$\mathcal{I} \begin{pmatrix} & h \\ h^\dagger & \end{pmatrix} \mathcal{I} = - \begin{pmatrix} & h^\dagger \\ h & \end{pmatrix}, \tag{6.5.24}$$

and we can relate $\vec{v}_\mathrm{A}$ and $\vec{v}_\mathrm{B}$ directly by $\mathcal{I}$ next. The inversion symmetry imposed on both sides of the eigenvector equation in Eq. (6.5.1) and using $\mathcal{I}^2 = \mathbb{1}_{2N}$ grants

$$h^\dagger \, (\mathcal{I}_\mathrm{s} \, \vec{v}_\mathrm{B}) \; = \; -\lambda \, (\mathcal{I}_\mathrm{s} \, \vec{v}_\mathrm{A}) \, , \tag{6.5.25}$$

$$h \, (\mathcal{I}_\mathrm{s} \, \vec{v}_\mathrm{A}) \; = \; -\lambda \, (\mathcal{I}_\mathrm{s} \, \vec{v}_\mathrm{B}) \, . \tag{6.5.26}$$

Remarkably, our last two expressions are very similar to Eqs. (6.5.2), (6.5.3) and since the eigenvector space corresponding to λ has dimension one, the state $\mathcal{I}\vec{v}$ is essentially $\vec{v}$ itself apart from a phase factor. One finds

$$\vec{v}_\mathrm{B} \; = \; \mp \mathrm{i} \, \mathcal{I}_\mathrm{s} \, \vec{v}_\mathrm{A}, \tag{6.5.27}$$

obeying the constraint $|\vec{v}_\mathrm{B}| = |\vec{v}_\mathrm{A}|$. The imaginary unit follows from the eigenvector equation, as we set the entries of $\vec{v}_\mathrm{A}$ to be real. In turn, the normalized eigenstate $\vec{v}$ reads

$$\vec{v}_\mathrm{c} \; = \; \frac{1}{\sqrt{2}|\vec{v}_\mathrm{A}|} \begin{pmatrix} \vec{v}_\mathrm{A} \\ \mp \mathrm{i} \, \mathcal{I}_\mathrm{s} \, \vec{v}_\mathrm{A} \end{pmatrix}, \tag{6.5.28}$$

where the two signs reflect the particle-hole (chiral) symmetry $\mathcal{P} = \mathbb{1}_{2N} \, \mathcal{K}$ ($\mathcal{C} = \tau_z \otimes \mathbb{1}_N$) in real space. The normalization constant involves non linear combinations of Tetranacci polynomials[14] so we do not intend to calculate this factor. The relation between the entries ξ_j, σ_j reads ($j = 1, \ldots, N$)

$$\sigma_j \; = \; \mp \mathrm{i} \, \xi_{N+1-j}. \tag{6.5.29}$$

and thus we have

$$\sigma_{N+1-j} \; = \; \mp \mathrm{i} \sum_{i=-2}^{1} \xi_i \, \mathcal{T}_i(j). \tag{6.5.30}$$

[14] Non linear recursion formulas for Tetranacci polynomials can be derived in principle. Unfortunately, they depend on the initial values, which precisely change here with the eigenvalue and the parameters.

Although the two signs in Eq. (6.5.30) correspond to the energy eigenvalues $\pm\lambda$, the relation depends on the parameters in agreement with numerical investigations. Concretely, the Eqs. (6.5.18), (6.5.20), (6.5.29) yield

$$\lambda\, s \;=\; \frac{\mu \;+\; (\Delta + t)\,\left(\frac{\xi_{-2}}{\xi_1}\,\mathcal{T}_{-2}(2) \;+\; \frac{b}{a}\,\mathcal{T}_{-1}(2) \;+\; \mathcal{T}_1(2)\right)}{\frac{\xi_{-2}}{\xi_1}\,\mathcal{T}_{-2}(N) \;+\; \frac{b}{a}\,\mathcal{T}_{-1}(N) \;+\; \mathcal{T}_1(N)} \tag{6.5.31}$$

where s represents the sign in Eq. (6.5.30). All expressions on the r.h.s are already known to us, particularly λ enters only in even powers. Thus, s has to be chosen properly. However, for most practical applications this sign does not matter and the physical quantities for which we will look later depend only on the absolute value of the eigenvector entries, where the sign drops out.

The eigenstate $\vec{v}_\mathrm{c}$ is associated to the fermionic operator $\hat{\psi}$. Explicitly, we have

$$\hat{\psi} \;=\; \frac{1}{\sqrt{2}|\vec{v}_\mathrm{A}|}\left(\sum_{j=1}^{N} \xi_j\,\gamma_j^{A} \;+\; \sigma_j\,\gamma_j^{B}\right) \tag{6.5.32}$$

satisfying

$$\hat{\psi}^2 \;=\; \frac{1}{2\sqrt{2}|\vec{v}_\mathrm{A}|}\left(\sum_{j=1}^{N} \xi_j^2 \;+\; \sigma_j^2\right) \;=\; \frac{1}{2\sqrt{2}|\vec{v}_\mathrm{A}|}\left(\sum_{j=1}^{N} \xi_j^2 \;-\; \xi_{N+1-j}^2\right) \;=\; 0. \tag{6.5.33}$$

We may decompose $\hat{\psi} = (\hat{\psi}_\mathrm{A} \;+\; \mathrm{i}\,\hat{\psi}_\mathrm{B})/\sqrt{2}$ into Majorana fermions

$$\hat{\psi}_\mathrm{A} \;=\; \frac{1}{|\vec{v}_\mathrm{A}|}\sum_{j=1}^{N} \xi_j\,\gamma_j^{A}, \tag{6.5.34}$$

$$\hat{\psi}_\mathrm{B} \;=\; \frac{1}{|\vec{v}_\mathrm{B}|}\sum_{j=1}^{N} \mathrm{Im}(\sigma_j)\,\gamma_j^{B}, \tag{6.5.35}$$

obeying $\hat{\psi}_{\mathrm{A,B}}^\dagger = \hat{\psi}_{\mathrm{A,B}}$, $\hat{\psi}_{\mathrm{A,B}}^2 = 1/2$ and $\left\{\hat{\psi}_\mathrm{A},\, \hat{\psi}_\mathrm{B}\right\} = 0$.

In order to relate our results back to Fig. 6.12, one has to transform the eigenstate $\vec{v}_\mathrm{c}$ into the BdG basis $\hat{\psi}_\mathrm{BdG} \;=\; \left(d_1, \ldots, d_N, d_1^\dagger, \ldots, d_N^\dagger\right)$. In turn, the particle (hole) $\vec{u} = \vec{v}_\mathrm{A} - \mathrm{i}\vec{v}_\mathrm{B}$ ($\vec{v} \;=\; \vec{v}_\mathrm{A} + \mathrm{i}\vec{v}_\mathrm{B}$) components are found. For the non-degenerate energy eigenstates, Eq. (6.5.27) implies that either the electronic or the hole sector of the eigenstate has even parity w.r.t. to spatial inversion. The other component is then odd. This behavior is reverted for $\lambda \to -\lambda$ as the relative sign between $\vec{v}_\mathrm{A}$ and $\vec{v}_\mathrm{B}$ at fixed parameters is changed.

6.5.2. Degenerate finite energy eigenstates

We discussed the degenerate energies, i.e. the crossings, already in section 6.4.3, but we have not proven the given statements yet. The reason behind this decision was to lower the level of abstraction for the reader. Initially, the only available information related to degenerate energies is that hermitian matrices such as $\mathcal{H}_\mathrm{c}$ are always diagonalisable[15] (even for degeneracies). As for instance Fig. 6.11 suggests, we find only two-fold degenerate eigenvalues for $\mu \neq 0$ and $t^2 \neq \Delta^2$, $t\Delta \neq 0$. In the following derivation, we assume a $D \geq 2$-fold degeneracy in the beginning and we prove that only $D = 2$ is allowed.

The D-fold degeneracy reflects the existence of D linearly independent eigenvectors denoted by $\vec{v}_\mathrm{c}^{(d)}$ with $d = 1, \ldots, D \geq 2$. Here, we adapt the notation of the non-degenerate case. The sublattice structure of $\mathcal{H}_\mathrm{c}$ suggests to set $\vec{v}_\mathrm{c}^{(d)} = \left(\vec{v}_\mathrm{A}^{(d)}, \vec{v}_\mathrm{B}^{(d)}\right)^\mathrm{T}$. Since $\vec{v}_\mathrm{c}^{(d)}$ is an eigenvector of $\mathcal{H}_\mathrm{c}$, $\vec{v}_\mathrm{A,B}^{(d)}$ obey

$$h\,\vec{v}_\mathrm{B}^{(d)} = \lambda\,\vec{v}_\mathrm{A}^{(d)}, \tag{6.5.36}$$

$$h^\dagger\,\vec{v}_\mathrm{A}^{(d)} = \lambda\,\vec{v}_\mathrm{B}^{(d)}, \tag{6.5.37}$$

for all $d = 1, \ldots, D \geq 2$. Here, λ is the D-fold degenerate eigenvalue, which is not known to us at the moment. In analogy to the Eqs. (6.5.4), (6.5.5), $|\vec{v}_\mathrm{A}^{(d)}| = |\vec{v}_\mathrm{B}^{(d)}|$ holds.

We decouple both sublattice vectors, granting

$$h\,h^\dagger\,\vec{v}_\mathrm{A}^{(d)} = \lambda^2\,\vec{v}_\mathrm{A}^{(d)} \tag{6.5.38}$$

and exchanging the order of h, $h^\dagger$ yields the equation for $\vec{v}_\mathrm{B}^{(d)}$. Further, we set $\vec{v}_\mathrm{A}^{(d)} = (\xi_1^{(d)}, \ldots, \xi_N^{(d)})^\mathrm{T}$, $\vec{v}_\mathrm{B}^{(d)} = (\sigma_1^{(d)}, \ldots, \sigma_N^{(d)})^\mathrm{T}$ for convenience. The entries $\xi_j^{(d)}$, $\sigma_j^{(d)}$ obey still the Tetranacci recursion formula

$$\xi_{j+2}^{(d)} = \frac{\lambda^2 + a^2 + b^2 - \mu^2}{ab}\,\xi_j^{(d)} - \xi_{j-2}^{(d)} - \mathrm{i}\mu\frac{a-b}{ab}\left(\xi_{j+1}^{(d)} + \xi_{j-1}^{(d)}\right) \tag{6.5.39}$$

$$\sigma_{j+2}^{(d)} = \frac{\lambda^2 + a^2 + b^2 - \mu^2}{ab}\,\sigma_j^{(d)} - \sigma_{j-2}^{(d)} - \mathrm{i}\mu\frac{a-b}{ab}\left(\sigma_{j+1}^{(d)} + \sigma_{j-1}^{(d)}\right) \tag{6.5.40}$$

since the eigenvector equation has not changed. Crucially, the coefficients in Eq. (6.5.39) do not depend on d, since λ is degenerate. Thus, the eigenvectors $\vec{v}_\mathrm{c}^{(d)}$ differ only due to the initial values of $\xi_{j+2}^{(d)}$ and $\sigma_{j+2}^{(d)}$. Further, the basic Tetranacci polynomials $\mathcal{T}_i(j)$ obey Eq. (6.5.39) as well and since their initial values are fixed by the selective property from Eq. (6.5.14), they do not depend on d either. In turn, we have

$$\xi_{j+2}^{(d)} = \sum_{i=-2}^{1} \xi_i^{(d)}\,\mathcal{T}_i(j), \tag{6.5.41}$$

$$\sigma_{j+2}^{(d)} = \sum_{i=-2}^{1} \sigma_i^{(d)}\,\mathcal{T}_i(j). \tag{6.5.42}$$

[15] This is for arbitrary square matrices not necessarily the case.

In analogy to the prior non degenerate case, only $\vec{v}_{\mathrm{A}}^{(d)}$ has to be determined as $\vec{v}_{\mathrm{B}}^{(d)}$ follows immediately from Eq. (6.5.37). Consequently, we can solely focus on $\xi_{-2}^{(d)}, \ldots, \xi_{1}^{(d)}$. Since the structure of the eigenvector equation is the same as in the non-degenerate case, $\vec{v}_{\mathrm{A}}^{(d)}$ has to obey

$$\xi_0^{(d)} = \xi_{N+1}^{(d)} = b\,\xi_{N+2}^{(d)} - a\,\xi_N^{(d)} = b\,\xi_1^{(d)} - a\,\xi_{-1}^{(d)} = 0. \tag{6.5.43}$$

Hence, only are $\xi_1^{(d)}$ and $\xi_{-2}^{(d)}$ are required to know.

Importantly, the eigenvector equation is linear, i.e. any superposition of its solutions is still an eigenvector. In the context of Eqs. (6.5.36)-(6.5.41), this superposition is translated straightforwardly to a linear combination of the initial values $\xi_{-2}^{(d)}, \ldots, \xi_{1}^{(d)}$ without changing the used coefficients. As one can show easily, this allows to set $\xi_1^{(d)}$ and $\xi_{-2}^{(d)}$ arbitrarily. We choose

$$\xi_1^{(1)} = 1,\ \xi_{-2}^{(1)} = 0, \tag{6.5.44}$$

$$\xi_1^{(2)} = 0,\ \xi_{-2}^{(2)} = 1, \tag{6.5.45}$$

without restrictions since $d = 1, \ldots, D \geq 2$ holds. In turn,

$$\xi_{-1}^{(1)} = \frac{b}{a},\ \xi_0^{(1)} = 0, \tag{6.5.46}$$

$$\xi_{-1}^{(2)} = 0,\ \xi_0^{(2)} = 0, \tag{6.5.47}$$

are fixed by the boundary condition. According to Eq. (6.5.41), linear combinations of $\xi_j^{(1)}$ and $\xi_j^{(2)}$ allow the construction of any $\xi_j^{(d)}$ $(d \neq 1, 2)$. Thus, the eigevectors $\vec{v}_{\mathrm{c}}^{(d)}$ for $d > 3$ are linearly dependent to $\vec{v}_{\mathrm{c}}^{(1,2)}$ which is a contradiction to the hermiticity of $\mathcal{H}_{\mathrm{c}}$. Consequently, only twofold degeneracies are allowed for $\mu \neq 0$ and $t^2 \neq \Delta^2$, $t\Delta \neq 0$.

We keep the setting in Eqs. (6.5.44), (6.5.45). Next, one has to truly satisfy the boundary condition from Eq. (6.5.43), in order to determine the eigenvalue λ and the associated eigenvectors.

The boundary conditions and the closed form for the Tetranacci polynomials yield

$$\mathcal{T}_1(N+1) + \frac{b}{a}\,\mathcal{T}_{-1}(N+1) = 0 \tag{6.5.48}$$

$$b\left[\mathcal{T}_1(N+2) + \frac{b}{a}\,\mathcal{T}_{-1}(N+2)\right] - a\left[\mathcal{T}_1(N) + \frac{b}{a}\,\mathcal{T}_{-1}(N)\right] = 0 \tag{6.5.49}$$

and also

$$\mathcal{T}_{-2}(N+1) = 0 \tag{6.5.50}$$

$$b\mathcal{T}_{-2}(N+2) - a\mathcal{T}_{-2}(N) = 0. \tag{6.5.51}$$

Notice that the two-fold degeneracy allowed a splitting of the boundary conditions compared to the non-degenerate case since two equations respectively for $N+1$ (N and

$N+2$) are found. In appendix I, we demonstrate that the Eqs. (6.5.48) - (6.5.51) alone imply

$$k_{1,2}d \,=\, \frac{n\pi}{N+1}, \quad n \,=\, 1\,\ldots,\,N. \tag{6.5.52}$$

Here, all combinations of $k_{1,2}d$ are a-priori allowed.

Still, any other choice of $\xi_1^{(1,d)}$, $\xi_{-2}^{(1,d)}$ as done in Eqs. (6.5.44), (6.5.45) corresponds to degenerate eigenvectors. In particular, a splitting of the boundary conditions can be prevented. Thus, the general quantization rule of the Kitaev chain from Eq. (6.3.28) has still to be satisfied. Further, the Tetranacci polynomials demand directly the equal energy constraint on k_1 and k_2 such that only specific combinations from Eq. (6.5.52) are left. This grants directly the criterion from section 6.4.3 expressed in terms of $k_\Sigma \,=\, (k_1+k_2)/2$, $k_\Delta \,=\, (k_1-k_2)/2$ for convenience. In other words the parameter constraints on t, Δ, μ and the twofold degenerate eigenvalues are known to us. In turn, $\vec{v}_{\rm A}^{\,(1,2)}$ are fixed.

Similar to the non-degenerate case, one can show that

$$\vec{v}_{\rm B}^{\,(d)} \,=\, \mp{\rm i}\,\mathcal{I}_{\rm s}\,\vec{v}_{\rm A}^{\,(d)} \tag{6.5.53}$$

holds. Notice, the eigenvector space has dimension two. The identification granting Eq. (6.5.53) uses that $\xi_1^{(1)}$, $\xi_{-2}^{(2)}$ can be varied independently from $\xi_1^{(1)}$, $\xi_{-2}^{(2)}$.

The two signs in Eq. (6.5.53) reflect the particle-hole (chiral) symmetry. Due to the degeneracy, the eigenvectors rearrange into even/ odd ones under the action of the inversion symmetry. Finally, the expression for the fermionic field operator associated to $\vec{v}_{\rm c}^{\,(d)}$, and the corresponding Majorana fermions generalize straightforwardly from the non-degenerate case.

We are left to calculate the zero energy eigenstates.

6.5.3. Zero energy eigenstates

For zero energy, the eigenvector equation Eq. (6.5.1) becomes

$$\begin{bmatrix} & h \\ h^\dagger & \end{bmatrix} \vec{v} \,=\, \vec{0}. \tag{6.5.54}$$

Since zero energy is (if existent) always degenerate due to the particle-hole symmetry, one can set indeed $\vec{v}_1 \,=\, (\vec{v}_{\rm A},\,\vec{0})^{\rm T}$, $\vec{v}_2 \,=\, (\vec{0},\,\vec{v}_{\rm B})^{\rm T}$. Any superposition of the two solutions is possible and we thus refer only to $\vec{v}_{\rm A,\,B}$. From Eq. (6.5.54) we find the decoupled equations

$$h^\dagger\,\vec{v}_{\rm A} \,=\, 0, \tag{6.5.55}$$

$$h\,\vec{v}_{\rm B} \,=\, 0, \tag{6.5.56}$$

and we consider here only the case of $\mu \neq 0$ and $t\Delta \neq 0$, $t^2 \neq \Delta^2$. In order to proceed, we set $\vec{v}_{\rm A} = (\xi_1,\,\ldots,\,\xi_N)^{\rm T}$, $\vec{v}_{\rm B} = (\sigma_1,\,\ldots,\,\sigma_N)^{\rm T}$ and the constraints on the entries read

$$-a\,\xi_{j-1} \,+\, {\rm i}\,\mu\,\xi_j \,+\, b\,\xi_{j+1} \,=\, 0, \tag{6.5.57}$$

$$-b\,\sigma_{j-1} \,-\, {\rm i}\,\mu\,\sigma_j \,+\, a\,\sigma_{j+1} \,=\, 0. \tag{6.5.58}$$

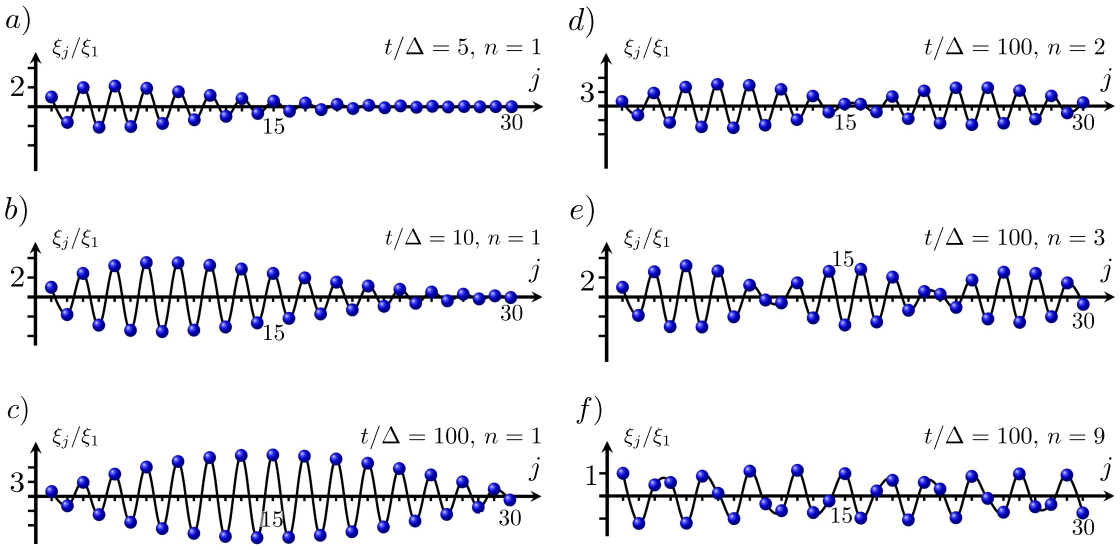

Figure 6.16.: Spatial profile of the Majorana zero modes $\vec{v}_{\mathrm{A}}$. ξ_j/ξ_1 (•) is depicted according to Eq. (6.5.62) and the black line is a guide to the eye. The parameters are $N = 30$ and $\mu_n = 2\sqrt{t^2 - \Delta^2}\cos(n\pi/N+1)$. Left column: We have fixed $n = 1$ and vary $t/\Delta = 5,\ 10,\ 100$. For small values t/Δ, the state is localized at the left end and gets further extended by increasing t/Δ. Right column: We set $t/\Delta = 100$ constant and n is varied. The chemical potential causes oscillations of the MZM.

Here, we extend to all $j \in \mathbb{Z}$ granting in turn the boundary conditions $\xi_0 = \xi_{N+1} = 0$ and $\sigma_0 = \sigma_{N+1} = 0$. We need to solve only for ξ_j as σ_j follows directly by $a \leftrightarrow b$ and $\mu \to -\mu$. Since the entries ξ_j form a Fibonacci sequence

$$\xi_{j+1} = -\frac{\mathrm{i}\,\mu}{b}\,\xi_j + \frac{a}{b}\,\xi_{j-1} \equiv x\,\xi_j + y\,\xi_{j-1} \tag{6.5.59}$$

we apply Eqs. (4.1.2), (4.1.17). We get

$$\xi_j = \xi_1\,\mathcal{F}(j) = \xi_1\,\frac{R_+^j - R_-^j}{R_+ - R_-}, \quad R_\pm = \frac{-\mu \pm \sqrt{\mu^2 + 4\,(\Delta^2 - t^2)}}{2\,(\Delta + t)}, \tag{6.5.60}$$

in agreement with [69, 70]. Here, we used only $\xi_0 = 0$ and ξ_1 accounts for the normalization. The constraint $\xi_{N+1} = 0$ is not yet imposed. Instead, the values[16] for $R_\pm$ are not quantized so far.

Similar to all prior Fibonacci sequences, we can make the standard ansatz $\mu = 2\sqrt{t^2 - \Delta^2}\cos(\theta)$, $\theta \in \mathbb{C}$ yielding $R_\pm = -\mathrm{sign}(t)\sqrt{(t-\Delta)/(t+\Delta)}\,\exp(\mp\mathrm{i}\theta)$. In turn, we have

$$\xi_j = \xi_1\,[-\mathrm{sign}(t)]^{j-1}\,\frac{\sin(\theta\,j)}{\sin(\theta)}\,\left(\frac{t-\Delta}{t+\Delta}\right)^{\frac{j-1}{2}}. \tag{6.5.61}$$

[16] We follow here essentially the footsteps of Kitaev, since his $x_\pm$ is $R_\pm$ [2].

The open boundary condition at the right end of the system $\xi_{N+1} = 0$ is only satisfied for $\theta \equiv \theta_n = n\pi/(N+1)$, $n = 1 \ldots, N$. Thus, our ansatz $\mu = 2\sqrt{t^2 - \Delta^2}\cos[n\pi/(N+1)] \equiv \mu_n$ becomes automatically the criterion for the zero energy lines, see Eq. (6.3.7) and $t^2 \geq \Delta^2$ must hold true. Notice that in chapter 6.4.2 we have shown $\theta_n = k_\Sigma d$.

The calculation for σ_j is analogues and we find

$$\xi_j = \xi_1 \, [-\mathrm{sign}(t)]^{j-1} \, \frac{\sin(\theta_n \, j)}{\sin(\theta_n)} \, \left(\frac{t-\Delta}{t+\Delta}\right)^{\frac{j-1}{2}}, \tag{6.5.62}$$

$$\sigma_j = \sigma_1 \, [-\mathrm{sign}(t)]^{j-1} \, \frac{\sin(\theta_n \, j)}{\sin(\theta_n)} \, \left(\frac{t+\Delta}{t-\Delta}\right)^{\frac{j-1}{2}}, \tag{6.5.63}$$

and $j = 1, \ldots, N$. We see that for $t/\Delta > 0$ ($t/\Delta < 0$) the sublattice vector $\vec{v}_\mathrm{A}$ is localized closer to the left (right) end, i.e. it reaches its maximum at $j = 1$ ($j = N$), and $\vec{v}_\mathrm{B}$ decays always from the other side. Remember that the inversion symmetry applied to the Kitaev chain turns $\Delta \to -\Delta$ which connects here the structures of ξ_j and σ_j. We extract the decay length ξ as

$$\xi = \frac{2d}{\left|\ln\left(\frac{t-\Delta}{t+\Delta}\right)\right|} \tag{6.5.64}$$

and we may write

$$\xi_j = \xi_1 \, [-\mathrm{sign}(t)]^{j-1} \, \frac{\sin(\theta_n \, j)}{\sin(\theta_n)} \, e^{-(j-1)d/\xi}, \tag{6.5.65}$$

$$\sigma_j = \sigma_1 \, [-\mathrm{sign}(t)]^{j-1} \, \frac{\sin(\theta_n \, j)}{\sin(\theta_n)} \, e^{(j-1)d/\xi} \tag{6.5.66}$$

in case of $(t - \Delta) < (t + \Delta)$ and otherwise we have to replace $\xi \to -\xi$. The chemical potential μ_n is kept inside θ_n and causes the wavefunction to oscillate in space. The possible change $\mu_n \to -\mu_n$, see Fig. 6.9, shifts $\theta_n \to \theta_n + \pi$ corresponding to a local phase shift. In Fig. 6.16 we depicted the spatial behavior of the zero energy modes. For $|\Delta| \lesssim |t|$ the two states become localized at opposite edges, reducing properly to only the first/ last site for $|\Delta| = |t|$, imposing $\mu_n = 0$, in agreement with the prior discussion of the Kitaev points. In contrast, both extend along the Kitaev chain in case of $|t| \gg |\Delta|$.

The values of ξ_j, σ_j fix the eigenvectors $\vec{v}_1 = (\vec{v}_\mathrm{A}, \vec{0})^\mathrm{T}$, $\vec{v}_2 = (\vec{0}, \vec{v}_\mathrm{B})^\mathrm{T}$. Since, ξ_1, σ_1 can be chosen to be real, $\vec{v}_{1,2}$ are eigenstates of the particle-hole symmetry $\mathcal{P} = \mathcal{K}\,\mathbb{1}_{2N}$, i.e. they are Majorana zero modes. The associated operators $\hat{\psi}_{\mathrm{A,B}}$ read

$$\hat{\psi}_\mathrm{A} = \frac{1}{|\vec{v}_\mathrm{A}|} \sum_{j=1}^{N} \xi_j \, \gamma_j^A, \tag{6.5.67}$$

$$\hat{\psi}_\mathrm{B} = \frac{1}{|\vec{v}_\mathrm{B}|} \sum_{j=1}^{N} \sigma_j \, \gamma_j^B, \tag{6.5.68}$$

satisfying $\hat{\psi}^{\dagger}_{\mathrm{A,B}} = \hat{\psi}_{\mathrm{A,B}}$, $\hat{\psi}^{2}_{\mathrm{A,B}} = 1/2$ and $\left\{\hat{\psi}_{\mathrm{A}}, \hat{\psi}_{\mathrm{B}}\right\} = 0$.

Notice, that the "Fibonacci" ξ_j, σ_j are in fact Tetranacci polynomials for $E_{\pm}(kd) = \lambda = 0$. The easy proof is $hh^{\dagger}\vec{v}_{\mathrm{A}} = \vec{0}$, $h^{\dagger}h\vec{v}_{\mathrm{B}} = \vec{0}$ following from Eqs. (6.5.55), (6.5.56) and recalling the derivation of Tetranacci recursion formula. Alternatively, we use Eq. (6.5.57) at $j \to j \pm 1$. The multiplication with $b \neq 0$ and $a \neq 0$ yields

$$ab\,\xi_{j-2} = b^2\,\xi_j + \mathrm{i}\mu b\,\xi_{j-1} \tag{6.5.69}$$

$$ab\,\xi_{j+2} = a^2\,\xi_j - \mathrm{i}\mu a\,\xi_{j+1}. \tag{6.5.70}$$

Further, we multiply Eq. (6.5.57) with $\mathrm{i}\mu$

$$0 = \mathrm{i}\mu b\,\xi_{j+1} - \mathrm{i}\mu a\,\xi_{j-1} - \mu^2\,\xi_j. \tag{6.5.71}$$

The sum of the last expressions grants

$$\xi_{j+2} = \frac{a^2 + b^2 - \mu^2}{ab}\,\xi_j - \xi_{j-2} + \mathrm{i}\mu\frac{b-a}{ab}\,(\xi_{j+1} + \xi_{j-1})\,, \tag{6.5.72}$$

the promised Tetranacci recursion formula at $\lambda = 0$ after rearranging the terms. Before we conclude in section 6.7, we first discuss the promised similarities between the Kitaev chain and the n.n.n. chain from Chapter 3.

6.6. Relations between the Kitaev chain and the atomic chain with n.n.n. hopping

Although the first notion of the n.n.n. chain and the Kitaev chain Eqs. (3.1.1), (5.1.1) seems contradictory, both models are quite similar after deeper investigation. We saw that both models obey the Tetranacci sequence from Eq. (4.2.1) for different ζ, η. In case of the Kitaev chain this is possibly surprising as this model contains only nearest neighbor terms by definition. However, the BdG Hamiltonian of the Kitaev chain possess the n.n.n. term ab after the decoupling of the γ^A, γ^B Majorana operators. In order to support this statement, we repeat this decoupling process and derive the entries of $hh^{\dagger}$, see Eq. (6.3.13), shown in a pictorial from in Fig. 6.17. Notice that the matrix h ($h^{\dagger}$) accounts for terms of the form $\gamma^A_j\ \gamma^B_i$ ($\gamma^A_i\ \gamma^B_j$) such that $hh^{\dagger}$ describes effective hopping processes from γ^A_j to $\gamma^A_{j'}$ mediated via $\gamma^B_{j''}$. We consider a mid-chain position γ^A_j far away from the boundaries at first for simplicity, as indicated in Fig. 6.17. At first we focus on effective nearest neighbor terms γ^A_j to γ^A_{j+1} following the arrows. We find the two independent options (in this order) $a\,\mathrm{i}\mu$ ($\searrow\ \uparrow$) and $-\mathrm{i}\mu\,b$ ($\downarrow\ \nearrow$). The only n.n.n. term from γ^A_j to γ^A_{j+2} is ab ($\searrow\nearrow$) without intermediate rest at a single $\gamma^A_{j'}$. The effective onsite "hoppings" from γ^A_j to γ^A_j itself are $-\mathrm{i}\mu\,(\mathrm{i}\mu)$ ($\downarrow\uparrow$), $a\,(-a)$ ($\searrow\nwarrow$) and $(-b)\,b$ ($\swarrow\nearrow$). Notice here that for the latter two processes the neighboring $\gamma^B_{j\pm1}$ has to exist. Thus, we have to exclude these processes partially at the ends of the Kitaev chain granting $-b^2(1-\delta_{j1})$ and $-a^2(1-\delta_{jN})$. We simplify the stated products and in turn

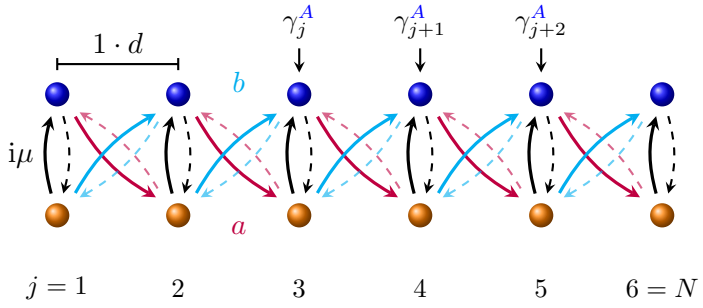

Figure 6.17.: Kitaev Hamiltonian in chiral basis for $N = 6$ sites. The Majorana operators γ^A (•), γ^B (•) form connected sublattices. Pictorially, one can decouple both parts of the system by focusing on processes from γ_j^A to γ_{j+1}^A (γ_{j+2}^A) via γ^B. These terms are kept in $hh^\dagger$ and more details are stated in the main text. The solid arrows depict $a = \mathrm{i}(\Delta - t)$ (purple), b=i($\Delta + t$) (cyan) and $\mathrm{i}\mu$ (black). Dashed arrows account for $-a$, $-b$ and $-\mathrm{i}\mu$, respectively.

γ_j^A is connected to $\gamma_{j'}^A$ by

$$\left[\mu^2 - a^2(1-\delta_{jN}) - b^2(1-\delta_{j1})\right]\delta_{j,j'} + \mathrm{i}\mu(a-b)\left(\delta_{j,j'+1} + \delta_{j+1,j'}\right) + ab\left(\delta_{j,j'+2} + \delta_{j+2,j'}\right). \tag{6.6.1}$$

Here, we added the Kronecker deltas to distinguish between onsite, n.n. and n.n.n. terms. Notice that Eq. (6.6.1) is exactly $(hh^\dagger)_{jj'}$ from Eq. (6.3.13). The diagonal term of λ^2 enters only via the eigenvector equation. In section 6.3 we showed that Eq. (6.6.1) yields the Tetranacci recursion formula and the boundary conditions. Further, the Kitaev chain is still by definition a n.n. model, its boundary condition (even after the decoupling of both Majorana sublattices) deviates from the one of the n.n.n. chain from chapter 3.

Since the Kitaev (n.n.n.) chain has three (two) parameters μ, t, Δ (t, m) influencing the quantization rule in case of finite number of sites N with open boundary conditions and since both models fall into different topological classifications, their spectra cannot be quantitatively mapped to each other. However, they match qualitatively very well as Fig. 6.18 shows, when they are plotted in terms of their respective ζ, η.

The distinct quantization rules of both models are still of the same type depending on either $N + 1$ for the Kitaev chain or $N + 2$ for the n.n.n. chain. In this respect, notice that the criterion for (avoided) crossings can be mapped from the n.n.n. chain to the Kitaev chain by replacing $N \to N + 1$. This shift also exchanges the roles for even and odd system sizes for both models in limiting cases properly, as can be seen from Fig. 6.18. At $\eta = 0$, the Kitaev chain shows avoided crossings and the n.n.n. chain degenerated energies.

Finally, we discovered in Ch. 3 that replacing $m \to -m$ changes the eigenvalues (measured w.r.t. μ) of the n.n.n. chain into their negative value; thus, turning the

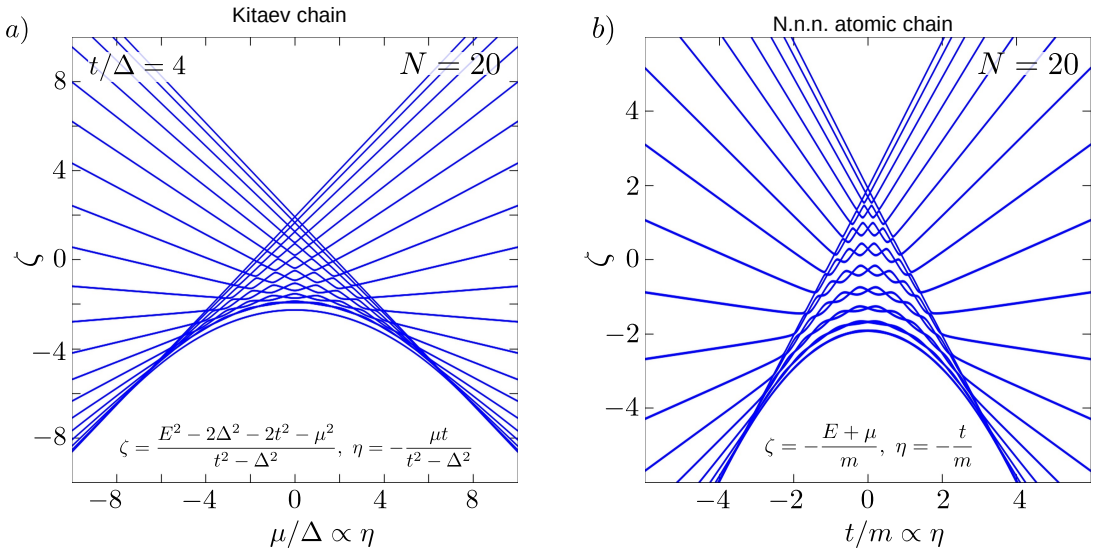

Figure 6.18.: The finite size spectrum of the Kitaev chain and the n.n.n. chain for $N = 20$ converted into their Tetranacci coefficients ζ, η. A quantitative mapping is not possible because of the different role the chemical potential μ adopts in both systems. Note the former in-gap states of the Kitaev chain are converted into the lowest blue line, close to the center of panel a).

arrow-like region with crossings upside down, see for instance Fig. 3.2 a), b). In case of the Kitaev chain, this happens also when the effective n.n.n. hopping $ab = \Delta^2 - t^2$ switches sign, as can be seen back in Fig. 6.11 a), d). However, the coefficient η imposes a different spatial positioning of the crossings for the Kitaev chain. For $\Delta > t$, the degenerate energies are widely separated by η and the arrowhead disappears.

Usually, spectral investigations are done numerically for good reasons. Nonetheless, in case one finds a similar shape, the arrow may be pointing towards a Tetranacci sequence.

6.7. Conclusion

We derived exact analytic expressions for the eigenvectors and the quantization rule (or eigenvalues) for generic parameters t, Δ and μ for Kitaev chain of finite length in case of the open boundary condition(s). Thus, the results stated in Ref. [69–72, 75–77] concerning the Kitaev chain were extended.

The most crucial finding of the approach is that the finite sized Kitaev chain with open boundary condition can be understood based on two constraints: First, the bulk relations obtained in the limit $N \to \infty$ and second, the finite size condition. In case of the former, we have mentioned the well known bulk dispersion relation [2, 7, 19]

$$E_{\pm}(k) = \pm\sqrt{[\mu + 2t\cos(kd)]^2 + 4\Delta^2\sin^2(kd)}. \tag{6.7.1}$$

The open boundary conditions demanded the use of $k_{1,2}$ instead of only "k" obeying the equal energy constraint

$$\cos(k_1 d) + \cos(k_2 d) = -\frac{\mu t}{t^2 - \Delta^2}, \tag{6.7.2}$$

which can be extracted from the dispersion relation. The real space approach to the spectrum and the eigenstates granted the Tetranacci recursion formula for the Kitaev chain, from where the dispersion relation was found as well. On the other hand, the open boundary condition and the finite size of the model yield discrete energy levels and thus quantized wavevectors $k_{1,2}$ at fixed parameters. Information from pure bulk considerations is therefore limited. In particular, recall here the zero energy criterion from Eq. (6.3.7); zero energy was restricted to discrete lines for only $t^2 \geq \Delta^2$ (except N odd and $\mu = 0$) which could not be deduced from only Eq. (6.7.1).

In this respect, we critically analyzed the decay length in section 6.2.3. We found that the (quantized) decay length extracted from the quantized wavevectors $k_{1,2}$ associated to finite energy in-gap states (which can be exponentially small), may deviate from the decay length solely extracted from recursion formulas/ pure bulk arguments. Thus, setting Eq. (6.7.1) to zero and obtaining k without imposing quantization, has to be seen critically. In this scope, we recommend also to revisit Eqs. (6.5.60), (6.5.61) from section 6.5.3.

We demonstrated that energy and spatial profile of an eigenstate are correlated. However, changes in the former are not caused by the latter; rather, the quantization rule ($k_\Sigma = (k_1 + k_2)/2$, $k_\Delta = (k_1 - k_2)/2$)

$$\frac{\sin^2[k_\Sigma d(N+1)]}{\sin^2[k_\Delta d(N+1)]} = \frac{1 + \left(\frac{\Delta}{t}\right)^2 \cot^2(k_\Delta d)}{1 + \left(\frac{\Delta}{t}\right)^2 \cot^2(k_\Sigma d)}, \tag{6.7.3}$$

is the origin of both. In this scope, we proved that energy oscillations as function of the chemical potential in both the sub- and supra-gap regime originate from an interplay of Eq. (6.7.2) and the quantization rule. Physically, μ was forced into its role by the superconducting pairing constant Δ and the Pauli principle for fermions embedded in the BdG construction. For more details, consult for instance appendix E.

We demonstrated in appendix H that the topological phase diagram of the Kitaev chain can be extracted from the quantization rule in Eq. (6.7.3) for $N \to \infty$. In this case, the mid-gap excitations adopt exact zero energy everywhere within the topologically non trivial phase as expected.

Returning to finite N, the bulk constraints Eqs. (6.7.1), (6.7.2) together with finite size constraint from Eq. (6.7.3) demonstrate beautifully the bulk-edge correspondence. In other words, the topological predictions, based for instance on the winding number topological invariant for $N \to \infty$, correctly predict the presence of edge states in the case of open boundary conditions and N finite [7, 31, 105]. One has only to respect the finite size of the model and one should avoid a too naive belief in the arguments based on the bulk properties.

We believe that our conclusions are not limited to the Kitaev chain alone. They might be quantitatively true also in other non-trivial topological classified models. As a perspective, we investigate in chapter 10 in part III, the proximitized Rashba nanowires based on our understanding of the Kitaev chain. The first results are promising. Next, we start by investigating the transport properties of the finite Kitaev chain in sub- and supra-gap regime.

7. Non equilibrium Green's function formalism (NEGF)

The results in sections 7.3, 7.4 have been published partially in [5].

7.1. Motivation

In the first part of the work, we discussed in depth the BdG spectrum of the Kitaev chain and we saw the emergence of the topologically predicted exotic in-gap states known as Majorana fermions. A part of the current research concerns their application as building blocks for quantum computers with a sufficient fault tolerance [2, 63–65]. However, physical devices hosting Majorana fermions have to be built [6, 25–27, 30, 66] and a first important step towards the final goal is to achieve unambiguous detection of the Majorana fermions. In this respect, one possibility relies on electronic charge transport measurements. Naturally the physical properties of a given model influence the behavior of an observed current I w.r.t. to an applied bias V. In particular, the differential conductance $\partial I/\partial V$ at small temperatures $T \approx 0\,\mathrm{K}$ depends strongly on the spectrum of the considered device. Majorana fermions are known to cause a stable quantized zero bias conductance peak in multiples of the conductance quantum e^2/h [7, 27, 45–49]. Although quantized zero bias peaks where already observed experimentally [67, 106], they can have various origins. For instance topologically trivial Andreev bound states; not to mention the influence of imperfections such as disorder and defects in experimental devices etc. [27, 52–55, 107, 108].

Further, the theoretical approaches are -because of the difficulty of realistic setups- mostly restricted to numerical investigations, although a few analytical advances were made including approximations [8, 32, 109]. Here, we derive exact results for both the linear and non-linear transport regime which can be used as a benchmark for interpreting the numerical results of realistic systems. We begin our study by introducing the setup and we guide the reader through the main issues of the current calculation.

7.2. Introduction into the NEGF method

The non-equilibrium Green's function (NEGF) method is a technique to treat the time evolution of observables or expectation values in out-of equilibrium situations [44, 91, 110–115]. In a generic situation, we will not be able to solve the problem exactly and one seeks a perturbative expansion. In this scope, the NEGF approach is advantageous since the obtained expansion is similar to the equilibrium expressions. Generally, a

Green's function is the solution of a differential equation containing a Dirac-delta as inhomogeneity, typically for us in time. This can be seen for example from the retarded G^{r} and advanced G^{a} (single particle) Green's function

$$G^{\mathrm{r}}(t,\,t') \;\coloneqq\; -\frac{\mathrm{i}}{\hbar}\,\theta(t-t')\,\Big\langle\,\Big\{\hat{\psi}(t),\,\hat{\psi}^{\dagger}(t')\Big\}\,\Big\rangle, \tag{7.2.1}$$

$$G^{\mathrm{a}}(t,\,t') \;\coloneqq\; \frac{\mathrm{i}}{\hbar}\,\theta(t'-t)\,\Big\langle\,\Big\{\hat{\psi}(t),\,\hat{\psi}^{\dagger}(t')\Big\}\,\Big\rangle \tag{7.2.2}$$

here in terms of a given fermionic field $\hat{\psi}$. In case of bosonic operators, the anticommutator is replaced by the commutator. A both short and intuitive introduction into Green's function using first quantization and in equilibrium can be found in the chapter "Time independent Lippmann-Schwinger equation" of Ref. [112]. There, the retarded (advanced) GF is introduced as time propagator of an initial wave function forward (backward) in time. In general, the definition of G^{r}, G^{a} does not change and typically for non-equilibrium scenarios, G^{r}, G^{a} depend on both t and t', rather than on only the time difference $t-t'$ as the Heaviside function indicates.

Closely related to G^{r}, G^{a} are the so called greater $G^{>}$ and lesser $G^{<}$ Green's functions

$$G^{>}(t,\,t') \;\coloneqq\; -\frac{\mathrm{i}}{\hbar}\,\Big\langle\,\hat{\psi}(t)\,\hat{\psi}^{\dagger}(t')\,\Big\rangle, \tag{7.2.3}$$

$$G^{<}(t,\,t') \;\coloneqq\; \frac{\mathrm{i}}{\hbar}\,\Big\langle\,\hat{\psi}^{\dagger}(t')\,\hat{\psi}(t)\,\Big\rangle, \tag{7.2.4}$$

even though both are not GF in the strict sense, as no Dirac-Delta arises in their time evolution. Independent of the concrete context, one of the relations between GF is $G^{\mathrm{r}}-G^{\mathrm{a}}=G^{>}-G^{<}$. For completeness, we mention the time-ordered G^{T} and the anti time-ordered GF $G^{\bar{\mathrm{T}}}$

$$G^{\mathrm{T}}(t,t') \coloneqq -\frac{\mathrm{i}}{\hbar}\Big\langle\,\hat{T}\left[\hat{\psi}(t)\,\hat{\psi}^{\dagger}(t')\right]\Big\rangle \;=\; \theta(t-t')\,G^{>}(t,t') \;+\; \theta(t'-t)\,G^{<}(t,t') \tag{7.2.5}$$

$$G^{\bar{\mathrm{T}}}(t,t') \coloneqq -\frac{\mathrm{i}}{\hbar}\Big\langle\,\hat{\bar{T}}\left[\hat{\psi}(t)\,\hat{\psi}^{\dagger}(t')\right]\Big\rangle \;=\; \theta(t'-t)\,G^{>}(t,t') \;+\; \theta(t-t')\,G^{<}(t,t'), \tag{7.2.6}$$

using the ordinary time (anti time) ordering operator $\hat{T}$ ($\hat{\bar{T}}$). Recall that $\hat{T}$ places the latest time left and exchanging two fermionic fields causes a minus sign [113]. The definitions of G^{r}, G^{a}, $G^{>}$, $G^{<}$, G^{T}, $G^{\bar{\mathrm{T}}}$ are not restricted to operators manipulating the same degree of freedom as we did so far, see for instance Eq. (7.3.7) below. The involved degrees of freedom are denoted by indices later.

A generic out of equilibrium situation can be described by the Hamiltonian $\hat{H}_{\mathrm{tot}}$

$$\hat{H}_{\mathrm{tot}} \;=\; \hat{h} \;+\; \hat{H}'(t), \tag{7.2.7}$$

where h is meant as initial Hamiltonian which is exposed to a time dependent perturbation $\hat{H}'$ acting only after some initial time t_0. Explicitly, $\hat{H}'$ can include external fields and interactions. For us, $\hat{H}'$ accounts for the coupling to the leads later [111, 114]. The

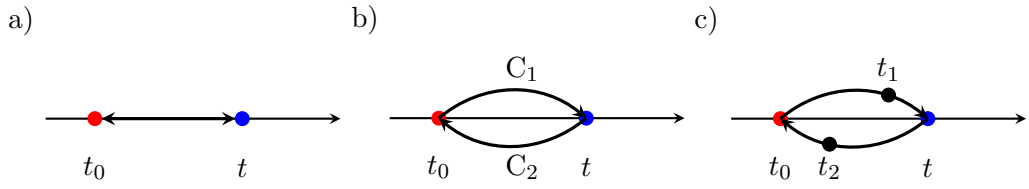

Figure 7.1.: The actual shape of contour C_t is shown in a). The horizontal line displays the time axis and the vertical spacing in the following has no meaning. b) The same contour drawn more usefully with separated forward and backward branches C_1, C_2. c) The contour time ordering $\hat{T}_{C_t}$ and later $\hat{T}_C$ is independent of the usual time ordering. On the contour t_2 is later than t_1, denoted as $t_1 \subset t_2$, although $t_2 < t_1$ is true. Consequently, we have $\hat{T}_{C_t}\left[\hat{\psi}(t_1)\,\hat{\psi}^\dagger(t_2)\right] = -\hat{\psi}^\dagger(t_2)\hat{\psi}(t_1)$ and $\hat{T}\left[\hat{\psi}(t_1)\,\hat{\psi}^\dagger(t_2)\right] = \hat{\psi}(t_1)\hat{\psi}^\dagger(t_2)$.

Hamiltonian $\hat{h} = \hat{H}_0 + \hat{H}_{\text{int}}$ is meant as time independent. Here, $\hat{H}_0$ does not contain interactions and $\hat{H}_{\text{int}}$ accounts for all internal correlations.

The basic idea of the NEGF method is to relate the time evolution of an expectation value, given by the full system $\hat{H}_{\text{tot}}$, to expressions connected to the evolution imposed by $\hat{H}_0$. Since $\hat{H}_0$ describes free particles, Wick's theorem can be applied and many body GF reduce to single particle (s.p.) ones. Thus, the out of equilibrium situation is approached by the equilibrium case. However, one has to account for the full time evolution of the considered GF. Fortunately for us, the relations between Schrödinger/ Heisenberg and interaction picture, which translate the time evolution of $\hat{H}_{\text{tot}}$ with its increments, can be written more advantageously. For instance, the time evolution of the operator $\hat{A}$ meant in the Heisenberg picture w.r. to $\hat{H}_{\text{tot}}$, is associated to $\hat{A}_{\hat{h}}(t)$ in interaction picture w.r.t. to $\hat{H}'(t)$ by [111, 114]

$$\hat{A}(t) = u(t_0,\, t)\,\hat{A}_{\hat{h}}(t)\,u(t,\, t_0). \tag{7.2.8}$$

Here, the time evolution of $\hat{A}_{\hat{h}}$ is determined only by $\hat{h} = \hat{H}_0 + \hat{H}_{\text{int}}$, $u(t_0,\, t)$ reads

$$u(t_0,\, t) = \hat{T}\left\{\exp\left[-\mathrm{i}\int_{t_0}^{t}\hat{H}'_{\hat{h}}(t')\,\mathrm{d}t'\right]\right\} \tag{7.2.9}$$

where $\hat{H}'_{\hat{h}}(t')$ is

$$\hat{H}'_{\hat{h}}(t') = e^{\mathrm{i}\,h(t'-t_0)}\,\hat{H}'(t')\,e^{-\mathrm{i}\,h(t'-t_0)}. \tag{7.2.10}$$

Importantly, one can unite the two operators $u(t,\, t_0)$, $u(t_0,\, t)$ from Eq. (7.2.8) formally into one

$$\hat{A}(t) = \hat{T}_{C_t}\left\{\exp\left[-\mathrm{i}\int_{C_t}\hat{H}'_{\hat{h}}(\tau)\,\mathrm{d}\tau\right]\,\hat{A}_{\hat{h}}(t)\right\}, \tag{7.2.11}$$

by introducing the contour C_t depicted in Fig. 7.1 and the associated contour time ordering operator $\hat{T}_{\mathrm{C}_t}$. The contour C_t treats the "forward" evolution captured by $u(t_0,\, t)$ from t_0 to t and the "backward" evolution kept by $u(t_0,\, t)$ from t back to t_0 as two different branches. Thus, the contour runs on the real axis from t_0, passes through t and back. A cancellation of the two branches and thus a trivial result is prevented by the contour time ordering $\hat{T}_{\mathrm{C}_t}$. Explicitly, time ordering along the contour meant that points visited (following the arrows of the contour) prior to others, are called earlier. For instance, in Fig. 7.1 c) we have that t_2 is later than t_1 along the contour denoted as $t_1 \subset t_2$. Undoubtedly, the time ordering along the contour is distinct from the usual one on the real time axis since $t_1 > t_2$ holds and *this* is the reason behind the identity in Eq. (7.2.11) as shown in Ref. [114].

Further, we introduce the shorthand notation for Eq. (7.2.11) as

$$\hat{A}(t) \;=\; \hat{T}_{\mathrm{C}_t}\, \left[S_{\mathrm{C}_t}^{\hat{H}_{\mathrm{tot}}}\, \hat{A}_{\hat{h}}(t) \right], \tag{7.2.12}$$

where we set

$$S_{\mathrm{C}_t}^{\hat{H}_{\mathrm{tot}}} \;\coloneqq\; \exp\left[-\mathrm{i} \int_{\mathrm{C}_t} \hat{H}'_{\hat{h}}(\tau)\, \mathrm{d}\tau \right]. \tag{7.2.13}$$

Thus, the time evolution for a product of operators $\hat{\psi}(t)\, \hat{\psi}^{\dagger}(t')$ is

$$\hat{\psi}(t)\, \hat{\psi}^{\dagger}(t') \;=\; \left[\hat{T}_{\mathrm{C}_t}\, S_{\mathrm{C}_t}^{\hat{H}_{\mathrm{tot}}}\, \hat{\psi}_{\hat{h}}(t) \right] \cdot \left[\hat{T}_{\mathrm{C}_{t'}}\, S_{\mathrm{C}_{t'}}^{\hat{H}_{\mathrm{tot}}}\, \hat{\psi}_{\hat{h}}^{\dagger}(t') \right], \tag{7.2.14}$$

which is almost the looked for expression for single particle GFs at the end. Notice that depending on how one interprets Eq. (7.2.14), the operator $\hat{\psi}_{\hat{h}}(t)$ is sandwiched again by two time evolution operators. The last unification of two such entities demanded the introduction of contour time ordering. However, we are not allowed to impose contraints on t and t', as both $t > t'$ and $t' > t$ can be true. Yet, the new contour C shown in Fig. 7.2 a) grants

$$\hat{\psi}(t)\, \hat{\psi}^{\dagger}(t') \;=\; \hat{T}_{\mathrm{C}}\, \left[S_{\mathrm{C}}^{\hat{H}_{\mathrm{tot}}}\, \hat{\psi}_{\hat{h}}(t)\, \hat{\psi}_{\hat{h}}^{\dagger}(t') \right] \tag{7.2.15}$$

where the involved contour time ordering $\hat{T}_{\mathrm{C}}$ behaves as $\hat{T}_{\mathrm{C}_t}$ did earlier and the gained expression holds for arbitrary t, t'. The used quantity $S_{\mathrm{C}}^{\hat{H}_{\mathrm{tot}}}$ is

$$S_{\mathrm{C}}^{\hat{H}_{\mathrm{tot}}} \;=\; \exp\left[-\mathrm{i} \int_{\mathrm{C}} \hat{H}'_{\hat{h}}(\tau)\, \mathrm{d}\tau \right]. \tag{7.2.16}$$

Still, Eq. (7.2.15) is merely a new formulation of Eq. (7.2.8) for $\hat{\psi}(t)$, $\hat{\psi}^{\dagger}(t')$. The standard identities of time evolution operators allow to shorten the term $u(t,\, t_0)\, u(t_0,\, t') = u(t,\, t')$, which is placed in between $\hat{\psi}(t)$ and $\hat{\psi}^{\dagger}(t')$ [110]. Thus, the deformation and even the extension of the contour is strictly allowed and grants later the so called Langreth's rules [114, 116].

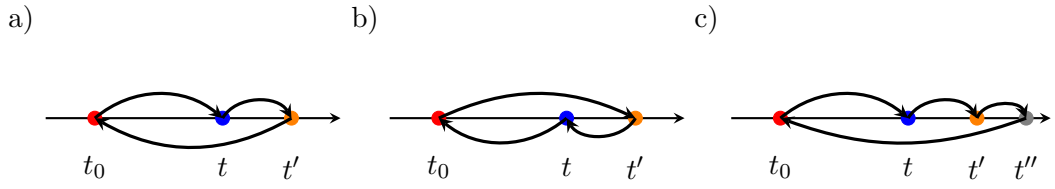

Figure 7.2.: The Contour C in the scenario of $t' > t$. a) The initial contours C_t, $\mathrm{C}_{t'}$ are combined into C. The contour time ordering $\hat{T}_\mathrm{C}$ acts as $\hat{T}$ on the forward branch. b) The properties of the time evolution operator u, for instance that $\hat{1} = u(t,\, t) = u(t,\, t')\, u(t',\, t)$ is true, allows the deformation of C. On the backward branch $\hat{T}_\mathrm{C}$ behaves as the antitime ordering operator. c) The time evolution can be used to introduce t'', here for $t'' > t$. The limits $t'' \to \infty$ and $t_0 \to -\infty$ grant the Keldysh contour [110, 111].

Next, we exploit the fact that the r.h.s. of Eq. (7.2.15) is already contour time ordered. Further, Eq. (7.2.15) holds for arbitrary t, t' on the contour. Therefore, we have

$$\left\langle \hat{T}_\mathrm{C} \left[\hat{\psi}(t)\, \hat{\psi}^\dagger(t') \right] \right\rangle = \left\langle \hat{T}_\mathrm{C} \left[S_\mathrm{C}^{\hat{H}_\mathrm{tot}}\, \hat{\psi}_{\hat{h}}(t)\, \hat{\psi}^\dagger_{\hat{h}}(t') \right] \right\rangle, \tag{7.2.17}$$

and we can finally introduce the contour time ordered GF G^c as

$$G^\mathrm{c}(t,\, t') \coloneqq -\frac{\mathrm{i}}{\hbar} \left\langle \hat{T}_\mathrm{C} \left[\hat{\psi}(t)\, \hat{\psi}^\dagger(t') \right] \right\rangle, \tag{7.2.18}$$

imitating the form of $G^\mathrm{T}(t, t')$. Since one can deform the contour transforming the case of $t \subset t'$ into $t' \subset t$ as illustrated Fig. 7.2 a), b), the contour ordered GF G^c is an interesting object. For instance, we have that

$$G^\mathrm{c}(t,\, t') = \begin{cases} G^<(t,\, t'), & t \subset t' \\ G^>(t,\, t'), & t' \subset t \end{cases}, \tag{7.2.19}$$

independent on whether $t > t'$ or $t < t'$ is true. Further, the contour C can be changed such that both t, t' are on the forward (backward) branch, where the contour time ordering $\hat{T}_\mathrm{C}$ acts as $\hat{T}$ ($\bar{\hat{T}}$). We call C_1 the forward and C_2 the backward part of the contour C. Thus, we have

$$G^\mathrm{c}(t,\, t') = \begin{cases} G^\mathrm{T}(t,\, t'), & t, t' \in C_1 \\ G^{\bar{\mathrm{T}}}(t,\, t'), & t, t' \in C_2 \\ G^<(t,\, t'), & t \in C_1,\, t' \in C_2 \\ G^>(t,\, t'), & t \in C_2,\, t' \in C_1 \end{cases}, \tag{7.2.20}$$

for all t, t'. This unification of several GF, especially the lesser and greater ones into G^c, is helpful to shorten the calculations in terms of Green's functions.

The identity in Eq. (7.2.15) is universal and does not rely on the properties of the Hamiltonian. In turn, we can relate $\hat{\psi}_{\hat{h}}(t)\, \hat{\psi}^\dagger_{\hat{h}}(t')$ and $\hat{\psi}_{\hat{H}_0}(t)\, \hat{\psi}^\dagger_{\hat{H}_0}(t')$ using a second

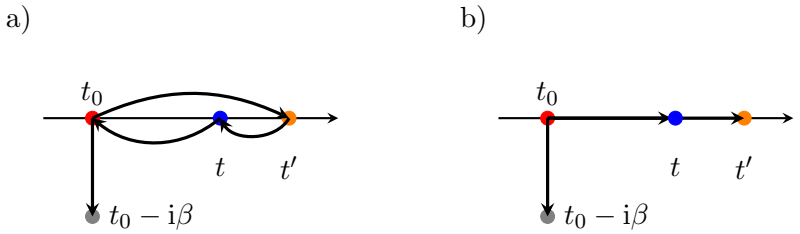

Figure 7.3.: The contour C_v originates from C by accounting for finite temperatures T encoded in $1/\beta = k_\mathrm{B}T$. This attachment only is related to a shift away from the real axis as illustrated in b).

contour accounting for $\hat{H}^\mathrm{int}$. Typically, one is interested expectation values at finite temperature such that the statistical operator ρ ($k_\mathrm{B}T = 1/\beta$)

$$\rho \;=\; \frac{e^{-\beta\,\hat{H}_\mathrm{tot}}}{Z}, \qquad Z = \mathrm{Tr}\left\{e^{-\beta\,\hat{H}_\mathrm{tot}}\right\} \tag{7.2.21}$$

has to be considered. For non-equilibrium scenarios, we do not find the Fermi-Dirac distribution. Nonetheless, we can cure this by simply accounting for the evolution of $\hat{H}_\mathrm{tot}$ w.r.t. to $\hat{H}_0$. For consistent perturbative or diagrammatic expansions, one has to include those terms into the evolution of the operators $\hat{A}$, $\hat{B}$. The first step is to observe that

$$e^{-\beta\,\hat{H}_\mathrm{tot}} \;=\; e^{-\beta\,\hat{H}_0}\,v(t_0 - \mathrm{i}\beta,\,t_0) \tag{7.2.22}$$

holds, where we introduced an imaginary time scale and the used time evolution operator reads

$$v(t,\,t_0) \;=\; \hat{T}\,\exp\left[-\mathrm{i}\int_{t_0}^{t}\hat{H}^\mathrm{int}_{\hat{H}_0}(t')\,\mathrm{d}t'\right]. \tag{7.2.23}$$

This imaginary time strip can be attached at the "end" of the contour, see Fig. 7.3 respecting thereby the contour time ordering and we denote this new quantity by C_v [111, 114]. As $\langle\hat{\psi}(t)\,\hat{\psi}^\dagger(t')\rangle$ and $G^\mathrm{c}(t,\,t')$ are related according to Eq. (7.2.18), we find

$$G^\mathrm{c}(t,\,t') \;=\; -\frac{\mathrm{i}}{\hbar}\frac{\left\langle\,\hat{T}_{\mathrm{C}_v}\,\left[S^i_{\mathrm{C}_v}\,S'_\mathrm{C}\;\hat{\psi}_{\hat{H}_0}(t)\,\hat{\psi}^\dagger_{\hat{H}_0}(t')\right]\,\right\rangle_0}{\left\langle\,\hat{T}_{\mathrm{C}_v}\,\left[S^i_{\mathrm{C}_v}\,S'_\mathrm{C}\right]\,\right\rangle_0}, \tag{7.2.24}$$

where $\langle\;\rangle_0$ is meant as the expectation value w.r. to $\rho_0 = \exp(-\beta\hat{H}_0)/\mathrm{Tr}[\exp(-\beta\hat{H}_0)]$. The complete time evolution is related back to the simple one imposed by $\hat{H}_0$

$$S'_\mathrm{C} \;=\; \exp\left[-\mathrm{i}\int_\mathrm{C}\hat{H}'_{\hat{H}_0}(\tau)\,\mathrm{d}\tau\right], \tag{7.2.25}$$

$$S^i_{\mathrm{C}_v} \;=\; \exp\left[-\mathrm{i}\int_{\mathrm{C}_v}\hat{H}^\mathrm{int}_{\hat{H}_0}(\tau)\,\mathrm{d}\tau\right], \tag{7.2.26}$$

which allows a pertubative/ diagrammatic approach for G^{c} in out of equilibrium cases [111, 114]. However, this is more knowledge than required for us, because in the following we will be working without interactions. To summarize, the contour allows the unification of the full time evolution of two operators as discussed.

In the next section, we introduce the transport setup for the Kitaev chain and we carry out the main steps towards the final expression of the current. We use the contour time ordered GF and the equation of motions (EOM). The equation of motion itself accounts for the time derivative of the considered GF and no internal interactions ($\hat{H}_{\mathrm{int}} \equiv 0$) are present. The initial separation of the Kitaev chain and the contacts allows all equations to close and Eq. (7.2.24) does not have to be used directly. The EOM allows a very intuitive understanding of the current calculation. The reason to show Eq. (7.2.24) was that the NEGF is not limited to such simple cases as we consider in the following.

7.3. The N-S-N transport configuration for the finite Kitaev chain

In our approach, the Kitaev chain

$$\hat{H}_{\mathrm{KC}} = -\mu \sum_{j=1}^{N} \left(d_j^\dagger d_j - \frac{1}{2} \right) + \sum_{j=1}^{N-1} \left(\Delta\, d_{j+1}^\dagger d_j^\dagger - t\, d_{j+1}^\dagger d_j + \mathrm{h.c.} \right), \tag{7.3.1}$$

containing solely the p-wave superconducting (S) pairing constant Δ, is placed in between two normal (N) conducting contacts $\hat{H}_{L,R}$. We consider the leads to be non interacting and spinless like the Kitaev chain and we use the chemical potential μ in $\hat{H}_{\mathrm{KC}}$ as reference energy. In their respective eigenbasis, the grand-canonical Hamiltonians read

$$\hat{H}_\alpha^{\mathrm{gc}} = \hat{H}_\alpha - \mu\, \hat{N}_\alpha = \sum_k \epsilon_{k\alpha}\, c_{k\alpha}^\dagger c_{k\alpha}, \quad \alpha = L, R, \tag{7.3.2}$$

where $c_{k\alpha}^\dagger$ ($c_{k\alpha}$) creates (annihilates) a spinless fermion in state k of lead α and $\hat{N}_{k\alpha} = c_{k\alpha}^\dagger c_{k\alpha}$ denotes the corresponding particle number operator. Please notice, the sum over k depends on the concrete choice for the contacts. The values for k are generic.

The tunneling Hamiltonian

$$\hat{H}_{\mathrm{T}} = \sum_k \left(t_L\, d_1^\dagger\, c_{kL} + t_L^*\, c_{kL}^\dagger\, d_1 \right) + \sum_k \left(t_R\, d_N^\dagger\, c_{kL} + t_R^*\, c_{kL}^\dagger\, d_N \right) \tag{7.3.3}$$

establishes a connection between the three formerly independent parts of the model and allows now the transfer of charge between them. The tunneling elements $t_\alpha(k)$ are allowed to depend on k for the respective contact and the limited number of terms inside $\hat{H}_{\mathrm{T}}$ will be very helpful to obtain the analytical results for the conductance in the end.

The entire system is given by $\hat{H}_{\mathrm{tot}}(t)$

$$\hat{H}_{\mathrm{tot}}(t) = \hat{H}_{\mathrm{KC}} + \hat{H}_L^{\mathrm{gc}} + \hat{H}_R^{\mathrm{gc}} + \theta(t - t_0)\, \hat{H}_{\mathrm{T}}. \tag{7.3.4}$$

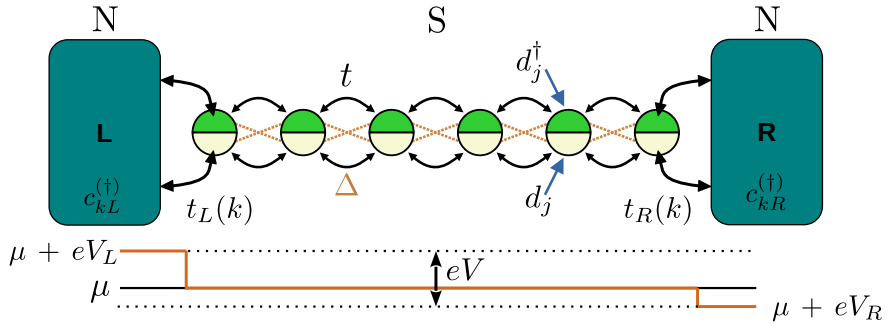

Figure 7.4.: The Kitaev chain in contact with two normal leads $\alpha = L,\, R$ forming the N-S-N configuration.The tunneling amplitude $t_{L,R}(k)$ from $\hat{H}_{\mathrm{T}}$ enables charge transfer between the leads and the Kitaev chain. In case of $V \neq 0$ and when μ lies in between $\mu_{L,R} = \mu + eV_{L.R}$ a net current is observed.

where the Heaviside function $\theta(t-t_0)$ activates the tunneling Hamiltonian after an initial time t_0 and we consider no interaction between $\hat{H}_L$, $\hat{H}_R$. Here, $\theta(t-t_0)\,\hat{H}_{\mathrm{T}}$ adopts the role of $\hat{H}'$ of section 7.2. The contacts act as electron reservoirs and prior to t_0, they were brought to their thermodynamic equilibrium with temperature T_α and the chemical potentials $\mu_{L,R}$ are associated with the left and right lead respectively [91, 110, 112, 114, 117]. The N-S-N configuration is sketched in Fig. 7.4 and in case of an applied bias V between the contacts, i.e. $\mu_L \neq \mu_R$ and for $t > t_0$, a current I flows through the system. Further, we wish to respect and compare scenarios of differently arranged bias drops and therefore we set $\mu_\alpha = \mu + e\,V_\alpha$, with $\mu_L - \mu_R = eV$, in terms of the elementary charge e and V_α being the piece of V applied to lead α, measured with respect to μ. We may use $V_L = \eta V$, $V_R = (\eta - 1)V$ $(\eta \in \mathbb{R})$ for more convenience.

In *reality*, charge is conserved and we thus can measure or calculate the current I at any position in our system. It is especially simple to look inside the leads; let us focus for instance on I_L. The electronic current (for fixed spin) in the left lead is by definition

$$I_L(t) = -e\,\frac{d}{dt}\,\langle \hat{N}_L(t)\rangle \;=\; -e\,\sum_k \frac{d}{dt}\,\langle \hat{N}_{kL}(t)\rangle, \tag{7.3.5}$$

and analogously for I_R. The time evolution of our system is given by $\hat{H}_{\mathrm{tot}}(t)$ and we thus face generally an out of equilibrium situation as all of the initially independent parts $\hat{H}_{L,R}$, $\hat{H}_{\mathrm{KC}}$ influence each other for $t > t_0$. We can proceed in the Heisenberg picture and we need to know $\left[\hat{H}_{\mathrm{tot}}(t),\, \hat{N}_{kL}(t)\right] = \left[\hat{H}_{\mathrm{T}}(t),\, \hat{N}_{kL}(t)\right]$. The last equality holds since both operators are given at the same time, i.e. the fermionic anticommutation relations at initial time apply here. Straightforwardly, one finds

$$I_L(t) \;=\; -\mathrm{i}\frac{e}{\hbar}\,\theta(t-t_0)\,\sum_k \left[t_L\,\langle d_1^\dagger(t)\,c_{kL}(t)\rangle \;-\; t_L^*\,\langle c_{kL}^\dagger(t) d_1(t)\,\rangle\right] \tag{7.3.6}$$

where it is intuitively clear that particles can travel only towards the center, i.e. into the Kitaev chain, supposed that $t > t_0$ is true. This is also true for $I_R(t)$ but the spatial direction of the electronic flow is opposite; therefore, $I_L(t) = -I_R(t)$ must hold for conserved number of particles.

Well, charge conservation is not granted per se within our theoretical model since the Kitaev chain is given by a mean field Hamiltonian, see Eq. (7.3.1), which is a subtle point. First of all, the mean field approach replaces the expectation value of two creation/ annihilation operators by a constant term Δ [91]. The main issue is then precisely the value of Δ; so far we treated the superconducting pairing as a free parameter but in fact its value has to be self consistently calculated in order to properly represent the expectation value [45, 118, 119]. Otherwise, the superconducting part of H_{KC} in Eq. (7.3.1) breaks the particle number conservation as the two creation (annihilation) operators imply. This in turn yields a finite contribution to the current which actually should be zero if the mean field pairing constant is treated properly [118]. The self-consistent treatment within the scope of the nonequilibrium Green's function technique requires a lesser GF of the central system, but in presence of the leads. Naturally within this method, the lesser GF of the isolated leads are closely intertwined and Δ depends essentially on every other parameter of the model: $\Delta = \Delta(t,\, \mu,\, \epsilon_{kL}\, \epsilon_{kR},\, V_L,\, V_R,\, t_L,\, t_R)$. However, there is indeed a way to circumvent the self-consistency cycle while still conserving the particle number [45], but we defer this issue for now.

Next, we transform the expression for the current $I_L(t)$ into one in terms of Green's functions. As the time evolution is given by $\hat{H}_{\mathrm{tot}}(t)$, all operators in Eq. (7.3.6) depend on Δ; thus, we shall account directly for the unusual terms containing two creation and annihilation operators. Therefore, we generalize the (scalar) lesser mixed GF

$$G^{<}_{k\alpha,\,j}(t,t') \;=\; \frac{\mathrm{i}}{\hbar}\,\langle\, d_j^{\dagger}(t')\, c_{k\alpha}(t)\,\rangle \tag{7.3.7}$$

with

$$D_j \;=\; \begin{pmatrix} d_j \\ d_j^{\dagger} \end{pmatrix}, \quad C_{k\alpha} \;=\; \begin{pmatrix} c_{k\alpha} \\ c_{k\alpha}^{\dagger} \end{pmatrix} \tag{7.3.8}$$

into the 2×2 lesser mixed GF $\boldsymbol{G}^{<}_{k\alpha,\,j}(t,t')$, defined element-wise as

$$\Big(\boldsymbol{G}^{<}_{k\alpha,\,j}(t,t')\Big)_{n,m} \;\coloneqq\; \frac{\mathrm{i}}{\hbar}\,\langle\, \big(D_j(t')\big)^{\dagger}_{m}\; \big(C_{k\alpha}(t)\big)_n\,\rangle, \qquad n,\, m = 1,\, 2. \tag{7.3.9}$$

Explicitly, we have

$$\boldsymbol{G}^{<}_{k\alpha,\,j}(t,t') \;=\; \frac{\mathrm{i}}{\hbar}\begin{pmatrix} \langle\, d_j^{\dagger}(t')\, c_{k\alpha}(t)\,\rangle & \langle\, d_j(t')\, c_{k\alpha}(t)\,\rangle \\ \langle\, d_j^{\dagger}(t')\, c_{k\alpha}^{\dagger}(t)\,\rangle & \langle\, d_j(t')\, c_{k\alpha}^{\dagger}(t)\,\rangle \end{pmatrix}, \tag{7.3.10}$$

where the off-diagonal elements are the mentioned unconventional terms and the second element of the diagonal is indeed a (scalar) greater GF. Rewriting the current $I_L(t)$ in

terms of GFs can be tricky and depends on the concrete model and on the involved degrees of freedom. Nonetheless, we simply exploit here $c_{kL}^\dagger(t)d_1(t) = -d_1(t)\,c_{kL}^\dagger(t)$ due to the equal time constraint and we find

$$\begin{aligned} I_L(t) &= -\mathrm{i}\frac{e}{\hbar}\,\theta(t-t_0)\sum_k\Big[t_L\,\langle d_1^\dagger(t)\,c_{kL}(t)\rangle + t_L^*\,\langle d_1(t)c_{kL}^\dagger(t)\,\rangle\Big] \\ &= -\mathrm{i}\frac{e}{\hbar}\,\theta(t-t_0)\sum_k \mathrm{Tr}\left\{\begin{bmatrix} t_L & \\ & t_L^* \end{bmatrix}\begin{bmatrix} \langle\, d_1^\dagger(t)\,c_{kL}(t)\,\rangle & \langle\, d_1(t)\,c_{kL}(t)\,\rangle \\ \langle\, d_1^\dagger(t)\,c_{kL}^\dagger(t)\,\rangle & \langle\, d_1(t)\,c_{kL}^\dagger(t)\,\rangle \end{bmatrix}\right\} \\ &= -e\,\theta(t-t_0)\sum_k \mathrm{Tr}\Big\{\boldsymbol{T}_L\;\boldsymbol{G}^<_{kL,\,1}(t,t)\Big\} \\ &= -e\,\theta(t-t_0)\lim_{t'\to t}\sum_k \mathrm{Tr}\Big\{\boldsymbol{T}_L\;\boldsymbol{G}^<_{kL,\,1}(t,t')\Big\}, \end{aligned} \tag{7.3.11}$$

where "Tr" denotes the trace and $\boldsymbol{T}_L$ contains the tunneling elements $t_L^{(*)}$. We can now implement the NEGF technique and once $\boldsymbol{G}^<_{kL,\,1}(t,t')$ is found, the current for any point of time follows directly. We estimate $\boldsymbol{G}^<_{kL,\,1}(t,t')$ with the equation of motion technique and since the time evolution is given by $\hat{H}_{\mathrm{tot}}(t)$, every degree of freedom in the system knows about all the others. For every combination there is a GF and all are interrelated. Further, the different yet connected GF types such as lesser, greater, retarded and advanced enter too, not to mention the GF of the isolated system parts. Instead of aiming at $\boldsymbol{G}^<_{kL,\,1}(t,t')$ directly, we focus on the contour time ordered GF $\boldsymbol{G}^{\mathrm{c}}_{k\alpha,\,1}(\tau,\,\tau')$ $(\alpha = L, R)$

$$\big(\boldsymbol{G}^{\mathrm{c}}_{k\alpha,\,1}(\tau,\,\tau')\big)_{n,m} \coloneqq -\frac{\mathrm{i}}{\hbar}\,\langle\,\hat{T}_{\mathrm{c}}\Big[(C_{k\alpha}(\tau))_n\,\big(D_1(\tau')\big)^\dagger_m\Big]\,\rangle, \qquad n,\,m = 1,\,2. \tag{7.3.12}$$

since one treats formally the lesser, greater mixed GF simultaneously. In case of $\tau' \supset \tau$, $\boldsymbol{G}_{kL,\,1}(\tau,\tau')$ adopts the shape of $\boldsymbol{G}^<_{kL,\,j}(t,t')$ and one has only to set $t = \tau$ and $t' = \tau'$ afterwards. Further, we introduced τ, τ' to help the reader, as $\hat{T}_{\mathrm{c}}$ introduces generally Heaviside functions to account for the time ordering on the contour, which should not be misunderstood as $t' > t$ or $t > t'$.

The equation of motion (EOM) technique evaluates $\boldsymbol{G}^{\mathrm{c}}_{kL,\,1}(\tau,\,\tau')$ by calculating its time derivative for instance w.r.t. τ from the Heisenberg equation, here in terms of an arbitrary operator $A(\tau)$

$$\frac{d}{d\tau}\,A(\tau) = \frac{1}{\mathrm{i}\hbar}\Big[A,\,\hat{H}_{\mathrm{tot}}\Big](\tau) + (\partial_\tau\,A_{\mathrm{S}})_{\mathrm{H}} \tag{7.3.13}$$

in Heisenberg picture w.r.t. $\hat{H}_{\mathrm{tot}}$ and A_{S} denotes the corresponding Schrödinger representation. For convenience and following the usual notation, we denote $d_\tau \coloneqq d/d\tau$ as ∂_τ to remind the reader constantly of the independence of τ and τ', and also that the full time evolution w.r.t τ is meant.

This procedure can be carried out straightforwardly and we recommend first to write down $\partial_\tau \boldsymbol{G}^{\mathrm{c}}_{kL,\,1}(\tau,\,\tau')$ entry-wise using only the abstract definition of the contour time ordering[1] $\hat{T}_{\mathrm{c}}$. One finds

$$\begin{aligned}\mathrm{i}\hbar\,\partial_\tau\,\left(\boldsymbol{G}^{\mathrm{c}}_{kL,\,1}(\tau,\,\tau')\right)_{n,m} \;=\; -\,\frac{\mathrm{i}}{\hbar}\left\langle\,\hat{T}_{\mathrm{c}}\left\{\left[(C_{kL})_n\,,\,\hat{H}_{\mathrm{tot}}\right](\tau)\;(D_1(\tau'))^{\dagger}_m\right\}\right\rangle \\ +\;\delta(\tau-\tau')\left\langle\left\{(C_{kL})_n,\,(D_1)^{\dagger}_m\right\}(\tau)\right\rangle\end{aligned} \tag{7.3.14}$$

where due to the Dirac distribution $\delta(\tau-\tau')$ the last term drops. Implementing the commutator values and rewriting the terms in matrix form grants

$$(\mathrm{i}\hbar\,\mathbb{1}_2\,\partial_\tau\;-\;\epsilon_{kL}\,\tau_z)\;\boldsymbol{G}^{\mathrm{c}}_{kL,\,1}(\tau,\,\tau') \;=\; \begin{bmatrix} t^*_L & \\ & -t_L\end{bmatrix}\boldsymbol{G}^{\mathrm{c}}_{11}(\tau,\,\tau') \tag{7.3.15}$$

after reordering. Here, $\boldsymbol{G}^{\mathrm{c}}_{11}(\tau,\,\tau')$ is the contour time ordered GF corresponding to the first site of the Kitaev chain, including both electron and hole degrees of freedom. Notice that τ_z represents the Pauli matrix. Generally, these local GFs $\boldsymbol{G}^{\mathrm{c}}_{ij}(\tau,\,\tau')$ are defined as

$$\left(\boldsymbol{G}^{\mathrm{c}}_{ij}(\tau,\,\tau')\right)_{n,m} \coloneqq -\frac{\mathrm{i}}{\hbar}\,\langle\,\hat{T}_{\mathrm{c}}\left[(D_i(\tau\,))_n\,\left(D_j(\tau'\,)\right)^{\dagger}_m\right]\rangle, \qquad n,\,m=1,\,2 \tag{7.3.16}$$

for all sites $i,\,j=1,\,\ldots,\,N$ and i denotes the imaginary unit. Please notice, $\epsilon_{kL}\,\tau_z$ in Eq. (7.3.15) is the BdG matrix of the isolated left lead $\hat{H}^{\mathrm{gc}}_L$ in terms of C_{kL} (apart from a constant term). More convenient is

$$(\mathrm{i}\hbar\,\mathbb{1}_2\,\partial_\tau\;-\;\epsilon_{kL}\,\tau_z)\;\boldsymbol{G}^{\mathrm{c}}_{kL,\,1}(\tau,\,\tau') \;=\; \boldsymbol{T}^{\dagger}_L\,\tau_z\,\boldsymbol{G}^{\mathrm{c}}_{11}(\tau,\,\tau') \tag{7.3.17}$$

rather than the initial form of Eq. (7.3.15). Importantly, the EOM separated pure lead and tunneling coefficients and one can search for a specific form of this separation as we explain in the following. In this scope one can define the contour time ordered GF of the isolated lead α, that is $\boldsymbol{g}^{\mathrm{c}}_{k\alpha,\,k\alpha}(\tau,\,\tau')$, as

$$\left(\boldsymbol{g}^{\mathrm{c}}_{k\alpha,\,k\alpha}(\tau,\,\tau')\right)_{n,m} \coloneqq -\frac{\mathrm{i}}{\hbar}\,\langle\,\hat{T}_{\mathrm{c}}\left[(C_{k\alpha}(\tau))_n\,\left(C_{k\alpha}(\tau')\right)^{\dagger}_m\right]\rangle, \qquad n,\,m=1,\,2. \tag{7.3.18}$$

Its time evolution is given exclusively by $\hat{H}^{\mathrm{gc}}_\alpha$. Generally, we denote isolated GF, even for the central system, always by lowercase letters. The time evolution of $\boldsymbol{g}^{\mathrm{c}}_{kL,\,kL}(\tau,\,\tau')$ is trivial, but nonetheless we treat $\boldsymbol{g}^{\mathrm{c}}_{kL,\,kL}(\tau,\,\tau')$ similar as $\boldsymbol{G}^{\mathrm{c}}_{kL,\,1}(\tau,\,\tau')$ before. Since for both GFs τ enters via the same, first, operator we get for both similar expressions and commutator values apart from two differences: First, $\boldsymbol{g}^{\mathrm{c}}_{kL,\,kL}(\tau,\,\tau')$ is not a mixed GF as both indices refer to the same degrees of freedom and the Dirac distribution $\delta(\tau-\tau')$ appears. Secondly, none of the pieces of the EOM originating from $\hat{H}_{\mathrm{KC}}$, $\hat{H}_{\mathrm{T}}$ or $\hat{H}^{\mathrm{gc}}_R$ enters as we work with $\hat{H}^{\mathrm{gc}}_L$. Therefore, we find the rather neat equation

$$(\mathrm{i}\hbar\,\mathbb{1}_2\,\partial_\tau\;-\;\epsilon_{kL}\,\tau_z)\;\boldsymbol{g}^{\mathrm{c}}_{kL,\,kL}(\tau,\,\tau') \;=\; \delta(\tau-\tau')\,\mathbb{1}_2, \tag{7.3.19}$$

[1] That is $\hat{T}_{\mathrm{c}}\;[A(\tau)B(\tau')] \;=\; \theta(\tau-\tau')\,A(\tau)\,B(\tau') \,\pm\, \theta(\tau'-\tau)\,B(\tau')\,A(\tau)$ with $-$ $(+)$ for fermionic (bosonic) operators.

looking suspiciously similar to Eq. (7.3.17). Indeed $\boldsymbol{g}^{\mathrm{c}}_{kL,kL}(\tau,\,\tau')$ is a Green's function for $\boldsymbol{G}^{\mathrm{c}}_{kL,\,1}(\tau,\,\tau')$, thus granting

$$\boldsymbol{G}^{\mathrm{c}}_{kL,\,1}(\tau,\,\tau') \;=\; \int_{\mathrm{c}} \boldsymbol{g}^{\mathrm{c}}_{kL,\,kL}(\tau,\,s)\;\boldsymbol{T}^{\dagger}_{L}\tau_z\;\boldsymbol{G}^{\mathrm{c}}_{11}(s,\,\tau')\;\mathrm{d}s \tag{7.3.20}$$

where s runs along the contour. The proof relies essentially only on Eq. (7.3.19) and is obvious [110, 114]. Although we have the solution for $\boldsymbol{G}^{\mathrm{c}}_{kL,\,1}(\tau,\,\tau')$ the answer is unsatisfying as the GFs $\boldsymbol{g}^{\mathrm{c}}_{kL,\,kL}(\tau,\,s)$, $\boldsymbol{G}^{\mathrm{c}}_{11}(s,\,\tau')$ so far are not explicitly known to us. Yet we made in fact a huge progress since one of the Langreth rules [116] can be imposed on Eq. (7.3.20) as we show next.

In order to proceed, we return to $\boldsymbol{G}^{<}_{kL,\,1}(t,\,t')$ which can be extracted from $\boldsymbol{G}^{\mathrm{c}}_{kL,\,1}(\tau,\,\tau')$: We demand $\tau \subset \tau'$, which puts $\boldsymbol{G}^{\mathrm{c}}_{kL,\,1}(\tau,\,\tau')$ into the shape of a lesser GF and we set $t = \tau$, $t' = \tau'$. Again "$\subset$" is a contour time ordering and as such $\tau \subset \tau'$ does not impose any constraint on t, t'. Therefore, we first get

$$\boldsymbol{G}^{<}_{kL,\,1}(t,\,t') \;=\; \int_{\mathrm{c}} \boldsymbol{g}^{\mathrm{c}}_{kL,\,kL}(t,\,s)\;\boldsymbol{T}^{\dagger}_{L}\tau_z\;\boldsymbol{G}^{\mathrm{c}}_{11}(s,\,t')\;\mathrm{d}s \tag{7.3.21}$$

and the Langreth rules are essentially algebraic identities concerning the contour time ordered GF on the r.h.s. such that "ordinary" GF are integrated over real time intervals [114, 116]

$$\boldsymbol{G}^{<}_{kL,\,1}(t,\,t') \;=\; \int_{t_0}^{\infty} \boldsymbol{g}^{\mathrm{r}}_{kL,\,kL}(t,\,u)\;\boldsymbol{T}^{\dagger}_{L}\tau_z\;\boldsymbol{G}^{<}_{11}(u,\,t')\;\mathrm{d}u \;+\; \int_{t_0}^{\infty} \boldsymbol{g}^{<}_{kL,\,kL}(t,\,u)\;\boldsymbol{T}^{\dagger}_{L}\tau_z\;\boldsymbol{G}^{\mathrm{a}}_{11}(u,\,t')\;\mathrm{d}u. \tag{7.3.22}$$

The problem to find $\boldsymbol{G}^{<}_{kL,\,1}(t,\,t')$ separated into the calculation of the isolated lead GFs $\boldsymbol{g}^{\mathrm{r}}_{kL,\,kL}(t,\,u)$, $\boldsymbol{g}^{<}_{kL,\,kL}(t,\,u)$ and two GFs associated to the first site of the Kitaev chain, namely $\boldsymbol{G}^{<}_{11}(u,\,t')$ and $\boldsymbol{G}^{\mathrm{a}}_{11}(u,\,t')$, including the electron and hole degrees of freedom, but in presence of the entire system. Since the GF associated to the isolated leads are trivial to determine, we simply state their result at a suitable point and we focus on the mixed ones in the following.

As a guidance one should focus on $\boldsymbol{G}^{\mathrm{c}}_{11}(\tau,\,\tau')$ rather than on the lesser or advanced GF, since the contour GF unites lesser and greater, i.e. advanced and retarded follow directly. Furthermore, since all sites of the Kitaev chain are connected, once should directly consider $\boldsymbol{G}^{\mathrm{c}}_{ij}(\tau,\,\tau')$ as one otherwise crawls literally from site to site. Treating $\boldsymbol{G}^{\mathrm{c}}_{ij}(\tau,\,\tau')$ in a similar way as $\boldsymbol{G}^{\mathrm{c}}_{kL,\,1}(\tau,\,\tau')$ before, yields finally

$$\begin{aligned}
(\mathrm{i}\hbar\,\mathbb{1}_2\,\partial_\tau \;-\; \mu\,\tau_z)\,\boldsymbol{G}^{\mathrm{c}}_{ij}(\tau,\,\tau') \;=& \delta(\tau-\tau')\,\delta_{ij}\,\mathbb{1}_2 \;-\; (1-\delta_{i1})\;\tau_z\,(t\,\mathbb{1}_2 - \Delta\tau_x)\;\boldsymbol{G}^{\mathrm{c}}_{i-1,\,j}(\tau,\,\tau') \\
&-\; (1-\delta_{iN})\;\tau_z\,(t\,\mathbb{1}_2 + \Delta\tau_x)\;\boldsymbol{G}^{\mathrm{c}}_{i+1,\,j}(\tau,\,\tau') \\
&+\; \delta_{i1}\;\int_{\mathrm{c}} \boldsymbol{\Sigma}^{\mathrm{c}}_{L}(\tau,\,s)\;\boldsymbol{G}^{\mathrm{c}}_{ij}(s,\,\tau')\,\mathrm{d}s \\
&+\; \delta_{iN}\;\int_{\mathrm{c}} \boldsymbol{\Sigma}^{\mathrm{c}}_{R}(\tau,\,s)\;\boldsymbol{G}^{\mathrm{c}}_{ij}(s,\,\tau')\,\mathrm{d}s,
\end{aligned} \tag{7.3.23}$$

where we defined the contour time ordered self-energies $\boldsymbol{\Sigma}^{\mathrm{c}}_{\alpha}(\tau,\, s)$ as

$$\boldsymbol{\Sigma}^{\mathrm{c}}_{\alpha}(\tau,\, s) \coloneqq \sum_{k} \boldsymbol{T}_{\alpha}\, \tau_z\, \boldsymbol{g}^{\mathrm{c}}_{k\alpha,\, k\alpha}(\tau,\, s)\, \tau_z\, \boldsymbol{T}^{\dagger}_{\alpha}, \quad \alpha = L, R \tag{7.3.24}$$

and $\boldsymbol{T}_{\alpha}$ reads

$$\boldsymbol{T}_{\alpha} \,=\, \begin{bmatrix} t_{\alpha} & \\ & t^{*}_{\alpha} \end{bmatrix}. \tag{7.3.25}$$

Before we turn to the self-energies in more detail, let us comment on Eq. (7.3.23). The Kitaev chain contains apart from μ only the nearest neighbor terms t, Δ; thus, the only possible transfer $i \to i \pm 1$ is accompanied by Δ and t. The details of the processes are naturally different and as such t (Δ) connects electrons with electrons (holes) encoded in $\mathbb{1}_2$ (τ_x). Furthermore, electronic and hole-like processes are distinct by a sign change, hence τ_z. Since, the Kitaev chain possess a finite length, therefore hopping with t and pairing with Δ onto both leads is not possible and here originate the Kronecker-deltas. Instead, once the first or the last side is reached, further transport outwards is mediated by the tunneling Hamiltonian. Particularly, the EOM for $\boldsymbol{G}^{\mathrm{c}}_{ij}(\tau,\, \tau')$ contains a priori the GFs $\boldsymbol{G}^{\mathrm{c}}_{k\alpha,\, j}(\tau,\, \tau')$ and their respective integral representation results in the introduction of the self-energy terms into Eq. (7.3.23).

As one can see from Eq. (7.3.24), the self-energies contain the entire information about the leads and the tunneling Hamiltonian. Moreover, $\boldsymbol{\Sigma}^{\mathrm{c}}_{\alpha}$ is written w.r.t. $\boldsymbol{G}^{\mathrm{c}}_{ij}(\tau,\, \tau')$ as Eq. (7.3.23) implies. In turn, the Kitaev Hamiltonian, being in contact with the leads, gets modified in comparison to the isolated case.

In order to account for the entire system, we define a global contour ordered GF. We simply absorb the single sites

$$G^{\mathrm{c}}(\tau,\, \tau') \coloneqq \left\{\boldsymbol{G}^{\mathrm{c}}_{ij}(\tau,\, \tau')\right\}^{N,\, N}_{i,\, j=1} \equiv \begin{bmatrix} \boldsymbol{G}^{\mathrm{c}}_{11}(\tau,\, \tau') & \dots & \boldsymbol{G}^{\mathrm{c}}_{1N}(\tau,\, \tau') \\ \vdots & & \vdots \\ \boldsymbol{G}^{\mathrm{c}}_{N1}(\tau,\, \tau') & \dots & \boldsymbol{G}^{\mathrm{c}}_{NN}(\tau,\, \tau') \end{bmatrix}_{2N \times 2N}. \tag{7.3.26}$$

In this regard, $G^{\mathrm{c}}(\tau,\, \tau')$ is defined w.r.t. $\hat{\Psi}_{\mathrm{so}} = \left(d_1,\, d^{\dagger}_1,\, \dots,\, d_N,\, d^{\dagger}_N\right)^{\mathrm{T}} \equiv \left(D^{\mathrm{T}}_1,\, \dots,\, D^{\mathrm{T}}_N\right)$ as

$$G^{\mathrm{c}}(\tau,\, \tau') \coloneqq -\frac{\mathrm{i}}{\hbar}\Big\langle\, \hat{T}_{\mathrm{c}}\, \Big[\hat{\Psi}_{\mathrm{so}}(\tau)\, \hat{\Psi}^{\dagger}_{\mathrm{so}}(\tau')\Big]\, \Big\rangle, \tag{7.3.27}$$

and the acronym "so" means site(-wise) ordered. A short look into the Eqs. (7.3.8), (7.3.16) and treating the matrix product inside $G^{\mathrm{c}}(\tau,\, \tau')$ correctly, provides immediately the agreement of the two definitions for $G^{\mathrm{c}}(\tau,\, \tau')$ given in Eqs. (7.3.26), (7.3.27). Alternatively, one can leave Eq. (7.3.27) aside for a moment.

Returning to Eq. (7.3.23) and recalling that GF's are specific solution of differential equations, we might wonder which one $G^{\mathrm{c}}(\tau,\, \tau')$ obeys. Matrices acting on $G^{\mathrm{c}}(\tau,\, \tau')$

must have the same size as $G^{\mathrm{c}}(\tau,\,\tau')$ itself and have to contain naturally the combined information of all sites. We introduce the abbreviation

$$\boldsymbol{\alpha} \coloneqq -\tau_z\,(t\,\mathbb{1}_2 + \Delta\tau_x) \;=\; \begin{bmatrix} -t & -\Delta \\ \Delta & t \end{bmatrix} \tag{7.3.28}$$

and the Kitaev Hamiltonian reads

$$\mathcal{H}_{\mathrm{so}} \;=\; \begin{bmatrix} \mu\,\tau_z & \boldsymbol{\alpha} & & & & & \\ \boldsymbol{\alpha}^\dagger & \mu\,\tau_z & \boldsymbol{\alpha} & & & & \\ & \boldsymbol{\alpha}^\dagger & \mu\,\tau_z & \boldsymbol{\alpha} & & & \\ & & \ddots & \ddots & \ddots & & \\ & & & \boldsymbol{\alpha}^\dagger & \mu\,\tau_z & \boldsymbol{\alpha} & \\ & & & & \boldsymbol{\alpha}^\dagger & \mu\,\tau_z & \boldsymbol{\alpha} \\ & & & & & \boldsymbol{\alpha}^\dagger & \mu\,\tau_z \end{bmatrix}, \tag{7.3.29}$$

such that $\hat{H}_{\mathrm{KC}} = \frac{1}{2}\hat{\Psi}_{\mathrm{so}}^\dagger\,\mathcal{H}_{\mathrm{so}}\,\hat{\Psi}_{\mathrm{so}}$ holds. Indeed, by simply reading out the 2×2 block at position i, j of the product $\mathcal{H}_{\mathrm{so}}\,G^{\mathrm{c}}(\tau,\,\tau')$ reproduces exactly the terms in Eq. (7.3.23) for $\boldsymbol{G}^{\mathrm{c}}_{ij}(\tau,\,\tau')$ and $\boldsymbol{G}^{\mathrm{c}}_{i\pm1,\,j}(\tau,\,\tau')$ apart from the ones including the self-energies or the partial derivative w.r.t. τ. Hence, Eq. (7.3.23) becomes

$$\begin{aligned}\left[(\mathrm{i}\hbar\,\mathbb{1}_{2N}\,\partial_\tau \,-\, \mathcal{H}_{\mathrm{so}})\;G^{\mathrm{c}}(\tau,\,\tau')\right]_{ij} \;=\; \delta(\tau-\tau')\,\delta_{ij}\,\mathbb{1}_2 \,+\, \delta_{i1}\int_{\mathrm{c}} \boldsymbol{\Sigma}^{\mathrm{c}}_L(\tau,\,s)\;\boldsymbol{G}^{\mathrm{c}}_{1j}(s,\,\tau')\,\mathrm{d}s \\ +\;\delta_{iN}\int_{\mathrm{c}} \boldsymbol{\Sigma}^{\mathrm{c}}_R(\tau,\,s)\;\boldsymbol{G}^{\mathrm{c}}_{Nj}(s,\,\tau')\,\mathrm{d}s.\end{aligned} \tag{7.3.30}$$

We continue with the same strategy for the self-energy $\boldsymbol{\Sigma}^{\mathrm{c}}_L(\tau,\,s)$. We set

$$\Sigma^{\mathrm{c}}_L(\tau,\,s) \;=\; \begin{bmatrix} \boldsymbol{\Sigma}^{\mathrm{c}}_L(\tau,\,s) & \mathbf{0} & \dots & \mathbf{0} \\ \mathbf{0} & \mathbf{0} & \dots & \mathbf{0} \\ \vdots & \vdots & \ddots & \vdots \\ \mathbf{0} & \mathbf{0} & \dots & \mathbf{0} \end{bmatrix}_{2N\times 2N}, \quad \Sigma^{\mathrm{c}}_R(\tau,\,s) \;=\; \begin{bmatrix} \mathbf{0} & \dots & \mathbf{0} & \mathbf{0} \\ \vdots & \ddots & \vdots & \vdots \\ \mathbf{0} & \dots & \mathbf{0} & \mathbf{0} \\ \mathbf{0} & \dots & \mathbf{0} & \boldsymbol{\Sigma}^{\mathrm{c}}_R(\tau,\,s) \end{bmatrix}_{2N\times 2N} \tag{7.3.31}$$

accounting for the local character of the tunneling Hamiltonian $\hat{H}_{\mathrm{T}}$. Here, $\mathbf{0}$ denotes the 2×2 zero matrix. As one can show straightforwardly, we arrive at the compact, much simplified and yet exact expression

$$(\mathrm{i}\hbar\,\mathbb{1}_{2N}\,\partial_\tau \,-\, \mathcal{H}_{\mathrm{so}})\;G^{\mathrm{c}}(\tau,\,\tau') \;=\; \delta(\tau-\tau')\,\mathbb{1}_{2N} \,+\, \int_{\mathrm{c}} \left[\Sigma^{\mathrm{c}}_L(\tau,\,s) \,+\, \Sigma^{\mathrm{c}}_R(\tau,\,s)\right]\;G^{\mathrm{c}}(s,\,\tau')\,\mathrm{d}s \tag{7.3.32}$$

where all the coupled local contour GFs $\boldsymbol{G}^{\mathrm{c}}_{ij}(\tau,\,\tau')$ are intrinsically respected. Once we obtained the solution for $G^{\mathrm{c}}(\tau,\,\tau')$, we can then read out the result for $\boldsymbol{G}^{\mathrm{c}}_{11}(\tau,\,\tau')$; in

turn, $\boldsymbol{G}_{11}^{<,\mathrm{a}}(u,\, t')$ can be constructed. Consequently, our original goal to find $\boldsymbol{G}_{kL,\,1}^{<}(t,\, t')$ comes -finally- into reach. However, we do not know $G^{\mathrm{c}}(\tau,\, \tau')$ so far.

The current situation becomes apparently more tractable by thinking of the contour integral in Eq. (7.3.32) as one whole function in τ, τ', say $F^{\mathrm{c}}(\tau,\, \tau')$, which is undoubtedly the case as we integrate over s. In this scope, the structure of Eq. (7.3.32) reminds to the one of Eq. (7.3.17); therefore, we proceed as before and define a new contour time ordered GF $g^{\mathrm{c}}(\tau,\, \tau')$ for the isolated Kitaev chain. Explicitly, $g^{\mathrm{c}}(\tau,\, \tau')$ is defined as $G^{\mathrm{c}}(\tau,\, \tau')$ according to Eq. (7.3.27) but its time evolution is given only by $\hat{H}_{\mathrm{KC}}$. Thus, $g^{\mathrm{c}}(\tau,\, \tau')$ obeys the self-energy free version of Eq. (7.3.32) namely

$$(\mathrm{i}\hbar\, \mathbb{1}_{2N}\, \partial_\tau \,-\, \mathcal{H}_{\mathrm{so}})\; g^{\mathrm{c}}(\tau,\, \tau') \,=\, \delta(\tau - \tau')\, \mathbb{1}_{2N}. \tag{7.3.33}$$

In terms of $g^{\mathrm{c}}(\tau,\, \tau')$, we find

$$\begin{aligned} G^{\mathrm{c}}(\tau,\, \tau') \,&=\, g^{\mathrm{c}}(\tau,\, \tau') \,+\, \int_{\mathrm{c}'} g^{\mathrm{c}}(\tau,\, s')\, F^{\mathrm{c}}(s',\, \tau')\, \mathrm{d}s' \\ &=\, g^{\mathrm{c}}(\tau,\, \tau') \,+\, \int_{\mathrm{c}'} \int_{\mathrm{c}} g^{\mathrm{c}}(\tau,\, s')\, \left[\Sigma_L^{\mathrm{c}}(s',\, s) \,+\, \Sigma_R^{\mathrm{c}}(s',\, s)\right]\; G^{\mathrm{c}}(s,\, \tau')\, \mathrm{d}s'\, \mathrm{d}s \end{aligned} \tag{7.3.34}$$

where c$'$ is the same contour as c and s (s') runs along c (c$'$). Note Eq. (7.3.34) is a Dyson equation in the time domain [114] and can be used repeatedly for approximations. Temporarily, we cannot proceed due to the intricate time dependency displayed by Eq. (7.3.34). Nonetheless, Eq. (7.3.34) is an important milestone since the Langreth rules [114, 116] can be used here. One can show that Eq. (7.3.34) implies

$$G^s(t,\, t') \,=\, \int_{t_0}^{\infty} \int_{t_0}^{\infty} G^r(t,\, u)\, \left[\Sigma_L^s(u, v) \,+\, \Sigma_R^s(u, v)\right]\, G^a(v,\, t')\, \mathrm{d}u\, \mathrm{d}v \tag{7.3.35}$$

for $s =>, <$ and a similar expression can be found for G^r

$$G^r(t,\, t') \,=\, g^r(t,\, t') \,+\, \int_{t_0}^{\infty} \int_{t_0}^{\infty} g^r(t,\, u)\, \left[\Sigma_L^r(u, v) \,+\, \Sigma_R^r(u, v)\right]\, G^r(v,\, t')\, \mathrm{d}u\, \mathrm{d}v. \tag{7.3.36}$$

7.4. Steady state current formula

Let us now return to $G^{\mathrm{c}}(\tau,\, \tau')$. The double contour integral on the r.h.s. in Eq. (7.3.34) accounts for the time evolution of the central system in presence of the leads, i.e. originating from $\hat{H}_L^{\mathrm{gc}}$, $\hat{H}_R^{\mathrm{gc}}$ and $\hat{H}_{\mathrm{T}}$ as indicated by the self-energies. For times $t, t' \gg t_0$, i.e. long after connections between the leads and the Kitaev chain were established, the system may reach the steady state. Respecting the time domain in which we currently operate, one formulates the assumption that the GFs depend only on time difference

rather than on t, t' (τ, τ'). Consequently, the steady state is predestined for a Fourier transformation (FT) from time to frequency space

$$G^s(\omega) \;=\; \int\limits_{\mathbb{R}} G^s(t,\,t')\,e^{\mathrm{i}\omega(t-'t)}\,\mathrm{d}(t-t'). \tag{7.4.1}$$

Apart from the technical details, we are then able to determine all required GFs explicitly [110, 114]. Moreover, we consider the initial coupling of the central system at the leads to happen in the remote past and we thus employ the limit $t_0 \to -\infty$. In turn, the ordinary GFs are integrated over $\mathbb{R}$, rather then $[t_0,\,\infty)$.

For a systematic approach, we return to Eq. (7.3.11) and the inverse FT yields directly

$$I_L \;=\; -e\int\limits_{\mathbb{R}} \frac{\mathrm{d}\omega}{2\pi}\,\mathrm{Tr}\left\{\sum_k \boldsymbol{T}_L\;\boldsymbol{G}^{<}_{kL,\,1}(\omega)\right\}, \tag{7.4.2}$$

where we dropped the time argument in I_L, as this quantity specifies now the steady state current. The primary advantage of the steady state assumption can be seen already from Eq. (7.3.22) since the FT grants

$$\boldsymbol{G}^{<}_{kL,\,1}(\omega) \;=\; \boldsymbol{g}^{r}_{kL,\,kL}(\omega)\,\boldsymbol{T}^{\dagger}_L\tau_z\;\boldsymbol{G}^{<}_{11}(\omega) \;+\; \boldsymbol{g}^{<}_{kL,\,kL}(\omega)\,\boldsymbol{T}^{\dagger}_L\tau_z\;\boldsymbol{G}^{a}_{11}, \tag{7.4.3}$$

a product due to the convolution theorem. Thus, the current reads

$$I_L \;=\; -e\int\limits_{\mathbb{R}} \frac{\mathrm{d}\omega}{2\pi}\,\mathrm{Tr}\left\{\tau_z\,\left[\boldsymbol{\Sigma}^{r}_L(\omega)\,\boldsymbol{G}^{<}_{11} \;+\; \boldsymbol{\Sigma}^{<}_L(\omega)\,\boldsymbol{G}^{a}_{11}\right]\right\} \tag{7.4.4}$$

where we used the definition of the self-energy from Eq. (7.3.24) in the frequency domain and exploited $\tau_z^2 = \mathbb{1}_2$, $[\tau_z,\,\boldsymbol{T}_L] = 0$. Similarly Eq. (7.3.35) becomes

$$G^{<}(\omega) \;=\; G^{r}(\omega)\,\left[\Sigma^{<}_L(\omega) \;+\; \Sigma^{<}_R(\omega)\right]\,G^{a}(\omega). \tag{7.4.5}$$

We are left to find $\boldsymbol{g}^{<}_{k\alpha,\,k\alpha}(\omega)$, hidden inside the self-energies, and $G^{r,\,a}(\omega)$ in order to find $G^{<}$. Moreover, we have in fact $G^{a}(\omega) = [G^{r}(\omega)]^{\dagger}$ as usual, as one can show from their basic definition in the time domain and using the FT. The solution for G^r can be easily found from Eq. (7.3.36) which grants

$$G^{r}(\omega) \;=\; g^{r}(\omega) \;+\; g^{r}(\omega)\,[\Sigma^{r}_L(\omega) \;+\; \Sigma^{r}_R(\omega)]\;G^{r}(\omega). \tag{7.4.6}$$

We rearrange the terms and inserting $[\hbar\omega\mathbb{1}_{2N} \;-\mathcal{H}_{\mathrm{so}}]\;g^{r}(\omega) \;=\; \mathbb{1}_{2N}$ yields

$$G^{r}(\omega) \;=\; [\hbar\omega\mathbb{1}_{2N} \;-\mathcal{H}_{\mathrm{so}} \;-\; \Sigma^{r}_L(\omega) \;-\; \Sigma^{r}_R(\omega)]^{-1}\,. \tag{7.4.7}$$

The expression for $g^r(\omega)$ follows from Eq. (7.3.33).

Our last results imply that only the self-energies $\Sigma^{<,\,r}_{\alpha}(\omega)$ are missing to finally fix I_L and thus we have to find $\boldsymbol{g}^{<,r}_{k\alpha,\,k\alpha}(\omega)$. Since the time evolution of $\boldsymbol{g}^{<,r}_{k\alpha,\,k\alpha}(t,\,t')$ is given

only by the respective lead Hamiltonian, the task is trivial and we give only the results. We have ($\alpha = L,\, R$)

$$\begin{aligned} \boldsymbol{g}^{r}_{k\alpha,\,k\alpha}(\omega) \;&=\; \lim_{\eta\to 0} \begin{bmatrix} \frac{1}{\hbar\omega-\epsilon_{k\alpha}+\mathrm{i}\eta} & \\ & \frac{1}{\hbar\omega+\epsilon_{k\alpha}+\mathrm{i}\eta} \end{bmatrix} \\ &=\; P \begin{bmatrix} \frac{1}{\hbar\omega-\epsilon_{k\alpha}} & \\ & \frac{1}{\hbar\omega+\epsilon_{k\alpha}} \end{bmatrix} \;-\; \mathrm{i}\pi \begin{bmatrix} \delta(\hbar\omega-\epsilon_{k\alpha}) & \\ & \delta(\hbar\omega+\epsilon_{k\alpha}) \end{bmatrix}, \end{aligned} \tag{7.4.8}$$

where $\delta(\hbar\omega \mp \epsilon_{k\alpha})$ is the density of state (DOS) of state $k\alpha$ of the leads for electrons (-) and holes (+) respectively. Here, P denotes the principal value.

Generally, the imaginary part of a retarded GF contains the spectral function $\boldsymbol{A}_{k\alpha}(\omega) \coloneqq -2\,\mathrm{Im}[\boldsymbol{g}^{r}_{k\alpha,\,k\alpha}(\omega)]$. Analogously, the spectral function of lead α is $\boldsymbol{A}_{\alpha}(\omega) \coloneqq -2\,\mathrm{Im}[\sum_{k} \boldsymbol{g}^{r}_{k\alpha,\,k\alpha}(\omega)]$ and contains the information of the spectrum of the respective contact.

The lesser GF of the isolated leads read

$$\begin{aligned} \boldsymbol{g}^{<}_{k\alpha,\,k_\alpha}(\omega) \;&=\; 2\pi\mathrm{i} \begin{bmatrix} \delta(\hbar\omega-\epsilon_{k\alpha})\, f_{\alpha}(\hbar\omega \,-\, eV_{\alpha}) & \\ & \delta(\hbar\omega+\epsilon_{k\alpha})\, [1 - f_{\alpha}(\hbar\omega \,-\, eV_{\alpha})] \end{bmatrix} \\ &\equiv \mathrm{i}\boldsymbol{A}_{k\alpha}(\omega)\, \boldsymbol{F}_{\alpha}(\omega) \end{aligned} \tag{7.4.9}$$

containing both the spectral information and information about the occupations. This expression is known as the fluctuation-dissipation theorem in the literature [91, 114]. For convenience, we introduce the 2×2 Fermi matrix $\boldsymbol{F}_{\alpha}$

$$\boldsymbol{F}_{\alpha} \;=\; \begin{bmatrix} f^{-}_{\alpha} & \\ & f^{+}_{\alpha} \end{bmatrix}, \quad f^{\mp}_{\alpha} \coloneqq f_{\alpha}(\hbar\omega \,\mp\, eV_{\alpha}), \tag{7.4.10}$$

where $f_{\alpha}(\hbar\omega \,\mp\, eV_{\alpha})$ is the Fermi function for electrons (-) and holes (+) associated to the temperature T_{α} of the respective contact. The diagonal structure of $\boldsymbol{g}^{r,<}_{k\alpha,\,k_\alpha}(\omega)$ originates in their definition as normal conducting leads, i.e. the isolated leads do not experience the unusual off-diagonal elements corresponding to superconducting pairing. The results for the self-energies follow from Eq. (7.3.24) used for the frequency space quantities. Since $\boldsymbol{T}_{\alpha}$, τ_z and $\boldsymbol{g}^{r,<}_{k\alpha,\,k\alpha}(\omega)$ are all diagonal, we find the simplified expression

$$\boldsymbol{\Sigma}^{r,<}_{\alpha}(\omega) \;=\; \sum_{k} |t_{\alpha}(k)|^2\; \boldsymbol{g}^{r,<}_{k\alpha,\,k\alpha}(\omega). \tag{7.4.11}$$

Explicitly, we have the self-energies

$$\boldsymbol{\Sigma}^{r}_{\alpha}(\omega) \;=\; \begin{bmatrix} \Lambda^{-}_{\alpha}(\omega) - \mathrm{i}\gamma^{-}_{\alpha} & \\ & \Lambda^{+}_{\alpha}(\omega) - \mathrm{i}\gamma^{+}_{\alpha} \end{bmatrix}, \tag{7.4.12}$$

$$\boldsymbol{\Sigma}^{<}_{\alpha}(\omega) \;=\; \begin{bmatrix} 2\mathrm{i}\,\gamma^{-}_{\alpha}\, f^{-}_{\alpha} & \\ & 2\mathrm{i}\,\gamma^{+}_{\alpha}\, f^{+}_{\alpha} \end{bmatrix} \tag{7.4.13}$$

where we introduced the real valued abbreviations

$$\Lambda_\alpha^{\pm}(\omega) \coloneqq P\sum_k \frac{|t_\alpha(k)|^2}{\hbar\omega \pm \epsilon_{k\alpha}}, \tag{7.4.14}$$

$$\gamma_\alpha^{\pm}(\omega) \coloneqq \pi \sum_k |t_\alpha(k)|^2\ \delta(\hbar\omega \pm \epsilon_{k\alpha}), \tag{7.4.15}$$

and $-$ $(+)$ refers to electrons (holes) as usual. The imaginary part of the self-energy, i.e. $\gamma_\alpha^{\pm}(\omega)$ introduces a finite life time for particle/holes inside the central system, such that they travel according to the applied bias V. Importantly, we see now that $G^<(\omega)$ from Eq. (7.4.5) depends via the lesser self-energies on the Fermi functions of the leads.

Our results displayed in Eqs. (7.4.5), (7.4.7) and Eqs. (7.4.8) - (7.4.11) uniquely determine the current I_L; however, the latter is still written w.r.t to local 2×2 matrices and we remove this downside next for convenience. The global self-energy $\Sigma_\alpha^{r,<}(\omega)$ is defined analogously as $\Sigma_\alpha^{\mathrm{c}}(\tau,\, s)$ was, only in frequency space. We thus replace $\mathbf{\Sigma}_\alpha^{\mathrm{c}}(\tau,\, s) \to \mathbf{\Sigma}_\alpha^{r,<}(\omega)$ in Eq. (7.3.31). In this respect one can easily show that

$$\mathrm{Tr}\left\{\Sigma_\alpha^{s}(\omega)\, G^{s'}(\omega)\right\} \;=\; \mathrm{Tr}\left\{\mathbf{\Sigma}_\alpha^{s}(\omega)\, \boldsymbol{G}_{11}^{s'}(\omega)\right\}, \quad s,\, s' =<,\, r,\, a \tag{7.4.16}$$

holds and in turn the current I_L becomes

$$I_L \;=\; -e\int\limits_{\mathbb{R}} \frac{\mathrm{d}\omega}{2\pi}\, \mathrm{Tr}\left\{\mathbb{1}_N \otimes \tau_z\, \left[\Sigma_L^{r}(\omega)\, G^{<}(\omega) \;+\; \Sigma_L^{<}(\omega)\, G^{a}(\omega)\right]\right\}, \tag{7.4.17}$$

Here, $\mathbb{1}_N \otimes \tau_z$ originates from the Pauli matrix τ_z and accounts for positive (negative) signs for electron (hole) contributions. Nonetheless, a more suitable form can be obtained using the realness of I_L, i.e. $2\, I_L = I_L + I_L^\dagger$, exploiting the skew hermiticity of the lesser GF/ self-energies and using the properties of the trace. Doing so grants

$$I_L \;=\; -\frac{e}{2}\int\limits_{\mathbb{R}} \frac{\mathrm{d}\omega}{2\pi}\mathrm{Tr}\left\{\mathbb{1}_N \otimes \tau_z\, \left[-\mathrm{i}\Gamma_L(\omega)\, G^{<}(\omega) \;-\; \Sigma_L^{<}(\omega)\, \left[G^{r}(\omega) - G^{a}(\omega)\right]\right]\right\}, \tag{7.4.18}$$

where we introduced here the $2N\times 2N$ broadening matrices

$$\Gamma_\alpha\,(\omega) = \,\mathrm{i}\,\left[\Sigma_\alpha^{r}(\omega) - \Sigma_\alpha^{a}(\omega)\right] \;=\; -2\,\mathrm{Im}\left\{\Sigma_\alpha^{r}(\omega)\right\} \tag{7.4.19}$$

containing the spectral functions of the leads. Explicitly, we have $(s =<, r)$

$$\Gamma_L(\omega) \;=\; \begin{bmatrix} \mathbf{\Gamma}_L(\omega) & \mathbf{0} & \dots & \mathbf{0} \\ \mathbf{0} & \mathbf{0} & \dots & \mathbf{0} \\ \vdots & \vdots & \ddots & \vdots \\ \mathbf{0} & \mathbf{0} & \dots & \mathbf{0} \end{bmatrix}_{2N\times 2N}, \quad \Gamma_R(\omega) \;=\; \begin{bmatrix} \mathbf{0} & \dots & \mathbf{0} & \mathbf{0} \\ \vdots & \ddots & \vdots & \vdots \\ \mathbf{0} & \dots & \mathbf{0} & \mathbf{0} \\ \mathbf{0} & \dots & \mathbf{0} & \mathbf{\Gamma}_R(\omega) \end{bmatrix}_{2N\times 2N} \tag{7.4.20}$$

with

$$\mathbf{\Gamma}_\alpha(\omega) \;=\; -2\,\mathrm{Im}\,\{\mathbf{\Sigma}^r_\alpha\} \equiv \begin{bmatrix} 2\,\gamma^-_\alpha(\omega) & \\ & 2\,\gamma^+_\alpha(\omega) \end{bmatrix}. \tag{7.4.21}$$

We can further express $\Sigma^<_\alpha(\omega)$

$$\Sigma^<_\alpha(\omega) \;=\; \mathrm{i}\,\Gamma_\alpha(\omega)\;[\mathbb{1}_N \otimes \boldsymbol{F}_\alpha(\omega)] \tag{7.4.22}$$

in terms of $\Gamma_\alpha(\omega)$ and we may write the current in the form

$$I_L \;=\; \frac{\mathrm{i}\,e}{2}\int\limits_{\mathbb{R}} \frac{\mathrm{d}\omega}{2\pi}\mathrm{Tr}\left\{(\mathbb{1}_N \otimes \tau_z)\;\Gamma_L\left[G^< \;+\; (\mathbb{1}_N \otimes \boldsymbol{F}_L)\;(G^r - G^a)\right]\right\}, \tag{7.4.23}$$

where we dropped the argument ω only for shortness. Please notice, the current formula agrees with the more general expression found by Meir and Wingreen in case of non-interacting leads [117]. In principle the current calculation ends here, since all quantities are at least implicitly known to us and we could move on to discuss the results and compare them to our earlier spectral findings. However, we would like to first demonstrate that the current vanishes in equilibrium, i.e. without applied bias $V = 0$, and second we wish to reshape I_L into a more appealing form.

We can write $G^<$ from Eq. (7.4.5) as

$$G^< \;=\; \mathrm{i}\,G^r\left[\sum_{\alpha=L,R}\Gamma_\alpha\;(\mathbb{1}_N \otimes \boldsymbol{F}_\alpha(\omega))\right] G^a. \tag{7.4.24}$$

by inserting Eq. (7.4.22). Further, one can show that

$$G^r \;-\; G^a \;=\; -\mathrm{i}\,G^r\,(\Gamma_L \;+\; \Gamma_R)\;G^a \tag{7.4.25}$$

holds. As we see, the last two expressions are quite similar and the only distinction relies on the Fermi functions contained inside $\boldsymbol{F}_\alpha$. For $V = 0$, we find $V_L = \eta eV = 0$, $V_R = (\eta - 1)eV = 0$ and thus $\boldsymbol{F}_\alpha = \mathbb{1}_2$. Therefore, we have $\mathbb{1}_N \otimes \boldsymbol{F}_\alpha|_{V=0} = \mathbb{1}_{2N}$ and the current vanishes in equilibrium due to Eqs. (7.4.24), (7.4.25).

The most suitable candidate to reshape the current expression is the (default) BdG basis $\hat{\psi}_{\mathrm{BdG}} \;=\; \left(d_1,\,\ldots,d_N,\,d_1^\dagger,\,\ldots,d_N^\dagger\right)^{\mathrm{T}}$ where the Kitaev Hamiltonian is reordered into electronic and hole blocks, see Eq. (6.0.1), and both are coupled by the superconducting pairing. We denote quantities w.r.t. $\hat{\psi}_{\mathrm{BdG}}$ with a subscript "BdG" for clarity until the end of this section. The reason for this choice can be seen at best from the matrices $\mathbb{1}_N \otimes \tau_z$ and $\mathbb{1}_N \otimes \boldsymbol{F}_\alpha$ as they transform to

$$\mathbb{1}_N \otimes \tau_z \;\to (\mathbb{1}_N \otimes \tau_z)_{\mathrm{BdG}} \;=\; \tau_z \otimes \mathbb{1}_N \;=\; \begin{bmatrix} \mathbb{1}_N & \\ & -\mathbb{1}_N \end{bmatrix}, \tag{7.4.26}$$

$$\mathbb{1}_N \otimes \boldsymbol{F}_\alpha \;\to (\mathbb{1}_N \otimes \boldsymbol{F}_\alpha)_{\mathrm{BdG}} \;=\; \boldsymbol{F}_\alpha \otimes \mathbb{1}_N \;=\; \begin{bmatrix} \mathbb{1}_N\,f^-_\alpha & \\ & \mathbb{1}_N\,f^+_\alpha \end{bmatrix}, \tag{7.4.27}$$

i.e. uniting the electronic (hole) information into the upper (lower) diagonal block matrix, which we exploit soon. This is essentially the opposite ordering w.r.t $\hat{\Psi}_{\mathrm{so}} = \left(d_1,\, d_1^\dagger,\, \ldots,\, d_N,\, d_N^\dagger\right)^{\mathrm{T}}$ which primarily orders according to the sites and then to electron and holes respectively. In principle, one has to verify the given expressions by explicit proof using the basis transformation matrix which maps $\hat{\Psi}_{\mathrm{so}}$ on $\hat{\psi}_{\mathrm{BdG}}$. However, one can bypass this calculation by simply remembering if an entry corresponds to electron or holes and to which site. For instance, the electronic (hole) components of $\mathbf{\Gamma}_\alpha$ acting on the first (last) site for $\alpha = L$ ($\alpha = R$), read now entry-wise ($n,\, m = 1,\, \ldots,\, 2N$)

$$\left[\Gamma_{L,\,\mathrm{BdG}}(\omega)\right]_{n\,m} = 2\gamma_L^-\ \delta_{n\,1}\,\delta_{m\,1} + 2\gamma_L^+\ \delta_{n\,N+1}\,\delta_{m\,N+1}, \tag{7.4.28}$$

$$\left[\Gamma_{R,\,\mathrm{BdG}}(\omega)\right]_{n\,m} = 2\gamma_R^-\ \delta_{n\,N}\,\delta_{m\,N} + 2\gamma_R^+\ \delta_{n\,2N}\,\delta_{m\,2N}, \tag{7.4.29}$$

and the retarded self-energies behave of course analogously

$$\left[\Sigma^r_{L,\,\mathrm{BdG}}(\omega)\right]_{n\,m} = \left[\Lambda_L^- - \mathrm{i}\gamma_L^-\right]\ \delta_{n\,1}\,\delta_{m\,1} + \left[\Lambda_L^+ - \mathrm{i}\gamma_L^+\right]\ \delta_{n\,N+1}\,\delta_{m\,N+1}, \tag{7.4.30}$$

$$\left[\Sigma^r_{R,\,\mathrm{BdG}}(\omega)\right]_{n\,m} = \left[\Lambda_R^- - \mathrm{i}\gamma_R^-\right]\ \delta_{n\,N}\,\delta_{m\,N} + \left[\Lambda_R^+ - \mathrm{i}\gamma_R^+\right]\ \delta_{n\,2N}\,\delta_{m\,2N}. \tag{7.4.31}$$

Further, the retarded GF G^r_{BdG} obeys

$$G^r_{\mathrm{BdG}} = \left[E\mathbb{1}_{2N} - \mathcal{H}_{\mathrm{BdG}} - \Sigma^r_{L,\,\mathrm{BdG}} - \Sigma^r_{R,\,\mathrm{BdG}}\right]^{-1} = \begin{bmatrix} C_- & -S \\ -S^\dagger & C_+ \end{bmatrix}^{-1}_{2N\times 2N} \tag{7.4.32}$$

with S from Eq. (6.0.4) and

$$C_\mp = \begin{bmatrix} E \pm \mu - \Lambda_L^\mp + \mathrm{i}\gamma_L^\mp & \pm t & & & & & & & \\ \pm t & E \pm \mu & \pm t & & & & & & \\ & \pm t & E \pm \mu & \pm t & & & & & \\ & & \ddots & \ddots & \ddots & & & & \\ & & & \pm t & E \pm \mu & \pm t & & & \\ & & & & \pm t & E \pm \mu & \pm t & & \\ & & & & & \pm t & E \pm \mu & \pm t & \\ & & & & & & \pm t & E \pm \mu - \Lambda_R^\mp + \mathrm{i}\gamma_R^\mp \end{bmatrix} \tag{7.4.33}$$

where we set $E = \hbar\omega$.

Since a trace is basis invariant one can symbolically replace the matrices in I_L from Eq. (7.4.23) by the ones w.r.t. $\hat{\psi}_{\mathrm{BdG}}$. Particularly physically relevant is Eq. (7.4.26), as it allows us to split the full trace in I_L into the contributions from the first N, corresponding to only electronic degrees of freedom, and the last N associated to the holes. The difference of both partial traces yields the full current following Eqs. (7.4.23), (7.4.26). In fact, the respective partial trace represents the particle or hole current (in presence of the superconducting pairing constant Δ) and we have to respect both pieces. Further, the Kitaev chain enters naturally in the NEGF formalism as BdG matrix in a given basis, see for instance Eq. (7.3.29), and thus respects intrinsically the particle-hole symmetry. The intuitive expectation that both the electronic and the hole current contribute equally is indeed correct, since the particle-hole symmetry is preserved by the self-energies.

8. Quasi-particle transport properties of the finite size Kitaev chain

The main results of the chapter have been published partially in [5].

The trace inside the current formula (7.4.23) can be simplified since the self-energies are sparse matrices. We find

$$\begin{aligned} I_L \;=\; \frac{e}{h} \int\limits_{\mathbb{R}} \mathrm{d}E \; \big\{ & \Gamma_L^- \, \Gamma_R^- \, |G^r_{1,N}|^2 \, \left[f_L^- - f_R^- \right] \\ & + \; \Gamma_L^- \, \Gamma_L^+ \, |G^r_{1,N+1}|^2 \, \left[f_L^- - f_L^+ \right] \\ & + \; \Gamma_L^- \, \Gamma_R^+ \, |G^r_{1,2N}|^2 \, \left[f_L^- - f_R^+ \right] \big\} \,, \end{aligned} \tag{8.0.1}$$

where $\Gamma_\alpha^\pm \coloneqq 2\gamma_\alpha^\pm = 2\pi \sum\limits_k |t_\alpha(k)|^2 \delta(E \pm \epsilon_{k\alpha})$ represents the non-zero entries of the broadening matrices. Here, $f_\alpha^\pm = f(E \pm eV_\alpha)$ is the Fermi-Dirac distribution for electrons $(-)$ and holes $(+)$ in lead $\alpha = L,\, R$ at temperature T_α. The quantities $G^r_{i,j}$ are the entries of G^r_{BdG} from Eq. (7.4.32) and we dropped the subscript BdG for shortness. Further, we substituted $E = \hbar\omega$ for convenience (all terms beneath the integral depend on E) and the earlier prefactor $1/2$ canceled due to the particle-hole symmetry.

The information provided by the current formula from Eq. (8.0.1) is depicted in Fig. 8.1. We have a direct term ($G^r_{1,N}$), the Andreev reflection ($G^r_{1,N+1}$) and the crossed Andreev process ($G^r_{1,2N}$). Explicitly, the direct term describes the quasiparticle transport of an electron through the Kitaev chain originating from the left lead and towards the right lead, in presence of the superconducting pairing Δ. The Andreev reflection relies on the superconductivity such that the electron entering the Kitaev chain from the left lead is back reflected as hole into the contact. Meanwhile, a right moving Cooper-pair is formed inside the Kitaev chain [120, 121]. Similarly to the Andreev reflection, the crossed Andreev process accounts for electrons from the left lead, only that the hole leaves the Kitaev chain towards the right lead and we find a left moving Cooper pair. In this scope, transmission probabilities of each process are the product of the respective values of $\Gamma_\alpha^\pm$ and the absolute value squared of the corresponding entry of the GF.

Due to their physical appearance, one considers the Andreev reflection as *local* process contrary to the *non-local* crossed Andreev and direct terms. Indeed, one should consider these assignments literally since decaying states, localized around the systems ends, favor the Andreev reflection. In contrast extended states contribute mostly by the direct and crossed Andreev terms. Further, the ratio between the latter two depends highly on the chosen parameters which determine the quasi-particle character of the

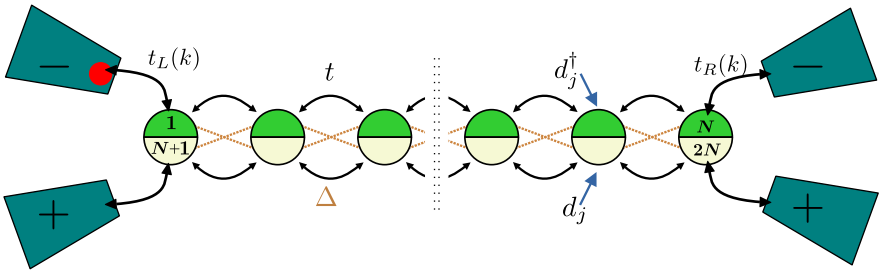

Figure 8.1.: The N-S-N configuration with separated electron (−) and hole (+) tunneling per contact. An electron for instance from the left lead (red sphere) has three possibilities to participate in the charge transfer: First to re-enter the same contact as a hole (Andreev reflection) or using the Kitaev chain to arrive at the other contact either as electron (Direct) or as hole (crossed Andreev). Particle (hole) degrees of freedom are represented by $1, \ldots, N$ ($N+1, \ldots, 2N$) w.r.t $\hat{\psi}_{\mathrm{BdG}}$. The depicted numbers 1, N, $N+1$, $2N$ refer to the entries of G^r_{BdG} which determine the current, see Eq. (8.0.1).

charge carrying state. For instance, in the case of very weak superconducting pairing the crossed Andreev process and the Andreev reflection become weaker and disappear entirely for $\Delta = 0$.

In case the mean-field superconducting pairing constant is not properly handled by a self-consistent calculation, the charge is not conserved [109, 118, 119] and $I_L \neq -I_R$. The self-consistent treatment implies $\Delta = \Delta(t, \mu, \epsilon_{kL}\, \epsilon_{kR}, V_L, V_R, t_L, t_R)$ and has to be done numerically. However, in case of $\Sigma^r_L = \Sigma^r_R$, $V_L = -V_R = V/2$ and $T_L = T_R$ both contacts are physically indistinguishable and charge is automatically conserved for generic Δ [45]. The constraint from the self-energy translates as $\gamma^\pm_L = \gamma^\pm_R$, $\Lambda^\pm_L = \Lambda^\pm_R$. We refer to this charge conserving scenario as the symmetric case from now on.

In section 8.1, we discuss in more detail how the values of $V_{L,R}$ influence the conductance formula. For instance, in case of $V_L = V_R \neq 0$, no bias is applied between the leads, but quasiparticle transport is still possible. Only Andreev and crossed Andreev reflection contribute to the conductance [47, 122]. Further, the quantized conductance peak value is also influenced by $V_{L,R}$. In the symmetric case of $V_L = -V_R = V/2$, we expect quantized values of e^2/h [45–47] for the conductance while we find $2e^2/h$ [7, 27, 48, 49] in the case when one lead is grounded ($V_R \equiv 0$).

The conductance results presented and discussed in the next section extends the ones stated in Ref. [109]. There, several analytical results for the conductance in special parameter situations are presented. Here, we give exact results for generic parameter values with and without the wide band limit for the conductance and all independent contributions to it. We also investigate later the supra-gap transport regime in section 8.2.

8.1. Linear transport and generic applied bias

The linear conductance $G = \lim_{V\to 0} \partial I/\partial V$ is generally determined by Eq. (8.0.1) and we first examine the generic situation in order to introduce the used notation. The chemical potentials of the leads $\mu_{L,R}$ deviate from the one of the Kitaev chain, μ, by $V_{L,R}$ such that $V = V_L - V_R$. We can understand $V_L = \eta V$, $V_R = (\eta - 1)V$ as fractions of the total applied bias and since μ, $\mu_{L,R}$ are observable, η is in fact a physical, although not always known, quantity. In case of zero temperature for both contacts, the conductance G follows from Eq. (8.0.1) as

$$G \,=\, \frac{e^2}{h}\, \left\{ \Gamma_L^-\, \Gamma_R^-\, |G^r_{1,N}|^2 \,+\, 2\eta\, \Gamma_L^-\, \Gamma_L^+\, |G^r_{1,N+1}|^2 \,+\, (2\eta - 1)\; \Gamma_L^-\, \Gamma_R^+\, |G^r_{1,2N}|^2 \right\}_{E=0} . \tag{8.1.1}$$

The constraint of $E = 0$ originates from the Fermi functions and e^2/h is the conductance quantum. Since distinct values for η change only the weights of the second and third term in Eq. (8.1.1), we define the Direct/ Andreev/ Crossed Andreev conductance contributions as

$$G_{\mathrm{D}} \coloneqq \frac{e^2}{h}\, \left\{ \Gamma_L^-\, \Gamma_R^-\, |G^r_{1,N}|^2 \right\}_{E=0} , \tag{8.1.2}$$

$$G_{\mathrm{A}} \coloneqq \frac{e^2}{h}\, \left\{ \Gamma_L^-\, \Gamma_L^+\, |G^r_{1,N+1}|^2 \right\}_{E=0} , \tag{8.1.3}$$

$$G_{\mathrm{CA}} \coloneqq \frac{e^2}{h}\, \left\{ \Gamma_L^-\, \Gamma_R^+\, |G^r_{1,2N}|^2 \right\}_{E=0} \tag{8.1.4}$$

whereby the (total) conductance G reads

$$G \,=\, 1 \cdot G_{\mathrm{D}} \,+\, 2\eta\; G_{\mathrm{A}} \,+\, (2\eta - 1)\; G_{\mathrm{CA}}. \tag{8.1.5}$$

The definition of G_{D}, G_{A}, G_{CA} is strategically advantageous as the required GF entries and $\Gamma_\alpha^\pm$ are independent of η. In other words, the functional dependence of the three contributions to G on all involved parameters, namely t, Δ, μ, $\gamma_{L,R}^\pm = \Gamma_\alpha^\pm/2$ and $\Lambda_{L,R}^\pm$, does not change with η. A quantitative understanding of G requires the self-consistent calculations $\Delta \equiv \Delta(t,\, \mu,\, \epsilon_{kL}\, \epsilon_{kR},\, V_L,\, V_R,\, t_L,\, t_R)$ in order to ensure the charge conservation [118, 119]. However, a qualitative understanding of G_{D}, G_{A}, G_{CA} and even their relative ratio does not require the self-consistency cycle as all three rely on the same value of Δ.

In order to provide an overview, we show the results for G_{D}, G_{A}, G_{CA} immediately. The involved abbreviations are explained in section 8.1.1. Generally, the introduction of

$p := t + \Delta$, $m := t - \Delta$ (p, $m \in \mathbb{R}$) was helpful to shorten the exact expressions

$$G_{\mathrm{A}} = \frac{e^2}{h} \frac{\gamma_L^2 \gamma_R^2 \left(p^{2N-2} - m^{2N-2}\right)^2}{\left[|q_+|^2 + \gamma_L \gamma_R \left(p^{N-1} + m^{N-1}\right)^2\right]^2}, \tag{8.1.6}$$

$$G_{\mathrm{D}} = \frac{e^2}{h} \frac{\gamma_L \gamma_R \left(p^{N-1} + m^{N-1}\right)^2}{\left[|q_+|^2 + \gamma_L \gamma_R \left(p^{N-1} + m^{N-1}\right)^2\right]^2} |q_-|^2, \tag{8.1.7}$$

$$G_{\mathrm{CA}} = \frac{e^2}{h} \frac{\gamma_L \gamma_R \left(p^{N-1} - m^{N-1}\right)^2}{\left[|q_+|^2 + \gamma_L \gamma_R \left(p^{N-1} + m^{N-1}\right)^2\right]^2} |q_+|^2 \tag{8.1.8}$$

where $\gamma_{L,R} := \gamma^{\pm}_{L,R}|_{E=0} = 2\Gamma^{\pm}_{L,R}|_{E=0}$ is used. Explicitly, we have

$$\gamma_\alpha = \pi \sum_k |t_\alpha(k)|^2 \, \delta(\epsilon_{k\alpha}), \tag{8.1.9}$$

$$\Lambda^{\pm}_\alpha|_{E=0} = P \sum_k \frac{|t_\alpha(k)|^2}{E \pm \epsilon_{k\alpha}}\bigg|_{E=0} = \pm P \sum_k \frac{|t_\alpha(k)|^2}{\epsilon_{k\alpha}} =: \pm \Lambda_\alpha \tag{8.1.10}$$

from Eqs. (7.4.14), (7.4.15).

Let me give three short remarks before we discuss the details. First, in case of $\Delta = 0$, one finds as expected that $G_{\mathrm{CA}} = G_{\mathrm{A}} = 0$. Secondly, G_{D}, G_{CA} are very similar and differ only in a few negative signs while G_{A} deviates from both. The physical reasons behind this originates simply from the fact that the direct and the crossed Andreev process are both non-local, i.e. the internal structure of the Kitaev chain has a large impact. Finally, we will soon see that all results rely in the end on the spectrum of the finite and isolated Kitaev chain which enters via $q_\pm$.

In the next section, we introduce the quantities $q_\pm$ in detail and we discuss the conductance results for $V_L = -V_R = V/2$.

8.1.1. Conductance in the symmetric bias and charge conserved scenario

The setting $V_L = -V_R = V/2$ implies $\eta = 1/2$ and the conductance G becomes

$$G = \frac{e^2}{h} \left\{\Gamma^-_L \Gamma^-_R |G^r_{1,N}|^2 + \Gamma^-_L \Gamma^+_L |G^r_{1,N+1}|^2\right\}_{E=0} = G_{\mathrm{D}} + G_{\mathrm{A}}. \tag{8.1.11}$$

Although G_{CA} is finite, the term dropped as the population of electrons in the left and holes in the right lead is the same for $\eta = 1/2$.

As one can see from Eq. (7.4.32), the GF are peaked around values for E close to the eigenvalues of the central system thus the sub-gap regime is probed by the linear conductance. For simplicity, we consider first the so called wide band limit in which the density of states and the tunneling amplitudes $t_{L,R}$ for both leads are constant. This treatment causes the real part of the self-energies $\Lambda_{L,R} = 0$ to vanish and the imaginary

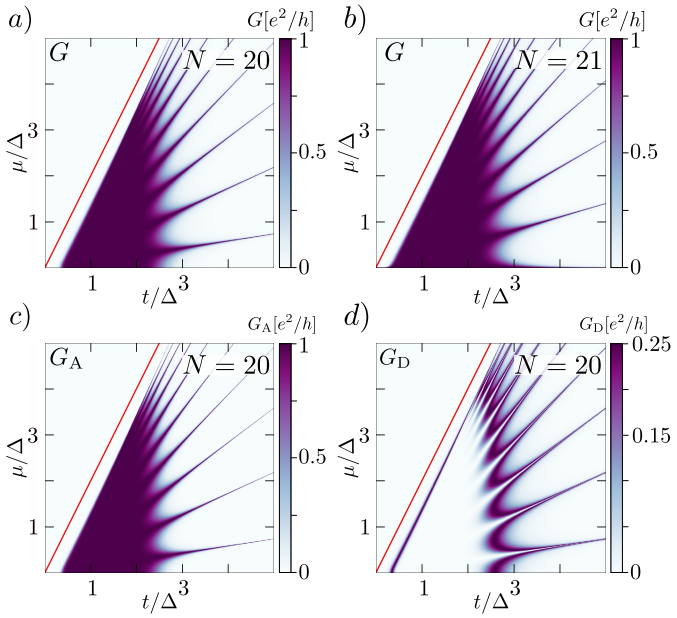

Figure 8.2.: Zero temperature conductance G as function of μ/Δ, t/Δ in the wide band limit for $\gamma_{L,R}/\Delta = 0.001$ in units of e^2/h. The topological phase boundary is depicted in red. a) The conductance of about e^2/h forms a triangular-like plateau from which the discrete Majorana lines emerge, when system size and decay length become comparable in magnitude. Those lines follow the parameter constraint of Eq. (6.3.7). b) For odd N, exponentially small energies reside always close to horizontal axis. c) The Andreev contribution G_A dominates the conductance $G = G_A + G_D$ for the given parameter ranges. d) The direct term G_D emerges when the Andreev contribution weakens, and slightly broadens the conductance plateau.

part becomes constant, $\gamma_L = \text{const.}$, $\gamma_R = \text{const.}$. Moreover, we focus first on G rather than G_D or G_A. Once G is discussed, we turn back to G_D, G_A. In a last step we leave the wide-band approximation and discuss the generic situation for $\eta = 1/2$. Finally, without the self-consistent calculation of Δ, charge is only conserved for $\gamma_L = \gamma_R$ and $\Lambda_L = \Lambda_R$.

It is intuitively clear that, proper transmission functions $\Gamma_L \Gamma_R |G^r_{1,N}|^2$, $\Gamma_L \Gamma_L |G^r_{1,N+1}|^2$ vary only between 0 and 1 in the case when the number of particles is conserved. Thus, we can naively expect conductance values up to $2\, e^2/h$. However, this is not the case as both functions do not reach their maxima simultaneously since the underlining physical processes are distinct. We refer here to Fig. 8.2 for a first impression. Instead, we find conductance values up to e^2/h and reached only for zero or near zero energy modes of the Kitaev chain. The exact result for G at $\eta = 1/2$ is

$$G = \frac{e^2}{h} \frac{\gamma_L \gamma_R \left(p^{N-1} + m^{N-1}\right)^2}{|q_+|^2 + \gamma_L \gamma_R \left(p^{N-1} + m^{N-1}\right)^2}. \tag{8.1.12}$$

From Eq. (8.1.12), one observes directly that $G = e^2/h$ ($G < e^2/h$) holds in case of $|q_+| = 0$ ($|q_+| \neq 0$). In order to give a expression for $q_\pm$, we introduce $x_{j,0}$ as

$$x_{j,0} = \frac{r_+^{j+1} - r_-^{j+1}}{r_+ - r_-}, \quad j \in \mathbb{Z} \tag{8.1.13}$$

with $2r_\pm = \left(-\mu \pm \sqrt{\mu^2 - 4\,mp}\right)/p$. The function $x_{j,0}$ is real valued, dimensionless and contains the spectral information of the isolated Kitaev chain with j sites. Explicitly, we have $\det(\mathcal{H}_\mathrm{c}) = (-1)^N p^{2N} x_{N,0}^2$ as one can easily verify with Eq. (6.3.9). In the wide band limit, the function

$$q_s \coloneqq p^{N-2}\left[sp^2\, x_{N,0} + \mathrm{i}p\, x_{N-1,0}\,(s\,\gamma_L - \gamma_R) + x_{N-2,0}\,\gamma_L\gamma_R\right], \quad s = \pm, \tag{8.1.14}$$

modifies $x_{j,0}$ due to the presence of the contacts. Note that one has to adapt q_s slightly for non-wide band scenarios.

Let us examine the conduction for parameters corresponding to exact or nearly zero energy first. Especially simple are the Kitaev points at $\mu = 0$, $|t| = |\Delta|$ since exact zero energy are found here independent of the system length, i.e. we have $x_{j,0} \equiv 0$ for $j = N, N-1, N-2$. In turn, $q_+ = 0$ holds and the conductance adopts the maximal value of e^2/h. Besides these specific points, zero or close to zero energies can be found, implying that $x_{N,0} \approx 0$ is small. Thus, $q_+ \approx 0$ gives only a minor contribution as we are forced to use $\gamma_L = \gamma_R$ eliminating the $x_{N-1,0}$ term. $x_{N-2,0}$ behaves similar as $x_{N,0}$ and is especially suppressed for small values of $\gamma_{L,R}$. Thus, we find $G \approx e^2/h$ for close to or even exact zero energy modes. Consequently, the maximum conductance appears in the triangular shaped region in Fig. 8.2 similar to the one of minimal in-gap energy from Fig. 6.10. Further away from the Kitaev points, the conductance G touches e^2/h only on or very close to the Majorana lines corresponding to the parameters given in Eq. (6.3.7) as only $x_{N,0} = 0$ holds there. At the edges of the roughly e^2/h conductance plateau, the value of $\gamma_L\gamma_R\, x_{N-2,0}$ becomes important.

The difference between even and odd N as shown in Fig. 8.2 a), b) originates back in the $\mu = 0$ case, where for odd N we found zero energy for all ratios of t/Δ, later identified as one of the zero energy lines given in Eq. (6.3.7). Since the conductance is continuous in all parameters, the e^2/h value smears out for smaller values of μ/Δ and t/Δ.

In the limit $N \to \infty$, the conductance becomes e^2/h for all parameters within the topological non-trivial region as expected see Fig. 8.3 for comparison.

Next, we turn to G_D, G_A,

$$G_\mathrm{D} = \frac{e^2}{h}\,\frac{\gamma_L\gamma_R\left(p^{N-1} + m^{N-1}\right)^2}{\left[|q_+|^2 + \gamma_L\gamma_R\left(p^{N-1} + m^{N-1}\right)^2\right]^2}\,|q_-|^2, \tag{8.1.15}$$

$$G_\mathrm{A} = \frac{e^2}{h}\,\frac{\gamma_L^2\gamma_R^2\left(p^{2N-2} - m^{2N-2}\right)^2}{\left[|q_+|^2 + \gamma_L\gamma_R\left(p^{N-1} + m^{N-1}\right)^2\right]^2}, \tag{8.1.16}$$

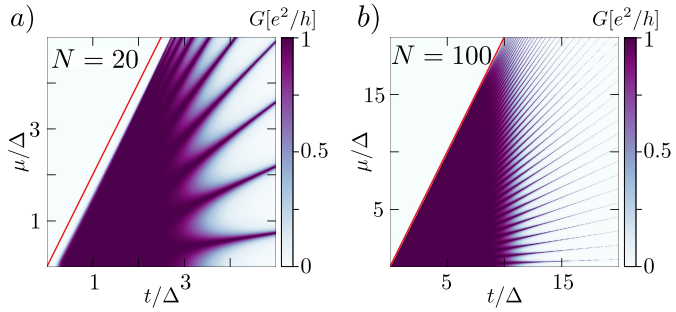

Figure 8.3.: Conductance for $N = 20$, $\gamma_{L,R}/\Delta = 0.01$ in a) and for $N = 100$, $\gamma_{L,R}/\Delta = 0.001$. a) Larger values of $\gamma_{L,R}$ broaden the e^2/h conductance region compared to smaller ones, see also Fig. 8.2 a). b) The conductance plateau grows with N until the entire topologically non-trivial phase is occupied in the limit $N \to \infty$.

in order to improve our understanding of G. The most important observation concerning $G_{\mathrm{D,A}}$ is their dependency on q_s: we have $G_{\mathrm{D}} \sim |q_-|^2/|q_+|^4$ and $G_{\mathrm{A}} \sim 1/|q_+|^4$. Thus, for parameters such that $q_+ \approx 0$ holds, we find no significant direct contribution $G_{\mathrm{D}} \approx 0$ as shown in Fig. 8.2 d), since q_- behaves similar to q_+ by virtue of Eq. (8.1.14). In contrast, G_{A} can be approximated as

$$G_{\mathrm{A}} \approx \frac{e^2}{h} \left(\frac{p^{N-1} - m^{N-1}}{p^{N-1} + m^{N-1}} \right)^2 , \tag{8.1.17}$$

and the dependency on μ dropped with q_+. Note that our approximation is very naive: the gained expression has a pole at $t = 0$ while G_{A} has an upper bound $G_{\mathrm{A}} \leq G \leq e^2/h$. Our treatment fails as q_s counters the divergence for small $|\Delta| \gg |t|$ thus $q_+ \approx 0$ imposes an implicit constraint on t, Δ and μ. However, for $t \approx \pm\Delta$ we find $p \approx 0$ or $m \approx 0$ and thus G_{A} is close to e^2/h. Hence, the conductance G is mostly given by G_{A} around the Kitaev points within the triangular-shaped region, as we see also from Fig. 8.2.

The situation changes in the moment in which q_+ is not sufficiently small. The direct term $G_{\mathrm{D}} \sim |q_-|^2/|q_+|^4$ starts to contribute since q_- behaves similar to q_+. This happens only at the edges of the conductance plateau as the in-gap energies grow exponentially there and a further increase leads directly to a decline of G_{D} again. Large values of $q_\pm$ diminish G_{A} and since $G = G_{\mathrm{A}} + G_{\mathrm{D}}$ is limited by e^2/h, the direct term can literally be seen as the frame enclosing significant contributions of the Andreev reflection.

So far, we have discussed the conductance and its contributions from merely an energetic point of view. We can improve our understanding in terms of the standard terminology for Majorana fermions: the decay length ξ given earlier in Eq. (5.4.1) adds the aspect of localization. For parameters associated to the triangular region in Fig. 8.2, we have that $\xi \ll Nd$, i.e. the in-gap states are localized at the system's end. Here, the Andreev term contributes primarily, with almost e^2/h and the direct term is suppressed. We conclude that localized states favour the local Andreev reflection. Close to edges of the conductance plateau, the direct term contributes more strongly. Here, the energy of

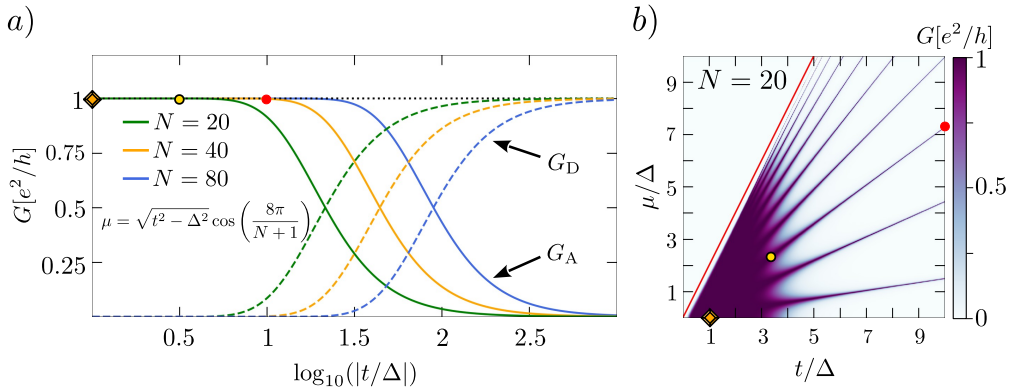

Figure 8.4.: Conductance contributions G_A (solid), G_D (dashed) in the wide band limit at $T_{L,R} = 0\,\mathrm{K}$ following the zero energy $\mu_8 = 2\sqrt{t^2 - \Delta^2}\cos(8\pi/N+1)$ line for $N = 20$, $N = 40$ and $N = 80$. a) For $|t/\Delta| = 1$, i.e. at the Kitaev points, the total conductance (black, dotted) arises only from the Andreev reflection which diminishes for larger t/Δ. Instead the direct term grows and becomes finally the dominant or exclusive contribution to G. Larger system sizes stabilize the $G_A = e^2/h$ plateau. b) Conductance G as function of μ/Δ, t/Δ for $N = 20$ as orientation. We have chosen $\gamma_{L,R}/\Delta = 0.02$ in both a), b) in order to enhance the line thickness in b). The conductance along distinct zero energy lines behaves similarly and is not strongly affected by $\gamma_{L,R}$.

the in-gap states grows and they are thus more extended along the Kitaev chain than before.

One might get the impression that the ratio G_A/G_D is determined by the spatial profile of the zero/ near zero energy state. This is indeed correct as one can see in Fig. 8.4, where we tracked G_A, G_D along one of the Majorana lines. The conductance is constantly about e^2/h, while the ratio between G_A/G_D changes continuously with t/Δ, starting with $G_A = e^2/h$, $G_D = 0$ at the Kitaev point and ending with $G_D = e^2/h$, $G_A = 0$. At $t/\Delta = 1$ (imposing here $\mu = 0$), the states are localized exclusively on the first/last site of the chain see Eqs. (5.3.7), (5.3.8) and the zero modes start to extend with increasing t/Δ as depicted in Fig. 6.16. For a critical value of t/Δ, the spatial extend favors direct charge transfer rather than the Andreev reflection. We confirm this result later in Ch. 9.

8.1.2. Conductance in non-wide band limit and with onsite disorder

We generalize our prior findings and we leave the wide band limit. Here, we have to account for $\Lambda^{\pm}_{L,R}|_{E=0} = \pm\Lambda_{L,R} \neq 0$ from Eq. (8.1.10). Fortunately only the functions q_s are modified to ($s = \pm$)

$$\begin{aligned} q_s \;=\; p^{N-2}\,\big[& sp^2\, x_{N,0} \,+\, p\, x_{N-1,0}\,(\mathrm{i}s\,\gamma_L \,-\, \mathrm{i}\,\gamma_R \,-\, s\,\Lambda_L \,-\, s\,\Lambda_R) \\ & +x_{N-2,0}\;(\Lambda_L \,-\, \mathrm{i}\,\gamma_L)\,(s\,\Lambda_R \,+\, \mathrm{i}\,\gamma_R)\big]\,, \end{aligned} \tag{8.1.18}$$

reducing back to the former expression given in Eq. (8.1.14) if $\Lambda_{L,R} = 0$. Notice, the values for $\gamma_{L,R}$ have to be taken from Eq. (8.1.9) and they are not necessarily constant. Still, avoiding the self-consistency cycle of Δ requires $\gamma_L = \gamma_R$, $\Lambda_L = \Lambda_R$. A further generalization of q_s including onsite disorder is possible. In case that the chemical potential of the Kitaev chain on the first (last) site is changed from $\mu \to \mu_1 = \mu + \nu_1$ ($\mu \to \mu_N = \mu + \nu_N$) for $\nu_{1,N} \in \mathbb{R}$, one only has to replace Λ_L (Λ_R) by $\tilde{\Lambda}_L \coloneqq \Lambda_L + \nu_1$ ($\tilde{\Lambda}_R \coloneqq \Lambda_R + \nu_N$) in q_s from Eq. (8.1.18). This simple extension was possible since the exact results for the GF entries G^r_{N+1}, $G^r_{1,N}$, $G^r_{1,2N}$ stated in appendix K can obtained for generic additions on the first/last site of the Kitaev chain. Any further change requires a recalculation of G^r_{N+1}, $G^r_{1,N}$, $G^r_{1,2N}$ or a numerical treatment. Please notice that the replacement $\mu \to \mu_1 = \mu + \nu_1$, $\mu \to \mu_N = \mu + \nu_N$ breaks the symmetry of the Kitaev chain w.r.t. $\mu \to -\mu$.

The given formulae for G, G_{A}, G_{D} and G_{CA} are still exact. One has only to account for the proper values of $\gamma_{L,R}$, $\Lambda_{L,R}$ in Eqs. (8.1.9), (8.1.10) and q_s in Eq. (8.1.18). However, the "small" adaptations change G, G_{A}, G_{D} (G_{CA}) qualitatively as we see next. For simplicity we consider $\tilde{\Lambda}_{L,R}$ as non-zero constants which is not necessarily true in reality but justified due to $\nu_{1,N}$.

As we discussed before, for small values of $|q_+|$ the conductance is about e^2/h. Finite values of $\tilde{\Lambda}_{L,R}$ enlarge q_+ and thus suppress G as depicted in Fig. 8.5 a), c), d). Possibly surprising though, $\tilde{\Lambda}_{L,R}$ can even enhance locally the conductance compared to the prior situation as we can see from Fig. 8.5 b). The reason is that the zero energy criterion from Eq. (6.3.7) does not hold anymore due to $\tilde{\Lambda}_{L,R} \neq 0$ as shown in appendix J in detail.

As short verification, recall the retarded GF $G^r = (E\,\mathbb{1}_{2N} - \mathcal{H}_{\mathrm{KC}} - \Sigma^r_L - \Sigma^r_R)^{-1}$ at generic E. For disorder, we have to adapt the Kitaev Hamiltonian. In case that E is close to the real part of an eigenvalue of $\mathcal{H}_{\mathrm{KC}} - \Sigma^r_L - \Sigma^r_R$, the GF is largest. A conductance peak of e^2/h is found in the vicinity of a vanishing real part, which changed since the real part of the self-energies is given by $\Lambda^{\pm}_{L,R}|_{E=0} = \pm\Lambda_{L,R} \neq 0$. Thus, the zero energy lines of the isolated Kitaev chain from Eq. (6.3.7) are modified. This modification depends also on the parameters t, Δ.

We have shown that in the case of large N the influence of $\tilde{\Lambda}_{L,R}$ vanishes as expected and depicted in Fig 8.6 a). However, in case that N is not large enough one finds also zero energy for $\Delta^2 \geq t^2$, which were forbidden for $\tilde{\Lambda}_{L,R} = 0$. Since the energy is itself continuous in the parameters, one finds in the vicinity of the zero energy lines always exponentially small energy eigenvalues. The modification by $\tilde{\Lambda}_{L,R}$ is such that in-gap

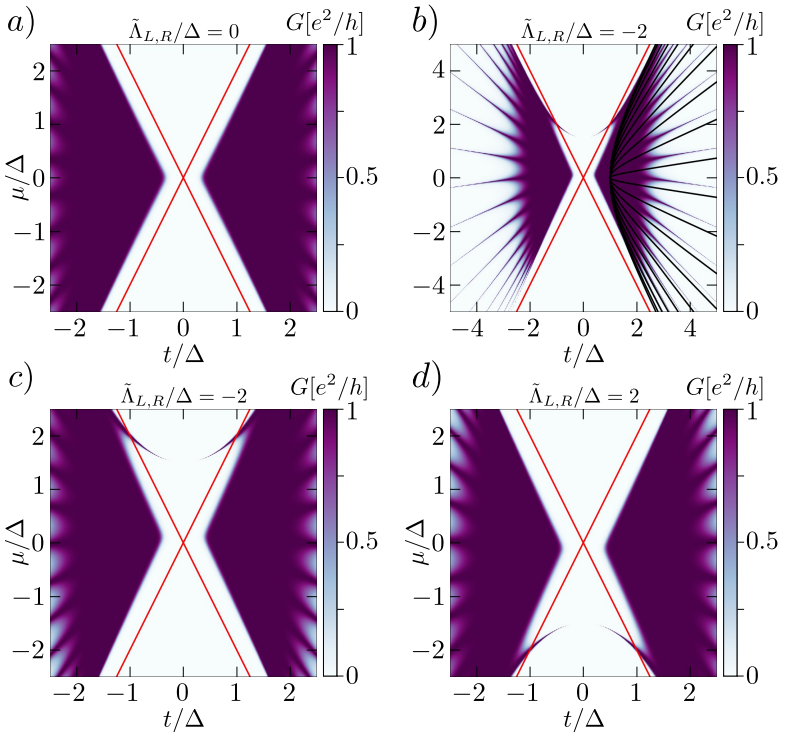

Figure 8.5.: Conductance of the Kitaev chain in non-wide band regime with onsite disorder as function of μ/Δ, t/Δ. We have chosen the parameters $N = 20$, $\gamma_{L,R}/\Delta = 0.001$. a) Conductance in wide band limit and without disorder ($\tilde{\Lambda}_{L,R}/\Delta = 0$) as comparison. b) For $\tilde{\Lambda}_{L,R}/\Delta = -2$, the zero energy lines are modified compared to the ones at $\tilde{\Lambda}_{L,R}/\Delta = 0$ (black). The e^2/h conductance plateau leaks into the topologically trivial phase. c) Zoom of b) around $\mu = t = 0$. The symmetry w.r.t to μ/Δ is broken and the entire conductance plateau is slightly moved upwards. This effect is more pronounced in the vicinity of the line openings at the left/right boundary as G gets locally suppressed. d) Similar to b) only for $\tilde{\Lambda}_{L,R}/\Delta = 2$. More details are given in the text.

energies leak into the topologically trivial phase. There, the (isolated) Kitaev chain does not support in-gap states by itself, and thus e^2/h conductance fingerprints are restricted. Notice, for large values of the imaginary part of the self-energies $\gamma_{L,R}$, the product $\gamma_R\gamma_L$ also influences the zero energy condition, see appendix M.

In Fig. 8.6, we also investigated Andreev and the direct term. Still, the Andreev term is dominant even within the topologically trivial phase. In section 9, we analyse more closely the dependence of G_A and G_D on the spatial profile of the charge carrying state. We find that the e^2/h conductance peak leaking into the topologically trivial phase, is caused by a localized in-gap state.

In the next section, we shortly return to the generic bias situation.

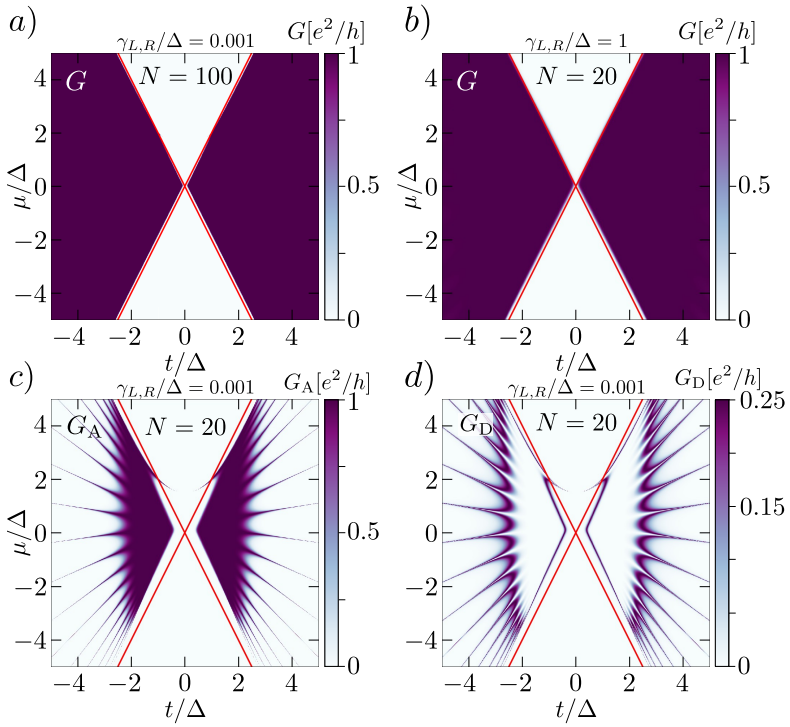

Figure 8.6.: Conductance and contributions $G_{A,D}$ in non-wide band regime with onsite disorder $\tilde{\Lambda}_{L,R}/\Delta = -2$ as function of μ/Δ, t/Δ. a) For $N = 100$, the influence of onsite disorder and the real part of the self-energies vanishes. Still, the symmetry in $\mu \to -\mu$ is slightly broken. b) Large values of $\gamma_{L,R}$ also reduce the impact of $\tilde{\Lambda}_{L,R}/\Delta = -2$. c) Andreev conductance G_A for $N = 20$ and small $\gamma_{L,R}/\Delta = 10^{-3}$ is still the main contribution to G in both topological phases. d) Analogous to c), but for the direct term. G_D is a minor term in G and merely broadens the e^2/h plateau of G_A.

8.1.3. Conductance for generic applied bias and $V_R = 0$

We have stated earlier that the conductance is in general given by $G = G_D + 2\eta\, G_A + (2\eta - 1)\, G_{CA}$ and we just finished the discussion of G_D, G_A and G for $\eta = 1/2$. In order to understand the conductance for arbitrary η, we are left to investigate G_{CA} given in Eq. (8.1.8). The expressions for G_A, G_D from Eqs. (8.1.6), (8.1.7) are still valid with q_s from either Eq. (8.1.14) (wide band limit, no onsite disorder) or generally from Eq. (8.1.18). In Fig. 8.7, we depicted the crossed Andreev and the direct contribution as a function of μ/Δ and t/Δ. Both are seemingly identical. This results from the fact that $q_\pm$ behave similarly as we discussed before and that $|t/\Delta|$ is not too large. In case of $|t| \gg |\Delta|$ however, the numerators in Eqs. (8.1.7), (8.1.8) behave differently, since Δ becomes an unimportant energy scale. In turn, G_{CA} diminishes and becomes zero at $\Delta = 0$. Contrary, G_D can still be finite. For instance, the extreme case belongs to the zero energy lines, where we find $G_D \to e^2/h$ and $G_{CA} \to 0$ for $|t/\Delta| \to \infty$. Note that

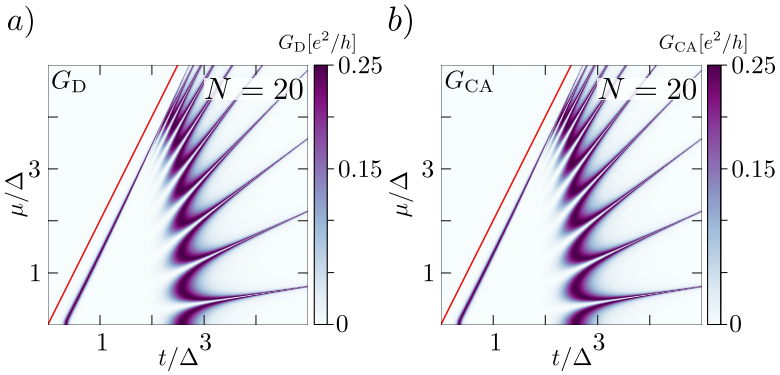

Figure 8.7.: Direct and crossed Andreev conductance in wide band limit for $N = 20$, $\gamma_{L,R}/\Delta = 0.001$ as function of μ/Δ, t/Δ. G_{D} in a) and G_{CA} in b) behave nearly identically for $|\Delta|$, $|t|$ being of the same order of magnitude.

setting $\gamma_L = \gamma_R$ can change the physical reality. In the wide band limit and $\gamma_L = \gamma_R$, one finds $G_{\mathrm{CA}}|_{\mu=0} = 0$ for odd N and generic η.

Recall that for generic η and $\Lambda_L \neq \Lambda_R$, $\gamma_L \neq \gamma_R$, one has to calculate Δ self-consistently [45, 118, 119]. Particularly interesting is the case of $V_R = 0$, corresponding to $\eta = 1$. The conductance G is then given by

$$G = 2\,G_{\mathrm{A}} + G_{\mathrm{D}} + G_{\mathrm{CA}} \tag{8.1.19}$$

and inserting the formulae for G_{A}, G_{D} and G_{CA} yields

$$G = \frac{2e^2}{h}\,\frac{\gamma_L\gamma_R\left(p^{2N-2} + m^{2N-2}\right)}{|q_+|^2 + \gamma_L\gamma_R\left(p^{N-1} + m^{N-1}\right)^2}, \tag{8.1.20}$$

Thus, localized zero/ near zero energy modes are identified by $2\,e^2/h$ originating from the Andreev reflection, contrary to extended ones associated with at least $G = e^2/h$. Our result for G is exact. In the limit of $\mu = 0$, without onsite disorder and in wide band limit our findings for $\eta = 1$ agree with the ones given in [109] for both even and odd N.

We discuss next the differential conductance and investigate also the supra-gap regime.

8.2. Non-linear transport characteristics: Differential conductance

The differential conductance $\partial I/\partial V$ misses by definition only the restriction to $V \to 0$ in comparison to the conductance G. In this respect, the $\partial I/\partial V$ characteristics include the sub-gap transport phenomena and yet allow the investigation of the higher energetic excitation. We discuss only the case of symmetrically applied bias $V_L = -V_R = V/2$ ($\eta = 1/2$) in wide-band limit ($\Lambda_\alpha^\pm = 0$) at $T_{L,R} = 0\,\mathrm{K}$ with $\gamma_L = \gamma_R$, to ensure current

conservation. From Eq. (8.0.1), we find

$$\frac{\partial I}{\partial V} = \frac{e^2}{2h} \sum_{E=\pm V/2} \left(\Gamma_L^- \Gamma_R^- |G^r_{1,N}|^2 + \Gamma_L^- \Gamma_L^+ |G^r_{1,N+1}|^2 \right) \tag{8.2.1}$$

where we temporarily kept $\Gamma_\alpha^\pm$ to illustrate that $\partial I/\partial V$ recovers G in Eq. (8.1.11) for $V \to 0$. More importantly though, we evaluate the former integration variable E at $\pm V/2$. We expect significant differential conductance peaks in the case when $V/2$ is close to an eigenvalue of the isolated Kitaev chain, as we can estimate following the definition of the retarded GF in Eq. (7.4.32). Analogously to the linear conductance before, the differential conductance is composed of Andreev and direct contributions for $V_L = -V_R = V/2$. For shortness, we introduce the notation

$$\frac{\partial I_\mathrm{A}}{\partial V} = \frac{e^2}{2h} \sum_{E=\pm V/2} \Gamma_L^- \Gamma_L^+ |G^r_{1,N+1}|^2, \tag{8.2.2}$$

$$\frac{\partial I_\mathrm{D}}{\partial V} = \frac{e^2}{2h} \sum_{E=\pm V/2} \Gamma_L^- \Gamma_R^- |G^r_{1,N}|^2, \tag{8.2.3}$$

and we have

$$\frac{\partial I}{\partial V} = \frac{\partial I_\mathrm{A}}{\partial V} + \frac{\partial I_\mathrm{D}}{\partial V}. \tag{8.2.4}$$

The exact expressions of $G^r_{1,N}$ and $G^r_{1,N+1}$ are given in appendix K. The investigation of $\partial I_{\mathrm{A,\,D}}/\partial_V$ separately rather than $\partial I/\partial_V$ is more interesting as can be anticipated directly from Fig. 8.8. Here, the first impression is as possibly expected: the Andreev term dominates the sub-gap transport and a stable signal mostly covering the region around $\mu = \pm 2t$ is found. The supra-gap regime, corresponding to higher excitations, features less pronounced contributions of $\partial I_\mathrm{A}/\partial_V$. Here, and in contrary to the Andreev term, $\partial I_\mathrm{D}/\partial V$ is strongest. In total, the differential conductance reaches e^2/h.

However, this simple picture is not correct as the direct term is present as well in the sub-gap regime, as we noticed already for the conductance. This is shown in Fig. 8.8 b). The striped pattern is caused by the formation of small islands or pockets of enhanced values of $\partial I_\mathrm{D}/\partial_V$ as it can be seen in panel d). In order to understand these islands, we turn first to the Andreev term. We discover that the value of $\partial I_\mathrm{A}/\partial_V$ varies with μ, reaching its maximum only at discrete and critical values of μ. Those originate from the exact zero energy lines given in Eq. (6.3.7). To put it into context, the horizontal line at $V = 0$ in panel d) of Fig. 8.8 is essentially a vertical cut at $t/\Delta = 4.1$ in Fig. 8.2, only for different $\gamma_{L,R}$. Thus, we find $\partial I_\mathrm{A}/\partial_V \approx e^2/h$, $\partial I_\mathrm{D}/\partial_V \approx 0$ around those points due to the line broadening introduced by $\gamma_{L,R}$. In between, sub-gap states still exists but their associated energy is slightly larger. Similarly to the conductance, the direct term increases at the edges of $\partial I_\mathrm{A}/\partial_V \approx e^2/h$ contributions yielding the pockets.

More interesting though is the Andreev term for higher excitations. Possibly surprising, we find typical values of up to $e^2/4h$, i.e. a quarter of the conductance quantum for $t/\Delta = 4.1$. In order to understand this result better, we consider first the situation for

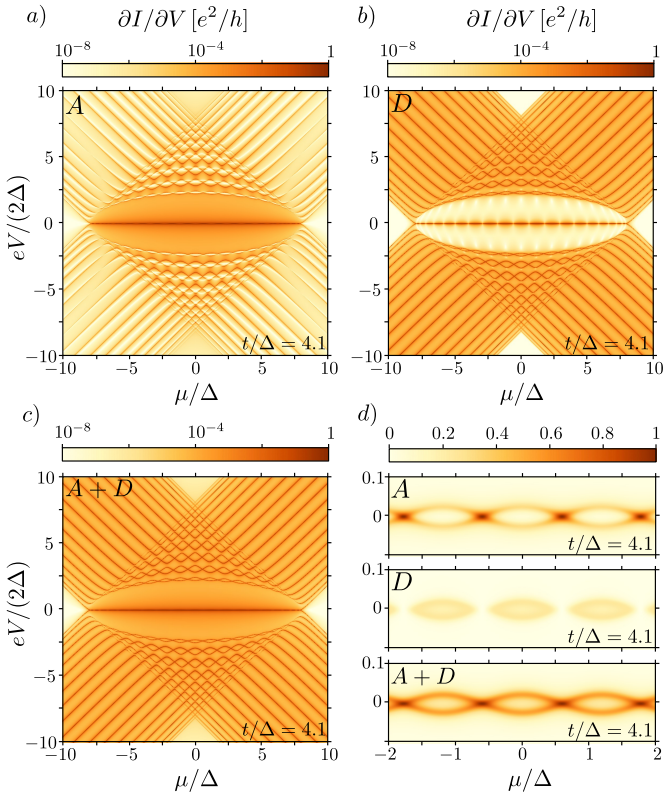

Figure 8.8.: Differential conductance for $\gamma_{L,R}/\Delta = 0.02$, $t/\Delta = 4.1$, $N = 20$ as function of μ/Δ and $eV/(2\,\Delta)$. a) The Andreev term dominates the in-gap transport and is still present for higher energy eigenstates. b) The direct term contributes in and outside of the superconducting gap regime. Its magnitude inside the gap depends on the parameters. c) The differential conductance as sum of direct and Andreev terms. d) The seemingly stable in-gap signal has in fact a substructure where $\partial I/\partial V$ is largest around values of μ following from Eq. (6.3.7). (This Figure is published in Ref. [5])

$t/\Delta = 1$ which is depicted in Fig. 8.9. As discussed before in Ch. 6.4.3, all crossings and avoided ones collapse into a single crossing at $\mu = 0$. For these parameters, the eigenstates of the isolated Kitaev chain are given by the dimerized pairs between n.n. sites (eigenvalues $E_\pm = \pm 2t$, degenerate) and two zero energy modes residing on the first/ last site as shown in Fig. 5.2 a).

In Fig. 8.9, the extended states at $\mu = 0$ are associated to the dark spots at $eV/(2\Delta) = \pm 2t$ in panel a) and thus; they contribute with $\partial I_\mathrm{A}/\partial_V \approx e^2/h$ and $\partial I_\mathrm{D}/\partial_V \approx 0$ to the differential conductance. The physical reason behind these results relies on three facts: First, these eigenstates possess equal particle and hole weights. In turn, perfectly balanced quasiparticles are formed as shown in panel d). Second, these bulk states are found at both ends of the system and a direct connection through the Kitaev chain is

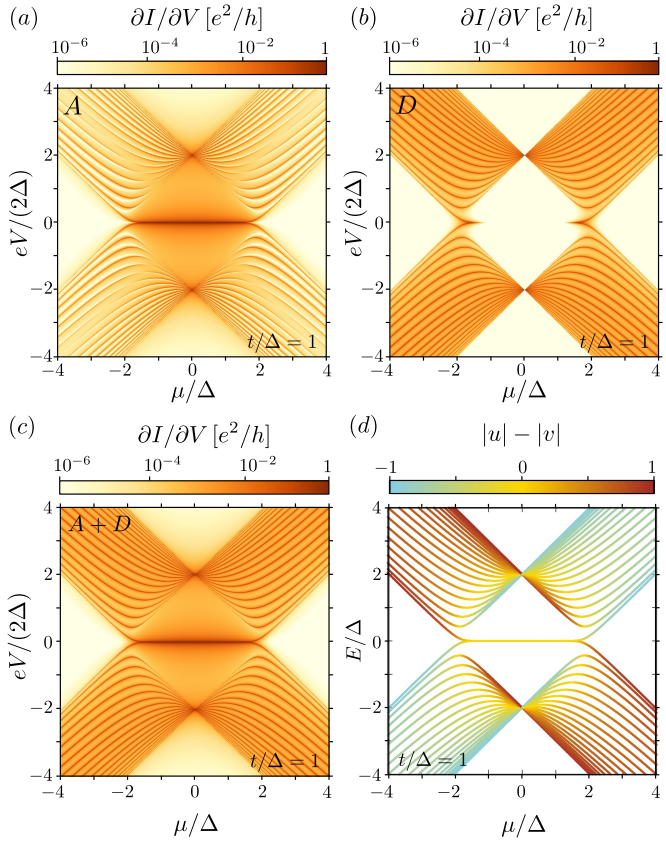

Figure 8.9.: Differential conductance as function of μ/Δ and $eV/(2\,\Delta)$ for $\gamma_{L,R}/\Delta = 0.02$, $N = 20$ and $|t/\Delta| = 1$. a) The Andreev term is largest close to $V = 0$. At $\mu = 0$ and $V = \pm 4\Delta$, the Andreev reflection dominates the supra-gap transport. b) The direct term behaves in a way complementary to the Andreev contributions. $\partial I_{\mathrm{D}}/\partial_V$ vanishes at $\mu = 0$ and $V = \pm 4\Delta$. c) The differential conductance as sum of both Andreev and direct terms. d) The particle (hole) character in brown (blue) varies within the spectrum of the isolated Kitaev chain. The Andreev term is more pronounced for states with balanced particle and hole parts (yellow). (This Figure is published in Ref. [5])

prohibited by $\mu = 0$. Quite intuitively, this results in favouring the Andreev reflection rather than the direct charge transfer, supposing N is large enough. For finite values of the chemical potential, a direct channel is opened yielding to an increase of $\partial I_{\mathrm{D}}/\partial_V$. We conclude that the Andreev reflection, dominating usually the sub-gap transport as shown in Fig. 8.9 a) and b), does not require exclusively complex wavevectors $k_{1,2}$. Instead, the wavefunction's weight at the edges of the system is essential. As qualitative comparison consult Fig. 6.5 panels c), d) where supra-gap eigenstates for even N at $\mu = 0$ are shown.

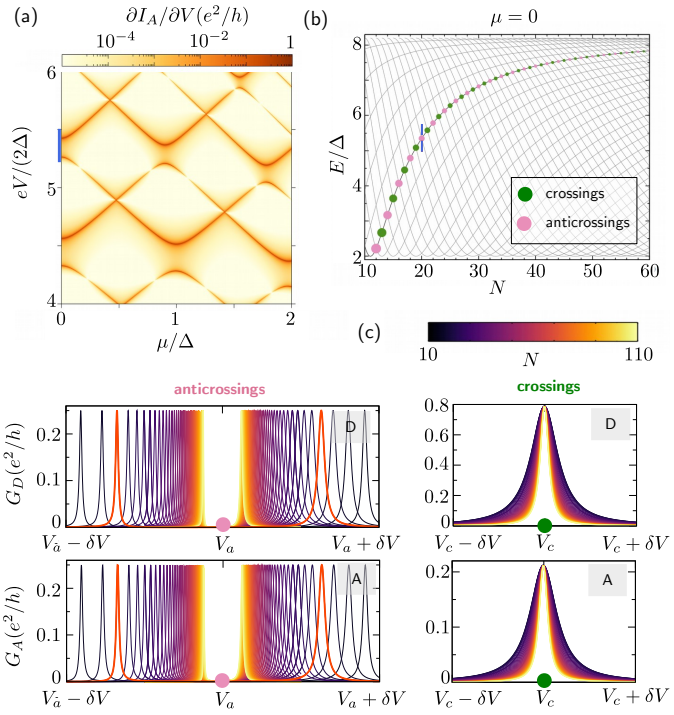

Figure 8.10.: Differential conductance as function of μ/Δ and $eV/(2\,\Delta)$ for $\gamma_{L,R}/\Delta = 0.02$ and $t/\Delta = 4.1$. a) Zoom into Fig. 8.8 a). The typical pattern of exact crossings and avoided crossings is visible in the Andreev term for $N = 20$. b) The grey lines follow $E_{\pm}(n\pi/(N+1))$ with $n = 1, \ldots, N$ and avoided crossings/ crossings at $\mu = 0$, $n = 6$ are tracked for varying N; their positions are indicated by pink and green dots, respectively. c) An adaptive bias window $V_a - \delta V$ to $V_a + \delta V$ is adjusted at every N in order to resolve the peak values of the direct/ Andreev contributions. The blue band in a) belongs the red depicted peaks in c) and indicates the $N = 20$ and the corresponding bias range in b). (This Figure is published in Ref. [5])

Before we continue, let us revisit Fig. 6.13. We observe that eigenstates at avoided crossings consist of equal particle and hole components, while this is not the case in the vicinity of the crossings. In order to understand the Andreev process for higher energetic excitations better, we investigated their dependence on the system length, shown in Fig. 8.10. We restricted ourselves to $\mu = 0$ for simplicity and we tracked $k_1 d = 6\pi/(N+1)$, see Fig. 6.13 b) which is a crossing (avoided crossing) for odd (even) N there. For more details consult Ch. 6.4.3. The typical situation is shown in Fig. 8.8 panel a) for $N = 20$ and Fig. 8.10 a) is a close up. At crossings, we find $\partial I_{\mathrm{D}}/\partial_V \approx 0.8\,e^2/$, $\partial I_{\mathrm{A}}/\partial_V \approx 0.2\,e^2/$, i.e. the direct contribution is about four times larger than the Andreev term and the differential conductance is close to the conductance quantum. For larger system sizes, the peak width for the direct and Andreev term diminishes while the peak value remains.

The avoided crossings on the other hand, are more interesting. Both $\partial I_{\mathrm{D}}/\partial V$ and $\partial I_{\mathrm{A}}/\partial V$ contribute with about $e^2/(4h)$ per peak nearly independently of the number of sites. The reason for this behaviour originates from the perfect quasiparticle mixing and the non-equidistant quantization rule, granting naively unexpected large probabilities for particles to reside close to the system's ends as shown qualitatively in Fig. 6.5. The peak value of $e^2/(4h)$ can be explained quite intuitively. Recall that former avoided crossings turn into crossings at $\Delta = 0$, as we have proven earlier in Ch. 6.4.3. Without superconductivity, the Andreev contribution vanishes entirely as particles and holes remain distinct entities and no quasiparticle mixing can occur. The eigenstates conduct then with about e^2/h solely due to the direct charge transfer. Increasing now Δ to some finite value opens the gaps inside the excitations regime and the avoided crossings are formed. Naively, we might expect the former peak to split into two contributing with $e^2/(2h)$ each, but superconductivity leads to quasiparticle states and the Andreev reflection arises. Thus, we find a peak splitting into four equal contributions. Similar to our prior findings for the BdG excitation spectrum of the Kitaev chain, we conclude that the qualitative impact of the superconducting pairing constant is strongest around the avoided crossings in the Figs. 8.8, 8.10. In total, we find that the gap openings between excitations, i.e. the avoided crossings, qualitatively mimic the bulk conduction gap.

Part III.

From minimal models of 1d topological superconductors to Rashba nanowires

9. Minimal model

In the third part of the thesis, we discuss a minimal model to investigate the transport characteristics for generic 1d topological superconductors. Although a similar approach was already considered in Ref. [12, 45, 123], we demonstrate here that this approach is not limited to qualitative agreements. Rather, one can also reproduce numerical findings or exact analytical results quantitatively, supposing that the self-energies defined within the scope of the minimal model are treated properly.

For convenience we first introduce in section 9.1 the transport setup and discuss the results within the framework of the minimal model only. At the end of this section, we explain how one achieves the quantitative agreement. Hereafter in section 9.2, we demonstrate explicitly that the minimal model properly reproduces the exact analytical results for the conductance of the Kitaev chain as a function of the chemical potential, the hopping parameter and the p-wave superconducting pairing constant. In the scope of the minimal model, we will find again that the quantitative results for the Andreev reflection and direct conductance indeed depend on the spatial profile of the charge carrying state as discussed earlier.

9.1. General case study

The basic idea of the minimal model considers initially a generic diagonal and fermionic Hamiltonian

$$\hat{H}_{\mathrm{g}} = \sum_{n} \epsilon_n \, \hat{\Psi}_n^\dagger \, \hat{\Psi}_n. \tag{9.1.1}$$

Here, ϵ_n describes the energy levels w.r.t. to the chemical potential μ and $\hat{\psi}_n$ is a fermionic operator. The energies ϵ_n depend on the actual parameters of the full model, for instance magnetic fields or superconducting pairing in case of a topological superconductor. Please notice that the approach is not limited to topological superconductors since $\hat{H}_{\mathrm{g}}$ is generic; for instance $\hat{H}_{\mathrm{g}}$ can also represent the linear chain or the n.n.n. chain from part I of the thesis.

We are interested in the transport properties and we thus truncate $\hat{H}_{\mathrm{g}} \to \hat{H}_{\mathrm{M}}$ to the relevant energy scale

$$\hat{H}_{\mathrm{M}} = \epsilon \, \hat{\Psi}^\dagger \, \hat{\Psi}. \tag{9.1.2}$$

In case of a topological superconductor and focusing on sub-gap transport at zero temperature, ϵ may accounts for the in-gap energy. Transformed into Majorana fermions

$\hat{\psi}_\mathrm{A}$, $\hat{\psi}_\mathrm{B}$

$$\begin{pmatrix}\hat{\psi}_\mathrm{A}\\ \hat{\psi}_\mathrm{B}\end{pmatrix} \coloneqq \frac{1}{\sqrt{2}}\begin{bmatrix}1 & 1\\ -\mathrm{i} & \mathrm{i}\end{bmatrix}\begin{pmatrix}\hat{\Psi}\\ \hat{\Psi}^\dagger\end{pmatrix}, \tag{9.1.3}$$

and apart from an unimportant constant, our model reads

$$\hat{H}_\mathrm{M} = \mathrm{i}\,\epsilon\,\hat{\psi}_\mathrm{A}\,\hat{\psi}_\mathrm{B}. \tag{9.1.4}$$

From the definition Eq. (9.1.3), we find

$$\left[\hat{\psi}_i,\,\hat{\psi}_j\right] = \delta_{ij}, \tag{9.1.5}$$

$$\hat{\psi}_j^\dagger = \hat{\psi}_j, \tag{9.1.6}$$

and $\hat{\psi}_j^2 = 1/2$ for $i,\,j = A,\,B$. The transport setup requires two reservoirs and we introduce the two normal conducting leads ($\alpha = L, R$)

$$\hat{H}_\alpha - \mu\hat{N}_\alpha = \sum_k \epsilon_{k\alpha}\,c_{k\alpha}^\dagger\,c_{k\alpha}, \tag{9.1.7}$$

where $c_{k\alpha}^\dagger$ creates an electron in the state k and lead α. We consider the chemical potential $\mu_\alpha = eV_\alpha + \mu$ in lead α and the bias is $V = V_L - V_R$. In the case that the Hamiltonian $\hat{H}_\mathrm{g}$ contained superconductivity, we have a N-S-N setup. The most generic tunneling Hamiltonian $\hat{H}_\mathrm{T} = \hat{H}_\mathrm{T,L} + \hat{H}_\mathrm{T,R}$ in our approach contacts both $\hat{\psi}_\mathrm{A}$ and $\hat{\psi}_\mathrm{B}$ to $\hat{H}_\alpha$

$$\hat{H}_{\mathrm{T},\alpha} = \sum_{k,\,j=\mathrm{A,B}}\left[V_{\alpha,\,j}(k)\,\hat{\psi}_j\,c_{k\alpha} + V_{\alpha,\,j}^*(k)\,c_{k\alpha}^\dagger\,\hat{\psi}_j\right]. \tag{9.1.8}$$

In order to receive later quantitative results, the tunneling amplitudes $V_{\alpha,\,\mathrm{A}}$, $V_{\alpha,\,\mathrm{B}}$ for the minimal model have to be extracted from the transport setup for the generic Hamiltonian $\hat{H}_\mathrm{g}$. For instance the spatial extension of the Majorana fermions $\hat{\psi}_\mathrm{A}$, $\hat{\psi}_\mathrm{B}$ will be important as we discuss later in more detail.

The transport setup for the minimal model is

$$\hat{H}_\mathrm{tot} = \hat{H}_L + \hat{H}_\mathrm{M} + \hat{H}_R + \theta(t - t_0)\,\hat{H}_\mathrm{T}, \tag{9.1.9}$$

and we impose later $t_0 \to \infty$ for steady state results. Similar as in section 7.3, we calculate the current $I_\alpha(t) = -e\langle\partial_t\,\hat{N}_\alpha\rangle$ inside the contacts. Only the tunneling Hamiltonian contributes to I_α and we find

$$I_\alpha(t) = -\mathrm{i}\frac{e}{\hbar}\theta(t - t_0)\sum_{k,\,j=\mathrm{A,B}}\left[V_{\alpha,\,j}(k)\,\langle\hat{\psi}_j\,c_{k\alpha}\rangle + V_{\alpha,\,j}^*(k)\,\langle\hat{\psi}_j\,c_{k\alpha}^\dagger\rangle\right]. \tag{9.1.10}$$

The dynamics of the system are treated by the NEGF method. As guidance, one can define a lesser GF of dimension 2×2, element-wise by ($n,\,m = 1,\,2$)

$$\left(\boldsymbol{G}_{k\alpha,\mathrm{M}}^<(t,\,t')\right)_{n,m} \coloneqq \frac{\mathrm{i}}{\hbar}\left\langle\left(\Psi_\mathrm{M}(t')\right)_m^\dagger\,\left(C_{k\alpha}(t)\right)_n\right\rangle, \tag{9.1.11}$$

where we set $\Psi_{\mathrm{M}} \coloneqq \left(\hat{\psi}_{\mathrm{A}},\, \hat{\psi}_{\mathrm{B}}\right)^{\mathrm{T}}$, $C_{k\alpha} = \left(c_{k\alpha},\, c^{\dagger}_{k\alpha}\right)^{\mathrm{T}}$. The definitions for retarded, advanced, greater and the contour GF are analogous. In terms of $\boldsymbol{G}^{<}_{k\alpha,\mathrm{M}}$ and the tunneling matrix

$$\boldsymbol{V}_{\alpha} = \begin{bmatrix} V_{\alpha,\mathrm{A}} & V^{*}_{\alpha,\mathrm{A}} \\ V_{\alpha,\mathrm{B}} & V^{*}_{\alpha,\mathrm{B}} \end{bmatrix}, \tag{9.1.12}$$

the current $I_{\alpha}(t)$ reads

$$I_{\alpha}(t) = -e\,\theta(t-t_0) \sum_{k} \mathrm{Tr}\left\{ \boldsymbol{V}_{\alpha}(k)\; \boldsymbol{G}^{<}_{k\alpha,\mathrm{M}}(t,\,t) \right\}. \tag{9.1.13}$$

The steady state current I_{α} can be straightforwardly derived and we state only the final results. As expected, the quasi-particle current is

$$I_{\alpha} = \frac{e}{h} \int\limits_{\mathbb{R}} \left[M^{--}_{\alpha,\bar{\alpha}} \left(f^{-}_{\alpha} - f^{-}_{\bar{\alpha}} \right) + M^{-+}_{\alpha,\alpha} \left(f^{-}_{\alpha} - f^{+}_{\alpha} \right) + M^{-+}_{\alpha,\bar{\alpha}} \left(f^{-}_{\alpha} - f^{+}_{\bar{\alpha}} \right) \right] \mathrm{d}E \tag{9.1.14}$$

composed by three contributions: the direct charge transfer $M^{--}_{\alpha,\bar{\alpha}}$, the Andreev reflection $M^{-+}_{\alpha,\alpha}$ and the crossed Andreev process $M^{-+}_{\alpha,\bar{\alpha}}$. Here, $f^{\pm}_{\alpha} = f(E \pm e\,V_{\alpha})$ denotes the Fermi functions. In Eq. (9.1.14), $\bar{\alpha}$ signifies "not" α, i.e. $\bar{\alpha} = R$ in case that $\alpha = L$. The transmission probability $M^{sz}_{\alpha,\beta}$ is defined as ($s,\, z = \pm,\, \alpha,\, \beta = L,\, R$)

$$M^{sz}_{\alpha,\beta}(E) \coloneqq \mathrm{Tr}\left\{ \boldsymbol{\Gamma}^{s}_{\alpha}\, \boldsymbol{G}^{r}_{\mathrm{MM}}\, \boldsymbol{\Gamma}^{z}_{\beta}\, \boldsymbol{G}^{a}_{\mathrm{MM}} \right\} \tag{9.1.15}$$

and depends on the retarded/ advanced GF $\boldsymbol{G}^{r,\,a}_{\mathrm{MM}}$ of the central system $\hat{H}_{\mathrm{M}}$ in presence of the leads. Here, we separated $\boldsymbol{\Gamma}_{\alpha} = -2\mathrm{i}\mathrm{Im}\left(\boldsymbol{\Sigma}^{r}_{\alpha}\right) = \boldsymbol{\Gamma}^{-}_{\alpha} + \boldsymbol{\Gamma}^{+}_{\alpha}$ into the electronic and hole components. The expressions for $\boldsymbol{G}^{r,\,a}_{\mathrm{MM}}$, $\boldsymbol{\Sigma}^{r}_{\alpha}$ and $\boldsymbol{\Gamma}^{\pm}_{\alpha}$ are shown in appendix N. The sign s (z) in $M^{sz}_{\alpha,\beta}$ can be intuitively considered as the charge of the particle leaving (entering) contact α (β).

Initially, the steady state current is given by six terms, respectively three for electrons and holes, where a factor $1/2$ prevents overcounting. Actually, the NEGF approach in terms of 2×2 matrices respects particle-hole symmetry $\mathcal{P} = \mathbb{1}_2\,\mathcal{K}$, which is preserved by the contacts. The transmission probabilities conserve $\mathcal{P}$ as well, and one can show that

$$M^{sz}_{\alpha,\beta}(E) = M^{-s\,-z}_{\alpha,\beta}(-E). \tag{9.1.16}$$

In turn, Eq. (9.1.16) reduces the number of terms contributing to transport in I_{α} from six to three and Eq. (9.1.14) is found. Note, the entries of the self-energies Σ^{r}_{α} within the framework of the minimal model are all non zero. The calculation of the conductance G is not a trivial task. We restrict ourselves to give the result in case of the Kitaev chain in section 9.2 below.

The retarded GF $\boldsymbol{G}^r_{\mathrm{MM}}$ is obtained from

$$\boldsymbol{G}^r_{\mathrm{MM}} \,=\, (E\,\mathbb{1}_2 \,-\, \mathcal{H}_{\mathrm{M}} - \Sigma^r_L - \Sigma^r_R)^{-1}\,, \tag{9.1.17}$$

where $\mathcal{H}_{\mathrm{M}}$ satisfies

$$\hat{H}_{\mathrm{M}} \,=\, \frac{1}{2}\,\Psi^\dagger_{\mathrm{M}}\,\mathcal{H}_{\mathrm{M}}\Psi_{\mathrm{M}}, \quad \mathcal{H}_{\mathrm{M}} = -\mathrm{i}\epsilon\,\sigma_y. \tag{9.1.18}$$

The minimal model reproduces the correct results supposed that we relate not only $\mathcal{H}_{\mathrm{M}}$ but also $\Sigma^r_{L,R}$ to the full model. Let $\Sigma^r_{\alpha,\mathrm{g}}$ denote the self-energies of lead α w.r.t. $\hat{H}_{\mathrm{g}}$. Then, we may transform $\Sigma^r_{\alpha,\mathrm{g}}$ into the eigenbasis of $\hat{H}_{\mathrm{g}}$ and read out the dominant contribution for the energy ϵ. Thus, we demand

$$\mathcal{H}_{\mathrm{M}} \,\stackrel{!}{=}\, [\mathcal{H}_{\mathrm{g}}]_{\mathrm{truncated}}\,, \quad \Sigma^r_\alpha \,\stackrel{!}{=}\, \left[\Sigma^r_{\alpha,\mathrm{g}}\right]_{\mathrm{truncated}}\,. \tag{9.1.19}$$

As a consequence of this approach, the entries of Σ^r_α are set as joint objects of contributions from $\Sigma^r_{\alpha,\mathrm{g}}$ and the eigenvectors of the isolated and full model.

9.2. Application to the Kitaev chain

The minimal model can reproduce the conductance at $T = 0\,\mathrm{K}$ for the Kitaev chain, supposing Eq. (9.1.19) was used to relate the physical quantities. From $\mathcal{H}_{\mathrm{g}} \equiv \mathcal{H}_{\mathrm{KC}}$, we set $\epsilon = E_0$. Here, E_0 denotes here the smallest positive eigenvalue of the Kitaev chain. Notice, E_0 may or may not reside inside the gap. The self-energies $\Sigma^r_{\alpha,\mathrm{KC}}$ for the Kitaev chain in the N-S-N setup yield

$$\Sigma^r_L \,=\, -2\mathrm{i}\,\gamma_L \begin{bmatrix} |\xi_1|^2 & \\ & |\xi_N|^2 \end{bmatrix}, \quad \Sigma^r_R \,=\, -2\mathrm{i}\,\gamma_R \begin{bmatrix} |\xi_N|^2 & \\ & |\xi_1|^2 \end{bmatrix}, \tag{9.2.1}$$

with $\gamma_{L,R} = \gamma^{\pm}_{L,R}|_{E=0} = const.$ from Eq. (8.1.9) in wide band limit. Notice, the basis transformation of $\Sigma^r_{\alpha,\mathrm{KC}}$ into the eigenbasis of the isolated Kitaev chain results in a non-sparse $2N \times 2N$ matrix, even in wide band limit. Here we obtained the diagonal form of $\Sigma^r_{L,R}$ only by omitting all contributions from eigenvectors associated to energies different from E_0. Since their weight at the border sites is small compared to the weight of the sub-gap states, this approximation is justified. The quantities ξ_1, ξ_N account for the wavefunction's weight on the first/ last site of the Majorana sublattice vector $\vec{v}_{\mathrm{A}}$. Since the spatial inversion symmetry related $\vec{v}_{\mathrm{A}}$ and $\vec{v}_{\mathrm{B}}$, we were able to effectively eliminate the latter. The selection of only ξ_1 and ξ_N originates from the local character of the tunneling Hamiltonian in Eq. (7.3.3), which granted sparse self-energies $\Sigma^r_{\alpha,\mathrm{KC}}$.

In case of $\gamma_L = \gamma_R$ and $V_L = -V_R = V/2$, the current in Eq. (9.1.14) is conserved [45]. For generic E, one can determine the transmission functions for both the Andreev reflection $M^{-+}_{\alpha,\alpha}(E)$ and the direct process $M^{--}_{\alpha,\bar{\alpha}}(E)$. In terms of

$$D = E^2 - E_0^2 - 8\,\gamma_\alpha^2\,|\xi_1|^2\,|\xi_N|^2 \,-\, 4\gamma_\alpha^2\,\left(|\xi_1|^4 \,+\, |\xi_N|^4\right) \,+\, 4\mathrm{i}E\gamma_\alpha\left(|\xi_1|^2 \,+\, |\xi_N|^2\right)$$

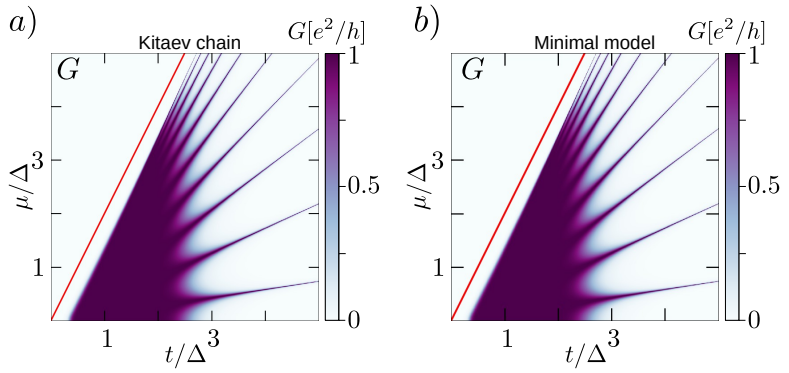

Figure 9.1.: Conductance comparison from the minimal and the full model as function of μ/Δ and t/Δ. a) The exact result for the Kitaev chain. b) The parameters ϵ and Γ_{eff} are calculated as stated in the text. The conductance of the minimal model reproduces the prior findings. We used the parameters $N = 20$ and $\gamma_{L,R}/\Delta = 0.001$.

we have that

$$M^{-+}_{\alpha,\alpha}(E) \;=\; 4\,\gamma_\alpha^2\;\frac{\left|E\,\left(|\xi_1|^2\,-\,|\xi_N|^2\right)\,+\,2\,\mathrm{i}\gamma_\alpha\,\left(|\xi_1|^4\,-\,|\xi_N|^4\right)^2\right|^2}{|D|^2}, \tag{9.2.2}$$

and

$$\begin{aligned} M^{--}_{\alpha,\bar{\alpha}}(E) \;=\; 4\,\gamma_\alpha^2\;&\frac{4|\xi_1\,\xi_N|^2\,\left[E^2\,+\,\left(|\xi_1|^2\,+\,|\xi_N|^2\right)^2\right]\,+\,E_0^2\,\left(|\xi_1|^2\,+\,|\xi_N|^2\right)^2}{|D|^2} \\ -\;4\,\gamma_\alpha^2\;&\frac{E_0\,E\,\left(|\xi_1|^2\,+\,|\xi_N|^2\right)}{|D|^2}, \end{aligned} \tag{9.2.3}$$

holds. It is important that ξ_1 and ξ_N enter differently in the Andreev reflection and the direct term. In case of a localized Majorana fermion in the Kitaev chain, either $\xi_1 \approx 0$ or $\xi_N \approx 0$ is true. This causes the direct term essentially to vanish ($M^{--}_{\alpha,\bar{\alpha}}(E) \approx 0$) for $E = 0$ and E_0 small. Thus, the conductance at zero temperature relies mostly on the Andreev reflection for in-gap states. In the extreme situation of extended in-gap states, i.e. $\xi_1 \approx \xi_N \neq 0$, the Andreev reflection gets suppressed. The conductance is then given mostly by the direct charge transfer, in agreement with chapter 8.1 and see especially Fig. 8.4. In turn, the observed conductance reflects the spatial profile involved eigenstate.

At zero temperature, the conductance G is

$$G \;=\; \frac{e^2}{h}\,\left[M^{-+}_{\alpha,\alpha}(0)\,+\,M^{--}_{\alpha,\bar{\alpha}}(0)\right]\;=\;\frac{e^2}{h}\,\frac{\Gamma_{\text{eff}}^2}{E_0^2\,+\,\Gamma_{\text{eff}}^2}, \tag{9.2.4}$$

reaching values only up to e^2/h. Here, the we defined Γ_{eff} as

$$\Gamma_{\text{eff}} = \Gamma_L \left(|\xi_1|^2 + |\xi_N|^2\right) \tag{9.2.5}$$

and $\Gamma_L = 2\gamma_L$ as usual. Notice, the structure of Eq. (9.2.4) agrees with the formula stated in [12, 45, 123]. However, Γ_{eff} in Eq. (9.2.5) depends also on the generic Hamillonian $\hat{H}_{\text{g}}$. In Fig. 9.1, we show G according to Eq. (9.2.4). The values of ξ_1, ξ_N and E_0 can be calculated either completely numerically or using the derived analytical formulae for the Kitaev chain.

We find that Eq. (9.2.4) reproduces the exact results. Interestingly though, the minimal models predicts $G = e^2/h$ exactly in case that $E_0 = 0$, contrary to the exact result in Eq. (8.1.12) which states $G \lesssim e^2/h$ (except at the Kitaev points $\mu = 0$, $|t| = |\Delta|$).

To summarize, we found that the different weight of the $G_{\text{D}}/G_{\text{A}}$ contributions to the linear conductance are caused by the spatial profile of the wavefunction. Further, the conductance could be reproduced by considering only low energy degrees of freedom. We exploit this property and investigate the transport signatures of the proximitized Rashba nanowires in section 10.4 next.

10. The proximitized semiconducting Rashba nanowires

The low-energy physics of a semiconducting nanowire with Rashba spin-orbit coupling, in proximity to a s-wave superconductor, when exposed to an external magnetic field is a realization of the low energy physics of the archetypal model for topological superconductors: the Kitaev chain [6, 7]. In the mentioned circumstances, the nanowire is predicted to host Majorana zero modes/ Majorana fermions. Because of this, the spectral and transport characteristics of the model have been object of intense investigation, see for instance Refs. [3, 8–11].

Due to the technical difficulties arising from the open boundary conditions and the finite wire length in analytical treatments, earlier studies were typically based on numerical treatments, semi-infinite approaches or pure bulk considerations. In contrast, we consider here a finite length nanowire and we take explicitly the open boundary condition into account. In analogy to our approach made for the finite sized Kitaev model (with open boundary conditions), we make an analytical attempt for the spectral and transport signatures of the nanowire beyond earlier investigations.

As perspective, zero energy is found on a set of discrete lines inside the topologically non-trivial phase. Those lines were found both numerically and analytically before [3, 13]. We derive the required analytical conditions taking the finite length of the nanowire and the open boundary condition explicitly into account. Our treatment can be generalized to finite energy modes and is not limited to any specific part of the topological phase diagram. Further, the earlier observed energy oscillations [3, 9, 12–17] as a function of the magnetic field strength or in the chemical potential are qualitatively understood by a mapping of the nanowire onto the Kitaev chain.

Some of our results hold only in the weak spin orbit regime. Currently, we try to avoid this limitation before we consider finite energy states. However, already our first attempts are promising and agree well with a numerical approach. Based on our success, we also investigate the transport properties of the nanowire in an N-S-N setup. We found an exact expression for the current, taking also finite energy modes into account. The conductance at zero temperature along the discrete zero energy lines extracted from the analytical formula is presented. We find that the conductance G in a symmetric bias setup reaches the conductance quantum.

The contributions of Andreev reflection G_{A} and the charge transfer G_{D} to the conductance G vary with the parameters. In the vicinity of the phase boundary, the Majorana fermions are strongly localized at both edges of the system and thus the Andreev reflection is the dominant contribution to G. Further away from the phase boundary but still along the zero energy lines within the topologically non-trivial parameter section,

the Majorana fermions start to extend and thus G_D becomes more significant and finally dominant. This behavior reflects the spatial profile of the Majorana fermions. As a consequence of the weak-spin orbit coupling limit, the Majorana fermions decay but may extend over long sections of the nanowire. Our findings are confirmed by numerical treatments and agree qualitatively with the expected behavior anticipated from the finite sized Kitaev chain with open boundary conditions. A publication is currently in preparation and the investigations were done within the framework of the Master thesis of Harald Schmid [124].

In the following section 10.1, we introduce the model and its known properties. Thereafter, we present our treatment and the main results.

10.1. Model, effective p-wave pairing and the low energy description

We consider a quasi-1d semiconducting Rashba nanowire of finite length L, oriented along the x-axis, with intrinsic Rashba spin orbit coupling and exposed to a uniform, external magnetic field $\boldsymbol{B} = |\boldsymbol{B}|\,\hat{z}$. This setup or similar ones have been object of intense study [6–10, 12, 24, 28, 66, 124, 125]. The Hamiltonian reads

$$\hat{H}_0 \;=\; \int_{-L/2}^{L/2} \hat{\psi}^\dagger(x) \left(-\frac{\hbar^2\,\partial_x^2}{2m} \;-\; \mu \;-\mathrm{i}\,\alpha_\mathrm{R}\,\sigma_y\,\partial_x \;+\; V_\mathrm{Z}\,\sigma_z \right) \hat{\psi}(x)\;\mathrm{d}x. \tag{10.1.1}$$

with $\hat{\psi}(x) = \left(\hat{\psi}_\uparrow(x),\, \hat{\psi}_\downarrow(x)\right)^\mathrm{T}$ where $\hat{\psi}_\sigma^\dagger$ creates an electron with spin $\sigma = \pm 1/2$ and effective mass m at position x. Here, μ represents the chemical potential, $V_\mathrm{Z} = g\,\mu_\mathrm{B}\,|\boldsymbol{B}|/2$ is the Zeeman energy and the Rashba spin orbit coupling α_R is aligned in $\hat{y}$ direction. Crucial is the competition between the Rashba spin orbit coupling and the Zeeman term as both together prevent a favored axis of spin alignment. In turn, the former spin degeneracy of the band for $V_\mathrm{Z} = \alpha_\mathrm{R} = 0$ is removed and the Zeeman term opens a gap for $\alpha_\mathrm{R} \neq 0$. The nanowire is in contact with a conventional s-wave superconductor and due to the proximity effect, superconductivity leaks into the wire, adding to the Hamiltonian the new term

$$\hat{H}_\Delta \;=\; \int_{-L/2}^{L/2} \Delta\,\hat{\psi}_\uparrow(x)\,\hat{\psi}_\downarrow(x)\;\mathrm{d}x \;+\; \mathrm{h.\;c.}, \tag{10.1.2}$$

assuming here a pairing potential constant in x. The complete setup is described by

$$\hat{H} \;=\; \hat{H}_0 \;+\; \hat{H}_\Delta \tag{10.1.3}$$

which has a similar structure as the Hamiltonian in Eq. (1.0.6) from the introduction. Typically the energy and length scales associated with the spin orbit coupling α_R are $E_\mathrm{so} = m\,\alpha_\mathrm{R}^2/\hbar \approx 0.1\,\mathrm{meV}$ and $l_\mathrm{so} = \hbar/(m\,\alpha_\mathrm{R}) \approx 100\,\mathrm{nm}$ in InAs. The Zeeman energy

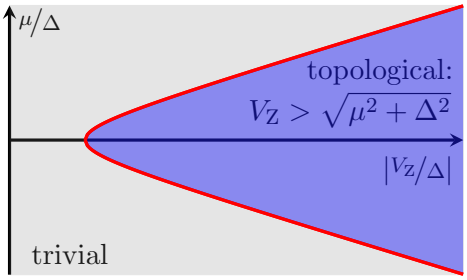

Figure 10.1.: Topological phase diagram of the proximitized semiconducting nanowire with Rashba spin orbit coupling in perpendicular magnetic field. The topological phase boundary $V_Z = \sqrt{\mu^2 + \Delta^2}$ shown in red separates the topologically non trivial phase ($V_Z > \sqrt{\mu^2 + \Delta^2}$, blue) from the trivial one ($V_Z < \sqrt{\mu^2 + \Delta^2}$).

$V_Z \approx 1\,\mathrm{meV}$ for $|\boldsymbol{B}| = 1\mathrm{T}$, is about one order of magnitude larger [126]. As we want to emphasize in this section, effective p-wave pairing is engineered basing on the the spin orbit coupling, the Zeeman term and the s-wave pairing constant. For more details we refer to Refs. [6, 7].

Initially, we consider periodic boundary conditions and apply $\hat{\psi}_\sigma(x) = \frac{1}{\sqrt{L}} \sum_k e^{\mathrm{i}\,kx}\, \hat{\psi}_{k\sigma}$ in order to determine the topological phase diagram. In terms of the Nambu spinor $\hat{\Psi}_k = \left(\hat{\psi}_{k\uparrow}, \hat{\psi}_{k\downarrow}, \hat{\psi}^\dagger_{-k\downarrow}, \hat{\psi}^\dagger_{-k\uparrow}\right)^{\mathrm{T}}$, we have

$$\hat{H} = \frac{1}{2} \sum_k \hat{\Psi}^\dagger_k\, \mathcal{H}_{\mathrm{BdG}}(k)\, \hat{\Psi}_k \tag{10.1.4}$$

where we introduced

$$\mathcal{H}_{\mathrm{BdG}}(k) = \begin{bmatrix} \frac{\hbar^2 k^2}{2m} - \mu + V_Z & -\mathrm{i}\,\alpha_R k & -\Delta^* & 0 \\ \mathrm{i}\,\alpha_R k & \frac{\hbar^2 k^2}{2m} - \mu - V_Z & 0 & \Delta^* \\ -\Delta & 0 & -\frac{\hbar^2 k^2}{2m} + \mu + V_Z & -\mathrm{i}\,\alpha_R k \\ 0 & \Delta & \mathrm{i}\,\alpha_R k & -\frac{\hbar^2 k^2}{2m} + \mu - V_Z \end{bmatrix}. \tag{10.1.5}$$

Although we discuss the consequences of the chemical potential and the Zeeman term in more detail in sec. 10.3, notice their switching signs along the diagonal in Eq. (10.1.5). In case of the Kitaev chain with open boundary condition, the finite size quantization of the wavevectors depended non trivially on the chemical potential yielding the energy oscillations in μ below and above the gap. We naturally expect the same here and these oscillations were already observed, see for instance [3, 9, 12, 14–17].

For simplicity, we consider $\Delta \in \mathbb{R}$ from now on and the dispersion relation can be

extracted from Eq. (10.1.5). We find ($l = \pm 1$)

$$E_l^2(k) = \left(\frac{\hbar^2 k^2}{2m} - \mu\right)^2 + \alpha_{\mathrm{R}}^2 k^2 + V_{\mathrm{Z}}^2 + \Delta^2 + 2l\sqrt{\left(\frac{\hbar^2 k^2}{2m} - \mu\right)^2 \left(V_{\mathrm{Z}}^2 + \alpha_{\mathrm{R}}^2 k^2\right) + V_{\mathrm{Z}}^2 \Delta^2}, \tag{10.1.6}$$

and $E_l(k) = E_l(-k)$ holds. Importantly, a gap closing occurs at $k = 0$ for $V_{\mathrm{Z}} = \sqrt{\mu^2 + \Delta^2}$, reflecting a topological phase transition. In fact, the topologically trivial and non-trivial phases depend on the relation of the Zeeman term, the chemical potential and the pairing contant [10, 24]

$$V_{\mathrm{Z}} > \sqrt{\mu^2 + \Delta^2} \quad \text{(non-trivial)}, \tag{10.1.7}$$

$$V_{\mathrm{Z}} < \sqrt{\mu^2 + \Delta^2} \quad \text{(trivial)}, \tag{10.1.8}$$

supposing $\alpha_{\mathrm{R}} \neq 0$. The topological phase diagram is shown in Fig. 10.1.

The physics of the model and the relation to the Kitaev chain become apparent[1] by expressing the Hamiltonian $\hat{H}$ in a suitable basis as we show in the following [6, 7]. The operators $\hat{\phi}_{\nu,k}$ ($\nu = 1, 2$) obeying

$$\begin{pmatrix} \hat{\psi}_{k\uparrow} \\ \hat{\psi}_{k\downarrow} \end{pmatrix} = \begin{bmatrix} u_k & v_k \\ v_k & u_k \end{bmatrix} \begin{pmatrix} \hat{\phi}_{1,k} \\ \hat{\phi}_{2,k} \end{pmatrix} \tag{10.1.9}$$

diagonalize $\hat{H}_0$

$$\hat{H}_0 = \sum_{\nu=1,2,} \sum_k \epsilon_\nu(k)\, \hat{\phi}_{\nu,k}^\dagger\, \hat{\phi}_{\nu,k} \tag{10.1.10}$$

with single particle energy $\epsilon_\nu(k) = (\hbar^2 k^2)/(2m) - \mu \pm \sqrt{V_{\mathrm{Z}}^2 + \alpha_{\mathrm{R}}^2 k^2}$. The quantities u_k, v_k introduced in Eq. (10.1.9) are

$$u_k = \left(V_{\mathrm{Z}} + \sqrt{V_{\mathrm{Z}}^2 + \alpha_{\mathrm{R}}^2 k^2}\right) N_k, \quad v_k = \mathrm{i}\,\alpha_{\mathrm{R}} k\, N_k \tag{10.1.11}$$

with N_k being the normalization constant such that $|u_k|^2 + |v_k|^2 = 1$ holds. In terms of $\hat{\phi}_{\nu,k}$, the Hamiltonian $\hat{H}$ reads ($\bar{k} \coloneqq -k$)

$$\begin{aligned} \hat{H} = \sum_{\nu=1,2,\,k} \epsilon_\nu(k)\, \hat{\phi}_{\nu,k}^\dagger\, \hat{\phi}_{\nu,k} + \frac{1}{2} \sum_k \Big[& \mathrm{i}\Delta_{\mathrm{p}} \left(\hat{\phi}_{2,k}\, \hat{\phi}_{2,\bar{k}} - \hat{\phi}_{1,k}\, \hat{\phi}_{1,\bar{k}}\right) \\ & + \Delta_{\mathrm{s}} \left(\hat{\phi}_{1,k}\, \hat{\phi}_{2,\bar{k}} - \hat{\phi}_{2,k}\, \hat{\phi}_{1,\bar{k}}\right) + \mathrm{h.c.}\Big], \end{aligned} \tag{10.1.12}$$

where the s-wave pairing amplitude is rescaled into

$$\Delta_{\mathrm{s}}(k) = \frac{\Delta\, V_{\mathrm{Z}}}{\sqrt{V_{\mathrm{Z}}^2 + \alpha_{\mathrm{R}}^2\, k^2}} \tag{10.1.13}$$

[1] A similar mapping exists also for proximitized semi-conducting carbon nanotubes [30].

and an effective p-wave pairing constant is found

$$\Delta_{\mathrm{p}}(k) \,=\, \frac{\Delta\,\alpha_{\mathrm{R}}\,k}{\sqrt{V_{\mathrm{Z}}^2 \,+\, \alpha_{\mathrm{R}}^2\,k^2}}. \tag{10.1.14}$$

Notice, the effect of the initial pairing potential Δ was separated and $\Delta^2 = \Delta_{\mathrm{s}}^2 + \Delta_{\mathrm{p}}^2$ holds. In Eq. (10.1.12), Δ_{p} (Δ_{s}) acts as inter- (intra-) band pairing. In order to demonstrate the similarity between the Kitaev chain and the current nanowire model, we impose a second (unitary) transformation[30]

$$\begin{pmatrix} \hat{\phi}_{1,k} \\ \hat{\phi}_{2,k} \\ \hat{\phi}_{1,\bar{k}}^{\dagger} \\ \hat{\phi}_{2,\bar{k}}^{\dagger} \end{pmatrix} \,=\, \begin{bmatrix} m & 0 & 0 & n \\ 0 & -n & -m & 0 \\ 0 & m & -n & 0 \\ -n & 0 & 0 & m \end{bmatrix} \begin{pmatrix} \hat{b}_{k,+} \\ \hat{b}_{\bar{k},+}^{\dagger} \\ \hat{b}_{k,-} \\ -\hat{b}_{\bar{k},-}^{\dagger} \end{pmatrix} \tag{10.1.15}$$

with m, n defined as

$$2\,m^2 \,=\, 1 \,+\, \frac{\epsilon_1 \,+\, \epsilon_2}{\sqrt{(\epsilon_1 \,+\, \epsilon_2)^2 \,+\, 4\,\Delta_{\mathrm{s}}^2}}, \tag{10.1.16}$$

$$2\,n^2 \,=\, 1 \,-\, \frac{\epsilon_1 \,+\, \epsilon_2}{\sqrt{(\epsilon_1 \,+\, \epsilon_2)^2 \,+\, 4\,\Delta_{\mathrm{s}}^2}}. \tag{10.1.17}$$

Here, $\epsilon_{1,2}$ are the single particle energies of $\hat{H}_0$ given above. The structure of the transformation respects the action of Δ_{s} naturally by $\hat{b}_{ks}^{\dagger}\,\hat{b}_{ks}$ terms, contrary to Δ_{p} and; thus the nanowire Hamiltonian becomes

$$\hat{H} \,=\, \frac{1}{2} \sum_{k,\,s=\pm} \left[\xi_s\,\hat{b}_{ks}^{\dagger}\,\hat{b}_{ks} \,+\, \mathrm{i}\Delta_{\mathrm{p}}\,\hat{b}_{ks}^{\dagger}\,\hat{b}_{\bar{k}s}^{\dagger} \,+\, \mathrm{h.c.}\right]. \tag{10.1.18}$$

The effective single particle energy $\xi_{\pm}$ is

$$\xi_{\pm} \,=\, \sqrt{\left(\frac{\hbar^2\,k^2}{2m} - \mu\right)^2 \,+\, \Delta_{\mathrm{s}}^2} \,\pm\, \sqrt{V_{\mathrm{Z}}^2 \,+\, \alpha_{\mathrm{R}}^2\,k^2}, \tag{10.1.19}$$

and the relation to the eigenvalues stated in Eq. (10.1.6) is $E_l^2(k) = \xi_{\pm}^2 + \Delta_{\mathrm{p}}^2$ for $l = \pm 1$.

We may express next the Hamiltonian $\hat{H}$ w.r.t. to the Nambu spinor $\hat{\Psi} \,=\, \left(\hat{b}_{k+},\, \hat{b}_{\bar{k}+}^{\dagger},\, \hat{b}_{k-},\, \hat{b}_{\bar{k}-}^{\dagger}\right)^{\mathrm{T}}$ granting

$$\hat{H} \,=\, \frac{1}{2} \sum_{k} \hat{\Psi}^{\dagger} \begin{bmatrix} \mathcal{H}_{+}(k) & \\ & \mathcal{H}_{-}(k) \end{bmatrix} \hat{\Psi}, \tag{10.1.20}$$

where $\mathcal{H}_{-}$ ($\mathcal{H}_{+}$) accounts for the low-energy (high-energy) degrees of freedom of the nanowire Hamiltonian. We have $\mathcal{H}_{\pm} = \xi_{\pm}\tau_z + \Delta_{\mathrm{p}}\,\tau_y$. For parameters within the topologically non-trivial phase, the energies associated to $\mathcal{H}_{\pm}$ are well separated.

The block diagonal form of $\hat{H}$ is an important intermediate result and basing on Eq. (10.1.20), we derive analytical expressions for the zero energy wavevector quantization in sec. 10.2 and the conductance in sec. 10.4 at $T = 0\,\mathrm{K}$, for L finite and open boundary conditions.

Since the low energy physics of the nanowire model is fully captured by $\mathcal{H}_-$, we have to demonstrate that the topological properties of the model are contained in the low energy description. Importantly, $\mathcal{H}_\pm = \xi_\pm\tau_z + \Delta_\mathrm{p}\,\tau_y$ adopts the form of the Kitaev Hamiltonian stated earlier in Eq. (5.1.5). The operator $\hat{b}_{k\pm}$ contains both spin degrees of freedom and thus, $\mathcal{H}_\pm$ are indeed effectively spinless. Consequently, $\mathcal{H}_-$ has the same symmetries as the Kitaev chain, namely the (pseudo) time reversal symmetry $\mathcal{T} = \mathcal{K}\mathbb{1}_2$, the particle-hole symmetry $\mathcal{P} = \mathcal{K}\,\sigma_x$ (by construction) and also the chiral symmetry $\mathcal{C} = \sigma_x$. Hence, the nanowire is placed in the BDI class [41]. The chiral symmetry allows the usage of the winding number topological invariant ν [39, 98]

$$\nu = \frac{1}{2\pi}\int\limits_{\mathbb{R}} \partial_k \arctan\left(\frac{\xi_-(k)}{\Delta_\mathrm{p}(k)}\right)\,\mathrm{d}k. \tag{10.1.21}$$

We find $\nu = 1$ for $V_\mathrm{Z} > \sqrt{\Delta^2 + \mu^2}$ and otherwise zero in agreement with the phase diagram. We conclude that the low energy part of the nanowire $\mathcal{H}_-(k)$ contains the topological properties of the system and thus; our analytical approach will treat $\mathcal{H}_-(k)$ rather than the full Hamiltonian.

During the work on the Kitaev chain, we experienced that finite size effects of the model with open boundary conditions particularly the finite size quantization have to be considered in order to receive quantitative results. In the following section, we derive the constraints for zero energy modes for the nanowire with open boundary conditions and L finite.

10.2. Discrete zero energy lines in the weak spin orbit regime

Generally, the zero energy criterion for the nanowire demands $E_l^2(k) = 0$ and a quantization constraint on k. We call the former the bulk zero energy constraint, which relates the parameters μ, V_Z and Δ to the momentum k. This relation alone in the situation of open boundary conditions and L finite is insufficient as the quantized value of k is missing. For simplicity, we first derive the quantization rule for zero energy from $\mathcal{H}_-(k)$.

The open boundary conditions demand the quasi-particle wavefunction $\psi(x)$ to vanish at both ends of the wire, i.e. $\psi(\pm L/2) = 0$. Since $\mathcal{H}_-$ is a 2×2 matrix and we have two boundaries, one has to satisfy in total four constraints. Similar to the Kitaev chain, we use two left moving $k_{1,2}$ and two right moving solutions $-k_{1,2}$ of the eigenvalue equation

for $\mathcal{H}_-$. The normalized eigenvectors $\chi_{1,2}(k)$ of $\mathcal{H}_-$ are

$$\chi_1(k) \;=\; \frac{1}{\sqrt{2\,|E_-|(\xi_- + |E_-|)}} \begin{pmatrix} \xi_- + |E_-| \\ \Delta_\mathrm{p} \end{pmatrix}, \tag{10.2.1}$$

$$\chi_2(k) \;=\; \frac{1}{\sqrt{2\,|E_-|(\xi_- + |E_-|)}} \begin{pmatrix} -\Delta_\mathrm{p} \\ \xi_- + |E_-| \end{pmatrix}, \tag{10.2.2}$$

where χ_1 (χ_2) corresponds to the positve (negative) energy eigenvalue $E_- = \pm\sqrt{\xi_-^2 \,+\, \Delta_\mathrm{p}^2}$. In case of $E_- = 0$, the ansatz for $\psi(x)$ is

$$\psi(x) \;=\; \sum_{j=1,2} \Big[a_j\, \chi_j(k_j)\, e^{\mathrm{i}\, k_j x} \,+\, b_j\, \chi_j(-k_j)\, e^{-\mathrm{i}\, k_j x} \Big], \tag{10.2.3}$$

where $k_{1,2}$ are complex due to the gapped spectrum. We are allowed to use both χ_1 and χ_2 in the same eigenstates because we are looking for a zero energy solutions. Here, we respect the condition $E_-(k_{1,2}) \;=\; \sqrt{\xi_-^2(k_{1,2}) + \Delta_\mathrm{p}^2(k_{1,2})} \;\overset{!}{=}\; 0$ only implicitly with $\Delta_p(k_j) \;=\; \pm\mathrm{i}\xi_-(k_j)$. The expressions for $k_{1,2}$ are complicated and so far not explicitly required. The equal (zero) energy constraint on $k_{1,2}$ relates them non-trivially (in full analogy to the Kitaev chain), i.e. $k_1 \neq \pm k_2$ and $k_{1,2} \neq 0$ must be true for the proper ansatz.

A second zero energy mode exists, namely $\mathcal{P}\,\psi(x)$, due to particle-hole symmetry. In turn, one can construct with $\psi(x)$ and $\mathcal{P}\,\psi(x)$ the two Majorana zero modes for the proximitized nanowire taking explicitly the system's size into account.

Notice that a similar ansatz as in Eq. (10.2.3) for finite energy eigenstates can be made, using a composition of either $\chi_1(\pm k_{1,2})$ or $\chi_2(\pm k_{1,2})$ exclusively[2]. The equal energy constraint $E_-(k_1) \;=\; E_-(k_2) \;\neq\; 0$ must hold, restricting again $k_1 \neq \pm k_2$ and $k_{1,2} \neq 0$. Thus, the open boundary conditions prevent here generally the gap closing for parameters on the topological phase boundary $V_\mathrm{Z} = \sqrt{\mu^2 \,+\, \Delta^2}$ as $k_{1,2} \neq 0$. Further, a connection to the Tetranacci polynomials from the Kitaev chain can be made. Consider transforming $\mathcal{H}_-$ in its eigenbasis, where $\chi_1 \to (1,\,0)^\mathrm{T}$, $\chi_2 \to (0,\,1)^\mathrm{T}$ holds. This unitary transformation cannot change the physical reality at the boundary and $\pm k_{1,2}$ have still to be used. Then, the non-trivial part in the superposition of χ_1 (χ_2) using $\pm k_{1,2}$ displays exactly the closed form of a Tetranacci as stated in Eq. (4.3.5) for a continuous system ($j\,d \to x$).

Returning to the zero energy case and Eq. (10.2.3), the constraint $\psi(\pm L/2) = 0$ yields a homogeneous set of four equations. In order to avoid a trivial solution, we demand the coefficient matrix constructed by the entries of $\chi_j(\pm k_j)$ and the exponentials $e^{\pm\mathrm{i}\, k_j x}$ to vanish. After some manipulations, we find the semi final result

$$\frac{\sin^2\left(\frac{k_1+k_2}{2}L\right)}{\sin^2\left(\frac{k_1-k_2}{2}L\right)} \;=\; \frac{\xi_-(k_1)\,\xi_-(k_2) \;-\; \Delta_\mathrm{p}(k_1)\,\Delta_\mathrm{p}(k_2)}{\xi_-(k_1)\,\xi_-(k_2) \;+\; \Delta_\mathrm{p}(k_1)\,\Delta_\mathrm{p}(k_2)} \tag{10.2.4}$$

[2]Meanwhile, we were able to find the quantization rule for generic energy eigenvalues of the Rashba nanowire in case of finite length and open boundary condition from the mentioned ansatz. This result and the constraint for the Kitaev chain from Eq. (6.3.28) can be united into one common condition.

where we used fractions rather than the correct product form only for shortness. The reason to show Eq. (10.2.4), is the apparent similarity to the quantization rule of the Kitaev chain in Eq. (6.3.28). Notice though, Eq. (10.2.4) is only valid for $E_- = 0$.

The zero energy condition, i.e. $\Delta_p(k_j) = \pm \mathrm{i}\xi_-(k_j)$, can be used a last time and from Eq. (10.2.4) we have

$$\sin^2(k_\Sigma L) = 0 \tag{10.2.5}$$

in terms of $k_{\Sigma,\Delta} \coloneqq (k_1 \pm k_2)/2$ without restrictions. Hence, we find the exact result

$$k_\Sigma = \frac{n\pi}{L}, \quad n \in \mathbb{N}. \tag{10.2.6}$$

The condition of integer multiples of π/L was already stated in the literature [8, 13] but not derived for finite L and open boundary conditions. As we can clearly see from Eq. (10.2.6), k_1 and k_2 share the same imaginary part. Indeed, one can show that $k_1 = k_2^*$ holds for parameters associated with the topologically non-trivial phase. Thus, we have $\mathrm{Re}\,(k_{1,2}) = k_\Sigma$.

In order to finally determine $k_{1,2}$, a second constraint has to be derived which is extracted from $E_-(k_{1,2}) = \sqrt{\xi_-^2(k_{1,2}) + \Delta_\mathrm{p}^2(k_{1,2})} = 0$. Since $k_{1,2}$ are complex and the energy depends on $k_{1,2}^2$, a naive reordering according to real and pure imaginary terms yields coupled equations. Still, these two equations relate on the one hand the parameters V_Z, μ and Δ to $k_{1,2}$ imposing constraints (see Eq. (10.2.16) below) similar to those on μ for the Kitaev chain in Eq. (6.3.7). On the other hand, a condition on the imaginary part of $k_{1,2}$ is found.

Unfortunately, solving $E_-(k_{1,2}) = 0$ exactly is difficult and thus we apply approximations from now on. As the spin orbit coupling may yield the smallest energy scale as stated above, we restrict our approach to the weak spin orbit regime, i.e. $E_\mathrm{so} = m\,\alpha_\mathrm{R}^{2\,2}/\hbar \ll V_\mathrm{Z}, \Delta$. Previous works in this limit can be found in the literature [3, 8, 9, 125], but we respect here the exact quantization from Eq. (10.2.6).

For small α_R, we approximate Δ_p, ξ_- by

$$\xi_- \approx \sqrt{\left(\frac{\hbar^2 k^2}{2m} + \Delta^2\right)} - V_\mathrm{Z}, \tag{10.2.7}$$

$$\Delta_\mathrm{p} \approx \frac{\Delta\,\alpha_\mathrm{R}\,k}{V_\mathrm{Z}}, \tag{10.2.8}$$

where the effective p-pairing constant became linear in k. We demand $E_-^2(k_{1,2}) = \xi_-^2(k_{1,2}) + \Delta_\mathrm{p}^2(k_{1,2}) = 0$ in terms of the approximated expression for ξ_-, Δ_p and the substitution $\Delta\,\sinh(x_j) \coloneqq \hbar^2 k_j^2/(2m) - \mu$ ($j = 1, 2$, $x_j \in \mathbb{C}$) grants

$$[\Delta\,\cosh(x_j) - V_\mathrm{Z}]^2 + \frac{2m\,\alpha_\mathrm{R}^2\,\Delta^2}{\hbar^2\,V_\mathrm{Z}^2}\,[\Delta\,\sinh(x_j) + \mu] = 0, \tag{10.2.9}$$

a simplified zero energy constraint. A second replacement $u_j \coloneqq e^{x_j}$ grants a quartic equation for u_j

$$u_j^4 + (\epsilon - \beta)\, u_j^3 + \gamma\, u_j^2 - (\epsilon + \beta)\, u_j + 1 = 0. \tag{10.2.10}$$

with coefficients $\epsilon = 4m\,\alpha_{\mathrm{R}}^2\,\Delta/(\hbar^2\,V_{\mathrm{Z}}^2)$, $\beta = 4V_{\mathrm{Z}}/\Delta$ and $\gamma = 2 + 2(\mu\epsilon/\Delta) + \beta^2/4$. Importantly, the criterion for the topological phase, i.e. $V_{\mathrm{Z}} > \sqrt{\Delta^2 + \mu^2}$ is still present in the discriminant D of Eq. (10.2.10) in the dominant order of α_{R}

$$D \propto \frac{\epsilon^2}{\Delta^6}\left(V_{\mathrm{Z}}^2 - \Delta^2\right)^2\left(\mu^2 + \Delta^2 - V_{\mathrm{Z}}^2\right). \tag{10.2.11}$$

In case of $V_{\mathrm{Z}} > \sqrt{\Delta^2 + \mu^2}$, one finds two non-real, complex roots for u_j from Eq. (10.2.10) as expected. We approximate these roots and inserting them into the inverse transformation

$$k_j = \pm\sqrt{\frac{2m}{\hbar}}\,\sqrt{\Delta\,\sinh\left[\ln\left(u_j\right)\right] + \mu}, \tag{10.2.12}$$

grants a condition on k_j^2. We find ($s'\,, s = \pm 1$)

$$\frac{\hbar^2\,k_j^2}{2m} = \mu + s\sqrt{\left(V_{\mathrm{Z}} - f_{s's}\right)^2 - \Delta^2} \tag{10.2.13}$$

and the function $f_{s's}$

$$f_{s's} = s\epsilon_{\mathrm{so}} + 2s'\,\sqrt{\epsilon_{\mathrm{so}}^2 - 2s\left(V_{\mathrm{Z}} - \mu\right)\epsilon_{\mathrm{so}}} \tag{10.2.14}$$

accounts for corrections in the spin orbit coupling. Here, $\epsilon_{\mathrm{so}} = E_{\mathrm{so}}\,\Delta^2/V_{\mathrm{Z}}^2 = m\alpha_{\mathrm{R}}^2\,\Delta^2/(\hbar^2 V_{\mathrm{Z}}^2)$ represents the reduced spin orbit energy.

Since $k_{1,2}$ are complex, one can in principle use the ansatz $k_1 = (n\pi/L) + \mathrm{i}q$, $k_2 = (n\pi/L) - \mathrm{i}q$, due to Eq. (10.2.6), where q represents the unknown imaginary part. Separating in Eq. (10.2.13) real and imaginary terms yields non-linear coupled equation in q. Still, Eq. (10.2.13) is an important result.

In appendix O, we explain the derivation of the imaginary part

$$q = \frac{2m^2\,\alpha_{\mathrm{R}}\,\Delta}{\hbar^4}\left(\frac{\pi^2\,n^2}{L^2} - \frac{m\,\mu}{\hbar^2}\right)^{-1} + \mathcal{O}(\alpha_{\mathrm{R}}^3), \tag{10.2.15}$$

where the quantization due to the open boundary condition and finite L is directly embedded. Notice, the decay length $\xi = 1/|\mathrm{Im}(k_{1,2})| = 1/|q|$ of the zero energy modes can be extracted from Eq. (10.2.15). Importantly, we find in the weak spin orbit regime $\xi \propto 1/|\alpha_{\mathrm{R}}|$ and the proportionality is in agreement with prior works [9].

Since we now have q and the real parts of $k_{1,2}$ stated in Eq. (10.2.6), we can insert both into Eq. (10.2.13). We find a constraint on the chemical potential, namely

$$\mu \equiv \mu_n = \frac{n^2\pi^2\,\hbar^2}{2m\,L^2} \pm \sqrt{{V_{\mathrm{Z}}}^2 - \Delta^2 - V_{n,\,\mathrm{so}}} - 4\epsilon_{\mathrm{so}} \tag{10.2.16}$$

where $V_{n,\mathrm{so}} = 4\epsilon_{\mathrm{so}}\, n^2\pi^2\hbar^2/(mL^2) + 10\,\epsilon_{\mathrm{so}}\, V_{\mathrm{Z}}$. Similar to the Kitaev chain, see Eq. (6.3.7), the quantization imposed by finite L and open boundary condition restricts zero energy to discrete lines.

We compared our analytical findings with a pure numerical approach which uses a discrete version of the Hamiltonian from Eq. (10.1.1) stated in Ref. [127]. The numerics include all orders in α_{R} and both agree reasonably well, as shown in Fig. 10.2. Clearly, one has to approach Eq. (10.2.16) critically for to large and positive values of μ.

The discrepancies of the analytical findings compared to the numerical results arise from the used approximations. In particular, tuning the spin orbit coupling α_{R} changes significantly the slope of the numerical zero energy lines for $\mu > 0$ close to the topological phase boundary. Thus, our treatment has to be taken carefully there. Because of this, we used in a second treatment the zero energy conditions stated in the supplementary material of Ref. [3] and imposed the finite size quantization from Eq. (10.2.6). Again, numerics and analytics did not match perfectly. We concluded that weak spin orbit approximations has to be done with even more care. Currently, we try an exact approach which is not finished yet and will not be included in this thesis[3].

One now can insert the values for $k_{1,2}$ back into the ansatz for $\psi(x)$ and determine the remaining coefficients. Since $\mathcal{P}\psi(x)$ will be also a zero energy solution, one can determine the (approximated) wave function for the Majorana zero mode(s) by superposition(s).

Concerning the zero energy rings outside the topological non-trivial region found numerically, they were already observed in Ref. [13] and correspond to fermionic parity switches. For increasing system length L, these lines start to disappear as expected.

In the next section, we relate explicitly our findings for the proximitized Rashba nanowire back to the Kitaev chain. Although the former is a continuous model and the latter discrete, our results match quantitatively. The comparison allows a deeper understanding of the finite sized nanowires.

[3] Meanwhile, we found a much better analytical condition on the parameters for zero energy, which overcomes all prior attempts.

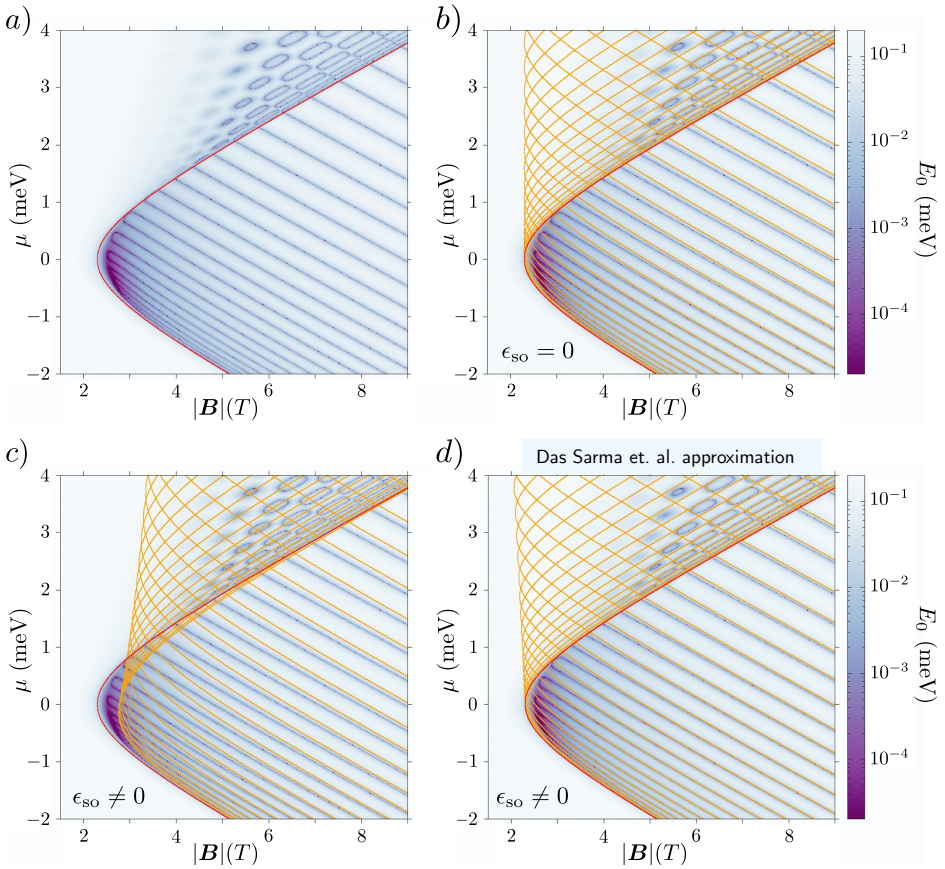

Figure 10.2.: Numerically calculated in-gap (positive) energy E_0 and the analytical zero energy lines (orange) in the weak spin orbit regime as function of μ and the magnetic field strength $|\boldsymbol{B}|$. The used parameters are $m = 0.04\, m_e$, $\alpha_R = 0.1\,\text{meV Å}$ ($E_{so} = 0.05\,\text{meV}$), $g = 15$, $N = 1600$ sites. The topological phase boundary is shown in red. a) Only numerical data. We find discrete, mostly parallel zero energy lines within the topologically non trivial region. In vicinity to the phase boundary for $\mu > 0$, two of the lines connect pairwise into loops, particularly at $\mu \approx 0$, $|\boldsymbol{B}| \lesssim 3\,\text{T}$. The deep purple region corresponds to lowest in-gap energies. b) Analytical zero energy lines according to Eq. (10.2.16) without spin-orbit correction ($V_{n,so} = \epsilon_{so} = 0$). c) Similar as b), with spin orbit correction. d) We used here the unquantized zero energy condition given in the supplementary part of Ref. [3] and applied Eq. (10.2.6). Inside the topological region, the agreement overcomes our own approach. Numerical results provided by M. Marganska.

10.3. The Rashba nanowire as an effective Kitaev chain

Earlier in section 10.1, we concluded that the low energy description of the proximitized nanowire matches structurally the Kitaev Hamiltonian. Both are described by $\mathcal{H} = \xi\,\tau_z + \Delta\,\sigma_y$ using the proper expressions of the single particle energy and the pairing constant. Still, the dependence of the (effective) single particle energy and the p-wave pairing on k are generally different for the Kitaev chain and the nanowire. From Eq. (5.1.5), we extract for the former that

$$\xi_{\mathrm{K}} = -\mu_{\mathrm{K}} - 2t_{\mathrm{K}}\cos(kd), \tag{10.3.1}$$

$$\Delta_{\mathrm{p,\,K}} = 2\Delta_{\mathrm{K}}\sin(kd), \tag{10.3.2}$$

and expanding at small kd yields

$$\xi_{\mathrm{K}} \approx -\mu_{\mathrm{K}} - 2t_{\mathrm{K}} + t_{\mathrm{K}}\,(kd)^2, \tag{10.3.3}$$

$$\Delta_{\mathrm{p,\,K}} \approx 2\Delta_{\mathrm{K}}\,kd. \tag{10.3.4}$$

In case of the nanowire, we use the approximations for ξ_- and Δ_{p} in weak spin orbit from Eqs. (10.2.7), (10.2.8). Since ξ_- and ξ_{K} have a distinct dependence on k, we need to expand the former up to second order. We have to respect the possible double-well shape of ξ_- which depends on the chemical potential. Thus, the naive Taylor expansion up to second order for small k fails. However, one can show that ξ_- has two roots $\pm\tilde{k}$, supposing the nanowire parameter belongs to the topological non-trivial phase, i.e. for $V_{\mathrm{Z}} > \sqrt{\mu^2 + \Delta^2}$. We then approximate ξ_- with $\xi_{\mathrm{approx}} = \lambda\,(k^2 - \tilde{k}^2)$ in order to respect the symmetry in $k \to -k$. The value of λ is extracted from the equal slope constraint, i.e. $\partial_k\,\xi_-(\tilde{k}) = \partial_k\,\xi_{\mathrm{approx}}(\tilde{k})$, at $\tilde{k}$. Including the approximation for Δ_{p}, we have

$$\xi_- \approx \xi_{\mathrm{approx}} = \frac{\hbar^2\,k^2}{2m_{\mathrm{eff}}} - \mu_{\mathrm{eff}}, \tag{10.3.5}$$

$$\Delta_{\mathrm{p}}(k) \approx \Delta_{\mathrm{eff}}\,k \tag{10.3.6}$$

where we introduced the abbreviations

$$m_{\mathrm{eff}} := \frac{m}{\sqrt{1 - \frac{\Delta^2}{V_{\mathrm{Z}}^2}}}, \tag{10.3.7}$$

$$\mu_{\mathrm{eff}} := \sqrt{1 - \frac{\Delta^2}{V_{\mathrm{Z}}^2}}\left(\sqrt{V_{\mathrm{Z}}^2 - \Delta^2} + \mu\right), \tag{10.3.8}$$

$$\Delta_{\mathrm{eff}} := \frac{\Delta\,\alpha_{\mathrm{R}}}{V_{\mathrm{Z}}}. \tag{10.3.9}$$

The approximated expressions for the Kitaev chain and the nanowire have now the same dependence on k; thus, we can relate next the physical quantities. We find

$$\mu_{\mathrm{eff}} \to -\mu_{\mathrm{K}} - 2t_{\mathrm{K}}, \tag{10.3.10}$$

$$\frac{\hbar^2}{2m_{\mathrm{eff}}} \to t_{\mathrm{K}}d^2, \tag{10.3.11}$$

$$\Delta_{\mathrm{eff}} \to 2\Delta_{\mathrm{K}}\,d. \tag{10.3.12}$$

Crucial is the gained expression for the effective chemical potential μ_{eff} in Eq. (10.3.8) of the nanowire: The parameters V_{Z}, μ are now related to μ_{K} of the Kitaev chain. In case of open boundary condition, the latter influences the spectrum of the finite sized Kitaev chain as we demonstrated in Ch. 6.4. The implicit dependency of the wavenumbers $k_{\Sigma,\Delta}$ on μ_{K} caused the energy oscillations depicted in Fig. 6.11. In the virtue of Eq. (10.3.8), we can understand now qualitatively the energy oscillations in V_{Z} or μ shown in [3, 9, 12–17]. For semiconducting nanowires of length L and open boundary conditions, we expect a non-trivial quantization rule depending on μ and V_{Z}.

Next, we demonstrate that the Eqs. (10.3.10)-(10.3.12) transform the zero energy lines from the Kitaev chain nearly to the ones of the nanowire. Since we operate in weak spin orbit limit, the mapping demands an expansion in $\Delta_{\text{K}} \ll t_{\text{K}}$. We change $\mu_{\text{K}} \to -\mu_{\text{K}}$ in Eq. (6.3.7) freely[4] and for $n \ll N$ we find

$$\mu_{\text{K}} + 2t_{\text{K}} = \frac{\Delta_{\text{K}}^2}{t_{\text{K}}} + \frac{t_{\text{K}}\,\pi^2 n^2}{(N+1)^2} + \mathcal{O}\left(\frac{\Delta_{\text{K}}}{t_{\text{K}}}\right)\mathcal{O}\left(\frac{n^2}{N^2}\right). \tag{10.3.13}$$

We omit the last term, since it is at least one order of magnitude smaller than the others. Mapping the quantities in Eq. (10.3.13) into μ_{eff}, m_{eff} and Δ_{eff} grants upon reordering

$$\sqrt{V_{\text{Z}}^2 - \Delta^2} + \mu = \frac{\hbar^2}{2m}\frac{\pi^2\, n^2}{L^2} + \frac{m\,\alpha_{\text{R}}^2\,\Delta^2}{2\hbar^2\left(V_{\text{Z}}^2 - \Delta^2\right)}. \tag{10.3.14}$$

Here, we set $L \approx (N+1)d$ being justified for large N and recall $\epsilon_{\text{so}} = m\alpha_{\text{R}}^2\,\Delta^2/(\hbar^2 V_{\text{Z}}^2)$. For small values of α_{R} and deep within the topologically non-trivial phase, the two expressions in Eqs. (10.2.16), (10.3.14) agree.

In the next section, we introduce the N-S-N transport setup considered for the Rashba nanowire. We derive an exact current formula for the minimal model given by $\mathcal{H}_-$ and show the zero temperature conductance results in the end.

10.4. N-S-N transport setup and current formula

We consider the two normal conducting leads

$$\hat{H}_\alpha^{\text{gc}} = \hat{H}_\alpha - \mu\,\hat{N}_\alpha = \sum_p \epsilon_{p\sigma\alpha}\, c_{p\sigma\alpha}^\dagger c_{p\sigma\alpha}, \quad \alpha = L, R, \tag{10.4.1}$$

where $c_{p\sigma\alpha}^\dagger$ ($c_{p\sigma\alpha}$) creates (annihilates) a fermion in state p with spin σ in the lead α. We consider initially the full nanowire $\hat{H}$ of length L from Eq. (10.1.3), which is placed in between the leads and we consider the nanowire as floating. The tunneling Hamiltonian

$$\hat{H}_{\text{T}} = \sum_{\sigma=\uparrow\downarrow,\,\alpha} \int_{\mathbb{R}} \Big[t_\alpha(x,\,x')\, c_{\sigma\alpha}^\dagger(x)\,\hat{\psi}_\sigma(x') + \text{h.c.}\Big]\,\mathrm{d}x\,\mathrm{d}x' \tag{10.4.2}$$

[4]The Kitaev chain is symmetric in positive and negative values of the chemical potential. Thereby, we suppress an overall minus sign appearing in the end.

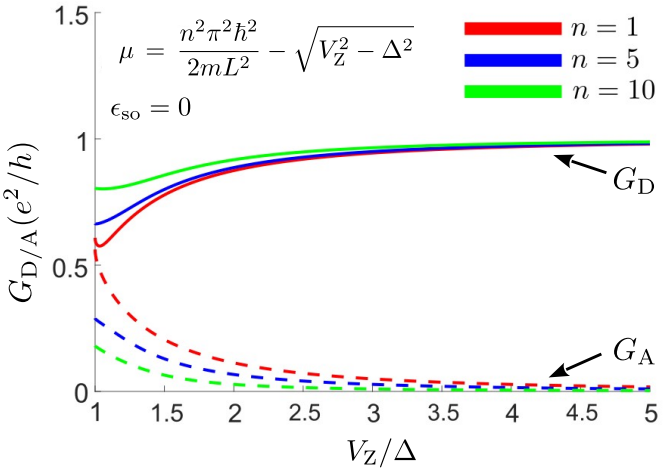

Figure 10.3.: Analytically calculated conductance at $T = 0\,\mathrm{K}$ as function of V_Z/Δ for weak spin orbit coupling. The chemical potential is determined by Eq. (10.2.16) for $n = 1, 5, 10$. For simplicity we neglected spin orbit corrections, i.e. $V_{n,\mathrm{so}}$ and ϵ_so, similar as in Fig. 10.2 b). Along the zero energy lines, the direct conductance G_D is usually larger than the Andreev contribution G_A. This changes close to the topological phase boundary ($V_\mathrm{Z}/\Delta \approx 1$). The total conductance $G = G_\mathrm{A} + G_\mathrm{D}$ reaches e^2/h. More details are given in the text. The used parameters are $\hbar^2/2m = 1\,\mu\mathrm{m}^2\,\mathrm{meV}$, $\alpha_\mathrm{R} = 0.05\,\mu\mathrm{m}\,\mathrm{meV}$, $\Delta = 1\,\mathrm{meV}$ and $L = 2.5\,\mu\mathrm{m}$. Figure adapted from Ref. [124]

allows spin conserving particle transfer. We consider (local) tunneling events from the leads to the nanowire to happen only at their respective contact surfaces ($x_L = -L/2$, $x_R = L/2$)

$$t_\alpha(x, x') = \tilde{t}\,\delta(x - x_\alpha)\,\delta(x' - x_\alpha), \tag{10.4.3}$$

with constant coupling strength $\tilde{t}$. One can convert $\hat{H}_\mathrm{T}$ into momentum space granting

$$\hat{H}_\mathrm{T} = \sum_{\sigma\alpha\,p,k} \left(t_{\alpha pk}\, d^\dagger_{p\sigma\alpha}\, \hat{\psi}_{k\sigma} \right) \tag{10.4.4}$$

where $t_{\alpha pk} = t \exp[-\mathrm{i}(p-k)x_\alpha]$ is the tunneling amplitude. Here, t and $\tilde{t}$ differ only by an unimportant normalization constant.

For clarity, we denote momenta of the nanowire (leads) with k (p). The values of k obey the quantization rule for the nanowire with open boundary conditions and are not restricted to zero energy modes. Only at the final stages of our calculation, we truncate the sum of k such that only the zero energy eigenstates of $\mathcal{H}_-$ are left. This procedure is justified in our explanation of the minimal model approach in Chapter 9.

Speaking about $\mathcal{H}_-$, we next use the basis transformation from Chapter 10.1, in order to split $\hat{H}$ into its high and low energy parts, see Eq. (10.1.18). We perform the same unitary transformation on the tunneling Hamiltonian, thereby separating $\hat{H}_{\mathrm{T}} \equiv \hat{H}_{\mathrm{T},-} + \hat{H}_{\mathrm{T},+}$ i.e. the high/ low energy tunneling events. Since we are in the end only interested in the conductance at zero temperature, we consider only the low energy piece $\hat{H}_{\mathrm{T},-}$

$$\hat{H}_{\mathrm{T},-} = \sum_{\sigma\alpha\, p,k} t_{\alpha p k} \left[c^\dagger_{p\uparrow\alpha} \left(u_k n_k\, b^\dagger_{\bar{k}-} + v_k m_k\, b_{k-} \right) + c^\dagger_{p\downarrow\alpha} \left(u_k m_k\, b_{k-} + v_k n_k\, b^\dagger_{\bar{k}-} \right) \right] + \mathrm{h.c.} \tag{10.4.5}$$

where u_k, v_k, n_k and m_k are the transformation coefficients given in Eqs. (10.1.11), (10.1.16), (10.1.17) respectively. The low energy transport setup for the nanowire is thus given by

$$\hat{H}_{\mathrm{tot}} = \hat{H}_L + \hat{H}_- + \hat{H}_R + \theta(t - t_0)\, \hat{H}_{\mathrm{T},-}, \tag{10.4.6}$$

and in the end we consider the limit $t_0 \to \infty$. The electronic current can be calculated in lead α

$$I_\alpha(t) = -e \langle \dot{N}_\alpha \rangle = \frac{\mathrm{i}e}{\hbar} \langle \Big[N_\alpha,\, \hat{H}_{\mathrm{tot}} \Big] \rangle, \tag{10.4.7}$$

where e is the elementary charge and $N_\alpha = \sum\limits_{p\sigma} c^\dagger_{p\sigma\alpha}\, c_{p\sigma\alpha}$. We used the NEGF method and the equation of motion technique to obtain the steady state current formula. In order to avoid the self-consistency cycle, due to the superconductivity hidden in $\mathcal{H}_-$, we considered equal tunneling amplitudes for both leads to the nanowire and set $V_L = -V_R = V/2$ [45, 118, 119]. Here, the quantity V represents the bias drop between the two leads. As a consequence of the setting, the current

$$I_L = \frac{e}{h} \int\limits_{\mathbb{R}} \left[M_{\mathrm{A}}(E) + M_{\mathrm{D}}(E) \right] \left(f^- - f^+ \right) \mathrm{d}E \tag{10.4.8}$$

is now conserved, i.e. $I_L = -I_R$, and the crossed Andreev term dropped. Here, $f^\pm := f(E \pm V/2)$ denotes the Fermi functions of the leads and M_{A} (M_{D}) is the transmission probability for the Andreev reflection (direct electron transfer). Note that the expression for I_L was obtained using the full dynamics of the system and is exact on the level of the low energy physics, i.e. for $\mathcal{H}_-$, since we considered non-interacting leads [117].

The transmission functions read explicitly

$$M_{\mathrm{A}} = \sum_{k_1\, k_2\, k_3\, k_4} \mathrm{Tr} \Big\{ \Gamma^e_L(k_1,\, k_2,\, E) G^r(k_2,\, k_3,\, E) \Gamma^h_L(k_3,\, k_4,\, E) G^a_L(k_4,\, k_1,\, E) \Big\}, \tag{10.4.9}$$

$$M_{\mathrm{D}} = \sum_{k_1\, k_2\, k_3\, k_4} \mathrm{Tr} \left\{ \Gamma^e_L(k_1,\, k_2,\, E) G^r(k_2,\, k_3,\, E) \Gamma^e_L(k_3,\, k_4,\, E) G^a_L(k_4,\, k_1,\, E) \right\}, \tag{10.4.10}$$

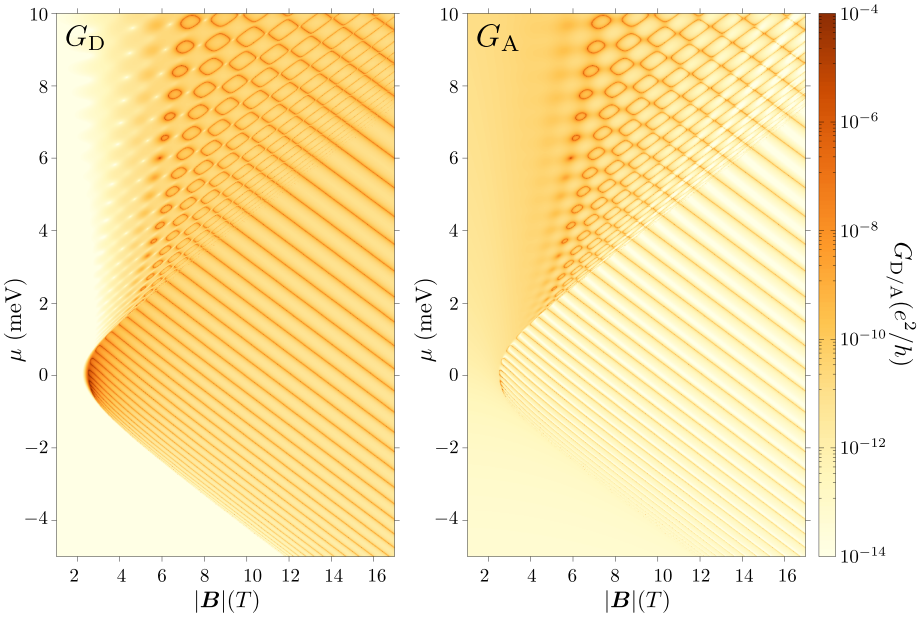

Figure 10.4.: Numerically calculated conductances G_A and G_D at $T = 0\,\mathrm{K}$ as a function of μ and $|\boldsymbol{B}|$. a),b) The direct conductance term is more dominant than the Andreev contribution. Qualitatively, the findings agree with the analytical approach. Notice though, the data points are selected by a dense grid, since the precise positions of the zero energy lines are not known. This causes a significant drop of the conductance results. The used parameters are $m = 0.04\,m_e$, $\alpha_\mathrm{R} = 0.1\,\mathrm{meV\ \AA}$ ($E_\mathrm{so} = 0.05\,\mathrm{meV}$), $g = 15$, $\gamma_{L,R} = 0.1\,\mathrm{meV}$ and $N = 1600$ sites. Numerical results provided by M. Marganska.

where the sums run over all the quantized momenta (open boundary conditions, finite L) associated with $\mathcal{H}_-$. The expressions for the rate matrices $\Gamma_L^{e,h}$ and for the retarded and advanced GF $G^{r,a}$ can be found in appendix P.

The conductance G at $T = 0\,\mathrm{K}$ can be extracted from Eq. (10.4.8)

$$G = \frac{e^2}{h}\,[M_\mathrm{A} + M_\mathrm{D}]_{E=0} = G_\mathrm{A} + G_\mathrm{D}. \tag{10.4.11}$$

Since only zero or close to zero energy eigenvalues contribute effectively to G, the sums over k_1, k_2, k_3, k_4 in the transmission probabilities can be truncated. Our analytical approach was so far restricted to zero energy modes in the weak spin-orbit coupling regime and thus k_1, k_2, k_3, k_4 can only adopt the values of $n\pi/L + \mathrm{i}q$ and $n\pi/L - \mathrm{i}q$ with q from Eq. (10.2.15). Please notice, the ansatz for $\psi(x)$ contains left and right movers, but this is already respected internally inside the transmission probabilities[5].

[5]Since zero energy modes yield in this setup conductance quanta of (up to) e^2/h, a mistreatment of the sums in M_A, M_G can easily produce wrong conductance peaks larger than e^2/h.

These solutions are restricted to discrete lines, see Eq. (10.2.16) and the associated conductance is shown in Fig. 10.3.

Recall that the decay length scales as $\xi \propto 1/|\alpha_{\mathrm{R}}|$ in the weak spin-orbit coupling regime, see Eq. (10.2.15). In turn, the zero energy modes associated to ξ can easily extend over large parts of the nanowire depending on the length L. Hence, we expect that G_{D} is at least comparable or even dominant compared to G_{A}, following the discussions of sections 8.1, 9. Since both spin degrees of freedom are not independent in this model and due to the particle number conservation, the conductance is restricted to values smaller or equal the conductance quantum e^2/h, confirmed by Fig. 10.3.

The tendency of G_{D} to increase for larger n is verified by Eq. (10.2.15). We expect the decay length to grow as n does; thus, for fixed L the zero modes extend further. In turn, the direct process is more favored than before.

Our analytical findings are qualitatively reproduced by numerical calculations shown in Fig. 10.4. Since the zero energy lines are discrete, small parameter deviations away from their precise position yields an immediate drop of the conductance results.

11. Acknowledgement

I would like to use the opportunity to thank several remarkable personalities for their support and their company during the three years of my PhD.

First of all, I would like to thank Milena Grifoni for her encouragement and the deep trust she put in me. It has been a pleasure to be your PhD student. I gratefully acknowledge Magdalena Margańska for her endless support and her simply unlimited endurance, especially while listening to my "cunning" mathematical plans. Magda without you, this thesis would not exist and you helped me a lot in several critical moments. Knowing both of you as my supervisors, the last three years have been a wonderful time. I will definitely miss our regular meetings to which Magdalena typically referred as: "The problem is, that we all agree."

Special thanks to Wolfgang Häusler for introducing me into theoretical physics. I would not have achieved so much in recent years without your guidance.

All the lovely persons in our group made the entire PhD period just adorable. In particular, Andrea Donarini and Paul Wenk for many "short" discussions and my office mate Luca Magazzù.

My students Harald Schmid and Eric Guenther, I enjoyed the time working with you on your projects.

My dear colleagues: Heng Wang, Matthias Stosiek, Michael Kammermeier, Patrick Grössing, Felix Weiner, Martin Wackerl, Lars Milz, Michael Niklas, Daniel Hernangómez Pérez, María Camarasa Gomez, Stefan Hartl and especially Jordi Picó-Cortés, Moritz Frankerl and Christoph Rohrmeier, thank your for the last years we spent together.

Sylvia and Robert Hrdina, Martin Puschmann and Paul Wenk, I appreciated the scientific and non-scientific discussions in our regular coffee ceremony.

Without the help of Sylvia Hrdina, Alexandra Prem and Claudia Zange, everyone facing the bureaucracy stands on lost ground. Thank you.

I would like to thank my dear friends Jens & Liz, Jakob & Patti, Steffi, Tobi & Andi, Fasi, Markus, Moritz, Max, Uli, Robert, Jacob, Kathi, Hannes, Ahmed, Simone, Masrya and Sayed.

In life, there are only a few things one can choose freely; family is definitely non of them. I however was extremely fortunate to have my parents Karin and Gerhard Leumer. I like to gratefully thank you for all your support and guidance during my way. I was further extremely lucky with my brother Sascha and my sister-in-law Pia. Thanks to you, to my uncle Hans-Peter Jung and to my grandparents.

Life without cats is possible but pointless. In loving memory, Nefertari.

This thesis was supported by the Deutsche Forschungsgemeinschaft via SFB 1277 and by the Elitenetzwerk Bayern via the doctorate program "Topologische Isolatoren".

A. The limit $t = 0$ and the n.n.n. chain quantization rule

A.1. N even

We have $k_{\mathrm{a},n} = k_{\mathrm{b},n} = 2k_1$ from Eqs. (3.2.45), (3.2.46) and thus

$$k_\Sigma d = \frac{n\pi}{N+2} + \frac{\pi}{2}, \quad n = 1, \ldots, N/2, \tag{A.1.1}$$

$$k_\Delta d = \frac{\pi}{2}. \tag{A.1.2}$$

The single terms of Eq. (3.2.32) become

$$\sin^2\left[k_\Sigma d\,(N+2)\right] = \sin^2\left(n\pi + \pi\frac{N+2}{2}\right) = 0, \tag{A.1.3}$$

$$\sin^2\left(k_\Sigma d\right) = \sin^2\left(\frac{n\pi}{N+2} + \frac{\pi}{2}\right) \neq 0 \tag{A.1.4}$$

and

$$\sin^2\left[k_\Delta d\,(N+2)\right] = \sin^2\left(\pi\frac{N+2}{2}\right) = 0, \tag{A.1.5}$$

$$\sin^2\left(k_\Sigma d\right) = \sin^2\left(\frac{\pi}{2}\right) = 1 \tag{A.1.6}$$

since $n = 1, \ldots, N/2$ and $(N+2)/2$ are integer values. Consequently, both sides in Eq. (3.2.32) vanish and the quantization rule is indeed satisfied.

A.2. N odd

Unfortunately, we have $k_{\mathrm{a},n} \neq k_{\mathrm{b},n}$ following from Eqs. (3.2.45), (3.2.46) and we have to show the validity for $k_{\mathrm{a},n} = 2k_1$ and $k_{\mathrm{b},n} = 2k_1$ separately. In the former case, we get

$$k_\Sigma d = \frac{n\pi}{N+3} + \frac{\pi}{2}, \quad n = 1, \ldots, (N+1)/2, \tag{A.2.1}$$

$$k_\Delta d = \frac{\pi}{2}. \tag{A.2.2}$$

Thus, we have

$$\sin^2\left[k_\Sigma d\,(N+2)\right] = \sin^2\left(n\pi\frac{N+2}{N+3} + \pi\frac{N+2}{2}\right) = \cos^2\left(n\pi\frac{N+2}{N+3}\right), \tag{A.2.3}$$

$$\sin^2\left(k_\Sigma d\right) = \sin^2\left(\frac{n\pi}{N+3} + \frac{\pi}{2}\right) = \cos^2\left(\frac{n\pi}{N+3}\right) \tag{A.2.4}$$

since $(N+2)/2$ is a half integer value. Secondly

$$\sin^2\left[k_\Delta d\,(N+2)\right] \;=\; \sin^2\left(\pi\frac{N+2}{2}\right) \;=\; 1, \tag{A.2.5}$$

$$\sin^2\left(k_\Delta d\right) \;=\; \sin^2\left(\frac{\pi}{2}\right) \;=\; 1, \tag{A.2.6}$$

setting the right hand side of Eq. (3.2.32) to one. Hence, if $\sin^2\left[k_\Sigma d\,(N+2)\right] = \sin^2\left(k_\Sigma d\right)$ holds, the quantization rule is satisfied. Indeed, we have further

$$\begin{aligned}\sin^2\left[k_\Sigma d\,(N+2)\right] \;=\; \cos^2\left(n\pi\frac{N+2}{N+3}\right) \;&=\; \cos^2\left(n\pi\frac{N+3-1}{N+3}\right)\\ &=\; \cos^2\left(n\pi-\frac{n\pi}{N+3}\right)\\ &=\; \cos^2\left(\frac{n\pi}{N+3}\right)\\ &\overset{\text{Eq.(A.2.4)}}{\equiv} \sin^2\left(k_\Sigma d\right)\end{aligned} \tag{A.2.7}$$

for all $n = 1, \ldots, (N+1)/2$. Thus, the quantization rule is confirmed for $k_1 = k_{\mathrm{a},n}/2$ and we can proceed with $k_1 = k_{\mathrm{b},n}/2$. Analogously, to the prior case, we have now

$$k_\Sigma d \;=\; \frac{n\pi}{N+1} \;+\; \frac{\pi}{2}, \quad n = 1, \ldots, (N-1)/2, \tag{A.2.8}$$

$$k_\Delta d \;=\; \frac{\pi}{2}. \tag{A.2.9}$$

Since

$$\begin{aligned}\sin^2\left[k_\Sigma d\,(N+2)\right] = \sin^2\left(n\pi\frac{N+2}{N+1}+\pi\frac{N+2}{2}\right) \;&=\; \cos^2\left(n\pi\frac{N+2}{N+1}\right)\\ &=\; \cos^2\left(n\pi+\frac{n\pi}{N+1}\right)\\ &=\; \cos^2\left(\frac{n\pi}{N+1}\right)\end{aligned} \tag{A.2.10}$$

and

$$\sin^2\left(k_\Sigma d\right) = \sin^2\left(\frac{n\pi}{N+1} \;+\; \frac{\pi}{2}\right) = \cos^2\left(\frac{n\pi}{N+1}\right) \tag{A.2.11}$$

hold, we find again the constraint $\sin^2\left[k_\Sigma d\,(N+2)\right] = \sin^2\left(k_\Sigma d\right)$ as validity check of the quantization rule. Indeed, we have

$$\sin^2\left[k_\Delta d\,(N+2)\right] \;=\; \sin^2\left(\pi\frac{N+2}{2}\right) = 1, \tag{A.2.12}$$

$$\sin^2\left(k_\Delta d\right) = \sin^2\left(\frac{\pi}{2}\right) = 1, \tag{A.2.13}$$

and the quantization rule in Eq. (3.2.32) is satisfied for odd N at $t = 0$, too.

B. Eigenstates of the extended chain

B.1. Non-degenerate case

The eigenvectors of the n.n.n. chain can be calculated in real space. We consider the quantization rule to be known, i.e. the eigenvalues λ, and we restrict ourselves to $m \neq 0$. We are left to determine the entries of $|\psi\rangle = (\xi_1, \xi_2, \ldots, \xi_N)^{\mathrm{T}}$, which obey the Tetranacci sequence in Eq. (4.2.1) for $\zeta = -(\lambda + \mu)/m$ and $\eta = -t/m$. Hence, we apply theorem 4.2.2 which states that

$$\xi_j \;=\; \sum_{i=-2}^{1} \xi_i \, \mathcal{T}_i(j), \qquad j \in \mathbb{Z} \tag{B.1.1}$$

holds. The basic Tetranacci polynomials obey the selective property. Since we know the values of ζ and η, the basic Tetranacci polynomials are fixed. One can either use the recursion formula or the closed form expressions.

We are left to determine the initial values ξ_{-2}, ξ_{-1}, ξ_0, ξ_1 such that the open boundary condition in Eq. (3.2.9) is satisfied. This implies $\xi_0 = \xi_{-1} = 0$ and we have

$$\xi_j \;=\; \xi_{-2} \, \mathcal{T}_{-2}(j) \;+\; \xi_1 \, \mathcal{T}_1(j). \tag{B.1.2}$$

Here in the non-degenerate energy case, we have by construction one degree of freedom which accounts for the normalization. Without restrictions, we choose $\xi_1 \neq 0$ freely and only ξ_{-2} is left.

The Tetranacci recursion formula and $\xi_0 = \xi_{-1} = 0$ yields

$$\xi_{-2} \;=\; \eta \, \xi_1 \;+\; \xi_2. \tag{B.1.3}$$

Obviously, ξ_{-2} depends on ξ_1 and on the right boundary. Since the basic Tetranacci polynomials are known to us, we apply the boundary condition for $j = N+1$, $N+2$ on Eq. (B.1.2). One can determine the value of ξ_{-2} as

$$\xi_{-2} \;=\; -\xi_1 \, \frac{\mathcal{T}_1(N+1)}{\mathcal{T}_{-2}(N+1)}, \tag{B.1.4}$$

supposing $\mathcal{T}_{-2}(N+1) \neq 0$. Otherwise, we have

$$\xi_{-2} \;=\; -\xi_1 \, \frac{\mathcal{T}_1(N+2)}{\mathcal{T}_{-2}(N+2)}, \tag{B.1.5}$$

assuming $\mathcal{T}_{-2}(N+2) \neq 0$. The situation of $\mathcal{T}_{-2}(N+1) = T_{-2}(N+2) = 0$ belongs to the degenerate case and is here excluded. For $\mathcal{T}_{-2}(N+2) \neq 0$ and $\mathcal{T}_{-2}(N+1) \neq 0$,

both equations yield the same value of ξ_{-2}, since the four boundary equations are linear dependent by means of the quantization rule. Thus, the non-degenerate eigenvectors are all known. The value of ξ_1 can be set by normalization.

B.2. Degenerate case and the crossing/ avoided crossing criteria

The case of degenerate eigenstates is closely related to the non-degenerate case. Although the quantization rules applies for the crossings, neither their energy nor the associated wavenumbers are initially known. Instead, we assume the eigenvalue λ to be $D \geq 2$ times degenerated. As we show soon, the system by means of the open boundary conditions support only $D = 2$. Due to the hermiticity of the Hamiltonian, we have to find n linear independent eigenvectors $|\psi_{(d)}\rangle = \left(\xi_1^{(d)}, \xi_2^{(d)}, \ldots, \xi_N^{(d)}\right)^{\mathrm{T}}$, where $d = 1, \ldots, D$ denotes the degeneracy. By definition, the entries of these states are all Tetranacci polynomials of the same recursion formula as in the non-degenerate case. Thus, we have

$$\xi_j^{(d)} = \xi_{-2}^{(d)} \mathcal{T}_{-2}(j) + \xi_1^{(d)} \mathcal{T}_1(j), \quad j \in \mathbb{Z}, d = 1, \ldots, D, \tag{B.2.1}$$

where we already used $\xi_{-1} = \xi_0 = 0$ from the boundary condition. Notice, also the basic Tetranacci's inherit the selective property, the degenerate eigenvalue λ is so far unknown to us. In turn, the basic Tetranacci are by now not fixed, as $\zeta = -(\lambda + \mu)/m$ is not. Crucial is, that all basic Tetranacci's obey the same recursion formula which is independent of d since λ is degenerate. This enabled us to write $\mathcal{T}_i(j)$ rather than $\mathcal{T}_i^{(d)}(j)$.

As all degenerate eigenstates share the same $\mathcal{T}_i(j)$, we can exploit this fact by considering suitable superpositions $|\psi_{(1)}\rangle, \ldots, |\psi_{(D)}\rangle$. By definition, these linear combinations are eigenstates associated to λ themselves, i.e. the entries obey the Tetranacci recursion formula. Importantly, the superposition of the eigenstates is pushed forward to the same combinations on the level of $\xi_{-2}^{(d)}, \xi_1^{(d)}$. Since the coefficients for the combinations of $|\psi_{(1)}\rangle, \ldots, |\psi_{(D)}\rangle$ can be chosen, we can always set

$$\xi_1^{(1)} = 1, \quad \xi_{-2}^{(1)} = 0, \tag{B.2.2}$$

$$\xi_1^{(2)} = 0, \quad \xi_{-2}^{(2)} = 1, \tag{B.2.3}$$

without restrictions. In turn and as consequence of Eq. (B.2.1), the vectors $|\psi_{(3)}\rangle, \ldots, |\psi_{(D)}\rangle$ are combinations of $|\psi_{(1)}\rangle$ and $|\psi_{(2)}\rangle$. This violates the constraint of linear independence and the dimension of the eigenspace associated to λ is less or equal 2. Thus, we have only two-fold degeneracies.

Importantly, the setting of $\xi_1^{(1,2)}$ and $\xi_{-2}^{(1,2)}$ implies that the boundary condition gets

effectively separated, as two constraints are always satisfied by triviality. We find

$$\mathcal{T}_1(N+2) = 0, \tag{B.2.4}$$
$$\mathcal{T}_1(N+1) = 0, \tag{B.2.5}$$
$$\mathcal{T}_{-2}(N+2) = 0, \tag{B.2.6}$$
$$\mathcal{T}_{-2}(N+1) = 0. \tag{B.2.7}$$

Converting now the constraints on $\mathcal{T}_{1,2}$ into ones for $\varphi_{1,2}$ using the closed formulas stated in Eqs. (4.2.42)-(4.2.45) grants after several manipulations

$$k_{1,2}d = \frac{j\pi}{N+2}, \quad j = 1, \ldots, N+1, \tag{B.2.8}$$

independently for $k_1 d$ and $k_2 d$. More details of the procedure are shown for the Kitaev chain in appendix I.

The separation of the boundary condition is only a specific situation and thus, the quantization rule in Eq. (3.2.32) must still be obeyed. Further, the Tetranacci character of the eigenvector entries demands that $k_{1,2}d$ obey the equal energy constraint in Eq. (3.2.28). These two constraints impose restriction on $k_{1,2}$ and carried out properly grants the crossing criterion from the main text. The avoided crossings follow in analogy to the Kitaev chain.

As discussed, the crossing criterion determines the energy and sets the relation on the parameters t, m. In turn, λ is known and the basic Tetranacci's are fixed. Thus, the two degenerated states are fixed by Eq. (B.2.1)-(B.2.3), apart from normalization.

C. Simplified expressions for the basic Tetranacci polynomials

A short comment about this section. Just a view days prior before finishing the thesis, I discovered the relations below. These properties of the basic Tetranacci are too useful to pass over but could not be set in the main part of the text anymore. For clarity, we consider the case of generic coefficients η, $\zeta \in \mathbb{C}$ outside of any physical context. We first prove the statement and explain then its usefulness in Eq. (C.0.12).

The stage is set by table C.1 obtained via the generic Tetranacci sequence from Eq. (4.2.1) using the selective property of basic Tetranacci polynomials. Using the marked point in the table as orientation, one can get the impression that the following relation possibly holds

$$\mathcal{T}_1(j) = \mathcal{T}_{-2}(-1-j), \tag{C.0.1}$$
$$\mathcal{T}_0(j) = \mathcal{T}_{-1}(-1-j), \tag{C.0.2}$$

for all $j \in \mathbb{Z}$. Given that the last expressions are true, one can set $l \coloneqq -1-j$ and after renaming, one finds the inverse relations

$$\mathcal{T}_1(-1-j) = \mathcal{T}_{-2}(j), \tag{C.0.3}$$
$$\mathcal{T}_0(-1-j) = \mathcal{T}_{-1}(j), \tag{C.0.4}$$

then again for all $j \in \mathbb{Z}$. Indeed the last four equations are all correct as we show now by induction over j.

j	-3	-2	-1	0	1	2
$\mathcal{T}_{-2}(j)$	η	1	0	0	0	-1
$\mathcal{T}_{-1}(j)$	ζ	0	1	0	0	η
$\mathcal{T}_0(j)$	η	0	0	1	0	ζ
$\mathcal{T}_1(j)$	-1	0	0	0	1	η

Table C.1.: The first few terms for the basic Tetranacci polynomials. The initial values are shown in the center $j = -2, \ldots, 1$. The values for $j = -3$ and $j = 2$ reveal a former hidden relation between the basic Tetranacci polynomials. The black point marks the inversion center.

Proof C.0.1

We show the correctness of Eq. (C.0.1) and Eq. (C.0.2) is analog. Then, Eq. (C.0.3) and Eq. (C.0.3) follow immediately as stated.

Initial values:

Since we deal with Tetranacci polynomials we prove Eq. (C.0.1) for four values of j in a row. We use $j = -3, \ldots, 0$

$$\begin{aligned} \mathcal{T}_{-2}(2) &= -1 \equiv \mathcal{T}_1(-3), && (j=-3) \\ \mathcal{T}_{-2}(1) &= \ 0 \equiv \mathcal{T}_1(-2), && (j=-2) \\ \mathcal{T}_{-2}(0) &= \ 0 \equiv \mathcal{T}_1(-1), && (j=-1) \\ \mathcal{T}_{-2}(-1) &= \ 0 \equiv \mathcal{T}_1(0), && (j=0) \end{aligned}$$

for which Eq. (C.0.1) holds.

Step $\{n-2,\, n-1,\, n,\, n+1\} \to n+2$:

Assume next Eq. (C.0.1), holds already for $n-2$, $n-1$, n and $n+1$ ($n \in \mathbb{Z}$ fixed). Remind that both $\mathcal{T}_{-2}(l)$ and $\mathcal{T}_1(l)$ obey the Tetranacci recursion formula for all $l \in \mathbb{Z}$. Thus, we can write

$$\mathcal{T}_i(l+2) + \mathcal{T}_i(l-2) = \zeta\, \mathcal{T}_i(l) + \eta\, [\mathcal{T}_i(l+1) + \mathcal{T}_i(l-1)] \tag{C.0.5}$$

for $i = -2,\, 1$. As n is an integer, we evaluate the last expression at $l = n$, granting

$$\mathcal{T}_1(n+2) + \mathcal{T}_1(n-2) = \zeta\, \mathcal{T}_1(n) + \eta\, [\mathcal{T}_1(n+1) + \mathcal{T}_1(n-1)]\,. \tag{C.0.6}$$

The assumption that $\mathcal{T}_1(j) = \mathcal{T}_{-2}(-1-j)$ holds for only $j \in \{n-2,\, n-1,\, n,\, n+1\}$ gives

$$\mathcal{T}_1(n+2) + \mathcal{T}_{-2}(1-n) = \zeta\, \mathcal{T}_{-2}(-1-n) + \eta\, [\mathcal{T}_{-2}(-2-n) + \mathcal{T}_{-2}(-n)]\,, \tag{C.0.7}$$

and we are left to identify $\mathcal{T}_1(n+2)$ as $\mathcal{T}_{-2}(-n-3)$. Since Eq. (C.0.5) holds for all integer l, we set $l = -1 - l'$ yielding

$$\mathcal{T}_{-2}(1-l') + \mathcal{T}_{-2}(-l'-3) = \zeta\, \mathcal{T}_{-2}(-1-l') + \eta\, \left[\mathcal{T}_{-2}(-l') + \mathcal{T}_{-2}(-2-l')\right] \tag{C.0.8}$$

for all $l' \in \mathbb{Z}$. We evaluate Eq.(C.0.8) at $l' = n$ which is allowed as n is an integer. We find

$$\mathcal{T}_{-2}(1-n) + \mathcal{T}_{-2}(-n-3) = \zeta\, \mathcal{T}_{-2}(-1-n) + \eta\, [\mathcal{T}_{-2}(-n) + \mathcal{T}_{-2}(-2-n)]\,. \tag{C.0.9}$$

Notice, that Eq. (C.0.7) and Eq. (C.0.8) share the same r.h.s. and $\mathcal{T}_{-2}(1-n)$ on the left. Thus, the difference of Eq. (C.0.7) and Eq. (C.0.8) reads

$$\mathcal{T}_1(n+2) \,-\, \mathcal{T}_{-2}(-n-3) \,=\, 0, \tag{C.0.10}$$

from where we find

$$\mathcal{T}_1(j)|_{j=n+2} \,=\, \mathcal{T}_1(n+2) \overset{\text{Eq. (C.0.10)}}{=} \mathcal{T}_{-2}(-1-(n+2)) \equiv \mathcal{T}_{-2}(-1-j)|_{j=n+2}\,.$$

Thus, Eq. (C.0.1) holds also at $n+2$, i.e. for all integers. □

The proof of Eq. (C.0.2) is analog and thus the Eqs. (C.0.1)-(C.0.4) are indeed all correct as stated. Please notice further, we never specified ζ, η and the derived relations hold always.

Simplified closed form expressions for non-degenerated roots: $\eta^2 + 4\,(\zeta+2) \neq 0$, $\eta \neq 0$

Returning to the statement that the found relations are useful. Remind Eq. (4.2.42)

$$\mathcal{T}_{-2}(j) \,=\, \frac{\varphi_2(j) - \varphi_1(j)}{S_1 - S_2}. \tag{C.0.11}$$

Due to Eq. (C.0.1), we find a much shorter closed form for $\mathcal{T}_1(j)$, namely

$$\mathcal{T}_1(j) \,=\, \frac{\varphi_2(-1-j) - \varphi_1(-1-j)}{S_1 - S_2}, \tag{C.0.12}$$

for all $j \in \mathbb{Z}$ in comparison to Eq. (4.2.45). Using the Eqs. (4.2.36)-(4.2.40) and $\varphi_{1,2}(0) = 0$, $\varphi_{1,2}(1) = 1$, one can easily verify the selective property of $\mathcal{T}_1(j)$ from Eq. (C.0.12). Since $\varphi_{1,2}(j)$ are Tetranaccis, the new form for $\mathcal{T}_1(j)$ is indeed correct.

Further, we apply Eq. (4.2.41)

$$\mathcal{T}_1(j) \,=\, \frac{\varphi_2(-1-j) - \varphi_1(-1-j)}{S_1 - S_2} \overset{\text{Eq. (4.2.41)}}{=} \frac{\varphi_1(j+1) - \varphi_2(j+1)}{S_1 - S_2}, \tag{C.0.13}$$

and thus, we find

$$\mathcal{T}_1(j) \,\equiv\, -\mathcal{T}_{-2}(j+1). \tag{C.0.14}$$

Most remarkable is the simplified form for $\mathcal{T}_1(j)$ which cannot be seen directly from Eq. (4.2.45). On the other side, the closed form expressions for $\mathcal{T}_{-1}(j)$, $\mathcal{T}_0(j)$ from Eqs. (4.2.43), (4.2.44) are similar to the original form for $\mathcal{T}_1(j)$. Since the algebraic way is possible difficult, we may try to guess the result instead. We focus on $\mathcal{T}_0(j)$.

The inspirations was taken from Eq. (C.0.12) and we make the ansatz

$$g(j) \,=\, \frac{\varphi_1(j+2) - \varphi_2(j+2)}{S_1 - S_2}. \tag{C.0.15}$$

j	$g(j)$	$g(j-1)$	$g(j)-(S_1-S_2)g(j-1)$
-2	0	0	0
-1	0	0	0
0	1	0	1
1	S_1-S_2	1	0

Table C.2.: The values of $g(j)$ and $g(j-1)$ allow the construction of $\mathcal{T}_0(j)$.

Here, the idea is to have the denominator of $S_1 - S_2$ and we need both $\varphi_{1,2}$ as otherwise $g(j)$ is a Fibonacci, not a Tetranacci. Using the argument $j+2$, was to ensure that $g(0) = 1$ holds. We have only to show that the function $g(j)$ obeys the selective property of $\mathcal{T}_0(j) = \delta_{0,j}$ for $j = -2, \ldots, 1$ in order to identify $\mathcal{T}_0(j) \to g(j)$.

Exploiting the properties of $\varphi_{1,2}$ in Eqs. (4.2.36)-(4.2.40) and $\varphi_{1,2}(0) = 0$, $\varphi_{1,2}(1) = 1$, one can calculate the values for $g(-2)$, $g(-1)$, $g(0)$ and $g(1)$. Since we have actually $g(j) \equiv \mathcal{T}_1(j+1)$, the ansatz is not correct, but *nearly* as shown in table C.2. One can show that the function $g(j) - (S_1 - S_2)g(j-1)$ has the correct initial values of $\mathcal{T}_0(j)$ and is by construction a Tetranacci. Thus, we have

$$\mathcal{T}_0(j) = \frac{\varphi_1(j+2) - \varphi_2(j+2)}{S_1 - S_2} - (S_1 + S_2)\,\frac{\varphi_1(j+1) - \varphi_2(j+1)}{S_1 - S_2} \tag{C.0.16}$$

and using Eqs. (C.0.13), (C.0.14) grants

$$\mathcal{T}_0(j) \equiv \mathcal{T}_1(j+1) - (S_1 + S_2)\,\mathcal{T}_1(j) \tag{C.0.17}$$

$$\equiv -\mathcal{T}_{-2}(j+2) + (S_1 + S_2)\,\mathcal{T}_{-2}(j+1). \tag{C.0.18}$$

The application of Eq. (C.0.4) grants the expression for $\mathcal{T}_{-1}(j)$. We find

$$\mathcal{T}_{-1}(j) = (S_1 + S_2)\,\frac{\varphi_1(j) - \varphi_2(j)}{S_1 - S_2} - \frac{\varphi_1(j-1) - \varphi_2(j-1)}{S_1 - S_2} \tag{C.0.19}$$

and thus

$$\mathcal{T}_{-1}(j) \equiv (S_1 + S_2)\,\mathcal{T}_1(j-1) - \mathcal{T}_1(j-2) \tag{C.0.20}$$

$$\equiv -(S_1 + S_2)\,\mathcal{T}_{-2}(j) + \mathcal{T}_{-2}(j-1). \tag{C.0.21}$$

D. Closed Form of the basic Tetranacci polynomials for degenerate roots and $\zeta \neq 0$

In the case of degenerated roots $\zeta = -2 - \eta^2/4$, we have $S_1 = S_2$ and thus $r_{\pm 1} = r_{\pm 2}$ following Eqs. (4.2.28), (4.2.29). In other words, r_{+1} (r_{-1}) and r_{+2} (r_{-2}) are linear independent and cannot be used both for a superposition as in Eq. (4.2.31). Still, we need four initial values for a Tetranacci polynomials for $\zeta \neq 0$, as the recursion formula Eq. (4.2.1) demands. Hence, four coefficients for the superposition are mandatory.

One can indeed prove that $j\, r_{\pm 1}^j$ satisfies the Tetranacci recursion formula only if $\zeta = -2 - \eta^2/4$ and we leave the prove for the reader. Importantly, $j\, r_{\pm 1}^j$ is independent of $r_{\pm 1}^j$ granting in total the four required coefficients

$$\xi_j \;=\; A\, r_{+1}^j \;+\; B\, r_{-1}^j \;+\; C\; j\, r_{+1}^j \;+\; D\, j\, r_{-1}^j. \tag{D.0.1}$$

The idea to look for $j\, r_{\pm 1}^j$ of Eq. (4.2.1) was done in analogy to ordinary differential equation of higher order (with constant coefficients), as becomes more apparent by rewriting $r_{+1} = e^{i\, k_1}$ from Eq. (4.3.4). Then, $j\, r_{\pm 1}^j = j e^{i\, k_1\, j}$ appears similar as a solution to the mentioned differential equation in case of degenerated roots of the respective characteristic equation.

The values of A, B, C and D are set by the initial values ξ_{-2}, ξ_{-1}, ξ_0 and ξ_1. Since the representation in terms of basic Tetranacci polynomials in Eq.(4.2.23) is also valid here, we focus on $\mathcal{T}_{-2}(j)$, ..., $\mathcal{T}_1(j)$ rather than ξ_j.

After some algebra one finds

$$\mathcal{T}_{-2}(j) \;=\; \frac{(1-j)\left(r_{+1}^{j+1} \,-\, r_{-1}^{j+1}\right) + (1+j)\left(r_{+1}^{j-1} \,-\, r_{-1}^{j-1}\right)}{\left(r_{+1} \,-\, r_{-1}\right)^3}, \tag{D.0.2}$$

$$\mathcal{T}_{-1}(j) \;=\; \frac{2(1-j)\left(r_{+1}^{j+3} \,+\, r_{-1}^{j+3}\right) - 3j\left(r_{+1}^{j+1} \,+\, r_{-1}^{j+1}\right) + (2+j)\left(r_{+1}^{j-3} \,+\, r_{-1}^{j-3}\right)}{\left(r_{+1} \,-\, r_{-1}\right)^4}, \tag{D.0.3}$$

$$\mathcal{T}_{0}(j) \;=\; \frac{(1-j)\left(r_{+1}^{j+4} \,+\, r_{-1}^{j+4}\right) + 3(j+1)\left(r_{+1}^{j} \,+\, r_{-1}^{j}\right) - 2(2+j)\left(r_{+1}^{j-2} \,+\, r_{-1}^{j-2}\right)}{\left(r_{+1} \,-\, r_{-1}\right)^4}, \tag{D.0.4}$$

and finally

$$\mathcal{T}_1(j) = \frac{j\left(r_{+1}^{j+3} + r_{-1}^{j+3}\right) - 2(j+1)\left(r_{+1}^{j+1} + r_{-1}^{j+1}\right) + (2+j)\left(r_{+1}^{j-1} + r_{-1}^{j-1}\right)}{\left(r_{+1} - r_{-1}\right)^4}. \tag{D.0.5}$$

E. A note on the competition between t and $\triangle$

In the general case with non zero t, Δ and μ we can naively repeat the technique for $t = 0$. The characteristic polynomial adopts still the seemingly harmless structure of the Hamiltonian from Eq. (6.0.2)

$$P_\lambda(\mathcal{H}_{\mathrm{BdG}}) \;=\; \det\left(\lambda \mathbb{1}_{2N} - \mathcal{H}_{\mathrm{BdG}}\right) \;=\; \det\begin{bmatrix} \lambda\mathbb{1}_N - C & -S \\ S & \lambda\mathbb{1}_N + C \end{bmatrix}. \tag{E.0.1}$$

The continuation of the calculation as done prior requires S and $\lambda\mathbb{1}_N + C$ to commute, being now prohibited by $t\Delta \neq 0$ as we show next. We introduce the matrix T_N defined by

$$T_N \coloneqq \begin{bmatrix} 0 & 1 & & & & & & \\ 1 & 0 & 1 & & & & & \\ & 1 & 0 & 1 & & & & \\ & & \ddots & \ddots & \ddots & & & \\ & & & 1 & 0 & 1 & & \\ & & & & 1 & 0 & 1 & \\ & & & & & 1 & 0 & \end{bmatrix}_{N\times N}, \tag{E.0.2}$$

for simplifications and to explain the physical reasonings for the non vanishing commutator after the performed calculation. The structure of C from Eq. (6.0.3) enables us to write $C = -\mu\mathbb{1}_N - t\,T_N$. Thus, $[S,\, \lambda\mathbb{1}_N + C] = [S,\, (\lambda - \mu)\,\mathbb{1}_N - t\,T_N] = -t\,[S,\, T_N]$ becomes independent of the chemical potential and only the matrices with Δ and t remain. Since S from Eq. (6.0.4) and T_N are sparse, we can obtain their commutator at best element wise using $(i,\, j = 1,\, \ldots,\, N)$

$$\begin{aligned} (T_N)_{ij} \;&=\; \delta_{j,i+1} \,+\, \delta_{i,j+1}, \\ S_{ij} \;&=\; \delta_{j,i+1} \,-\, \delta_{i,j+1}, \end{aligned}$$

on $([S,\, T_N])_{mn} \;=\; \sum\limits_{j=1}^{N} \left[(T_N)_{mj}\, S_{jn} \,-\, S_{mj}(T_N)_{jn}\right]$, $m,\, n = 1,\, \ldots,\, N$. We find that

$$\begin{aligned} -t\,([S,\, T_N])_{mn} \;&=\; -2t\Delta \sum_{j=1}^{N} \left[\delta_{m,j+1}\,\delta_{n,j+1} - \delta_{j,n+1}\,\delta_{j,m+1}\right] \\ &=\; -2t\Delta\,\delta_{n,m}\,(1 - \delta_{m,1}) + 2t\Delta\,\delta_{n,m}\,(1 - \delta_{N,n}) \\ &=\; 2t\Delta\,\delta_{n,m}\,(\delta_{1,n} - \delta_{N,n}) \end{aligned} \tag{E.0.3}$$

is zero exclusively for $N = 1$ when t (Δ) does not enter into C (S). In general, the commutator has two non zero elements $2t\Delta$ ($-2t\Delta$) for $m = n = 1$ ($m = n = N$). We conclude $[S,\, C] \neq 0$ and we cannot naturally continue to include $t \neq 0$ with the technique provided by Ref. [99]. In fact, the conflict between t and Δ originates mathematically in Eq. (E.0.3).

Physically, the non vanishing commutator is caused by Pauli's exclusion principle embedded inside the fermionic properties of $d_j^{(\dagger)}$ [91, 114] demanding the anticommutators $\left\{d_j^\dagger,\, d_{j+1}^\dagger\right\}$, $\{d_j,\, d_{j+1}\}$ to vanish. The BdG matrix in Eq. (6.0.2) relies on this aspect and generates in turn the sign modifications of Δ in S from Eq. (6.0.4). Precisely, this sign imbalance prevents $[S,\, C] = 0$, since we could otherwise write $S = \pm\Delta T_N$ granting $[S,\, C] \propto [T_N,\, T_N] = 0$.

F. Kitaev chain: characteristic polynomial at $\mu = 0$

The content of this appendix has been published previously in [4].

For simplicity, we introduce

$$\hat{\Psi}_{\mathrm{M,\,co}} \coloneqq \left(\gamma_1^A, \gamma_1^B, \gamma_2^A, \gamma_2^B, \ldots, \gamma_N^A, \gamma_N^B\right)^{\mathrm{T}}, \tag{F.0.1}$$

such that $\hat{H}_{\mathrm{KC}} = \frac{1}{2}\hat{\Psi}^\dagger_{\mathrm{M,\,co}}\mathcal{H}_{\mathrm{M,\,co}}\hat{\Psi}_{\mathrm{M,\,co}}$ holds. The BdG matrix $\mathcal{H}_{\mathrm{M,\,co}}$ reads

$$\mathcal{H}^{\mathrm{KC}}_{\mathrm{M,\,co}} = \begin{bmatrix} A & B & & & & \\ B^\dagger & A & B & & & \\ & B^\dagger & A & B & & \\ & & \ddots & \ddots & \ddots & \\ & & & B^\dagger & A & B \\ & & & & B^\dagger & A \end{bmatrix}_{2N\times 2N}, \tag{F.0.2}$$

where A, B are

$$A = \begin{bmatrix} 0 & -i\mu \\ i\mu & 0 \end{bmatrix}, \quad B = \begin{bmatrix} 0 & a \\ b & 0 \end{bmatrix}. \tag{F.0.3}$$

We calculate the spectrum at $\mu = 0$ using the to $\mathcal{H}^{\mathrm{KC}}_{\mathrm{M,\,co}}$ associated characteristic polynomial

$$P_\lambda = \det \begin{bmatrix} \lambda\mathbb{1} & -B & & & & \\ -B^\dagger & \lambda\mathbb{1} & -B & & & \\ & -B^\dagger & \lambda\mathbb{1} & -B & & \\ & & \ddots & \ddots & \ddots & \\ & & & -B^\dagger & \lambda\mathbb{1} & -B \\ & & & & -B^\dagger & \lambda\mathbb{1} \end{bmatrix}_{2N\times 2N}. \tag{F.0.4}$$

Due to the block tridiagonal structure, we use the technique given in Ref. [128, 129]. P_λ is then given by a recursive approach

$$\Lambda_j = \lambda\mathbb{1}_2 - B^\dagger\Lambda_{j-1}^{-1}B, \quad \Lambda_1 \coloneqq \lambda\mathbb{1}_2, \tag{F.0.5}$$

where $j = 1, ..., N$ and $P_\lambda = \prod_{j=1}^{N} \det(\Lambda_j)$ holds. The inversion of Λ_j imposes constraints on λ, for instance $\lambda \neq 0$ in the beginning. Thus, we consider λ initially as complex parameter to avoid these issues. However, the final result is independent of those restrictions.

Since Λ_1 is diagonal and B off-diagonal, one can easily show that Λ_j adopts the form $\Lambda_j \coloneqq \begin{bmatrix} x_j & 0 \\ 0 & y_j \end{bmatrix}$ (for all j). The relation between Λ_j and Λ_{j+1} from Eq. (F.0.5) gives

$$\begin{aligned} x_{j+1} &= \lambda + \frac{b^2}{y_j}, \\ y_{j+1} &= \lambda + \frac{a^2}{x_j}, \end{aligned}$$

with $x_1 = y_1 = \lambda$. In general x_j, y_j are fractions. We respect this and set ζ_j, ϵ_j, β_j and δ_j by

$$\begin{aligned} x_j &=: \frac{\zeta_j}{\beta_j}, \\ y_j &=: \frac{\epsilon_j}{\delta_j}, \end{aligned}$$

and one can demand

$$\zeta_1 = \epsilon_1 = \lambda, \tag{F.0.6}$$
$$\beta_1 = \delta_1 = 1. \tag{F.0.7}$$

The recursion formula for x_j (y_j) yields

$$\zeta_{j+1} = \lambda\,\epsilon_j + b^2\,\delta_j, \tag{F.0.8}$$
$$\epsilon_{j+1} = \lambda\,\zeta_j + a^2\,\beta_j, \tag{F.0.9}$$
$$\beta_{j+1} = \epsilon_j, \tag{F.0.10}$$
$$\delta_{j+1} = \zeta_j, \tag{F.0.11}$$

where j starts from 1. Hence, we have in fact

$$\zeta_{j+1} = \lambda\,\epsilon_j + b^2\,\zeta_{j-1}, \tag{F.0.12}$$
$$\epsilon_{j+1} = \lambda\,\zeta_j + a^2\,\epsilon_{j-1}, \tag{F.0.13}$$

and one can read out

$$\zeta_2 = \lambda^2 + b^2, \tag{F.0.14}$$
$$\epsilon_2 = \lambda^2 + a^2. \tag{F.0.15}$$

Starting from the Eqs. (F.0.13), (F.0.12) one can prove the relation $\zeta_j = \epsilon_j$ for all odd integer j. Also the mapping of ζ_l to ϵ_l for all integer l can be shown from here. Further,

Eq. (F.0.14), (F.0.15) show that the setting of the initial values in Eqs. (F.0.6), (F.0.7) yield the same ϵ_j, ζ_j as in the main text.

Extending the sequences of ζ_j and ϵ_j artificially backwards by using their respective recursion formula grants $\zeta_{-1} = \epsilon_{-1} = 0$. Notice, we do not extend x_j, y_j backwards and no corresponding x_0, y_0 or even x_{-1}, y_{-1} expressions exist. They would involve division by 0.

We can find the simplified expression for the characteristic polynomial

$$P_\lambda \;=\; \prod_{j=1}^{N} \det\left(\Lambda_j\right) \;=\; \prod_{j=1}^{N} x_j\, y_j \;=\; \zeta_N\, \epsilon_N, \tag{F.0.16}$$

using the properties of β_j and δ_j. Since the characteristic polynomial is unique and smooth, the r.h.s of Eq. (F.0.16) is. The restictions on λ are thus removed and can be taken as real again. We demonstrated in the main text how the eigenvalues are extracted.

G. Eigenstate entry relation at $\mu = 0$

The alternative expressions for x_l, y_l for even N given in Eqs. (6.2.50), (6.2.51) follow by solving for x_l using $x_{\frac{N}{2}}$ and $x_{\frac{N}{2}+1}$ as initial values. We do so by defining $\tilde{x}_l \coloneqq x_{\frac{N}{2}+1-l}$ with initial values $\tilde{x}_0 = x_{\frac{N}{2}+1}$, $\tilde{x}_1 = x_{\frac{N}{2}}$. Since x_l satisfies Eq. (6.2.43) for all l and this relation is symmetric in $x_{l\pm1}$, $\tilde{x}_l$ obeys this recursion relation as well. Thus, Eq. (4.1.17) is true for $\tilde{x}_l$ and we find

$$\tilde{x}_l \;=\; \tilde{x}_1\,\mathcal{F}(l) \;-\; \tilde{x}_0\,\mathcal{F}(l-1) \;=\; x_{N/2}\,\mathcal{F}(l), \tag{G.0.1}$$

since $\tilde{x}_0 \;=\; x_{\frac{N}{2}+1} \;=\; 0$ holds. The lattice constant of $2d$ for the SSH-like chain yield $\mathcal{F}(l) \;=\; \sin(2kd\,l)\,/\sin(2kd)$. As next step, we replace $\tilde{x}_l$ by its definition using in addition $l' = \frac{N}{2} + 1 - l$ $\tilde{x}_{\frac{N}{2}+1-l'} = x_{l'}$. We get that,

$$x_l \;=\; x_{N/2}\,\mathcal{F}(N/2 + 1 - l), \tag{G.0.2}$$

after renaming $l' \to l$. The remaining step is to show a hidden connection between $x_{N/2}$ and y_1. We use the form for y_l in Eq. (6.2.49) to replace $\mathcal{F}(N/2 + 1 - l)$ by

$$\mathcal{F}(N/2 + 1 - l) \;=\; y_{\frac{N}{2}+1-l}\,\frac{a}{x_1\,E_{\pm}(k)} \;=\; \frac{y_{\frac{N}{2}+1-l}}{y_1}, \tag{G.0.3}$$

and with Eq. (G.0.2) follows

$$x_l \;=\; x_{N/2}\,\frac{y_{\frac{N}{2}+1-l}}{y_1}. \tag{G.0.4}$$

The last expressions is seemingly not helpful; however the boundary condition in its earliest form in Eqs. (6.2.38), (6.2.39) gives rise to a similar expression. In case of $a \neq 0$, $\lambda = E_{\pm}(k) \neq 0$, we divide Eq. (6.2.38) by Eq. (6.2.39) yielding

$$-\frac{y_1}{x_{N/2}} \;=\; \frac{x_1}{y_{N/2}}, \tag{G.0.5}$$

while Eq. (G.0.4) at $l = 1$ states that

$$\frac{y_1}{x_{N/2}} \;=\; \frac{y_{N/2}}{x_1}. \tag{G.0.6}$$

The r.h.s. of the last two expression are the inverses of each other and we thus get

$$\left(\frac{x_{N/2}}{y_1}\right)^2 \;=\; -1 \quad\Rightarrow\quad \frac{x_{N/2}}{y_1} \;=\; \pm\mathrm{i}, \tag{G.0.7}$$

where the signs belong to the states of opposite energy. Replacing our finding back into Eq. (G.0.2) yields

$$x_l \;=\; \pm \mathrm{i} y_1 \, \mathcal{F}(N/2 + 1 - l). \tag{G.0.8}$$

Since x_1 was free to choose and $y_1 = x_1 E_{\pm}^{\mu=0}(k)/a$ holds, we choose $y_1 = \mp \mathrm{i}$. This grants directly Eq. (6.2.50) and Eq. (6.2.49) turns into Eq. (6.2.51).

H. Kitaev chain: Extracting the topological phase diagram from the quantization rule

In this section, we demonstrate how the topological phase diagram is obtained from Eq. (6.3.28) in the limit $N \to \infty$. The idea is to prove that Majorana fermions which are usually no eigenstates of the Kitaev Hamiltonian, become indeed (exact) zero energy eigenstates of $\hat{H}_{\mathrm{KC}}$ in this limit. This statement was proposed prior in the literature and the tendency of decreasing energy for growing system sizes (with open boundary conditions) was already observed, but not proven for open boundary conditions [3, 13]. As a reminder, we consider here initially the finite size Kitaev chain with open boundary conditions and arbitrary values for μ, t and Δ.

Initially, remind the dispersion relation in Eq. (6.3.34) in terms of $k_\Sigma d$, $k_\Delta d$ from which we find that zero energy is meet in case that

$$4\left(t^2-\Delta^2\right)\cos^2\left(k_\Sigma d\right) = \mu^2 \tag{H.0.1}$$

or

$$\left(t^2-\Delta^2\right)\cos^2\left(k_\Delta d\right) = t^2 \tag{H.0.2}$$

holds. Since the entire description of the Kitaev chain is invariant under the exchange of $k_\Sigma d$ and $k_\Delta d$, one of the given expressions is redundant. One can show that the bulk equal energy constraint from Eq. (6.3.27) convert indeed the two expressions into each other. Still, from the finite size perspective Eq. (H.0.1) is still without use, as we do not know if such a $k_\Sigma d$ exists per se and similar for increasing N. However, we showed already prior in Ch. 6.4.2 that

$$1+\left(\frac{\Delta}{t}\right)^2\cot^2(k_\Delta d) = 0 \tag{H.0.3}$$

is equivalent to Eq. (H.0.1), i.e. zero energy. Since Eq. (H.0.3) is part of the quantization rule, the idea is to make suitable choices for $k_\Sigma d$, $k_\Delta d$ such that the l.h.s. of Eq. (6.3.28) vanishes. Thus, this is a criterion for zero energy in the thermodynamic limit. Then, the constraints on μ, t and Δ follow from Eqs. (H.0.1), (H.0.3) and Eq. (6.3.27). Some choices for $k_\Sigma d$, $k_\Delta d$ grant zero energy for $N \to \infty$ and still lead to contradictions for the parameters; these cases are wrong and sometimes difficult to detect.

We start by inspecting Eq. (6.3.26) in order to find relation between $k_{1,2}d$ and in turn on $k_{\Sigma,\Delta} = (k_1 \pm k_2)d/2$. Since the parameters μ, t, Δ are real we find the constraints on the real parts $\mathrm{R}_{1,2} \coloneqq \mathrm{Re}\left(k_{1,2}\right)$ and imaginary parts $\mathrm{I}_{1,2} \coloneqq \mathrm{Im}\left(k_{1,2}\right)$ of $k_{1,2}$

1) $k_1 = k_2^*$.

2) $\mathrm{R}_1 = \mathrm{R}_2 = 0$,

3) $\mathrm{R}_1 = 0$, $\mathrm{R}_2 = \pi$,

4) $\mathrm{I}_1 = \mathrm{I}_2 = 0$,

5) $\mathrm{I}_1 = 0$, $\mathrm{R}_2 = 0$,

6) $\mathrm{I}_1 = 0$, $\mathrm{R}_2 = \pi$.

As one can easily verify, the cases 3) to 6) imposed on the quantization rule in Eq. (6.3.28) in the limit $N \to \infty$ do not grant Eq. (H.0.3). Thus, they do not correspond to zero energy in the thermodynamic limit. Contrary, the cases 1)-3) grant zero energy. We shortly summarize the results.

H.1. Case 1): $k_1 = k_2^*$

For shortness, we introduce r, $p \in \mathbb{R} \setminus \{0\}$ such that $k_1 d = 2r + 2\mathrm{i}p$, $k_2 d = 2r - 2\mathrm{i}p$, i.e. $k_\Sigma d = r$ and $k_\Delta d = \mathrm{i}p$. For $N \to \infty$, the quantization rule reduces to Eq. (H.0.3) which is equivalent to Eq. (H.0.1). Our ansatz imposes $t^2 > \Delta^2$ and $0 < \mu^2 \leq 4\left(t^2 - \Delta^2\right)$ since $0 < \cos^2(r) < 1$ is true. Using that $\cos^2(k_\Delta d) = \cosh^2(p) \geq \cos^2(r)$ demands $4t^2 \geq \mu^2$ from Eq. (H.0.2). These results form a subarea of the topological non trivial phase and rather unsurprisingly originate form the finite N zero energy lines in Eq. (6.3.7) for $N \to \infty$. The last pieces of the topological non-trivial phase are found from the cases 2) and 3). Thus, even for $N \to \infty$ Majorana fermions are not composed by complex conjugate momenta.

H.2. Case 2): $\mathrm{R}_1 = \mathrm{R}_2 = 0$

Here, we introduce $p_{1,2} \in \mathbb{R} \setminus \{0\}$ such that $k_{1,2} d = 2\mathrm{i}\, p_{1,2}$ granting $k_\Sigma d = \mathrm{i}(p_1 + p_2)$ and $k_\Delta d = \mathrm{i}(p_1 - p_2)$. Since the entire description of the Kitaev chain is invariant for $k_2 \to -k_2$ (similar for k_1) and under exchange $k_1 \to k_2$, we demand $p_1 > p_2 > 0$ without restrictions, i.e. $k_\Sigma d > k_\Delta d > 0$. The limit $N \to \infty$ on Eq. (H.0.3) yields

$$1 + \left(\frac{\Delta}{t}\right)^2 \cot^2(k_\Sigma d) = 0 \tag{H.2.1}$$

due to the constraints on $k_{\Sigma,\Delta}$, but has to be carried out carefully as both the numerator and denominator diverge. The gained expression is analog to Eq. (H.0.3) only for exchanged roles of $k_{\Sigma,\Delta}$. In total, we find the constraints $\cosh^2(p_1 + p_2) = t^2/(t^2 - \Delta^2)$ and $4\cosh^2(p_1 - p_2) = \mu^2/(t^2 - \Delta^2)$ from which $t^2 > \Delta^2$, $\mu^2 \geq 4\left(t^2 - \Delta^2\right)$ and $\mu^2 < 4t^2$ follows. Thus, these zero energy modes cover the piece of the topological non trivial phase which lies above the zero energy lines for finite N and is limited by $t^2 > \Delta^2$.

H.3. Case 3): $\mathrm{R}_1 = 0$, $\mathrm{R}_2 = \pi$

Similar as in case 2), we have $p_{1,2} \in \mathbb{R} \setminus \{0\}$ with $p_1 > p_2 > 0$ without restrictions and $k_1 d = 2\mathrm{i}\, p_1$, $k_1 d = \pi + 2\mathrm{i}\, p_2$. Thus, $k_{\Sigma,\Delta} d = \mathrm{i}(p_1 \pm p_2) \pm \frac{\pi}{2}$ holds. Again, the limit $N \to \infty$ on Eq. (H.0.3) has to be done properly grating finally $\cos^2(k_\Sigma d) = t^2/(t^2 - \Delta^2)$ and $4\cos^2(k_\Delta d) = \mu^2/(t^2 - \Delta^2)$. The $\pi/2$ term in $k_\Sigma d$ grants now $\Delta^2 \geq t^2$ and $k_\Delta d$ imposes no contradiction as $\mu^2 \geq 0$ is found. Comparing the cosine expressions for $k_{\Sigma,\Delta} d$ demands $\mu^2 < 4t^2$ since $p_1 + p_2 > p_1 - p_2 > 0$ holds. In turn, the entire topological non-trivial phase is covered with zero energy modes in the limit $N \to \infty$, starting from finite N and open boundary conditions.

A last comment. The cases 1) to 6) are all options to receive zero energy. Since only 1)-3) avoided contradictions and they belonged in the end to the topological non-trivial phase, zero energy is not found in the trivial phase for $N \to \infty$ as expected. However, this does not exclude zero/ near zero or simply in-gap energies for finite N for $\mu^2 > 4t^2$ and $\Delta \neq 0$ per se.

I. Deriving the wavevector quantization for degenerate energies

The content of this appendix has been partially published in [5].

The goal of this appendix is to show how to determine the wavevectors from the boundary condition in Eqs. (6.5.48)-(6.5.51). We focus initially on $\mathcal{T}_{-2}(N+1)=0$, as this yields directly to

$$\mathcal{T}_{-2}(N+1) \;=\; \frac{\varphi_2(N+1)-\varphi_1(N+1)}{S_1-S_2} \stackrel{!}{=} 0 \;\Rightarrow\quad \varphi_2(N+1)=\varphi_1(N+1)\;\&\;S_1\neq S_2. \tag{I.0.1}$$

and we find $\varphi_2(N+1)=\varphi_1(N+1)$ and $S_1\neq S_2$. Importantly, the latter means $k_1\neq\pm k_2$ according to Eq. (4.3.1). The calculation is shortest by keeping $\varphi_{1,2}$ as they are and using only their Fibonacci character from Eq. (4.2.15), namely that $\varphi_l(j+1)=S_l\,\varphi_l(j)-\varphi_l(j-1)$ holds for all j, $l=1,2$ ($\varphi_l(0)=0$, $\varphi_l(0)=1$). These properties imply

$$\begin{aligned}
\varphi_l(2) &= S_l\\
\varphi_l(3) &= S_l^2-1\\
\varphi_l(N+2) &= \varphi_l(2)\,\varphi_l(N+1)-\varphi_l(N)\\
\varphi_l(N+3) &= \varphi_l(3)\,\varphi_l(N+1)-\varphi_l(2)\,\varphi_l(N)\\
\varphi_l(N+4) &= S_l\,\left(S_l^2-2\right)\,\varphi_l(N+1)-\left(S_l^2-1\right)\,\varphi_l(N)
\end{aligned}$$

which we need soon. Next, we focus on $a\,\mathcal{T}_1(N+1)+b\,\mathcal{T}_{-1}(N+1)=0$ in Eq. (6.5.48). The closed forms given in Eqs. (4.2.43), (4.2.45) together with $\varphi_2(N+1)=\varphi_1(N+1)$ imply

$$\begin{aligned}
0 &= a\,\mathcal{T}_1(N+1)\;+\;b\,\mathcal{T}_{-1}(N+1)\\
&= \sum_{l=1}^{2}\{(a+b)\,[\varphi_l(3)\,\varphi_l(N+1)-\varphi_l(2)\varphi_l(N)]-a\,\varphi_{\bar{l}}(2)\,[\varphi_l(2)\varphi_l(N+1)-\varphi_l(N)]\\
&\quad +\varphi_l(N+2)\,[a-b\varphi_l(3)]+b\varphi_l(N)\varphi_{\bar{l}}(2)\}\\
&= \sum_{l=1}^{2}(S_l-S_{\bar{l}})\,[a\varphi_l(N+2)-b\varphi_l(N)]\,.
\end{aligned}$$

In order to derive at the last step, one has to use the given identities for $\varphi_l(2)$, $\varphi_l(3)$ multiple times and once the Fibonacci recursion formula for φ_l. Further, writing down

the sum explicit and rearranging the terms grants

$$\begin{aligned} 0 &= a\,\mathcal{T}_1(N+1) \,+\, b\,\mathcal{T}_{-1}(N+1) \\ &= (S_2 - S_1)\,\{a\,[\varphi_2(N+2) - \varphi_1(N+2)] - b\,[\varphi_2(N) - \varphi_1(N)]\}\,. \end{aligned}$$

Since $S_1 \neq S_2$ the terms inside the curly bracket vanishes; thus, from Eq. (4.2.42) implies $a\mathcal{T}_{-2}(N+2) - b\mathcal{T}_{-2}(N) = 0$. Please notice that Eq. (6.5.51) demands $b\,\mathcal{T}_{-2}(N+1) - a\,\mathcal{T}_{-2}(N) = 0$. Remind, we focus on the case where $a \neq 0$ and $b \neq 0$; hence, we have simply $\mathcal{T}_{-2}(N+2) = \mathcal{T}_{-2}(N) = 0$. Consequently, we have that

$$\varphi_1(n) = \varphi_2(m), \quad m = N,\, N+1,\, N+2, \tag{I.0.2}$$

taking the constraint on $N+1$ from above into account. As three terms in a row of two usually distinct Fibonacci sequences are the same, we have a look at $\varphi_l(N+2) = S_l\,\varphi_l(N+1) - \varphi_l(N)$, $l = 1, 2$ and we find that

$$0 \;=\; (S_1 - S_2)\,F_{1,2}(N+1) = 0, \tag{I.0.3}$$

must hold. Still $S_1 \neq S_2$ and from Eq. (4.3.7) follows then $k_{1,2} = n\pi/(N+1)$, $n = 1, \ldots, N$ as promised. The expressions for $\varphi_l(N+2)$, $\varphi_l(N+3)$ and $\varphi_l(N+4)$ can be used to show that the last and so far not touched boundary condition from Eq. (6.5.49) is indeed satisfied.

J. Criterion for zero energy in case of onsite disorder

One can quite easily show that zero energy lines can extend even for $\Delta^2 > t^2$ due onsite disorder or the real part of the self energies. Since only the sum of self-energies and Kitaev Hamiltonian enters into the retarded GF, we can extract Λ_α from the former and put it into the latter. This procedure replaces μ on the first (last) site by $\mu + \Lambda_L + \nu_1$ ($\mu + \Lambda_R + \nu_N$) for example in Eq. (7.3.29). A basis transformation into the chiral basis $\hat{\psi}_\mathrm{c} = \left(\gamma_1^A, \gamma_2^A, \ldots, \gamma_N^A, \gamma_1^B, \gamma_2^B, \ldots, \gamma_N^B\right)^\mathrm{T}$ yields

$$\tilde{\mathcal{H}}_\mathrm{c} = \begin{bmatrix} 0_{N,N} & \tilde{h} \\ \tilde{h}^\dagger & 0_{N,N} \end{bmatrix}. \tag{J.0.1}$$

Here, we added "$\sim$" to signal that the onsite disorder and the real part of the self energy are now incorporated into $\tilde{h}$

$$\tilde{h} = \begin{bmatrix} -\mathrm{i}(\mu + \Lambda_L + \nu_1) & a & & & & & & \\ -b & -\mathrm{i}\mu & a & & & & & \\ & -b & -\mathrm{i}\mu & a & & & & \\ & & \ddots & \ddots & \ddots & & & \\ & & & -b & -\mathrm{i}\mu & a & & \\ & & & & -b & -\mathrm{i}\mu & a & \\ & & & & & -b & -\mathrm{i}(\mu + \Lambda_R + \nu_N) \end{bmatrix}. \tag{J.0.2}$$

Remind now the standard definition of the retarded GF in frequency space $G_\mathrm{c}^r = (E\mathbb{1}_{2N} - \mathcal{H}_\mathrm{c} - \Sigma_L^r - \Sigma_R^r)^{-1}$ (here w.r.t. $\hat{\psi}_\mathrm{c}$), where only the imaginary part of $\Sigma_{L,R}^r$ acts on $\tilde{\mathcal{H}}_\mathrm{c}$ as the latter already includes the real parts. Thus, we have an *effective* wide band description and high conductance is now caused by zero energy eigenvalues of $\tilde{\mathcal{H}}_\mathrm{c}$. Analogously to the situation discussed for the pure Kitaev chain, we look for zero of $\det(\tilde{\mathcal{H}}_\mathrm{c})$. We have [99]

$$\det(\tilde{\mathcal{H}}_\mathrm{c}) = (-1)^N \left|\det(\tilde{h})\right|^2. \tag{J.0.3}$$

Thus, vanishing eigenvalues $\tilde{\eta}_n$ of $\tilde{h}$ signal now the discrete e^2/h conductance lines. These eigenvalues are [89]

$$\tilde{\eta}_n = -\mathrm{i}\mu + 2\sqrt{\Delta^2 - t^2}\,\cos(\tilde{\theta}_n), \tag{J.0.4}$$

where $\tilde{\theta}_n$ solves

$$0 = \left(\Delta^2 - t^2\right) \sin\left[\tilde{\theta}_n (N+1)\right] - \sqrt{t^2 - \Delta^2}\, (\Lambda_L + \Lambda_R + \nu_1 + \nu_N) \sin\left(N\tilde{\theta}_n\right) - (\Lambda_L + \nu_1)(\Lambda_R + \nu_N) \sin\left[\tilde{\theta}_n (N-1)\right]. \tag{J.0.5}$$

Notice, Eq. (J.0.5) modifies the old criterion for zero energy of the isolated Kitaev chain given in Eq. (6.3.7). Similar to our prior findings, the zero energy lines follow from

$$\mu = 2\sqrt{t^2 - \Delta^2}\cos(\tilde{\theta}_n), \tag{J.0.6}$$

but the values changed $\tilde{\theta}_n \neq n\pi/(N+1)$ $(n = 1, \ldots, N)$. Further, $t^2 < \Delta^2$ is not any more excluded, since $\tilde{\theta}_n$ is not necessarily real as we show below. Still, Eq. (J.0.6) becomes unphysically for non-real values of μ.

We first observe that $\mu = 2\sqrt{\Delta^2 - t^2}\,\mathrm{i}\cos(\tilde{\theta}_n)$ is true and we have only to ask whether or whether not real values of μ are found. Thus, we demand $\mathrm{i}\cos(\tilde{\theta}_n) \in \mathbb{R}$ for a complex $\tilde{\theta}_n =: x + \mathrm{i}y$ with x, y real. Trigonometric identities show that the constraint is satisfied by $x = \pi/2$ and arbitrary y. In order to determine $\tilde{\theta}_n$ fully, we are left to find y. Hence, we next focus on the terms like $\sin(\tilde{\theta}_n j)$ $(j \in \mathbb{Z})$ from Eq. (J.0.5). We find

$$\sin(\tilde{\theta}_n j) = \begin{cases} \mathrm{i}(-1)^{\frac{j}{2}} \sinh(y\,j) & j \text{ even} \\ (-1)^{\frac{j-1}{2}} \cosh(y\,j) & j \text{ odd} \end{cases}, \tag{J.0.7}$$

by inserting $x = \pi/2$. The required expressions for $\sin(\tilde{\theta}_n j)$ for $j = N \pm 1, N$ depend thus on N even/ odd. For N even we get

$$0 = \left(\Delta^2 - t^2\right) \cosh\left[y\,(N+1)\right] - \sqrt{\Delta^2 - t^2}\,(\Lambda_L + \Lambda_R + \nu_1 + \nu_N) \sinh(yN) + (\Lambda_L + \nu_1)(\Lambda_R + \nu_N) \cosh\left[y\,(N-1)\right] \tag{J.0.8}$$

and similarly for odd N

$$0 = \left(\Delta^2 - t^2\right) \sinh\left[y\,(N+1)\right] + \sqrt{\Delta^2 - t^2}\,(\Lambda_L + \Lambda_R + \chi_1 + \chi_N) \cosh(yN) + (\Lambda_L + \chi_1)(\Lambda_R + \chi_N) \sinh\left[y\,(N-1)\right]. \tag{J.0.9}$$

All coefficients became real and in turn one can find real solution(s) for y. However, the existence of y is still an issue of the involved parameters. Further, the ansatz for $\tilde{\theta}_n$ yields to $\mu = 2\sqrt{\Delta^2 - t^2}\,\sinh(y)$. Consequently, the zero energy/ e^2/h conductance lines may leak out into the region associated to the topologically trivial phase depending on the concrete values of y.

For large but still finite values of N such that $N + 1 \approx N, N - 1$ holds, we find $\tilde{\theta}_n \approx n\pi/(N+1)$ $(n = 1, \ldots, N)$ as solutions. Thus, for large N the line change due to $\Lambda_L + \nu_1$, $\Lambda_R + \nu_N$ declines and the zero energy lines approach the ones of the isolated Kitaev chain, i.e. they are limited to the parameters of the topologically non-trivial phase.

K. Exact expression for $G^r_{1,N}$, $G^r_{1,N+1}$ and $G^r_{1,2N}$

The content of this appendix has been published in [5].

The current formula in Eq. (8.1.1) requires $G^r_{1,N}$ $G^r_{1,N+1}$ and $G^r_{1,2N}$. These entries can be calculated analytically using the site-ordered Majorana basis $\hat{\Psi}_{\mathrm{M,\,co}} \coloneqq \left(\gamma_1^A, \gamma_1^B, \ldots, \gamma_N^A, \gamma_N^B\right)^{\mathrm{T}}$ since the Kitaev Hamiltonian and the self energies are reshaped into a block tridiagonal matrix, see Eq. (K.0.1) below. One can compare $\hat{\Psi}_{\mathrm{M,\,co}}$ with the standard BdG basis $\hat{\psi}_{\mathrm{BdG}} = \left(d_1, \ldots, d_N, d_1^\dagger, \ldots, d_N^\dagger\right)^{\mathrm{T}}$ and extract a basis transformation matrix. These matrix relates the retarded GF of both descriptions and after some algebra we find

$$
\begin{aligned}
G^r_{1,N+1} &= \frac{1}{2}\left\{(G^r_{\mathrm{M}})_{11} - (G^r_{\mathrm{M}})_{22} + i\left[(G^r_{\mathrm{M}})_{12} + (G^r_{\mathrm{M}})_{21}\right]\right\}, \\
G^r_{1,N} &= \frac{1}{2}\Big\{(G^r_{\mathrm{M}})_{1,2N-1} + (G^r_{\mathrm{M}})_{2,2N} \\
&\quad + i\left[(G^r_{\mathrm{M}})_{2,2N-1} - (G^r_{\mathrm{M}})_{1,2N}\right]\Big\}. \\
G^r_{1,2N} &= \frac{1}{2}\Big\{(G^r_{\mathrm{M}})_{1,2N-1} - (G^r_{\mathrm{M}})_{2,2N} \\
&\quad + i\left[(G^r_{\mathrm{M}})_{2,2N-1} + (G^r_{\mathrm{M}})_{1,2N}\right]\Big\},
\end{aligned}
$$

where G^r_{M} is defined in the basis of $\hat{\Psi}_{\mathrm{M,\,co}}$. Contrary to $G^r_{1,N}$ $G^r_{1,N+1}$ and $G^r_{1,2N}$, the entries of G^r_{M} *can* be calculated analytically using the method provided by Ref. [129]. As one finds in the end, the problem to determine $G^r_{1,N}$ $G^r_{1,N+1}$ and $G^r_{1,2N}$ is associated to non-linear combination of Tetranacci polynomials. The calculation is very long, intricate and requires several tricks. We state here only the initial situation and the results.

We define the matrix $\mathcal{M}$ in case of $N \neq 1$ as

$$
\begin{aligned}
\mathcal{M} &\coloneqq E\,\mathbb{1}_{2N} - \mathcal{H}_{\mathrm{M}} - \Sigma^r_{L,\mathrm{M}} - \Sigma^r_{R,\mathrm{M}} = \\
&= \begin{bmatrix}
\mathbf{A}_L & \mathbf{B} & & & & & \\
\mathbf{C} & \mathbf{A}_2 & \mathbf{B} & & & & \\
 & \mathbf{C} & \mathbf{A}_3 & \mathbf{B} & & & \\
 & & \ddots & \ddots & \ddots & & \\
 & & & \mathbf{C} & \mathbf{A}_{N-1} & \mathbf{B} & \\
 & & & & \mathbf{C} & \mathbf{A}_R &
\end{bmatrix},
\end{aligned}
\tag{K.0.1}
$$

where we set $(j = 2\,, \ldots, N-1)$

$$\mathbf{A}_j \;=\; \begin{bmatrix} E & i\mu \\ -i\mu & E \end{bmatrix}, \quad \mathbf{C}^\dagger = \mathbf{B} = \begin{bmatrix} 0 & -a \\ -b & 0 \end{bmatrix},$$
$$\mathbf{A}_\alpha \;= \mathbf{A}_2 \;+\; \begin{bmatrix} \sigma_{\alpha,p} & i\,\sigma_{\alpha,m} \\ -i\,\sigma_{\alpha,m} & \sigma_{\alpha,p} \end{bmatrix},$$

and $a = i(\Delta - t)$, $b = i(t + \Delta)$ as usual. In order to shorten the expressions, we introduced

$$\sigma_{\alpha,p} = -\frac{\Lambda_\alpha^+ \,+\, \Lambda_\alpha^-}{2} \,+\, \mathrm{i}\,\frac{\gamma_\alpha^+ \,+\, \gamma_\alpha^-}{2} \tag{K.0.2}$$
$$\sigma_{\alpha,m} = \frac{\Lambda_\alpha^+ \,-\, \Lambda_\alpha^-}{2} \,-\, \mathrm{i}\,\frac{\gamma_\alpha^+ \,-\, \gamma_\alpha^-}{2} \tag{K.0.3}$$

where $\Lambda_\alpha^\pm$, $\gamma_\alpha^\pm$are taken from Eqs. (7.4.14), (7.4.15). For $N = 1$, we have

$$\mathcal{M} \;=\; \mathbf{A}_2 + \sum_{\alpha=L,R} \begin{bmatrix} \sigma_{\alpha,p} & i\,\sigma_{\alpha,m} \\ -i\,\sigma_{\alpha,m} & \sigma_{\alpha,p} \end{bmatrix}.$$

In general, we have

$$G_{\mathrm{M}}^r \;=\; \mathcal{M}^{-1}. \tag{K.0.4}$$

Notice, the final expressions for $G_{1,N+1}^r$, $G_{1,N}^r$ and $G_{1,2N}^r$ unite the cases of $N = 1$ and $N \neq 1$. As first step, we consider the characteristic polynomial of the isolated Kitaev chain and include the self-energies in a second step; thus granting $\det(\mathcal{M})$ required for the inversion of $\mathcal{M}$. The method stated in Ref. [129] yields

$$\det\left(E\,\mathbb{1}_{2N} - \mathcal{H}_{\mathrm{M}}\right) \;=\; (-ab)^N \,\left(x_N\,\mathcal{Y}_N \;-\; y_N\,\chi_N\right), \tag{K.0.5}$$

where the functions x_N, $\mathcal{Y}_N$, y_N, χ_N are Tetranacci polynomials of order N. At first glance they obey two sets of coupled equations. The first is

$$x_{j+1} = \frac{-\mathrm{i}\mu}{b}\,x_j \,+\, \frac{a}{b}\,x_{j-1} \,+\, \frac{E}{b}\,y_j, \tag{K.0.6a}$$
$$\chi_{j+1} = \frac{-\mathrm{i}\mu}{b}\,\chi_j \,+\, \frac{a}{b}\,\chi_{j-1} \,+\, \frac{E}{b}\,\mathcal{Y}_j, \tag{K.0.6b}$$
$$y_{j+1} = \frac{\mathrm{i}\mu}{a}\,y_j \,+\, \frac{b}{a}\,y_{j-1} \,+\, \frac{E}{a}\,x_j, \tag{K.0.6c}$$
$$\mathcal{Y}_{j+1} = \frac{\mathrm{i}\mu}{a}\,\mathcal{Y}_j \,+\, \frac{b}{a}\,\mathcal{Y}_{j-1} \,+\, \frac{E}{a}\,\chi_j, \tag{K.0.6d}$$

and the second reads

$$x_{j+1} = \frac{-\mathrm{i}\mu}{b}\,x_j \,+\, \frac{a}{b}\,x_{j-1} \,+\, \frac{E}{a}\,\chi_j, \tag{K.0.7a}$$
$$\chi_{j+1} = \frac{\mathrm{i}\mu}{a}\,\chi_j \,+\, \frac{b}{a}\,\chi_{j-1} \,+\, \frac{E}{b}\,x_j, \tag{K.0.7b}$$
$$y_{j+1} = \frac{-\mathrm{i}\mu}{b}\,y_j \,+\, \frac{a}{b}\,y_{j-1} \,+\, \frac{E}{a}\,\mathcal{Y}_j, \tag{K.0.7c}$$
$$\mathcal{Y}_{j+1} = \frac{\mathrm{i}\mu}{a}\,\mathcal{Y}_j \,+\, \frac{b}{a}\,\mathcal{Y}_{j-1} \,+\, \frac{E}{b}\,y_j.. \tag{K.0.7d}$$

j	x_j	$\mathcal{Y}_j$	χ_j	y_j
-3	$\frac{\mathrm{i}\mu\, b}{a^2}$	$\frac{-\mathrm{i}\mu\, a}{b^2}$	$\frac{-E}{b}$	$\frac{-E}{a}$
-2	$\frac{b}{a}$	$\frac{a}{b}$	0	0
-1	0	0	0	0
0	1	1	0	0
1	$\frac{-\mathrm{i}\mu}{b}$	$\frac{\mathrm{i}\mu}{a}$	$\frac{E}{b}$	$\frac{E}{a}$

Table K.2.: The first terms of the Tetranacci sequences for x_j, y_j, χ_j and $\mathcal{Y}_j$.

One can show, that x_j, $\mathcal{Y}_j$, y_j, χ_j indeed obey the Tetranacci recursion formula for the Kitaev chain, e.g.

$$\begin{aligned} x_{j+2} \;=\; & \frac{E^2+a^2+b^2-\mu^2}{ab}\, x_j \;-\; x_{j-2} \\ & +\; \mathrm{i}\mu \frac{b-a}{ab}\,(x_{j-1}-x_{j+1})\,. \end{aligned} \tag{K.0.8}$$

In table K.2, we show their initial values and Eq. (4.2.23) gives their closed form expression. By definition $G^r_{1,N}$ $G^r_{1,N+1}$, $G^r_{1,2N}$ and $\det(\mathcal{M})$ depend also on the self-energies. After several manipulations and using the technique provided by Ref. [129] and can cast the self-energy contributions into coefficients. In particular the terms from Σ^r_R can be absorbed into four new Tetranacci polynomials d^y_j, $d^{\mathcal{Y}}_j$, d^x_j and d^χ_j. Explicitly, we have

$$d^y_j \;\coloneqq\; \sigma_{R,p}\; x_{j-1} \;+\mathrm{i}\,\sigma_{R,m}\; y_{j-1} \;+\; a\, y_j, \tag{K.0.9}$$

$$d^{\mathcal{Y}}_j \;\coloneqq\; \sigma_{R,p}\; \chi_{j-1} \;+\mathrm{i}\,\sigma_{R,m}\; \mathcal{Y}_{j-1} \;+\; a\, \mathcal{Y}_j, \tag{K.0.10}$$

$$d^x_j \;\coloneqq\; \sigma_{R,p}\; y_{j-1} \;-\mathrm{i}\,\sigma_{R,m}\; x_{j-1} \;+\; b\, x_j, \tag{K.0.11}$$

$$d^\chi_j \;\coloneqq\; \sigma_{R,p}\; \mathcal{Y}_{j-1} \;-\mathrm{i}\,\sigma_{R,m}\; \chi_{j-1} \;+\; b\, \chi_j. \tag{K.0.12}$$

All four obey again Eq. (K.0.8) and their initial values follow from Eqs. (K.0.9)- (K.0.12) and table K.2.

In the end, we have

$$\begin{aligned}\frac{\det(\mathcal{M})}{(-ab)^{N-1}} &= d_N^y\, d_N^\chi - d_N^x\, d_N^\mathcal{Y} + \frac{\sigma_{L,m}^2 - \sigma_{L,p}^2}{ab}\left[d_{N-1}^y\, d_{N-1}^\chi - d_{N-1}^x\, d_{N-1}^\mathcal{Y}\right] \\ &+ \frac{\sigma_{L,p}}{b}\left[d_N^y\, d_{N-1}^x - d_N^x\, d_{N-1}^y\right] + \frac{\sigma_{L,p}}{a}\left[d_N^\chi\, d_{N-1}^\mathcal{Y} - d_N^\mathcal{Y}\, d_{N-1}^\chi\right] \\ &+ \mathrm{i}\frac{\sigma_{L,m}}{a}\left[d_N^y\, d_{N-1}^\chi - d_N^x\, d_{N-1}^\mathcal{Y}\right] + \mathrm{i}\frac{\sigma_{L,m}}{b}\left[d_N^\mathcal{Y}\, d_{N-1}^x - d_N^\chi\, d_{N-1}^y\right], \quad \text{(K.0.13)}\end{aligned}$$

and $G_{1,N+1}^r$, $G_{1,N}^r$ and $G_{1,2N}^r$ read

$$\begin{aligned}G_{1,N+1}^r \frac{2\det(\mathcal{M})}{(-ab)^{N-2}} &= \frac{b^2}{a}\left[d_{N-2}^\mathcal{Y}\, d_{N-1}^\chi - d_{N-1}^\mathcal{Y}\, d_{N-2}^\chi\right] + \frac{a^2}{b}\left[d_{N-2}^y\, d_{N-1}^x - d_{N-1}^y\, d_{N-2}^x\right] \\ &+ \mathrm{i}a\left[d_{N-1}^\chi\, d_{N-2}^y - d_{N-1}^\mathcal{Y}\, d_{N-2}^x\right] - \mathrm{i}b\left[d_{N-1}^x\, d_{N-2}^\mathcal{Y} - d_{N-1}^y\, d_{N-2}^\chi\right], \quad \text{(K.0.14)}\end{aligned}$$

$$\begin{aligned}G_{1,2N}^r \frac{2\det(\mathcal{M})}{(-ab)^{N-1}} &= \frac{b}{a}\left[d_{N-2}^\chi - \mathrm{i}\, d_{N-2}^\mathcal{Y}\right] - \frac{a}{b}\left[d_{N-2}^y + \mathrm{i}\, d_{N-2}^x\right] \\ &+ \left(E - \Lambda_L^+ + \mathrm{i}\gamma_L^+ - \mu\right)\left[\frac{d_{N-1}^x - \mathrm{i}d_{N-1}^y}{b} - \frac{d_{N-1}^\mathcal{Y} + \mathrm{i}d_{N-1}^\chi}{a}\right], \quad \text{(K.0.15)}\end{aligned}$$

$$\begin{aligned}G_{1,N}^r \frac{2\det(\mathcal{M})}{(-ab)^{N-1}} &= \frac{b}{a}\left[d_{N-2}^\chi + \mathrm{i}\, d_{N-2}^\mathcal{Y}\right] + \frac{a}{b}\left[d_{N-2}^y - \mathrm{i}\, d_{N-2}^x\right] \\ &+ \left(E - \Lambda_L^+ + \mathrm{i}\gamma_L^+ - \mu\right)\left[\frac{d_{N-1}^x + id_{N-1}^y}{b} + \frac{d_{N-1}^\mathcal{Y} - \mathrm{i}d_{N-1}^\chi}{a}\right]. \quad \text{(K.0.16)}\end{aligned}$$

The results for $\det(\mathcal{M})$, $G_{1,N+1}^r$, $G_{1,N}^r$ and $G_{1,2N}^r$ are generic and exact. They apply all values of N, t, Δ, μ, E. The wide band limit is not used and the findings can be easily generalized to the case with onsite disorder on the last and/or on the first site.

My attempts to simplify the given expressions further, failed completely as non-linear recursion formulae for the Tetranacci polynomials d_j^y, $d_j^\mathcal{Y}$, d_j^x and d_j^χ are required. Although one finds many (and very easy) for x_N, $\mathcal{Y}_N$, y_N, χ_N during the calculation of Eq. (K.0.5), those non-linear relations depend on the initial values of Tetranacci polynomials and do not generalize to d_j^y, $d_j^\mathcal{Y}$, d_j^x and d_j^χ.

L. Derivation: conductance formulae

The content of this appendix has been published in [5] for the special wide-band limit case.

The conductance formulae G_{D}, G_{A} and G_{CA} defined in Eqs. (8.1.2)-(8.1.4) are required for the total conductance G from Eq. (8.1.5). We consider a generic bias situation in the beginning and demonstrate how G_{D}, G_{A} and G_{CA} are found from the GFs in Eqs. (K.0.14)-(K.0.16). Further, we consider the non-wide band situation, in which also the real parts of the self-energy enter.

The conductance at $T = 0\,\mathrm{K}$ relies on $|G^r_{1,N}|^2_{E=0}$, $|G^r_{1,N+1}|^2_{E=0}$ and $|G^r_{1,2N}|^2_{E=0}$. Notice, that the Tetranacci polynomials x_j, $\mathcal{y}_j$, y_j, χ_j at $E = 0$ are automatically decoupled and reduce to Fibonacci polynomials can be seen from Eqs. (K.0.6d)-(K.0.6). We have $\chi_j|_{E=0} = y_j|_{E=0} = 0$ from table K.2 and $x_{j,0} \coloneqq x_j|_{E=0}$, $\mathcal{y}_{j,0} \coloneqq \mathcal{y}_j|_{E=0}$ are

$$x_{j,0} = \frac{R_+^{j+1} - R_-^{j+1}}{R_+ - R_-}, \quad R_\pm = \frac{-\mathrm{i}\mu \pm \sqrt{4\,ab - \mu^2}}{2b}, \tag{L.0.1}$$

$$\mathcal{y}_{j,0} = \left(-\frac{b}{a}\right)^j x_{j,0} \tag{L.0.2}$$

In turn, d_j^y, $d_j^{\mathcal{y}}$, d_j^x and d_j^χ simplify to

$$\begin{aligned}
d_j^y|_{E=0} &= \mathrm{i}\,\gamma_R\; x_{j-1,0},\\
d_j^\chi|_{E=0} &= \mathrm{i}\,\gamma_R\; \mathcal{y}_{j-1,0},\\
d_j^{\mathcal{y}}|_{E=0} &= a\,\mathcal{y}_{j,0} + \mathrm{i}\Lambda_R\,\mathcal{y}_{j-1,0},\\
d_j^x|_{E=0} &= b\,x_{j,0} - \mathrm{i}\Lambda_R\,x_{j-1,0},
\end{aligned}$$

according to their definition in Eqs. K.0.9 - K.0.12. Further, we evaluate $\det(\mathcal{M})$ in Eq.

(K.0.13) at $E = 0$ and use Eq. (L.0.2). After some algebra one finds

$$\begin{aligned}\det\left(\mathcal{M}\right)|_{E=0}\, b^{2-2N} \;=\; & b^2\, x_{N,0}^2 - x_{N-1,0}^2\left(\gamma_L^2+\gamma_R^2\,+\,\Lambda_R^2\,+\,\Lambda_L^2\right)\\ & +\, x_{N-2,0}^2\,\left(\gamma_L^2\,+\,\Lambda_L^2\right)\left(\gamma_R^2\,+\,\Lambda_R^2\right)\, b^{-2},\\ & +\,\frac{2\mathrm{i}}{b}\, x_{N-1,0}\, x_{N-2,0}\left[\Lambda_R\,\left(\gamma_L^2\,+\,\Lambda_L^2\right)\,+\,\Lambda_L\,\left(\gamma_R^2\,+\,\Lambda_R^2\right)\right]\\ & -\,2\mathrm{i}b\, x_{N,0}\, x_{N-1,0}\,\left(\Lambda_R\,+\,\Lambda_L\right)\\ & -\,\gamma_L\gamma_R\left(x_{N-1,0}^2 - x_{N,0}\, x_{N-2,0}\right)\,\frac{a^{2N-2}+b^{2N-2}}{(-ab)^{N-1}}\\ & -\,2\Lambda_R\Lambda_L\left(x_{N-1,0}^2 + x_{N,0}\, x_{N-2,0}\right)\end{aligned} \tag{L.0.3}$$

Analogously, we have

$$G_{1,2N}^r\big|_{E=0} \;=\; (-1)^N\,\frac{a^{N-1}\,-\,(-b)^{N-1}}{2\det\left(\mathcal{M}\right)|_{E=0}}\, g_+, \tag{L.0.4}$$

$$G_{1,N}^r\big|_{E=0} \;=\; (-1)^{N-1}\,\frac{a^{N-1}\,+\,(-b)^{N-1}}{2\det\left(\mathcal{M}\right)|_{E=0}}\, g_-, \tag{L.0.5}$$

$$G_{1,N+1}^r\big|_{E=0} \;=\; -\mathrm{i}\,\gamma_R\,\frac{a^{2N-2}\,-\,b^{2N-2}}{2\det\left(\mathcal{M}\right)|_{E=0}}, \tag{L.0.6}$$

in terms of the function g_s $(s = \pm 1)$

$$g_s \coloneqq b^{N-1}\left[\mathrm{i}s\, b\, x_{N,0} + x_{N-1,0}\left(\mathrm{i}\gamma_R - \mathrm{i}\, s\gamma_L + s\Lambda_R + s\Lambda_L\right) - \frac{\mathrm{i}}{b} x_{N-2,0}\left(\mathrm{i}\gamma_L - \Lambda_L\right)\left(\mathrm{i}\gamma_R + s\Lambda_R\right)\right]. \tag{L.0.7}$$

One can prove easily from Eq. (K.0.6) and table K.2 that $x_{j,0}$ is real for all j. This information is crucial to demonstrate that

$$\begin{aligned}-|b^{1-N}\, g_s|^2 \;=\; & b^2\, x_{N,0}^2 - x_{N-1,0}^2\left[(\Lambda_R+\Lambda_L)^2 + (\gamma_R - s\,\gamma_L)^2\right]\\ & +\, x_{N-2,0}^2\, b^{-2}\,\left(\gamma_L^2\,+\,\Lambda_L^2\right)\left(\gamma_R^2\,+\,\Lambda_R^2\right) - 2\mathrm{i}\, b\, x_{N,0}\, x_{N-1,0}\,\left(\Lambda_R\,+\,\Lambda_L\right)\\ & -\,2\, x_{N,0}\, x_{N-2,0}\,\left(s\gamma_L\gamma_R + \Lambda_L\Lambda_R\right)\\ & +\,\frac{2\mathrm{i}}{b} x_{N-1,0}\, x_{N-2,0}\left[\Lambda_L\,\left(\gamma_R^2\,+\,\Lambda_R^2\right)\,+\,\Lambda_R\,\left(\gamma_L^2\,+\,\Lambda_L^2\right)\right]\end{aligned} \tag{L.0.8}$$

holds, using $s^2 = 1$ during the derivation. Importantly, the last expression appears similar to $\det\left(\mathcal{M}\right)|_{E=0}$. Indeed, we have

$$\det\left(\mathcal{M}\right)|_{E=0} = (-1)^N|g_s|^2 - \gamma_L\gamma_R\left[a^{N-1} + s(-b)^{N-1}\right]^2, \tag{L.0.9}$$

where $(-1)^{N-1}$ originates from b^{N-1} inside the absolute value from Eq. (L.0.8). In order to find Eq. (L.0.9), one needs to add and remove the terms $2s\,\gamma_L\,\gamma_R x_{N-1,0}^2\,+$ $2s\,\gamma_L\,\gamma_R x_{N,0} x_{N-2,0}$ to Eq. (L.0.3). Further, one relies on the identity

$$x_{j-1,0}^2 - x_{j,0}\, x_{j-2,0} \;=\; \left(-\frac{a}{b}\right)^{j-1}, \tag{L.0.10}$$

for $x_{j,0}$ which can be found with Eq. (L.0.1).

Next, we translate the findings from $a = -\mathrm{i}\,m$, $b = \mathrm{i}\,p$ into $p = t + \Delta$ and $m = t - \Delta$. The function q_s from the main text in Eq. (8.1.18) satisfies $|q_s|^2 = |g_s|^2$. In turn, one receives the expressions for G_A, G_CA and G_D from Eqs. (8.1.6)-(8.1.8).

In case of symmetric applied bias $V_L = -V_R = V/2$, the conductance $G = G_\mathrm{D} + G_\mathrm{A}$. We have

$$\begin{aligned}\frac{|2\det(\mathcal{M})|_{E=0}|^2}{4\gamma_L\gamma_R}\,\frac{h}{e^2}\,G \;&=\; \left(p^{N-1}+m^{N-1}\right)^2|q_-|^2 \;+\; \gamma_L\,\gamma_R\left(p^{2N-2}-m^{2N-2}\right)^2 \\ &= \left(p^{N-1}+m^{N-1}\right)^2\left[|q_-|^2+\gamma_L\gamma_R\left(m^{N-1}-p^{N-1}\right)^2\right], \quad \text{(L.0.11)}\end{aligned}$$

which is Eq. (8.1.12) after reordering.

For $V_L = V$, $V_R = 0$, we have $G = G_\mathrm{D} + G_\mathrm{CA} + 2\,G_\mathrm{A}$. Inserting the Eqs. (L.0.4)-(L.0.6) in G grants after reordering that

$$\begin{aligned}\frac{1}{4\gamma_L\gamma_R}\,\frac{G\,h}{e^2} \;=\; &\frac{\left(p^{2N-2}+m^{2N-2}\right)\left[|g_-|^2+|g_+|^2+2\gamma_L\gamma_R\left(p^{2N-2}+m^{2N-2}\right)\right]}{\left[|g_-|^2+|g_+|^2+2\gamma_L\gamma_R\left(p^{2N-2}+m^{2N-2}\right)\right]^2} \\ &+\; 2(mp)^{N-1}\,\frac{|g_-|^2-|g_+|^2-4\gamma_L\gamma_R(mp)^{N-1}}{\left[|g_-|^2+|.g_+|^2+2\gamma_L\gamma_R\left(p^{2N-2}+m^{2N-2}\right)\right]^2} \qquad \text{(L.0.12)}\end{aligned}$$

Here we used Eq. (L.0.9) for $s = +1$ and $s = -1$ to derive an expression for $\det(\mathcal{M})|_{E=0}$ in terms of both g_- and g_+. From Eq. (L.0.8) follows that $|g_-|^2 - |g_+|^2 - 4\gamma_L\gamma_R(mp)^{N-1} = 0$. Canceling the common factor in the first fraction and first reinserting $\det(\mathcal{M})|_{E=0}$ in the denominator and second using Eq. (L.0.8) for $s = +1$ grants Eq. (8.1.20) via $|q_s|^2 = |g_s|^2$.

M. Spectrum and self-energies

We consider first the trivial example of an linear chain in presence of two leads. The retarded GF for this setup can be directly extracted from the one for the Kitaev chain at $\Delta = 0$ shown in Eq. (7.4.32) by restricting to the electronic degrees of freedoms $C-$. Alternatively, one can calculate straightforwardly the N-N-N transport setup for the linear chain, i.e. Eq. (2.1.1), and the leads given in Eq. (7.3.2). For simplicity I recommend the tunneling Hamiltonian from Eq. (7.3.3) in this case. Either way, in wide band limit the inverse of the retarded GF in frequency space is

$$(G^r_{\mathrm{LC}})^{-1} = \begin{bmatrix} E+\mu+\mathrm{i}\gamma_L & t & & & & & & & \\ t & E+\mu & t & & & & & & \\ & t & E+\mu & t & & & & & \\ & & \ddots & \ddots & \ddots & & & & \\ & & & t & E+\mu & t & & & \\ & & & & t & E+\mu & t & & \\ & & & & & t & E+\mu & t & \\ & & & & & & t & E+\mu+\mathrm{i}\gamma_R \end{bmatrix}. \tag{M.0.1}$$

Here, $\gamma_{L,R}$ are real constants and represent the imaginary part of the self-energies. As usual, the retarded GF is the inverse of $E\mathbb{1}_N - \mathcal{H}_{\mathrm{LC}} - \Sigma^r_L - \Sigma^r_R$. The used basis is $\hat{\psi} = (d_1, \ldots, d_N)^{\mathrm{T}}$ such that $\hat{H}_{\mathrm{LC}} = \hat{\psi}^\dagger \mathcal{H}_{\mathrm{LC}} \hat{\psi}$ holds and $\hat{H}_{\mathrm{LC}}$ is taken from Eq. (2.1.1). Thus, the determinant of Eq. (M.0.1) yields the characteristic polynomial of the linear chain in presence of the leads. One can easily demonstrate that $\gamma_R\gamma_L$ change the real parts of the eigenvalues compared to $\gamma_L = 0$ or $\gamma_R = 0$

One can straightforwardly calculate $\det\left[E\mathbb{1}_N - \mathcal{H}_{\mathrm{LC}}\right] =: \theta_N$ [78]. We have

$$\theta_j = \mathcal{F}(j) \tag{M.0.2}$$

using Eq. (4.1.6) and $\mathcal{F}(j)$ is defined in (4.1.5). Further, $2R_\pm = E+\mu \pm \sqrt{(E+\mu)^2 - 4t^2}$ holds. Including $\gamma_{L,R}$ grants

$$\det\left(E\mathbb{1}_N - \mathcal{H}_{\mathrm{LC}} - \Sigma^r_L - \Sigma^r_R\right) = \mathcal{F}(N) - \gamma_L\,\gamma_R \mathcal{F}(N-2) + \mathrm{i}\left(\gamma_L + \gamma_R\right)\mathcal{F}(N-2). \tag{M.0.3}$$

Apparently the eigenvalues of the isolated system, i.e. $\mathcal{F}(N) = 0$, are changed due to $\gamma_{L,R}$. Although, $\gamma_L\,\gamma_R$ may be small itself, the term is weighted for instance by the hopping parameter t hidden in $\mathcal{F}(N-2)$. Notice the effect of $\gamma_L\,\gamma_R$ is largest around

eigenvalues of the isolated linear chain as $\mathcal{F}(N) = 0$ does not imply[1] $\mathcal{F}(N-2) = 0$. A quantization rule can be derived by applying Eq. (4.1.13). For similar results consult Ref. [88–90]. Notice, the effect of $\gamma_{L,R}$ to change the real parts of the eigenvalues is not a topological property, as the linear chain is topologically trivial.

In case of the Kitaev chain, we consider for simplicity $\mu = 0$ and the wide band limit. The general result is given in appendix K and only complicates the issue. The SSH-like basis from chapter 6.2 is most suitable for the calculation. We have a block diagonal structure

$$\mathcal{H}_{\text{SSH,open}} \,=\, E\,\mathcal{H}_{\text{SSH}} \,-\, \Sigma_{L,\text{SSH}} \,-\, \Sigma_{R,\text{SSH}} \,=\, \begin{bmatrix} P_N & \\ & Q_N \end{bmatrix}, \tag{M.0.4}$$

where P_N is

$$P_N \,=\, \begin{bmatrix} E+\mathrm{i}\gamma_L & -a & & & & & & \\ a & E & -b & & & & & \\ & b & E & -a & & & & \\ & & \ddots & \ddots & \ddots & & & \\ & & & a & E & -b & & \\ & & & & b & E & -a & \\ & & & & & a & E+\mathrm{i}\gamma_R \end{bmatrix} \tag{M.0.5}$$

for N even. The expression for odd N follows by removing the last line and last row in Eq. (M.0.5). Further, Q_N is follows always from P_N by exchanging $a = \mathrm{i}(\Delta - t)$ and $b = \mathrm{i}\,(\Delta + t)$. For your convenience, P_N (Q_N) is related to $\mathcal{H}_\alpha$ ($\mathcal{H}_\beta$) as can be seen from Eqs. (6.2.6), (6.2.7). Using the technique from Ref. [78] and the properties of $\det(\mathcal{H}_\alpha) = \epsilon_N$, $\det(\mathcal{H}_\beta) = \zeta_N$ given in section 6.2 or appendix F, one can derive the exact results

$$\det(P_N) \,=\, \epsilon_N \,-\, \gamma_L\,\gamma_R\,\zeta_{N-2} \,+\, \mathrm{i}\,(\gamma_R\,\epsilon_{N-1} \,+\, \gamma_L\,\zeta_{N-1}) \tag{M.0.6}$$

$$\det(Q_N) \,=\, \zeta_N \,-\, \gamma_L\,\gamma_R\,\epsilon_{N-2} \,+\, \mathrm{i}\,(\gamma_R\,\zeta_{N-1} \,+\, \gamma_L\,\epsilon_{N-1}) \tag{M.0.7}$$

for all N. The closed form expressions for ϵ_j, ζ_j ($j \in \mathbb{Z}$) are stated in Eqs. (6.2.23)-(6.2.20). The results for $\det(P_N)$, $\det(Q_N)$ can be proven via induction over N using an initial separation into even and odd N. I recommend to set first $\gamma_R = 0$ and to include $\gamma_R \neq 0$ in a second step manually exploiting the recursion formula in Ref. [78]. The proof is trivial and the result for $\det(Q_N)$ follows directly by exchanging a's and b's. Inserting the closed form expression for $\mathcal{F}(n) \propto \sin(2kd\,n)$ yields the quantization stated in Ref. [89] for $2kd \equiv \theta_k$ there.

Most importantly, are the second terms in Eqs. (M.0.6), (M.0.7). The minus sign originates from $\mathrm{i}^2 = -1$ and the term changes the real part of the eigenvalues of P_N, Q_N as $\gamma_{L,R} \in \mathbb{R}$. Since the characteristic polynomial of the Kitaev chain at $\mu = 0$ in presence of the leads (wide band limit) is given by the product $\det(P_N) \cdot \det(Q_N)$, their real part is changed as well.

[1] For finite t, the spectrum of the linear chain for N and $N-2$ are distinct.

N. Minimal model: Green's functions and self-energies

The retraded GF is

$$\boldsymbol{G}^r_{\mathrm{MM}} \,=\, (E\,\mathbb{1}_2 \,-\, \mathrm{i}\epsilon\,\tau_z\,\tau_x \,-\, \Sigma^r_L \,-\, \Sigma^r_R)^{-1}\,, \tag{N.0.1}$$

and the retarded self-energy is $\boldsymbol{\Sigma}^r_\alpha \,=\, \sum\limits_k \boldsymbol{V}_\alpha\,\tau_z\,\boldsymbol{g}^r_{k\alpha,k\alpha}\,\tau_z\,\boldsymbol{V}^\dagger_\alpha$, or explicitly

$$\boldsymbol{\Sigma}^r_\alpha \,=\, \lim_{\eta\to 0}\sum_k \begin{bmatrix} \frac{|V_{\alpha,\,\mathrm{A}}(k)|^2}{E-\epsilon_{k\alpha}+\mathrm{i}\eta} \,+\, \frac{|V_{\alpha,\,\mathrm{A}}|^2}{E+\epsilon_{k\alpha}+\mathrm{i}\eta} & \frac{V_{\alpha,\,\mathrm{A}}V^*_{\alpha,\,\mathrm{B}}}{E-\epsilon_{k\alpha}+\mathrm{i}\eta} \,+\, \frac{V^*_{\alpha,\,\mathrm{A}}V_{\alpha,\,\mathrm{B}}}{E+\epsilon_{k\alpha}+\mathrm{i}\eta} \\ \frac{V^*_{\alpha,\,\mathrm{A}}V_{\alpha,\,\mathrm{B}}}{E-\epsilon_{k\alpha}+\mathrm{i}\eta} \,+\, \frac{V_{\alpha,\,\mathrm{A}}V^*_{\alpha,\,\mathrm{B}}}{E+\epsilon_{k\alpha}+\mathrm{i}\eta} & \frac{|V_{\alpha,\,\mathrm{B}}(k)|^2}{E-\epsilon_{k\alpha}+\mathrm{i}\eta} \,+\, \frac{|V_{\alpha,\,\mathrm{B}}|^2}{E+\epsilon_{k\alpha}+\mathrm{i}\eta} \end{bmatrix}. \tag{N.0.2}$$

As usual we have $\boldsymbol{G}^a_{\mathrm{MM}} \,=\, (\boldsymbol{G}^r_{\mathrm{MM}})^\dagger$ and $\Gamma_\alpha \,=\, -2\mathrm{Im}\,(\boldsymbol{\Sigma}^r_\alpha)$. The quantities $\boldsymbol{\Gamma}^\pm_\alpha$ from the main text are the respective electron and hole parts, i.e. $\boldsymbol{\Gamma}_\alpha \,=\, \boldsymbol{\Gamma}^+_\alpha \,+\, \boldsymbol{\Gamma}^-_\alpha$ holds. We have

$$\boldsymbol{\Gamma}^-_\alpha(E) \,=\, 2\pi\sum_k \delta(E-\epsilon_{k\alpha}) \begin{bmatrix} |V_{\alpha,\,\mathrm{A}}(k)|^2 & V_{\alpha,\,\mathrm{A}}(k)\,V^*_{\alpha,\,\mathrm{B}}(k) \\ V^*_{\alpha,\,\mathrm{A}}(k)\,V_{\alpha,\,\mathrm{B}}(k) & |V_{\alpha,\,\mathrm{B}}(k)|^2 \end{bmatrix}, \tag{N.0.3}$$

$$\boldsymbol{\Gamma}^+_\alpha(E) \,=\, \mathcal{P}\,\boldsymbol{\Gamma}^-_\alpha(-E)\,\mathcal{P} \tag{N.0.4}$$

and $\mathcal{P} \,=\, \mathbb{1}_2\,\mathcal{K}$ denotes the particle-hole symmetry.

O. Rashba nanowire: Imaginary part of the sub-gap wavevector

The imaginary part q can be calculated exploiting the zero energy condition in a suitable fashion. Doubling $E_-(k_j)$ yields

$$\begin{aligned} 2E_-(k_j) \,=\, E_-(k_1) \,+\, E_-(k_2) \,&=\, \sum_{j=1,2} \xi_-^2(k_j) \,+\, \Delta_\mathrm{p}^2(k_j) \\ &\quad +\, 2\Delta_\mathrm{p}(k_1)\Delta_\mathrm{p}(k_2) \,-\, 2\Delta_\mathrm{p}(k_1)\Delta_\mathrm{p}(k_2) \\ &=\, \left[\Delta_\mathrm{p}(k_2) + \Delta_\mathrm{p}(k_1)\right]^2 \,+\, \left[\xi_-^2(k_1) - \xi_-^2(k_2)\right]^2, \end{aligned} \tag{O.0.1}$$

where we used that $E_-(k_j) = 0$ implies $\Delta_\mathrm{p}(k_j) \,=\, \pm\mathrm{i}\xi_-(k_j)$. In weak spin orbit approximation, Δ_p is linear in k. Since $k_1 = k_2^*$ and $(k_1 + k_2)/2 = n\pi/L$ holds, we find

$$\left(\frac{2\pi n}{L}\right)\left(\frac{\Delta\,\alpha_\mathrm{R}}{V_\mathrm{Z}}\right) \,+\, \left[\xi_-^2(k_1) - \xi_-^2(k_2)\right]^2 = 0. \tag{O.0.2}$$

Exploiting the weak spin orbit expression for $\xi_-^2(k)$ from Eq. (10.2.7) together with the substitution $\Delta\,\sinh(x_j) \coloneqq \hbar^2\,k_j^2/(2m) \,-\, \mu$ ($j = 1, 2$, $x_j \in \mathbb{C}$) grants

$$\cosh(x_1) - \cosh(x_2) \,=\, \pm\mathrm{i}\,\frac{\alpha_\mathrm{R}}{V_\mathrm{Z}}\,\frac{2\pi n}{L}. \tag{O.0.3}$$

Importantly, we can use Eq. (O.0.3) in order to eliminate terms in Eq. (10.2.9). We find

$$\left(\frac{\hbar^2}{2m}\right)^2 \left(k_1^4 - k_2^4\right) \,+\, \left(\frac{\Delta^2\,\alpha_\mathrm{R}^2}{V_\mathrm{Z}^2} - \frac{\hbar^2\mu}{m}\right) \,-\, 2\mathrm{i}\,\alpha_\mathrm{R}\Delta\,\frac{2\pi n}{L} \,=\, 0, \tag{O.0.4}$$

which is the equation of a hyperbola. Using binomic identities and that $k_1 + k_2 = 2\pi n/L$ gives a depressed cubic equation

$$(k_1 - k_2)^3 \,+\, g\,(k_1 - k_2) - 4\mathrm{i}\,\alpha_\mathrm{R}\Delta\left(\frac{2m}{\hbar}\right)^2 \,=\, 0 \tag{O.0.5}$$

with $k_1 - k_2 = 2\mathrm{i}\,q$. The coefficient g reads

$$g \,=\, 2\left[\left(\frac{2\pi n}{L}\right)^2 \,+\, \left(\frac{2m\,\Delta\,\alpha_\mathrm{R}}{\hbar^2\,V_\mathrm{Z}}\right)^2 \,-\, \frac{4\,m\mu}{\hbar^2}\right]. \tag{O.0.6}$$

and solving for q yields Eq. (10.2.15).

P. Rashba nanowire: retarded Green's functions and rate matrices

The rate matrices for the electronic degrees of freedom are

$$\Gamma^e_\alpha(k_1,\, k_2,\, E) \,=\, 2\pi\, t^2 \rho_\alpha(E)\, e^{-\mathrm{i}\,(k_1 - k_2^*)\, x_\alpha} \,\times \\ \times \begin{bmatrix} (u^*_{k_1}\, u_{k_2} \,+\, v^*_{k_1}\, v_{k_2})\, m^*_{k_1}\, m_{k_2} & (u^*_{k_1}\, v_{k_2} \,+\, v^*_{k_1}\, u_{k_2})\, m^*_{k_1}\, n_{k_2} \\ (u^*_{k_1}\, v_{k_2} \,+\, v^*_{k_1}\, u_{k_2})\, n^*_{k_1}\, m_{k_2} & (u^*_{k_1}\, u_{k_2} \,+\, v^*_{k_1}\, v_{k_2})\, n^*_{k_1}\, n_{k_2} \end{bmatrix}$$

with $x_L \,=\, -L/2$, $x_R \,=\, L/2$. Here, ρ_α is the density of states for lead α and t is the tunneling amplitude in $t_{\alpha p k} \,=\, t \exp[-\mathrm{i}(p - k) x_\alpha]$ from Eq. (10.4.4). For the hole components we have

$$\Gamma^h_\alpha(k_1,\, k_2,\, E) \,=\, 2\pi\, t^2 \rho_\alpha(-E)\, e^{-\mathrm{i}\,(k_1 - k_2^*)\, x_\alpha} \,\times \\ \times \begin{bmatrix} (u_{\bar{k}_1}\, u^*_{\bar{k}_2} \,+\, v_{\bar{k}_1}\, v^*_{\bar{k}_2})\, n_{\bar{k}_1}\, n^*_{\bar{k}_2} & (u_{\bar{k}_1}\, v^*_{\bar{k}_2} \,+\, v_{\bar{k}_1}\, u^*_{\bar{k}_2})\, n_{\bar{k}_1}\, m^*_{\bar{k}_2} \\ (u_{\bar{k}_1}\, v^*_{\bar{k}_2} \,+\, v_{\bar{k}_1}\, u^*_{\bar{k}_2})\, m_{\bar{k}_1}\, n^*_{\bar{k}_2} & (u_{\bar{k}_1}\, u^*_{\bar{k}_2} \,+\, v_{\bar{k}_1}\, v^*_{\bar{k}_2})\, m_{\bar{k}_1}\, m^*_{\bar{k}_2} \end{bmatrix},$$

and $\bar{k} = -k$. The retarded GF has to be obtained via the Dyson equation

$$G^r(k_1,\, k_2,\, E) \,=\, g^r(k_1,\, E) \left[\delta_{k_1 k_2} \,+\, \sum_{k_3, \alpha} \Sigma^r_\alpha(k_1,\, k_2,\, E)\, G^r(k_3,\, k_2,\, E) \right], \qquad \text{(P.0.1)}$$

where g^r is the retarded GF of the isolated (low energy) nanowire Hamiltonian $\mathcal{H}_-$

$$g^r(k_1,\, E) \,=\, \lim_{\eta \to 0} \left[(E \,+\, \mathrm{i}\eta)\, \mathbb{1}_2 \,-\, \mathcal{H}_-(k_1) \right]^{-1}. \qquad \text{(P.0.2)}$$

As usual $G^a(k_1,\, k_2,\, E) = [G^r(k_1,\, k_2,\, E)]^\dagger$ holds. The (complete) retarded self-energies are

$$\Sigma^r_\alpha(k_1,\, k_2,\, E) \,=\, \sum_p \left[T_{\alpha p k_1}\, g^r_{p\alpha}\, T_{\alpha p k_2} \,+\, S_{\alpha p k_1}\, g^r_{p\alpha}\, S_{\alpha p k_2} \right] \qquad \text{(P.0.3)}$$

related to the rate matrices by $\Gamma_\alpha \,=\, -2\mathrm{Im}\,(\Sigma^r_\alpha)$ and p runs over the momenta of the leads. Here, we used the abbreviations

$$T_{\alpha p k} \,=\, \begin{bmatrix} t^*_{\alpha p k} v^*_k m^*_k & t_{\alpha \bar{p} \bar{k}} v_{\bar{k}} n_{\bar{k}} \\ t^*_{\alpha p k} u^*_k n^*_k & t_{\alpha \bar{p} \bar{k}} u_{\bar{k}} m_{\bar{k}} \end{bmatrix}, \qquad \text{(P.0.4)}$$

$$S_{\alpha p k} \,=\, \begin{bmatrix} t^*_{\alpha p k} v^*_k m^*_k & t_{\alpha \bar{p} \bar{k}} v_{\bar{k}} n_{\bar{k}} \\ t^*_{\alpha p k} u^*_k n^*_k & t_{\alpha \bar{p} \bar{k}} u_{\bar{k}} m_{\bar{k}} \end{bmatrix}, \qquad \text{(P.0.5)}$$

and $g^r_{p\alpha}$ is the retarded self energy of the isolated leads, i.e.

$$g^r_{p\alpha} \;=\; \lim_{\eta\to 0}\,\left[(E \,+\, \mathrm{i}\eta)\,\mathbb{1}_2 \,-\, \epsilon_{p\alpha}\,\tau_z\right]^{-1}. \tag{P.0.6}$$

List of figures

Bibliography

[1]B. Stoker, *Dracula* (Archibald Constable and Company (London), 1897).

[2]A. Y. Kitaev, "Unpaired Majorana fermions in quantum wires", Phys. Usp. **44**, 131–136 (2001).

[3]S. D. Sarma, J. D. Sau, and T. D. Stanescu, "Splitting of the zero-bias conductance peak as smoking gun evidence for the existence of the Majorana mode in a superconductor-semiconductor nanowire", Phys. Rev. B **86**, 220506 (2012).

[4]N. Leumer, M. Marganska, B. Muralidharan, and M. Grifoni, "Exact eigenvectors and eigenvalues of the finite Kitaev chain and its topological properties", Journal of Physics: Condensed Matter **32**, 445502 (2020).

[5]N. Leumer, M. Grifoni, B. Muralidharan, and M. Marganska, "Linear and nonlinear transport across a finite Kitaev chain: An exact analytical study", Phys. Rev. B **103**, 165432 (2021).

[6]J. Alicea, "Majorana fermions in a tunable semiconductor device", Phys. Rev. B **81**, 125318 (2010).

[7]R. Aguado, "Majorana quasiparticles in condensed matter", La Rivista del Nuovo Cimento **40**, 523 (2017).

[8]J. Klinovaja and D. Loss, "Composite Majorana fermion wave functions in nanowires", Phys. Rev. B **86**, 085408 (2012).

[9]R. V. Mishmash, D. Aasen, A. P. Higginbotham, and J. Alicea, "Approaching a topological phase transition in Majorana nanowires", Phys. Rev. B **93**, 245404 (2016).

[10]Y. Oreg, G. Refael, and F. von Oppen, "Helical Liquids and Majorana Bound States in Quantum Wires", Phys. Rev. Lett. **105**, 177002 (2010).

[11]C. Fleckenstein, F. Domínguez, N. T. Ziani, and B. Trauzettel, "Decaying spectral oscillations in a Majorana wire with finite coherence length", Phys. Rev. B **97**, 155425 (2018).

[12]E. B. Hansen, "Majorana Bound States in Semiconductor-Superconductor Hybrid Devices", PhD thesis (University of Copenhagen, Faculty of Science, Niels Bohr Institute, 2018).

[13]G. Ben-Shach, A. Haim, I. Appelbaum, Y. Oreg, A. Yacoby, and B. I. Halperin, "Detecting Majorana modes in one-dimensional wires by charge sensing", Phys. Rev. B **91**, 045403 (2015).

[14]D. Rainis, L. Trifunovic, J. Klinovaja, and D. Loss, "Towards a realistic transport modeling in a superconducting nanowire with Majorana fermions", Phys. Rev. B **87**, 024515 (2013).

[15]E. Prada, R. Aguado, and P. San-Jose, "Measuring Majorana nonlocality and spin structure with a quantum dot", Phys. Rev. B **96**, 085418 (2017).

[16]A. Kobiałka, T. Domański, and A. Ptok, "Delocalisation of Majorana quasiparticles in plaquette–nanowire hybrid system", Sci. Rep. **9**, 1–12 (2019).

[17]J. Danon, A. B. Hellenes, E. B. Hansen, L. Casparis, A. P. Higginbotham, and K. Flensberg, "Nonlocal Conductance Spectroscopy of Andreev Bound States: Symmetry Relations and BCS Charges", Phys. Rev. Lett. **124**, 036801 (2020).

[18]J. D. Bjorken and S. D. Drell, *Relativistische Quantenmechanik* (Bibliographisches Institut AG, Mannheim, 1966).

[19]S. R. Elliott and M. Franz, "Colloquium: Majorana fermions in nuclear, particle, and solid-state physics", Rev. Mod. Phys. **87**, 137–163 (2015).

[20]F. Wilczek, "Majorana returns", Nature Physics **5**, 614–618 (2009).

[21]M. Leijnse and K. Flensberg, "Introduction to topological superconductivity and Majorana fermions", Semicond. Sci. Technol. **27**, 124003 (2012).

[22]M. Tinkham, *Introduction to Superconductivity* (McGraw-Hill Book Co., New York, 2004).

[23]C. Chamon, R. Jackiw, Y. Nishida, S.-Y. Pi, and L. Santos, "Quantizing Majorana fermions in a superconductor", Phys. Rev. B **81**, 224515 (2010).

[24]R. M. Lutchyn, J. D. Sau, and S. D. Sarma, "Majorana Fermions and a Topological Phase Transition in Semiconductor-Superconductor Heterostructures", Phys. Rev. Lett. **105**, 077001 (2010).

[25]M. Deng, S. Vaitiekėnas, E. B. Hansen, J. Danon, M. Leijnse, K. Flensberg, J. Nygård, P. Krogstrup, and C. M. Marcus, "Majorana bound state in a coupled quantum-dot hybrid-nanowire system", Science **354**, 1557–1562 (2016).

[26]Ö. Gül, H. Zhang, J. D. S. Bommer, M. W. A. de Moor, D. Car, S. R. Plissard, E. P. A. M. Bakkers, A. Geresdi, K. Watanabe, and T. Taniguchi, "Ballistic Majorana nanowire devices", Nat. Nanotechnology **13**, 192–197 (2018).

[27]E. Prada, P. San-Jose, M. W. A. de Moor, A. Geresdi, E. J. H. Lee, J. Klinovaja, D. Loss, J. Nygård, R. A. L. P., and Kouwenhoven, "From Andreev to Majorana bound states in hybrid superconductor-semiconductor nanowires", Nat. Rev. Phys. **2**, 575–594 (2020).

[28]P. Szumniak, D. Chevallier, D. Loss, and J. Klinovaja, "Spin and charge signatures of topological superconductivity in Rashba nanowires", Phys. Rev. B **96**, 041401 (2017).

[29]J. D. Sau, R. M. Lutchyn, S. Tewari, and S. D. Sarma, "Generic New platform for Topological Quantum Computation Using Semiconductor Heterostructures", Phys. Rev. Lett. **104**, 040502 (2010).

[30]M. Marganska, L. Milz, W. Izumida, C. Strunk, and M. Grifoni, "Majorana quasiparticles in semiconducting carbon nanotubes", Phys. Rev. B **97**, 075141 (2018).

[31]W. Izumida, L. Milz, M. Marganska, and M. Grifoni, "Topology and zero energy edge states in carbon nanotubes with superconducting pairing", Phys. Rev. B **96**, 125414 (2017).

[32]L. Milz, W. Izumida, M. Grifoni, and M. Marganska, "Transverse profile and three-dimensional spin canting of a Majorana state in carbon nanotubes", Phys. Rev. B **100**, 155417 (2019).

[33]J. D. Sau and S. Tewari, "Topological superconducting state and Majorana fermions in carbon nanotubes", Phys. Rev. B **88**, 054503 (2013).

[34]S. Nadj-Perge, I. K. Drozdov, B. A. Bernevig, and A. Yazdani, "Proposal for realizing Majorana fermions in chains of magnetic atoms on a superconductor", Phys. Rev. B **88**, 020407 (2013).

[35]S. Nadj-Perge, I. K. Drozdov, J. Li, H. Chen, S. Jeon, J. Seo, A. H. MacDonald, B. A. Bernevig, and A. Yazdani, "Observation of Majorana fermions in ferromagnetic atomic chains on a superconductor", Science **346**, 602–607 (2014).

[36]J. Klinovaja, P. Stano, A. Yazdani, and D. Loss, "Topological Superconductivity and Majorana Fermions in RKKY Systems", Phys. Rev. Lett. **111**, 186805 (2013).

[37]A. A. Zvyagin, "Possibility of Direct Observation of Edge Majorana Modes in Quantum Chains", Phys. Rev. Lett. **110**, 217207 (2013).

[38]H. Kim, A. Palacio-Morales, T. Posske, L. Rózsa, K. Palotás, L. Szunyogh, M. Thorwart, and R. Wiesendanger, "Toward tailoring Majorana bound states in artificially constructed magnetic atom chains on elemental superconductors", Sci. Adv. **4**, eaar5251 (2018).

[39]C.-K. Chiu, J. C. Y. Teo, A. P. Schnyder, and S. Ryu, "Classification of topological quantum matter with symmetries", Rev. Mod. Phys. **88**, 035005 (2016).

[40]A. B. Bernevig and T. L. Hughes, *Topological Insulators and Topological Superconductors* (Princeton University Press, 2013).

[41]A. Altland and M. R. Zirnbauer, "Nonstandard symmetry classes in mesoscopic normal-superconducting hybrid structures", Phys. Rev. B **55**, 1142–1161 (1997).

[42]A. Udupa, A. Banerjee, K. Sengupta, and D. Sen, "One-dimensional spin–orbit coupled Dirac system with extended s-wave superconductivity: Majorana modes and Josephson effects", Journal of Physics: Condensed Matter **33**, 145301 (2021).

[43]P. San-Jose, E. Prada, and R. Aguado, "Ac Josephson Effect in Finite-Length Nanowire Junctions with Majorana Modes", Phys. Rev. Lett. **108**, 257001 (2012).

[44]P. Sriram, S. S. Kalantre, K. Gharavi, J. Baugh, and B. Muralidharan, "Supercurrent interference in semiconductor nanowire josephson junctions", Phys. Rev. B. **100**, 155431 (2019).

[45]J. S. Lim, R. Lopez, and L. Serra, "Transport through Majorana nanowires attached to normal leads", New J. Phys. **14**, 083020 (2012).

[46]J. Ulrich and F. Hassler, "Majorana-assisted nonlocal electron transport through a floating topological superconductor", Phys. Rev. B **92**, 075443 (2015).

[47]X.-Q. Li and L. Xu, "Nonlocality of Majorana zero modes and teleportation: Self-consistent treatment based on the Bogoliubov–de Gennes equation", Phys. Rev. B **101**, 205401 (2020).

[48]K. Flensberg, "Tunneling characteristics of a chain of Majorana bound states", Phys. Rev. B **82**, 180516 (2010).

[49]K. T. Law, P. A. Lee, and T. K. Ng, "Majorana Fermion Induced Resonant Andreev Reflection", Phys. Rev. Lett. **103**, 237001 (2009).

[50]D. E. Liu and H. U. Baranger, "Detecting a Majorana-fermion zero mode using a quantum dot", Phys. Rev. B **84**, 201308 (2011).

[51]L. S. Ricco, F. A. Dessotti, I. A. Shelykh, M. S. Figueira, and A. C. Seridonio, "Tuning of heat and charge transport by Majorana fermions", Scientific reports **8**, 1–8 (2018).

[52]C.-X. Liu, J. D. Sau, T. D. Stanescu, and S. D. Sarma, "Andreev bound states versus Majorana bound states in quantum dot-nanowire-superconductor hybrid structures: Trivial versus topological zero-bias conductance peaks", Phys. Rev. B **96**, 075161 (2017).

[53]A. Vuik, B. Nijholt, A. R. Akhmerov, and M. Wimmer, "Reproducing topological properties with quasi-Majorana states", SciPost Phys. **7**, 61 (2019).

[54]H. Pan and S. D. Sarma, "Physical mechanisms for zero-bias conductance peaks in Majorana nanowires", Phys. Rev. Res. **2**, 013377 (2020).

[55]O. Dmytruk, D. Loss, and J. Klinovaja, "Pinning of Andreev bound states to zero energy in two-dimensional superconductor- semiconductor Rashba heterostructures", Phys. Rev. B **102**, 245431 (2020).

[56]C.-X. Liu, J. D. Sau, T. D. Stanescu, and S. D. Sarma, "Andreev bound states versus Majorana bound states in quantum dot-nanowire-superconductor hybrid structures: Trivial versus topological zero-bias conductance peaks", Phy. Rev. B **96**, 075161 (2017).

[57]J. Chen, B. D. Woods, P. Yu, M. Hocevar, D. Car, S. R. Plissard, E. Bakkers, T. D. Stanescu, and S. M. Frolov, "Ubiquitous Non-Majorana Zero-Bias Conductance Peaks in Nanowire Devices", Phys. Rev. Lett. **123**, 107703 (2019).

[58]B. D. Woods, J. Chen, S. M. Frolov, and T. D. Stanescu, "Zero-energy pinning of topologically trivial bound states in multiband semiconductor-superconductor nanowires", Phys. Rev. B **100**, 125407 (2019).

[59]M. T. Deng, S. Vaitiekėnas, E. Prada, P. San-Jose, J. Nygård, P. Krogstrup, R. Aguado, and C. M. Marcus, "Nonlocality of Majorana modes in hybrid nanowires", Phys. Rev. B **98**, 085125 (2018).

[60]M. Hell, K. Flensberg, and M. Leijnse, "Distinguishing Majorana bound states from localized Andreev bound states by interferometry", Phys. Rev. B **97**, 161401 (2018).

[61]H. Zhang, D. E. Liu, M. Wimmer, and L. P. Kouwenhoven, "Next steps of quantum transport in Majorana nanowire devices", Nature Commun. **10**, 1–7 (2019).

[62]S. D. Sarma and H. Pan, "Disorder-induced zero-bias peaks in Majorana nanowires", Phys. Rev. B **103**, 195158 (2021).

[63]S. D. Sarma, M. Freedman, and C. Nayak, "Majorana zero modes and topological quantum computation", npj Quantum Information **1**, 1–13 (2015).

[64]D. Aasen, M. Hell, R. V. Mishmash, A. Higginbotham, J. Danon, M. Leijnse, T. S. Jespersen, J. A. Folk, C. M. Marcus, K. Flensberg, and J. Alicea, "Milestones Toward Majorana-Based Quantum Computing", Phys. Rev. X **6**, 031016 (2016).

[65]T. E. O'Brien, P. Rożek, and A. R. Akhmerov, "Majorana-Based Fermionic Quantum Computation", Phys. Rev. Lett. **120**, 220504 (2018).

[66]J. Alicea, "New directions in the pursuit of Majorana fermions in solid state systems", Reports on progress in physics **75**, 076501 (2012).

[67]V. Mourik, K. Zuo, S. M. Frolov, S. R. Plissard, E. P. A. M. Bakkers, and L. P. Kouwenhoven, "Signatures of Majorana Fermions in Hybrid Superconductor-Semiconductor Nanowire Devices", Science **336**, 1003–1007 (2012).

[68]J. D. Sau and S. Tewari, "Topological superconducting state and Majorana fermions in carbon nanotubes", Phys. Rev. B **88**, 054503 (2013).

[69]H.-C. Kao, "Chiral zero modes in superconducting nanowires with Dresselhaus spin-orbit coupling", Phys. Rev. B **90**, 245435 (2014).

[70]K. Kawabata, R. Kobayashi, N. Wu, and H. Katsura, "Exact zero modes in twisted Kitaev chains", Phys. Rev. B **95**, 195140 (2017).

[71]S. Hegde, V. Shivamoggi, S. Vishveshwara, and D. Sen, "Quench dynamics and parity blocking in Majorana wires", New Journal of Physics **17**, 053036 (2015).

[72]A. A. Zvyagin, "Majorana bound states in the finite-length chain", Low Temp. Phys. **41**, 625–629 (2015).

[73]A. V. Loginov and Y. V. Pereverzev, "Classification of states and macroscopic degeneracy in an open XY-chain in transverse field", Low Temp. Phys. **23**, 534–540 (1997).

[74]E. Lieb, T. Schultz, and D. Mattis, "Two soluble models of an antiferromagnetic chain", Annals of Physics **16**, 407–466 (1961).

[75]A. Alase, E. Cobanera, G. Ortiz, and L. Viola, "Generalization of Bloch's theorem for arbitrary boundary conditions: Theory", Phys. Rev. B **96**, 195133 (2017).

[76]A. Alase, E. Cobanera, G. Ortiz, and L. Viola, "Exact Solution of Quadratic Fermionic Hamiltonians for Arbitrary Boundary Conditions", Phys. Rev. Lett. **117**, 076804 (2016).

[77]E. Cobanera, A. A. G. Ortiz, and L. Viola, "Exact solution of corner-modified banded block-Toeplitz eigensystems", Journal of Physics A: Mathematical and Theoretical **50**, 195204 (2017).

[78]R. Usmani, "Inversion of Jacobi's tridiagonal matrix", Comput. Math. Appl. **27**, 59–66 (1994).

[79]A. Böttcher and S. M. Grudsky, *Spectral Properties of Banded Toeplitz Matrices* (SIAM, 2005).

[80]W. F. Trench, "On the Eigenvalue Problem for Toeplitz Band Matrices", Linear Algebra and its Applications **64**, 199–214 (1985).

[81]V. E. Hoggatt Jr., *Fibonacci and Lucas numbers* (Houghton-Mifflin, PaloAlto, 1969).

[82]S. Vajda, *Fibonacci and Lucas numbers, and the Golden section: Theory and Applications* (Courier Corporation, 2008).

[83]W. A. Webb and E. A. Parberry, "Divisibility properties of Fibonacci polynomials", The Fibonacci Quaterly **7**, 457 (1969).

[84]V. E. Hoggatt Jr. and C. T. Long, "Divisibility properties of generalized Fibonacci polynomials", The Fibonacci Quaterly **12**, 113 (1974).

[85]M. Özvatan and O. K. Pashaev, "Generalized Fibonacci Sequences and Binet-Fibonacci Curves", arXiv:1707.09151 (2017).

[86]I. S. Gradsteyn and I. M. Ryzhik, *Table of Integrals, Series and Products* (Academic Press (New York), 1971).

[87]V. E. Hoggatt Jr.. and M. Bicknell, "Roots of Fibonacci polynomials", The Fibonacci Quaterly **11**, 271–274 (1973).

[88]S. Kouachi, "Eigenvalues and eigenvectors of some tridiagonal matrices with non-constant diagonal entries", Applicationes Mathematicae **35**, 107–120 (2008).

[89]S. Kouachi, "Eigenvalues and eigenvectors of tridiagonal matrices", ELA. Electron. J. Lin. Algebra **15**, `10.13001/1081-3810.1223` (2006).

[90]W.-C. Yueh, "Eigenvalues of several tridiagonal matrices", Applied Mathematics E-notes **5**, 210–230 (2005).

[91]K. Flensberg and H. Bruus, *Introduction to Many-Body Quantum Theory in Condensed Matter Physics* (Oxford Graduate Texts, New York, 2002).

[92]M. Feinberg, "Fibonacci-Tribonacci", The Fibonacci Quartely **1**, 70–74 (1963).

[93]F. Jishe, "More Identities On The Tribonacci Numbers", Ars Comb. **100**, 73–78 (2011).

[94]V. Hoggatt Jr. and M. Bicknell, "Generalized Fibonacci polynomials and Zeckendorf's theorem", The Fibonacci Quartely **11**, 457–465 (1973).

[95]M. E. Waddill, "The tetranacci sequence and generalizations", The Fibonacci Quarterly **30**, 9–19 (1992).

[96]R. Li, "Convolution identities for Tetranacci numbers", arXiv preprint arXiv:1609.05272 (2016).

[97]R. Wakatsuki, M. Ezawa, Y. Tanaka, and N. Nagaosa, "Fermion fractionalization to Majorana fermions in a dimerized Kitaev superconductor", Phys. Rev. B **90**, 014505 (2014).

[98]X. Wen and A. Zee, "Winding number, family index theorem, and electron hopping in a magnetic field", Nucl. Phys. B **316**, 641–662 (1989).

[99]J. R. Silvester, "Determinants of Block Matrices", The Mathematical Gazette **84**, 460–467 (2000).

[100]C. Li, X. Z. Zhang, G. Zhang, and Z. Song, "Topological phases in a Kitaev chain with imbalanced pairing", Phys. Rev. B **97**, 115436 (2018).

[101]J. Sirker, M. Maiti, N. Konstantinidis, and N. Sedlmayr, "Boundary fidelity and entanglement in the symmetry protected topological phase of the SSH model", J. Stat. Mech. **2014**, P10032 (2014).

[102]B. C. Shin, "A formula for Eigenpairs of certain symmetric tridiagonal matrices", Bull. Aust. Math. Soc. **55**, 249–254 (1997).

[103]C. W. J. Beenakker, D. I. Pikulin, T. Hyart, H. Schomerus, and J. P. Dahlhaus, "Fermion-Parity Anomaly of the Critical Supercurrent in the Quantum Spin-Hall Effect", Phys. Rev. Lett. **110**, 017003 (2013).

[104]B. Pekerten, A. M. Bozkurt, and İ. Adagideli, "Fermion parity switches of the ground state of Majorana billiards", Phys. Rev. B **100**, 235455 (2019).

[105]R. S. K. Mong and V. Shivamoggi, "Edge states and the bulk-boundary correspondence in Dirac Hamiltonians", Phys. Rev. B **83**, 125109 (2011).

[106]J. Chen, P. Yu, J. Stenger, M. Hocevar, D. Car, S. R. Plissard, E. P. A. M. Bakkers, T. D. Stanescu, and S. M. Frolov, "Experimental phase diagram of zero-bias conductance peaks in superconductor/semiconductor nanowire devices", Science advances **3**, e1701476 (2017).

[107]C.-H. Lin, J. D. Sau, and S. D. Sarma, "Zero-bias conductance peak in Majorana wires made of semiconductor/superconductor hybrid structures", Phys. Rev. B **86**, 224511 (2012).

[108]C. Moore, C. Zeng, T. D. Stanescu, and S. Tewari, "Quantized zero-bias conductance plateau in semiconductor-superconductor heterostructures without topological Majorana zero modes", Phys. Rev. B **98**, 155314 (2018).

[109]R. J. Doornenbal, G. Skantzaris, and H. T. C. Stoof, "Conductance of a finite Kitaev chain", Phys. Rev. B **91**, 045419 (2015).

[110]D. A. Ryndyk, *Theory of Quantum Transport at Nanoscale* (Springer, Cham, Heidelberg, New York, Dordrecht, London, 2016).

[111]J. Rammer and H. Smith, "Quantum field-theoretical methods in transport theory of metals", Rev. Mod. Phys. **58**, 323–359 (1986).

[112]M. Di Ventra, *Electrical Transport in Nanoscale Systems* (Cambride University Press, Cambridge, 2008).

[113]G. D. Mahan, *Many-Particle Physics* (Springer Science & Business Media, 2013).

[114]H. Haug and A.-P. Jauho, *Quantum Kinetics in Transport and Optics of Semiconductors* (Springer, Berlin, 1996).

[115]Z. Y. Zeng, B. Li, and F. Claro, "Electronic transport in hybrid mesoscopic structures: A nonequilibrium Green function approach", Phys. Rev. B **68**, 115319 (2003).

[116]D. C. Langreth, *Linear and nonlinear electron transport in solids*, Vol. 17 (Springer, New York, London, 1976).

[117]Y. Meir and N. S. Wingreen, "Landauer formula for the current through an interacting electron region", Phys. Rev. Lett. **68**, 2512–2515 (1992).

[118]A. L. Yeyati, A. Martín-Rodero, and F. J. García-Vidal, "Self-consistent theory of superconducting mesoscopic weak links", Phys. Rev. B **51**, 3743–3753 (1995).

[119]R. Mélin, F. S. Bergeret, and A. L. Yeyati, "Self-consistent microscopic calculations for nonlocal transport through nanoscale superconductors", Phys. Rev. B **79**, 104518 (2009).

[120]G. E. Blonder, M. Tinkham, and T. M. Klapwijk, "Transition from metallic to tunneling regimes in superconducting microconstrictions: Excess current, charge imbalance, and supercurrent conversion", Phys. Rev. B **25**, 4515 (1982).

[121]A. Andreev, "The Thermal Conductivity of the Intermediate State in Superconductors", JETP **19**, 1228 (1964).

[122]J. Nilsson, A. R. Akhmerov, and C. W. J.Beenakker, "Splitting of a Cooper Pair by a Pair of Majorana Bound States", Phys. Rev. Lett. **101**, 120403 (2008).

[123]J. Danon, E. B. Hansen, and K. Flensberg, "Conductance spectroscopy on Majorana wires and the inverse proximity effect", Phys. Rev. B **96**, 125420 (2017).

[124]H. Schmid, "Spectral and transport properties of a finite-size topological superconducting wire", MA thesis (University of Regensburg, 2020).

[125]S. Gangadharaiah, B. Braunecker, P. Simon, and D. Loss, "Majorana Edge States in Interacting One-Dimensional Systems", Phys. Rev. Lett. **107**, 036801 (2011).

[126]C. W. J. Beenakker, "Search for Majorana Fermions in Superconductors", Annu. Rev. Condens. Matter Phys. **4**, 113–136 (2013).

[127]T. D. Stanescu, R. M. Lutchyn, and S. D. Sarma, "Majorana fermions in semiconductor nanowires", Phys. Rev. B **84**, 144522 (2011).

[128]D. K. Salkuyeh, "Comments on "A note on a three-term recurrence for a tridiagonal matrix"", Appl. Math. Comput. **176**, 442–444 (2006).

[129]L. G. Molinari, "Determinants of block tridiagonal matrices", Linear Algebra Appl. **429**, 2221–2226 (2008).